



Norwegian University
of Life Sciences

Master's Thesis 2019 60 ECTS

Faculty of Chemistry, Biotechnology and Food Science

Characterisation of a Lytic Polysaccharide Monooxygenase from *Aspergillus fumigatus* belonging to Auxiliary Activity Family 11

Fredrik Gjerstad Støpamo

Master of science in biotechnology

Acknowledgements

This work would not have been possible without assistance and support from my colleagues. I owe a great deal of gratitude to my co-supervisor Sophanit Mekasha for her experimental guidance, lab work, and discussions which furthered my research. I would also like to thank my co-supervisor Dejan Petrovic for showing me how to operate in the lab, and providing me with the necessary equipment and techniques. Thank you to my thesis supervisor, Vincent G.H. Eijsink, for providing me with this research opportunity, guiding my progress, and for providing feedback on my text. Additionally, I would like to thank Åsmund Kjendseth for his help in solving the crystal structure of *Afu*LPMO11B. Without the moral support and writing assistance from Victoria Thomas, I fear I would not have survived this process. Finally, I would like to thank everyone in the PEP group for great cooperation and support and for creating an inclusive and professional environment, in which I was able to produce these results.

ABSTRACT

Studies with lytic polysaccharide monooxygenases (LPMOs) in recent years have shown promising results in the enzyme's ability to degrade recalcitrant carbohydrate biomass, a crucial property in future biomass utilization that have led to increasing interest for industrial purposes. The list of LPMO candidates with putative industrial applications continues to grow, with readily new characterized enzymes in the CAZy database. LPMOs are copper-dependent metalloenzymes that utilize an oxidative mechanism in degradation of polysaccharides. The intricate nature of the oxidation mechanism however, are hitherto unknown. Recent studies have found that LPMOs are able to utilize H_2O_2 as the catalytic co-substrate, and that this reaction is much faster than reactions using molecular oxygen (O_2). These finding have led to the debate of whether H_2O_2 is the true, and only co-substrate for LPMOs, or if O_2 also serve as a co-substrate. This study provides insight in enzymatic functions and structural arrangements of a novel LPMO from the AA family 11 (*AfuLPMO11B*) originating from *Aspergillus fumigatus*. *AfuLPMO11B* is a C1 oxidizing enzyme, active on α - and β - chitin substrates, with stable activity for 20+ hours on both substrates at 30 °C. The AA11 show great synergetic action with chitinase C (*SmChi18C*) when acting on α -chitin, and with an almost complete conversion of β -chitin to soluble products. Activity of the LPMO was boosted by adding H_2O_2 in reaction mixtures, yielding a so far maximum of 27-fold increase in catalytic rates from the apparent catalytic rate in standard aerobic conditions. The LPMO also show linear product formation up to 3 hours with 80 μ M H_2O_2 , and 6 hours with 50 μ M H_2O_2 from acting on β -chitin substrate. Earlier studies utilizing H_2O_2 in LPMO reactions have indicated that LPMOs are able to repeat catalytic cycles only using only H_2O_2 , after a first priming reduction. This ability was not observed for *AfuLPMO11B*. The enzyme binds equally well to α - and β -chitin in non-reduced state, with approximately 25 % bound protein after 6-hours of incubation. In glycosylated state with an N-linked glycan, the bound protein fraction is increased to 32 %, while reduced to 16 % on β , and α -chitin, respectively. Upon LPMO reduction, this binding trend is further increased. The N-glycan site is predicted to be on (Asn80), a residue that are not located close to the active site. *AfuLPMO11B* was crystallized, from which the protein structure was successfully elucidated from x-ray crystallography. The solved protein structure was similar to an earlier modelled structure which was used in structural studies.

ABBREVIATIONS

2,3-DHBA	-	2,3-dihydroxybenzoic acid
$^{18}\text{O}_2$	-	labelled molecular oxygen
ϵ	-	extinction coefficient
μl	-	microliter
μM	-	micromolar
A_{280}	-	absorbance at 280 nm, UV method – protein conc.
A_{595}	-	absorbance at 595 nm, Bradford assay – protein conc.
AA	-	auxiliary activity
CAN	-	acetonitrile
<i>Afu</i>	-	<i>Aspergillus fumigatus</i>
AscA	-	ascorbic acid
Asn	-	asparagine
Asp	-	aspartic acid
AU	-	absorbance unit
<i>Bc</i>	-	<i>Bacillus cereus</i>
BIS-Tris	-	2-[Bis(2-hydroxyethyl) amino]-2-(hydroxymethyl) propane-1,3-diol
BSA	-	bovine serum albumine
CAZy	-	carbohydrate active enzymes
CBM	-	carbohydrate-binding module
CBP	-	chitin-binding protein
Conc	-	concentration
Da	-	dalton
DMSO	-	dimethyl sulfoxide
DNA	-	deoxyribonucleic acid
DP	-	degree of polymerization
FASTA	-	fast-all (one letter codes for proteins or nucleic acids)
g	-	gram
GH	-	glycoside hydrolase
GlcNAc	-	<i>N</i> -Acetylglucosamine (2-(acetylamino)-2-deoxy-D-glucose)
GlcNAc1A	-	<i>N</i> -acetylglucosaminic acid
[GlcNAc] ₂ ^{ox}	-	<i>N,N'</i> -Diacetylchitobiose (Oxidized)
Glu	-	glutamic acid
H ₂ O ₂	-	hydrogen peroxide
HCl	-	hydrochloric acid
HIC	-	hydrophobic interaction chromatography
HILIC	-	hydrophilic interaction chromatography
His	-	histidine
HPAEC	-	high performance anion exchange chromatography
HPLC	-	high performance liquid chromatography

ICS	-	ion chromatography system
IEC	-	ion exchange chromatography
L	-	liter
LC	-	liquid chromatography
LPMO	-	lytic polysaccharide monooxygenase
M	-	molar
MALDI	-	matrix assisted laser desorption ionization
mAU	-	milli absorbance unit
ml	-	milliliter
mg	-	milligram
MS	-	mass spectrometry
MQ	-	milliQ-water
MWCO	-	molecular weight cut-off
NaCl	-	sodium chloride
NaOH	-	sodium hydroxide
nl	-	nano-Liter
nM	-	nano-Molar
O ₂	-	molecular oxygen
OH	-	hydroxide
PAD	-	pulsed amperometric detection
PAGE	-	polyacrylamide gel electrophoresis
PES	-	polyethersulfone
Phe	-	phenylalanine
pI	-	isoelectric point
psi	-	pounds per square inch
RCF	-	relative centrifugal force
RI	-	refractive index
ROS	-	reactive oxygen species
RPM	-	revolutions per minute
SDS	-	sodium dodecyl sulphate
SEC	-	size exclusion chromatography
Ser	-	serine
Std	-	standard
Thr	-	threonine
TOF	-	time of flight
Tyr	-	tyrosine
UPLC	-	ultra performance liquid chromatography
UV	-	ultraviolet
V	-	volt
w/v	-	weight/volume, where 1 g = 1 ml

Table of Contents

1. Introduction.....	1
1.1 Overview.....	1
1.2 Polysaccharides	2
1.2.1 Physiochemical properties of carbohydrates.....	2
1.2.2 Chitin	4
1.3 Enzymes.....	6
1.3.1 Enzymes that degrade recalcitrant polysaccharides.....	7
1.3.2 Chitinases	8
1.3.3 LPMOs.....	10
1.3.4 Synergy in biomass degradation	18
1.4 Glycosylation	19
1.4.1 Protein glycosylation	19
1.4.2 Deglycosylation of proteins.....	20
1.5 Protein structure elucidation	21
1.6 Carbohydrate product analysis	22
1.6.1 Liquid chromatography	22
1.6.2 Mass spectrometry.....	23
1.7 Protein production	25
1.7.1 Heterologous protein expression.....	25
1.7.2 Protein purification	27
1.7.3 Protein concentration	30
1.8 The goal of this study	32
2. Methods and materials	33
2.1 Solutions.....	33
2.1.1 Water.....	33
2.1.2 Buffers	33
2.1.3 Eluents	34
2.1.4 Ascorbic acid reductant.....	34
2.1.5 H ₂ O ₂ co-substrate	34
2.1.6 Enzyme stocks	35
2.1.7 Substrates.....	35
2.2 Protein production	35
2.2.1 Cultivation of <i>Pichia pastoris</i>	36
2.2.2 Purification of protein	37
2.2.3 Copper saturation.....	40

2.2.4 Protein concentration	40
2.3 Experimental setups	41
2.3.1 Deglycosylation	41
2.3.2 Substrate screening	42
2.3.3 Protein melting point	43
2.3.4 H ₂ O ₂ production by LPMO in the absence of substrate	43
2.3.5 Temperature screen	45
2.3.6 Comparing activity with AfuLPMO11B and BcLPMO10A	46
2.3.7 Comparing activity with glycosylated and deglycosylated AfuLPMO11B	46
2.3.8 Synergy experiment.....	47
2.3.9 H ₂ O ₂ feeding experiment.....	48
2.3.10 Protein-substrate binding.....	50
2.3.11 Crystallization	51
2.3.12 CHB treatment.....	54
2.4 Analytical methods.....	54
2.4.1 SDS-PAGE analysis	54
2.4.2 Product analysis with HPAEC-PAD.....	55
2.4.3 Product analysis with HILIC UPLC.....	55
2.4.4 Product analysis with MALDI-TOF MS.....	56
2.4.5 Quantification of GlcNAc and GlcNAcGlcNAc1A with RSLC.....	56
2.4.6 Thermal shift analysis.....	57
2.5 Calculations	57
2.5.1 Chemical concentrations	57
2.5.2 Progression curves	58
2.5.3 substrate conversion	58
2.5.4 Protein binding	59
2.5.5 Average DP estimation on (GlcNAc) _n GlcNAc1A reaction products	59
2.6 Bioinformatics	60
2.6.1 Protein modelling	60
2.6.2 Multiple sequence alignment.....	60
2.6.3 Glycosylation site predictions.....	61
2.7 AfuLPMO11B protein crystal structure	61
2.8 Materials.....	61
3. Results	67
3.1 Protein quality & AfuLPMO11B characteristics.....	67
3.1.1 Protein specifications and purified enzyme batch quality	67

3.1.2	Functional characterization of AfuLPMO11B - Substrate specificity.....	71
3.1.3	Functional characterization of AfuLPMO11B - Characterization of reaction products.....	74
3.1.4	Enzymatic H ₂ O ₂ -Production.....	78
3.1.5	Melting Point Analysis	79
3.2	Reaction kinetics & substrate binding.....	80
3.2.1	Temperature based activity screen on AfuLPMO11B	80
3.2.2	Comparison of AfuLPMO11B with another chitin-actve LPMO, BcLPMO10A.....	81
3.2.3	The effect of N-glycosylations on catalytic rate	82
3.2.4	Synergy between the LPMO and a chitinase	83
3.2.5	Activity of AfuLPMO11B with feeding of H ₂ O ₂ feeding	85
3.2.6	Substrate binding	89
3.3	Crystallization of <i>Afu</i> LPMO11B	92
3.3.1	Crystal screening kit	92
3.3.2	Reproducing crystallization conditions	93
3.4	Protein structure	94
3.4.1	Structural analysis by modelling.....	94
3.4.2	Protein structure by X-ray crystallographic analysis	98
4.	Discussion.....	100
4.1	Protein purification and quality control	100
4.2	<i>Afu</i> LPMO11B - functional characteristics.....	101
4.2.1	Substratespecificity	101
4.2.2	H ₂ O ₂ produced by AfuLPMO11B	104
4.2.3	Effects of temperature on LPMO activity.....	105
4.3	Kinetics	106
4.3.1	Comparing AfuLPMO11B and BcLPMO10A.....	106
4.3.2	Synergy with AfuLPMO11B and SmChi18C	107
4.3.3	H ₂ O ₂ -feeding reactions	109
4.4	The role of N-linked glycosylation on <i>Afu</i> LPMO11B	113
4.4.1	Binding and catalysis	114
4.4.2	Potential mishaps	117
4.5	Crystallization and protein modelling	120
4.5.1	Crystallization	120
4.5.2	Protein structure by SWISS-MODEL Homology Modelling.....	121
4.6	Comparability between experiments.....	122
5.	Conclusion and future perspectives	123
	References.....	125

Appendices	132
APPENDIX A	132
APPENDIX B	135
APPENDIX C	136
APPENDIX D	138
APPENDIX E.....	147
APPENDIX F.....	149
APPENDIX G.....	154

1. Introduction

1.1 Overview

Population growth, overconsumption, and use of fossil energy are debated as major contributors to anthropogenic climate change [1]. Climate issues have accumulated because there are too few sustainable solutions. The necessary solutions can be derived from advancements in biosciences, particularly biotechnology, which offer numerous approaches to solving environmental and societal issues. These numerous approaches have propelled biotechnology to the forefront of global interest [2]. A common goal in a broad perspective is to reduce the usage of fossil fuels. This, however, depends on the availability of a substitute material, so that net global energy demands can be met. In search of such a substitution, there has been considerable focus in recent years on the development and incorporation of biofuels [112].

Although biofuels are considered an eco-friendly solution to fossil fuels, there is currently no sustainable mechanism in biofuel production. Current biofuel production heavily relies on using plant derived sugars, such as starch and sucrose, which also are major sources for animal feed and human consumption. Suggested alternative resources in biofuel production are (non-edible) lignocellulosic- and chitinous biomass materials. The disadvantage of these materials is that they are recalcitrant and complex sugar-polymer structures, that require costly pretreatments for their conversion to simple sugars that can be utilized in fermentative biofuel production [111, 113].

As one application of biotechnology, enzymes can be used to convert the polysaccharides in biomass to simple sugars, which can further be utilized in production of biofuels or for other purposes, such as fermentative production of other products or microbial biomass (single cell protein), as well as chemical valorization. Biomass may be produced for direct utilization in such “biorefining” approaches, or one may use the enormous amounts of biomass by-products that are generated as a consequence of the inability of many industries to effectively utilize harvested materials.

Biomass is often composed of recalcitrant polysaccharides, which are essentially strong, organic materials, such as cellulose in plant cell walls and chitin in crustacean shells. These

materials are not very susceptible to enzymatic depolymerization. One biotechnological approach to solving this problem is to study how living organisms recycle recalcitrant polysaccharides in nature. Living organisms decompose these polysaccharides using complex enzymatic systems. By investigating the enzymes involved in natural decomposition processes and understanding the underlying enzymatic mechanisms, these systems can be exploited in industrial applications based on efficient enzymatic conversion technologies.

The insoluble polysaccharides cellulose and chitin are the most and second most abundant biopolymers available, respectively. It is thus important to better understand carbohydrate-active enzymes which can depolymerize these biopolymers. Such enzymes are typically glycoside hydrolases (GHs) and lytic polysaccharide monooxygenases (LPMOs) and are currently under intensive research [3, 4]. The goal of the research described in this thesis was to characterize a novel fungal LPMO from *Aspergillus fumigatus* from the LPMO family 11 (AA11), with possible applications in enzymatic processing of chitin. The results provide important information for applied science, but also give fundamental insights into LPMO (bio)chemistry, which can further our understanding of these important enzymes.

1.2 Polysaccharides

Polysaccharides are found in all living organisms and consist of polymeric or copolymeric materials. Polysaccharides are made up of mono-sugars, which are connected through ether-like bonds, typically called glycosidic linkages [5]. Polysaccharides may contribute to keeping organic structures stable, e.g. cellulose in plant cell walls, and play a fundamental role in energy storage, e.g. starch. Polysaccharides are also important in other biological systems, involving protein glycosylations, e.g. for antigenic modulations, regulatory processes, and protein transport mechanisms. [6, 7, 8].

1.2.1 Physicochemical properties of carbohydrates

Carbohydrates constitute a large class of polyhydroxylated ketones and aldehydes, which are generally referred to as sugars. Sugar is one of the four fundamental biomolecules in nature, alongside proteins, lipids, and nucleic acids. The stoichiometric description of this large class

of polyhydroxylated ketones and aldehydes, $C_m(CH_2O)_n$, reflects the carbon to water ratio of monosaccharides. Simple sugars, or monosaccharides, are single sugar units, containing typically three to seven carbon atoms in linear or cyclic arrangements. Each of these carbons are hydroxylated, except for one that is double bonded to oxygen, which is called the carbonyl group. In a linear arrangement, the carbonyl group is either an aldehyde or ketone, having an exo- (on the end) or endo- (within) position on the carbon chain, respectively.

The mono-sugar can rearrange from a linear to a cyclic configuration, when a nucleophile, such as a hydroxyl group (OH) attacks the carbonyl group. Both linear and cyclic forms are present in solution by back and forward reactions at equilibrium. In glucose, the nucleophilic reaction converts the carbonyl oxygen to an OH on C1 (carbon atom 1, by priority), and the nucleophilic hydroxyl group becomes the cyclic ether functional group [C1-O-C_n], more precisely named the hemiacetal group [OH-C1-O-C_n]. The OH on C1 may be positioned either cis or trans, meaning that there are two anomeric stereoisomers that are in equilibrium in solution. If the OH is in the cis-position, glucose is named β-glucose, while in trans-position it is called α-glucose [9].

Because the C1 in the cyclic configuration has chirality the two glucose forms (α and β) each constitute a pair of optical isomers (mirror-images), also known as enantiomers. In carbohydrate and amino acid chemistry particularly, these isomers are labeled D and L, which refers to the *right* and *left* handedness of a chiral center in a compound, and is further referred to D or L according to the orientation of the asymmetric carbon furthest from the carbonyl group. In nature, living organisms only use right-handed (D) sugars, and left-handed (L) amino-acids [19]. Natural sugars are therefore labeled as, e.g., β-D-glucose or α-D-glucose.

Simple sugars can be connected by glycosidic bonds and thereby form di-, oligo- or polysaccharides. Cellulose and chitin are linear polymers of glucose and *N*-acetylglucosamine, respectively, which are connected by so-called β(1,4)-linkages, where 1,4 refers to the C1 carbon and the C4 from the non-reducing end and reducing end monosaccharide, respectively. Short oligosaccharides are called di-, tri-, tetra-saccharides, or dimers, trimers, tetramers, and so on, and often referred to as oligomers. The length of both oligomers and polymers is often expressed by the term DP_n (for Degree of Polymerization, where n is the total number of mono-sugars). Polysaccharides can consist of thousands of interlinked sugar units, in both a linear and branched fashion [9].

Different functional characteristics have been observed for polysaccharides such as starch, cellulose and chitin. These differences stem from the chemistry of the mono-sugars and the various linear and branched polymeric arrangements. Starch is a highly branched α -glucose polymer with coiled chains and has low copolymeric- or inter-chain interaction. Therefore, starch interacts substantially with water. This gives starch a soft texture, becoming soluble in water when heated. Cellulose and chitin, however, are insoluble recalcitrant polymers, which are linear and engage strong inter-chain interactions. These polysaccharides are therefore strong and hard [10, 11].

Enzymatic degradation of complex recalcitrant polysaccharides causes low DP oligomers to disassociate. These solubilized oligomers can range from DP1 to \sim DP9, depending on the substrate type and solvent solution. The soluble oligomers are frequently used in quantitative product analyses, as they reflect the capability of the enzymes to solubilize an insoluble substrate. In the case of LPMO action, most of the soluble oligomers will contain an oxidized end, as discussed further below.

1.2.2 Chitin

Chitin and cellulose have similar linear, unbranched, polymer-arrangements. Chitin is composed of β -1,4-linked *N*-acetylglucosamine (GlcNAc), unlike cellulose, which is composed of β -1,4-linked glucopyranose (Glc). Both polymers have straight chains, composed of linked sugars that are oriented alternately with 180° , and self-associate into fibrils by inter-chain interaction because of hydrogen bonding [11]. The chitin monomer (GlcNAc) differs from glucose in that the second carbon (C_2) has a nitrogen (N) that is further connected to an acetyl group (Ac), hence the name *N*-acetylglucosamine, or more precisely 2-(acetamino)-2-deoxy-D-glucose. In contrast to cellulose, this N-linked acetyl group allows for a different inter-chain interaction with more hydrogen bonding. When substantial amounts of the acetyl group are removed from chitin, chitin becomes chitosan, which is a more flexible material that is soluble at slightly acidic pH [4]. The lack of the acetyl groups in chitosan causes inter-chain interactions to have less hydrogen bonding, resulting in a more flexible material.

Chitin occurs in three crystalline polymorphs called α -, β -, and γ -chitin (Fig 1). α -chitin is the strongest, least flexible form of the three, and is composed of antiparallel chain arrangements. This arrangement produces the most compact crystalline polymer structure,

which is least hydrated. α -chitin is the primary component in insect exoskeletons and crustacean shells. In β -chitin, the polysaccharide chains are arranged in a parallel fashion, which leads to a more open and less rigid crystalline structure. This arrangement is the most hydrated of the three and therefore the most flexible. β -chitin is found e.g. in fungal cell walls. γ -chitin has a mixture of parallel and antiparallel chain arrangements in a three-polymer chain system, where chain 1 and 2 are parallel to one another, and chain 3 is antiparallel to chain 1 and 2 [11, 126].

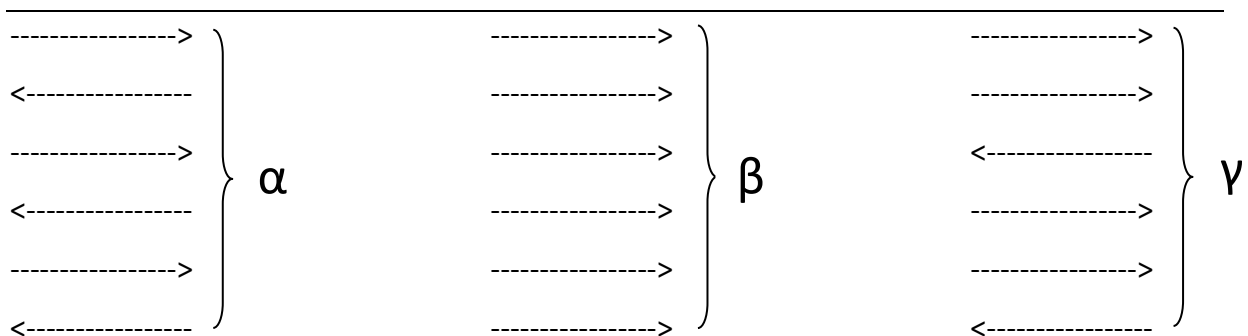


Fig 1. Chitin polymorphs. The figure illustrates the three allomorphic forms of chitin (α , β , and γ), where the polymer direction (arrows) relates to the carbohydrate reducing end.

It was estimated that 6.9 million tonnes of crustaceans were captured in 2014, of which more than a third was discarded as predominantly chitinous waste [11]. In nature, crustaceans, mollusks, insects, and fungi produce about 100 billion tonnes of chitin annually [127]. Concurrently, chitin is considered the least exploited available biomass on Earth [4]. Chitin, despite its recalcitrant nature and abundant production, does not accumulate in the environment, and, thus, there must be natural capabilities within the biosphere to degrade this material [12]. Consequently, several enzymes have been found and characterized for their ability to degrade chitin. Such enzymes are so-called carbohydrate-active enzymes (CAZymes), that are classified in the CAZy database (www.cazy.org) [13]. Hydrolytic enzymes, such as chitinases, are categorized in glycoside hydrolase (GH) families, whereas redox enzymes, including LPMOs, are categorized in auxiliary activity (AA) families. The CAZy classification is purely sequence-based. Enzymes for chitin degradation occur in families GH18 and GH19 and LPMO families AA10, AA11 and AA15.

1.3 Enzymes

Enzymes are catalytic proteins, complex bio-machines that drive nearly all processes of life, by catalyzing chemical reactions. Enzymes lower the energy barrier for a chemical transition in chemical reactions, thus speeding up (“catalyzing”) these reactions. The enzyme manipulates the electron orbital fields of substrates (compounds acted on by enzymes), thereby inducing particular chemical reactions, e.g. nucleophilic attacks on carbonyl groups and hydroxylation reactions. The compounds formed upon enzymatic catalysis are called products [98].

Unlike DNA, where sequence similarity is crucial in order to execute the biological function, proteins may differ in sequence, yet have the same structure and the same or similar functionality. This is possible because proteins operate in a three-dimensional space, allowing a larger set of possible solutions for the given function(s). It is important to note that the function of a protein, e.g. an enzyme, predominantly relies on its structure, rather than its sequence.

Proteins are chains of linked amino-acid residues, with on average 283, 311, and 438 residues in proteins from Archaea, Bacteria, and Eukaryotes, respectively. Nature uses 21 different amino acids in proteins (if one includes selenocysteine). All of these, except for proline, have the same core-structure, with an amine- (NH₂) and a carbonyl- (COOH) group covalently bound to a carbon-atom, known as C_α. The amino acid side chain extends from the C_α; glycine is special in that there is no side chain (only a hydrogen atom), whereas proline stands out because its side chain is covalently bound to its amino group. The amino acid changes in ionic forms depending on the pH environment (Fig 2), where positive ions (cations) are formed by protonation on the amine group at low pH (< 4), whilst negative ions (anions) are formed by deprotonation of the carboxylic group at high pH (> 8). Around neutral pH (~ 6), protonation and deprotonation of the amine- and carboxyl group occur simultaneously at back and forward reactions, resulting in a net-neutral charge.



Fig 2. Ionic change in amino acids. The figure illustrates the change in ionic forms of amino acids depending on the pH environment, where positive cations (blue) are formed under pH 4, while neutral or in switterionic form between pH 4-8, and negative anions (red) above pH 8.

Variation between amino acids arises from the varying side groups on C_α, also known as the functional groups, or R-group. Variations among these concern positive and negative charges, polarity, hydrophobicity and size. The size of the functional groups is an important factor, as it provides variation in steric hindrance and/or extended reach of the primary functional groups, e.g. an extended functional group with a charge, such as in lysine or arginine. The especial side chains of proline and glycine make these residues the least flexible and most flexible residues in a protein, respectively

Folding of a newly synthesized polypeptide, i.e., a polymer of amino acids, to a functional protein, e.g., an enzyme, depends on intra-molecular interactions involving main chain and side chain atoms. The final tertiary structure may be stabilized by covalent bonds between cysteine residues forming disulfide bridges. Folded functional units of proteins are called domains. Considerable numbers of proteins contain more than one domain. For example, carbohydrate-active enzymes may contain a carbohydrate-binding module (CBM) domain, next to a catalytic domain.

Newly synthesized proteins may undergo a multitude of post translational modifications of which N- and O-glycosylation are among the most abundant and best-known ones. Such modifications may be important for protein function and/or stability.

1.3.1 Enzymes that degrade recalcitrant polysaccharides

Until recently, it was believed that recalcitrant polysaccharide biomass was predominantly degraded by a wide variety of hydrolytic enzymes called glycoside hydrolases (GHs) [14, 96]. For example, members of GH families 18 and 19 break down chitin and are called chitinases. In many cases, GHs have an attached substrate binding domain called a CBM (carbohydrate-binding module), usually, but not always with flexible linker region in between. The CBM modules are catalytically inactive, but have substrate binding activity, particularly for crystalline carbohydrate substrates [15]. Because of the binding function of CBMs, they promote the hydrolytic activity of the attached GH, as the CBM operates as a substrate docking station.

In recent years however, a new group of enzymes called LPMOs has been discovered with a reaction mechanism that differs from the mechanism of the hydrolytic enzymes (GHs).

LPMOs catalyze oxidative reactions to cleave glycosidic linkages in recalcitrant polysaccharides and produce oxidized products [97]. Already in 2005, Vaaje-Kolstad et al. (2005) showed that a protein called CBP21 (chitin-binding protein) boosted the activity of chitinases during chitin degradation. At the time, CBP21 was thought not to have an enzymatic function, but rather to assist in chitinase activity by binding and manipulating the substrate surface [12]. However, in 2010, Vaaje-Kolstad et al. (2010), found that CBP21 in fact is an enzyme that cleaves chitin polymers and releases oxidized products. Today, CBP21 is known as *Sm*LPMO10A or *Sm*AA10A. Using mass spectrometry and labelled oxygen ($^{18}\text{O}_2$), it was shown that the oxygen incorporated at oxidized chain ends was derived from molecular oxygen (O_2), [16]. Research has since then, continued with increasing interest within the LPMO field, due to its promising results and putative applications. Continuously characterizing novel LPMOs is therefore important to understand the properties of these enzymes, and to provide biorefining industries with new LPMO candidates for industrial applications.

1.3.2 Chitinases

A multitude of chitinases belonging to the GH18 and GH19 families are now known and characterized. Chitinases, or 1,4- β -poly-*N*-acetylglucosaminidase (E.C 3.2.1.14), have been found in all domains of life [13]. Chitinases can be divided in two main categories, endo-chitinases and exo-chitinases. Endo-activity by GH refers to the binding and hydrolytic activity at random positions within the polymer chain. Exo-activity refers to enzymes that preferably bind to and act on chain ends. Exo-chitinases can further be divided into two groups: chitobiosidases (E.C 3.2.1.29), which catalyze the release of dimeric products (*N,N*-diacetylchitobiose) from the crystalline substrate, and 1-4- β -glucosaminidases (E.C. 3.2.1.30) which degrade soluble oligomeric products released by the former enzymes by cleaving of monomeric units of *N*-acetylglucosamine [17]. Chitobiosidases are often processive, which means that after binding to the substrate, they catalyze multiple successive releases of chitobiose, without fully dissociating from the substrate in between catalytic steps [106].

Many chitin harbouring organisms use chitinases for chitin remodeling, feeding, or as protection against harmful insects. Because of the multiple uses of chitinases, they are not only found in organisms possessing chitin, such as insects, crustaceans, yeast, and fungi, but also in organisms that lack chitin, such as bacteria, higher plants, and vertebrates [18]. One of

the most effective microbial chitin degraders known in nature, is the Gram-negative soil bacterium *Serratia marcescens*, with a characterized chitinolytic system (Fig 3). The bacterium produces four family 18 GHs, namely chitinase A, B, C, and D, also known as ChiA, ChiB, ChiC and ChiD, producing chitobiase, *SmGH20*, and a chitin-active LPMO (CBP21) [12, 106]. ChiA and ChiB are chitobiosidases (17), whereas ChiD has low activity and may not be involved in chitin conversion at all [128]. ChiC (*SmChi18C*) is an endo-active chitinase and was used in the work described in this thesis, as was (*SmGH20*). The latter enzyme may be used to convert oligomers in product mixtures to monomers, which facilitates product quantification [106]. This chitobiase acts at the non-reducing end of the oligomers, and sequentially cleaves off non-oxidized NAG monomers (GlcNAc). Oligomeric LPMO products carrying an oxidation at C1 (i.e., the former reducing end; see below) will also be degraded, except for the oxidized dimer [59].

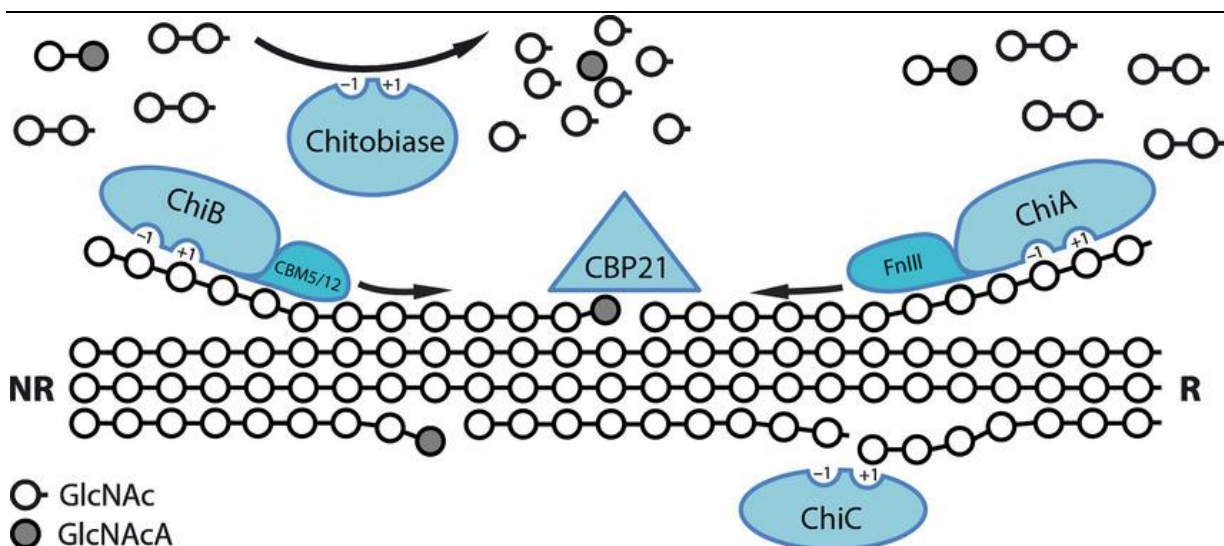


Fig 3. Chitinolytic machinery of *Serratia marcescens*. The figure illustrates the chitinolytic machinery, in *S. marcescens*, acting on chitin (ChiD not included). ChiA cleaves chains processively from the reducing end (R) and ChiB from the non-reducing end (NR), predominantly producing chitobiose ((GlcNAc)₂), while ChiC cleaves at random positions on more amorphous regions within the polymer substrate, making new chain ends for ChiA and ChiB activity. CBP21 (*SmLPMO10A*) performs oxidative cleavage in the more condensed and crystalline positions on the substrate, producing aldonic acids (GlcNAcA; dark circles) at the newly formed reducing end, and thus, also produces new chain ends for the processive enzymes, as well as disrupting substrate crystallinity, and therefore increasing ChiC activity. The released soluble products are further converted to monomers (GlcNAc) by Chitobiase, or oxidized dimers (GlcNAcGlcNAcA), if the soluble oligomers contain an aldonic acid, which inhibits the conversion to monomers. Figure source: Vaaje-Kolstad et al., (2013) [106].

1.3.3 LPMOs

Lytic polysaccharide monooxygenases (LPMOs) are mono-copper enzymes that break scissile glycosidic linkages using an oxidative mechanism, in an oxygen and reductant dependent manner [19]. LPMOs are unique in their catalytic mechanism, as opposed to classical GHs, as LPMOs are able to incorporate molecular oxygen (O₂) into the catalyzed product, rather than incorporating water [16]. It is important to note that many LPMOs, alongside several GHs, also have peptide linked CBMs, which may prevent LPMO inactivation, and possibly increase catalytic rates [20, 45].

Based on sequence similarities members of the LPMO superfamily are divided into various AA families, that is, AA9, AA10, AA11, AA13, AA14, AA15, and AA16 [21]. LPMOs vary in terms of occurrence and substrate specificity. LPMOs active on β (1-4) glucans may oxidize C1 or C4, whereas some LPMOs produce mixtures of C1- and C4-oxidized products. AA9s are fungal enzymes with known activities on substrates with a β -1,4-linked glucopyranose backbones as well as xylan. According to the CAZy database (as of May 2019) 29 fungal AA9s have been characterized so far. AA10s are known to act on chitin, cellulose, or both [11] and are found in all domains of life, but are primarily from bacterial origin. According to the CAZy database, so far, 21 AA10s have been characterized.

Only one known AA11 has been characterized according to the CAZy database, active on chitin, and originates from *Aspergillus oryzae*, known as AoLPMO11 [22]. This AA11 is so far, the only AA11 with a solved protein structure, and appear similar to AA9 and AA10 structures, but with a slightly more convex substrate-binding surface (as opposed to a rather flat surface observed in AA9s and AA10s) [22, 23]. The structure of AoLPMO11 also revealed a four-stranded antiparallel β -sandwich immunoglobulin-like fold at the core of the protein, which operates as the structural core of all LPMOs (Fig 4) [11, 23].

AA13s are fungal enzymes with known activity on starch. Three AA13s have so far been characterized according to the CAZy database [21]. AA14s are eukaryotic LPMOs predominantly originating in fungi, but also in sea anemones, stony corals, and plant pathogenic protists. Two fungal AA14s have so far been characterized according to the CAZy database, with known activity on xylan [21]. Two AA15s have also been characterized in the same database, one with known activity on chitin, while the other enzyme active on both chitin and cellulose. Two insect derived AA15s originating from *Thermobia domestica* have

also been characterized according to the CAZy database, as well as one eukaryotic AA16, active on cellulose [21].

1.3.3.1 LPMO structure

LPMOs have a completely conserved catalytic center, called the His-brace motif (Fig 4), coordinating a single copper (Cu) atom, and this catalytic center represents the only totally conserved structural motif across all LPMOs. The His-brace is positioned at the surface of the protein and is composed of two histidines that cooperatively provide binding and coordination for the catalytically active Cu-atom. The N-terminal histidine coordinates the copper, both with its terminal amino group and one nitrogen from its cyclic functional group, while the other histidine only coordinates with one nitrogen from its side chain.

Extending the perspective from the Cu-center and the His-brace of an LPMO, different conserved features can be found. This structural area is called the second shell, and refers to the residues that are thought to interact with cosubstrates (O_2 , H_2O_2 ; see below) and/or

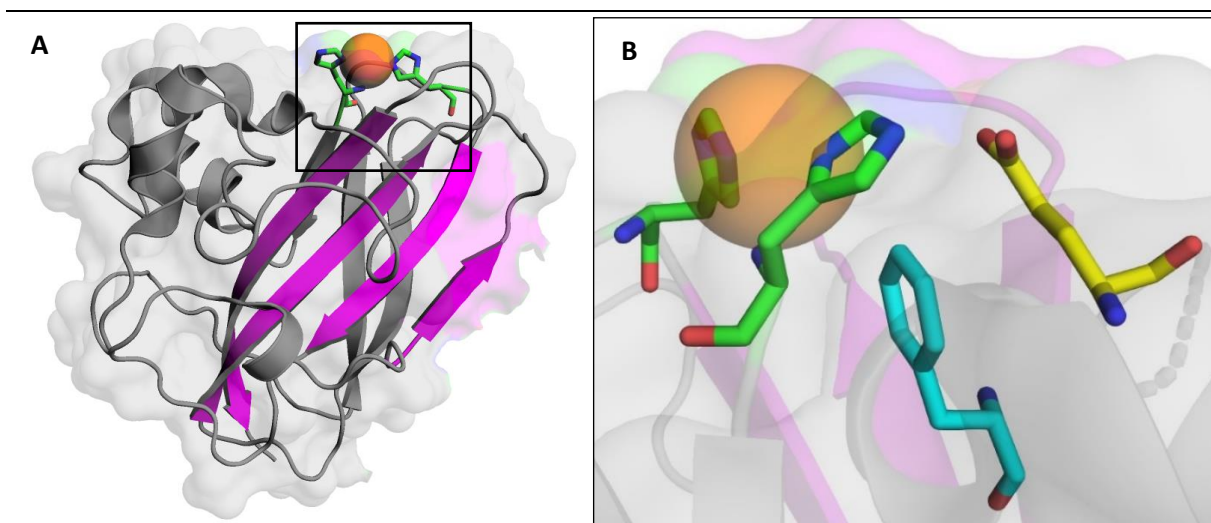


Fig 4. Illustration of general LPMO structural characteristics. *Sm*LPMO10A, also known as CBP21 (PDB accession number 2BEM) is used as example showing the conserved features across the LPMO superfamily. Panel A shows the four-stranded anti-parallel β -sandwich fold (magenta), as well as the exterior copper (orange sphere) -coordinating His-brace at the catalytic site (sticks with green carbons). Panel B shows a 90° right-hand rotation in respect to A, and provides a closer look at the catalytic site of CBP21, where the additional conserved residues are displayed: a buried copper coordinating aromatic residue, here phenylalanine (cyan carbons), and a second shell glutamate important for chitin activity (yellow carbons). The figures were generated using PyMOL (The PyMOL Molecular Graphics System, Version 2.2 Schrödinger, LLC.) [24].

the copper-binding histidines during catalysis. Within the second shell is a glutamate (Glu)

or glutamine (Gln), pointing towards the catalytic Cu-atom (Fig 4) in all LPMOs [19], where Glu has been found to relate with chitin activity [23], and Gln with cellulose activity [24].

LPMOs show low sequence homology between the AA-families but do show structural similarities. In addition to the core β -sandwich immunoglobulin-like fold and the highly conserved His-brace, LPMOs also have a buried aromatic residue pointing toward the Cu-atom (Fig 4). This residue is typically either phenylalanine (Phe) or tyrosine (Tyr), and is usually associated with bacterial and fungal LPMOs, respectively [19]. The entire LPMO structure also tends to have a triangle like shape, with one particularly flat side. This flat side incorporates the rather solvent exposed copper site and binds the substrate [43].

Although LPMOs are thought to primarily act on insoluble, crystalline substrates, some are able to catalyze soluble substrates, and even oligomeric substrates. For example, fungal NcLPMO9C is able to degrade xyloglucans, β -glucans, glucomannan and cellodextrins [25]. It has been suggested that this ability is due to an extended substrate binding surface with more polar binding regions [25, 129, 130].

1.3.3.2 LPMO catalytic mechanism

LPMOs were discovered to perform oxidoreductase activity, after labeled molecular oxygen ($^{18}\text{O}_2$) was found incorporated in oxidized lactone products. This was determined using mass spectrometric (MS) analyses and led to the belief that O_2 was the natural cosubstrate in LPMO catalysis [16]. Bissaro et al. (2017) recently challenged this belief, finding that LPMOs can utilize H_2O_2 as cosubstrate, and perhaps is the preferred cosubstrate [30]. Indeed, Bissaro et al. showed that H_2O_2 -driven LPMO reactions were much faster than O_2 -driven LPMO reactions. Thus, LPMOs should perhaps no longer be considered as classical monooxygenases. The increased catalytic speed using H_2O_2 was also supported by Kuusk et al., (2017) demonstrating H_2O_2 -driven reactions with as much as a 280-fold initial catalytic increase opposed to O_2 -driven reactions, using CBP21 (*SmAA10A*) [40].

Several parameters regarding the LPMO activity have been experimentally determined (Fig 5). First, to perform LPMO catalytic activity, the enzyme need to be reduced by a single electron reduction of the Cu-atom in the active site, going from a Cu(II) (inactive) state to a Cu(I) (active) state. Secondly, the active LPMO-Cu(I) interacts with O_2 or H_2O_2 and the

polysaccharide substrate and, somehow, performs oxidative cleavage of the scissile glycosidic bond by hydroxylation of the C1 or C4 carbon [16, 30]. This hydroxylation leads to spontaneous chain cleavage [31] producing an oxidized product that is either a lactone (C1 oxidation) or a keton (C4 oxidation). Both these products spontaneously react with water, which in the case of the lactone leads to the formation of aldonic acids [16, 31]. These oxidized products can be readily detected by chromatography, as discussed below.

The catalytic mechanism of LPMOs is not known in detail. Several quantum mechanical (QM) -and molecular mechanical (MM) simulations have been made however, using either molecular oxygen (O_2) or hydrogen peroxide (H_2O_2) as the catalytic cosubstrate [27, 28, 29]. Yet so far, no concrete evidence has been made in proving the explicit mechanisms.

Two main reaction pathways have been proposed for the LPMO catalytic mechanism, using either O_2 or H_2O_2 as the catalytic co-substrate (Fig 5). In both reaction pathways, the LPMO undergoes a single electron reduction by an externally delivered electron. This reduction can be performed by a wide range of reductants, such as ascorbic acid (AscA) or 2,3-dihydroxybenzoic acid (2,3-DHBA) [32, 33]. The first reduction of the LPMO is also known as the priming reduction and will be important in discussing H_2O_2 -driven reactions. After priming reduction, the two pathways have different suggested mechanisms, as elaborated below;

- O_2 -pathway: The reduced LPMO (Cu(I)) forms a bond with O_2 , producing a $[Cu(II)-O-O\cdot]$ radical superoxide intermediate [34]. Further delivery of a second electron and two protons, via various possible routes [35], the LPMO can hydroxylate the C1 or C4 carbon of the substrate and complete the catalytic cycle, with concomitant release of water [19]. After the catalytic cycle, the LPMO is in a resting state with Cu(II) and requires a new priming reduction in order to repeat the cycle. Of note, several of the proposed O -driven mechanisms also involve formation of a $[Cu(II)-O\cdot]$ (copper-oxyl) intermediate.
- H_2O_2 -pathway; The reduced LPMO [Cu(I)] interacts with H_2O_2 producing a $[Cu(II)-O\cdot]$ radical mono-oxygen intermediate, with subsequent release of water. This intermediate abstracts a hydrogen from the substrate carbon, producing a $[Cu(II)-OH]$ hydroxyl 2nd intermediate, and leaving a radical on the substrate carbon. The LPMO-OH-complex then hydroxylates the radical

1.3.3.3 H_2O_2 production by LPMOs

Non-substrate bound LPMOs in reduced states have been found to produce H_2O_2 in the presence of O_2 . The ability of LPMOs to produce H_2O_2 in the absence of substrates and reductants is well established. It is not clear however, if LPMOs produce H_2O_2 with a radical superoxide intermediate (described above) bound to the LPMO active site, or if the superoxide is released from the active site, and undergo reduction or dismutation in the solution, from which H_2O_2 is formed [19, 33]. The former H_2O_2 production pathway was suggested however, by Span et al., (2017), where two protons and a second electron needs to be delivered to the active site, in order to complete the two-electron reduction of molecular oxygen, producing H_2O_2 [36]. Importantly, H_2O_2 formed in reaction solutions are not always formed by LPMOs. Transition metals, sometimes present in solution or in carbohydrate substrates, can also produce H_2O_2 when interacting with O_2 and a reductant [19].

Although un-bound and reduced LPMOs produce H_2O_2 in aerobic conditions, H_2O_2 production has not been found in the same LPMO reactions containing substrates. The scientific community still debates why H_2O_2 is not found in these reactions. Some suggest that the H_2O_2 production by LPMOs is inhibited in reactions containing substrate, because of the binding of the enzyme to the substrate [39]. Others suggest that LPMO indeed produce H_2O_2 in these reactions, but is readily consumed by substrate-bound LPMOs [19, 30]. Since LPMOs generally show low binding proportions on substrates (described below), it seems apparent that the unbound and reduce LPMO in solution would produce H_2O_2 .

Due to the H_2O_2 -forming ability of LPMOs, a destructive component is induced regarding the LPMO health. Several studies have shown that LPMOs self-inactivate by oxidation [19], and that inactivation rates can be correlated to substrate binding efficiency [41, 42]. LPMOs can be denatured by externally supplied H_2O_2 , as well as by autooxidation during H_2O_2 production. Inactivation rates can be improved by increasing the binding efficiency of LPMOs [19], e.g. by polypeptide sequence mutations in the binding surface, or by attaching a linker and CBM module to the LPMO domain [45]. LPMOs autooxidation and inactivation is an important factor to consider when storing the enzyme stocks, as they may denature over time if the stock solution contains reducing agents. This may further

lead to false conclusions of e.g. true catalytic rates during characterization of new LPMOs [19].

1.3.3.4 LPMO binding

Because common substrate types for LPMOs often are recalcitrant and insoluble carbohydrate polymers, the study of LPMO-substrate interaction complexes have been challenging [11]. Protein structures are most commonly derived from X-ray crystallographic techniques, and thus require crystallization of the protein and/or protein-substrate complexes. Inter-chain polymeric substrates are often big and variable in size, which make them unsuitable for protein crystallizing techniques. Therefore, little is known about the molecular interactions between LPMOs and crystalline substrates.

Early mutation studies by Vaaje-Kolstad et al. (2005), did however, show that a single surface exposed residue (Tyr54) was important in binding to β -chitin for *SmAA10A* [23], and suggested that hydrophobic interactions are an important binding factor for LPMOs on crystalline substrates. LPMO binding on crystalline substrates have later been found to depend on a variety of physiochemical properties, including polar and hydrophilic interactions from both the rigid flat binding surface of LPMOs, as well as with flexible peptide looping regions in near proximity to the substrate binding side [43, 44].

Several binding interactions were shown by Frandsen et al. (2016) with a successful crystal structure of *LsLPMO9A* bound to cellotriose and cellohexaose. The findings show various hydrogen bonds, both direct protein-ligand interactions, as well as water-bridged interactions. The protein-substrate complex-structure also show a surface exposed tyrosine (Tyr203) in a similar position to *SmAA10A* (CBP21) (Tyr54). The complex-structure also revealed a glycosyl-linkage over the copper atom with an empty putative O₂ binding site [43].

Arora et al. (2018), demonstrated the importance of flexible looping regions on LPMOs for substrate binding, using “Elastic network Models” to investigate LPMO structural dynamics. They found that the flexible looping regions surrounding the catalytic site had structural dynamics needed for binding to a flat crystalline substrate. They also suggested that LPMOs were not as rigid as previously suggested by several experimental affirmations. They assumed that the natural oscillations in LPMO dynamics were not previously

observed, due to the time-scaling used in determining protein dynamics by NMR relaxation studies [44].

LPMOs show a large diversity in their binding efficiency toward various substrates, and can typically display a binding proportion between approximately 19-80 % bound protein [37, 38]. Another example, from binding analyses by Mutahir et al., (2018), it was demonstrated various binding efficiencies in wild-type and truncated versions of *BcLPMO10A*. The wild-type or full length LPMO (*BcLPMO10A-FL*) in the study, includes an attached CBM5 module, and showed a binding efficiency of seemingly 100 % on α -chitin, and ~ 95 % on β -chitin, after two hours incubation, with the LPMO in a non-reduced state. When detaching the CBM5 module however, the truncated version, only comprising the LPMO-domain, showed binding of ~ 25 % and ~ 50 % on α - and β -chitin respectively at a similar timepoint [45].

Mutahir et al. also found that during catalytic reactions on α -chitin, the truncated version (*BcLPMO10A*) showed a rapid inactivation, while activity of the full-length enzyme (*BcLPMO10A-CBM5*) remained stable. In reactions on β -chitin however, both versions relatively stable substrate catalysis. The inactivation may therefore be correlated with the binding efficiency of the LPMO to the substrate. The study by Mutahir et al. also found that both *BcLPMO10A-CBM5* and *BcLPMO10A* had similar initial catalytic rates, and suggest that the CBM module do not aid in catalytic speed, but rather prevent the LPMO from autoxidative damage. This prevention may be performed as the LPMO if more frequently bound to the substrate when harboring a CBM domain, and thus, is shielding the active site of the LPMO from the free solution [43, 45].

LPMO binding is an important factor to assess in LPMO characterization, and provides insight in both catalytic mechanisms and structurally important amino acids in accordance to the molecular morphology of the carbohydrate substrates and of the protein. Binding efficiency on insoluble crystalline substrates poses some issues in classic chemical analyses, because of its non-homogenous nature. Binding efficiency on crystalline substrates is therefore often performed by omitting the crystalline fraction using filtration techniques. The free protein in the supernatant thus reflect to some extent the amount of bound protein on the substrate. After filter separation, the protein in solution can be quantified in several ways, depending on the purity of the supernatant containing the protein, and/or other chemical interferences, e.g., contamination by filter membranes.

Some common methods in quantifying protein however, are with spectrophotometric methods using dye reagents, or ultraviolet absorbance, and sometimes with SDS-PAGE fluorescent emission relative intensity, further elaborated below.

1.3.4 Synergy in biomass degradation

Several enzyme studies on carbohydrate degradation have shown synergistic action between classical GHs and recently characterized LPMOs. Most of these experiments have been performed on lignocellulosic and chitinous biomass. In research, synergetic degradation experiments on lignocellulose and cellulose, are often performed with combination of cellulases and LPMO9s, while on chitinous substrates, LPMO10s and chitinases are frequently used [45, 54, 55, 56, 57, 58].

The mechanisms of the synergetic interplay are often observed to operate in apparent favor of the GHs, rather than for LPMOs, where LPMO activity on the substrate causes increase in GH activity. The most common synergetic value of these interactions is not necessarily in increased catalytic speed, but rather in final substrate conversion and catalytic stability, i.e., reacting for longer periods without catalytic inactivation. Sometimes, the total crystalline substrate is converted to soluble products in these synergy reactions. By observations that both GH and LPMO are unable to fully convert crystalline substrates independently, it is theorized that GH activity also benefit LPMO activity, and that these enzymes alternately prepare the substrate surface in favor of each-others activity. It is speculated that this synergetic favor is done, where GHs remove amorphous regions on the substrate, and expose a crystalline surface for LPMO activity, while LPMO disrupts this crystallinity by the oxidative action, and produces amorphous regions for GHs [45, 54, 55, 56, 57, 58].

Mutahir et al., [45] showed synergy experiments using *BcLPMO10A* and a chitinase cocktail encompassing *SmChi18A*, B and C. They also included a similar reactions using *SmLPMO10A* (CBP21) with the same chitinase cocktail, and found similar final substrate conversion in both experiments. In both cases, % final conversion yielded approximately 30 %, in total substrate conversion, compared to the sum of individually produced products by the GH cocktail and the LPMO [45]. In characterizing *AfuLPMO11B* described in this thesis, catalytic rates were compared between the AA11 and *BcLPMO10A*, and in synergy experiments with the AA11, *SmChi18C* was used. These are the same enzymes used by Mutahir et al. [45], and their

published paper, therefore, is a good comparative study in further discussing results obtained from characterizing *AfuLPMO11B*, and further leads to greater insight in chitin degradation between AA11s and GHs.

1.4 Glycosylation

1.4.1 Protein glycosylation

Many enzymes experience post-translational modifications by glycosylations from their host organism, which serves in a multitude of biologically relevant processes [46]. These glycosylations are divided in two general groups, i.e., N-linked glycosylations (N-glycans), and O-linked glycosylations (O-glycans) [11, 79]. The N-glycans are bound to asparagines (Asn) by a covalent N-glycosidic bond, where *N*-acetylglucosamine bound to Asn is the most common (GlcNAc β 1-Asn). The N-glycosylation site within a protein peptide is recognized by a three-amino acid (aa) sequence, starting with asparagine (Asn), followed by any amino acid except for proline, then ending with threonine (Thr) or serine (Ser). The three-aa sequences are called sequons (Asn-X-Thr/Ser), where the latter two residues aid in support of the bound glycan [47]. N-glycans are separated in three groups (Figure 6), where all groups have a common disaccharide, bound to the protein glycosylation site, composed of two linked *N*-acetylglucosamine sugars (GlcNAc), that are further connected to a branched three-mannose complex. The three N-glycan groups deviate in types and branching of further linked sugars that extend from the mannose complex, where the first group, called 'high mannose', is composed of branched and linear polymers of mannose explicitly. The second group, called 'complex', is composed of two linear polymer extending from the branched three-mannose complex, and contains several different sugars, additionally with a fucose linked to the protein-bound GlcNAc. The third group, called 'hybrid', is a hybrid version of the two former groups, with both linear and branched polymer arrangements, containing different sugar types.

O-linked glycosylations are covalently bound to either serine (Ser) or threonine (Thr) residues, and are also often found to be glycosylated by *N*-acetylglucosamine, e.g. in the case of mucins, but rather by an α -linked mannose in fungal expressed LPMOs [11]. O-glycans do

N-glycan types

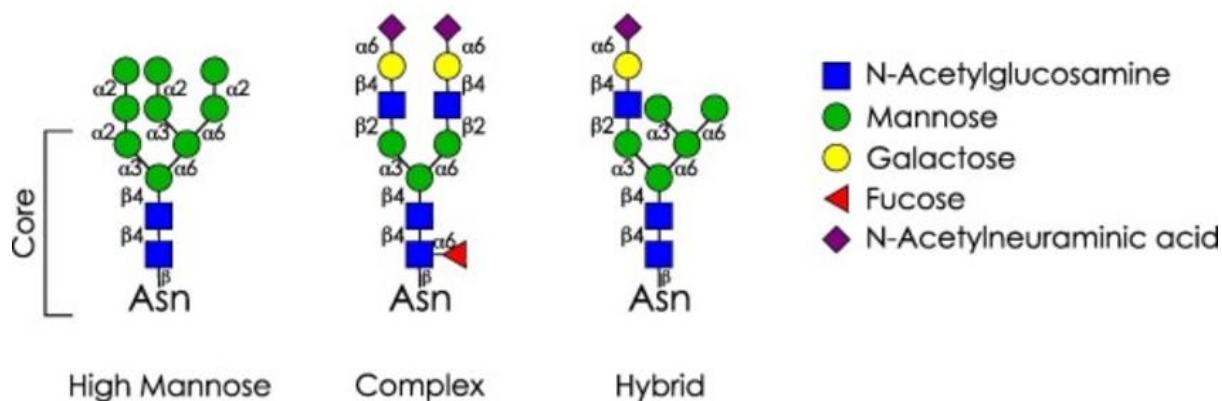


Fig 6. Types of N-glycans. The three groups (High Mannose, Complex and Hybrid) of N-glycans share a common core structure, including the two first N-acetylglucosamine and three first mannose residues. In higher regions, the groups vary both in sugar complexity and branching profiles. Figure source: Higel et al., (2016) [79].

not require sequons, and therefore yield more possible O-glycan sites, as opposed to N-linked sites [48]. N- and O-glycan sites are often predicted in protein research, based on the protein peptide sequence, using artificial neural network-based services, such as *NetNGlyc* [49] and *NetOGlyc* [50].

Glycosylations on carbohydrate active enzymes may induce structural support, and/or protect the enzyme from denaturing [11]. These suggested mechanisms are complemented e.g., by the findings that deglycosylation of a glucoamylase from *Aspergillus niger* led to a reduction in thermostability [51]. Little is known however, of how protein glycosylation affect LPMOs. Glycosylations become more relevant in enzyme studies using fungal protein expression systems, since fungal protein secretion often lead to glycosylated proteins, but not in proteins using bacterial protein expression systems (explained below) [11].

1.4.2 Deglycosylation of proteins

Glycosylations on proteins also lead to a non-biologically relevant issue, regarding protein crystallization, a technique used for protein structure elucidation by X-ray analyses (mentioned below). Protein glycans often are composed of large assemblies of branched sugars, with a flexible or less ordered molecular morphology. This, less ordered character of

the sugars, make protein crystallization difficult. Proteins that have glycosylations are therefore, often deglycosylated, e.g. by using commercial endoglycosidases, such as Endo-H [52]. However, Bøhle et al., (2011) described that deglycosylation can also be performed by an endo- β -*N*-acetylglucosaminidase from *Enterococcus faecalis*, called 'Endoglycosidase-18A' (*Ef*Endo18A), which hydrolyzes the glycosidic bond between the two first NAG (GlcNAc) units in N-glycans from the *High Mannose* and *Hybrid* group (Fig 6). This cleavage subsequently leaves one attached GlcNAc to the protein [53].

This thesis demonstrate one of few studies of N-linked glycans on LPMOs, testing for impacts in thermal stability, substrate specificity, binding efficiency, and crystallization optimization.

1.5 Protein structure elucidation

Most solved protein structures can be found in the Protein Data Bank (PDB) database (<https://www.rcsb.org/>) [60], where most entries are solved by X-ray crystallographic diffraction methods, and some, solved by the use of Solution NMR (nuclear magnetic resonance) methods. The NMR method provides structures typically with lower resolution, as the proteins are in solution, thereby being able to express structural dynamics. NMR studies are therefore better when analyzing flexibility and mechanical oscillations within proteins [44], as opposed to X-ray diffraction, where the proteins are fixed in protein crystals. On the other hand, structural analyses with X-ray diffraction methods generally produce protein structures with better resolution, ranging between $\sim 1.4 - 4.5$ angstrom (\AA) [60].

Increasing development in artificial neural networks, computing power, advancements in molecular dynamical and quantum mechanical modulations, as well as growing protein structural libraries, make it possible to predict reliable protein structure with the peptide sequence alone. These predictions can be generated with various online servers, some of which are SWISS-MODEL Homology Modelling [61], Phyre² – Protein Homology/analogy Recognition Engine V 2.0 [62], and I-TASSER Protein Structure & Function Predictions [63]. The servers commonly use multiple sequence alignment data, correlated with structural similarity of closely related proteins, and physiochemical properties for amino acid residues, with

calculated orientation of both the peptide main chain and amino acid functional groups functional groups, aiming for a low energy configuration [61].

1.6 Carbohydrate product analysis

carbohydrate products derived from enzymatic reactions can be analyzed by various methods, depending on the purity and type of the product sample, and the interest of the study. In many instances, oligosaccharides operate as reducing agents. With this property, chemical analyses such as titration, gravimetric, or colorimetric techniques can be performed, where, e.g., a reactant produces measurable optical properties when interacting with the sugars [64]. A more popular technique in studying carbohydrates however, are by using chromatographic separation in reference to commercial standards. High-performance liquid chromatography (HPLC) and ultra-performance liquid chromatography (UPLC) are modern LC methods that provide accurate results both in qualitative and quantitative studies from low-volume samples (see section 1.7.1). These methods are often performed in concert with mass spectrometric analyses (MS) (see section 1.7.2), providing concrete evidence, and in-depth analysis, of the investigated product(s) [66].

1.6.1 Liquid chromatography

Liquid chromatography (LC) is used to separate different compounds in a mixed solution, where the eluted and separated compounds can be measured, identified, and quantified. Technological development in recent years, have led to high precision LC instruments (HPLC), and furthermore UPLC/UHPLC (ultra high performance). Both HPLC and UPLC push liquid samples, also called “the mobile phase” through cylindrical tube columns with high pressure, separating different compounds in the sample solution. The columns are packed with specific materials, aimed to maximize the separation of respected compounds, i.e., charged-, aromatic-, polar-, and other chemical properties that may distinguish various molecules. The column, or column material, is called ‘the stationary phase’. HPLC operates with particles typically of less than 5 micrometer (μm) at a pressure of 500 – 6,000 psi, while particles less than 2 μm at 15,000 - 22,000 psi in UPLC analyses. The latter analysis provide significant

improvement in separation [65, 66, 68]. Compounds in the mobile phase (analyte) may separate because of different interactions with column material. The separated compounds are hence, eluted at different timepoints (elution time) from the column. The elution time of eluted compounds can be correlated to commercial standards, and thereby be identified. Elution of the compounds can be performed isocratically or by a gradient flow, where the latter involves a change in the mobile phase solvents. Isocratic elution refers to the mobile phase remaining constant throughout the analysis. Separated compounds from the analyte can be measured, using several techniques suited for the physiochemical nature of the analyte compounds, such as electrochemical and optical detection, and fluorescent emission [66].

UV-Vis detection (ultraviolet visible detection), is a photo-spectrometric method, and measures wavelengths (λ) in the range of maximum absorption (λ_{\max}) of a compound. Fluorescent detection provide greater detection than that of UV-Vis. Fluorescent detection measures the specific emission waves intensity from molecular transition states, i.e., excited and ground states of a molecule, induced by photoexcitation. A more cost-effective chromatographic product detection method is refractive index (RI) detection. This method measures variations in light-speed mitigation in the eluted mobile phase. The RI method is considered a universal detection method as it can detect any compound, but with the least sensitivity of the three described detection methods. Electrochemical detection serves as the best detection method to date, and are optimal for sensitive analyses, and well suited for oxidized product analyses [66, 67].

A wide range of columns are also available optimized for separating specific compounds. The HPLC/UPLC method that are used is often named according to the intended properties of the selected column, such as hydrophobic- or hydrophilic chromatography (see section 1.8.2 below). Some common chromatographic methods for analyzing sugars however, include Ion exclusion- (IEC) and hydrophilic interaction- (HILIC) chromatography [69].

1.6.2 Mass spectrometry

Mass spectrometry (MS) is a fundamental analytical tool used to precisely measure the masses of chemical compounds, such as carbohydrates and proteins. MS is crucial in producing direct evidence of specific compounds in many fields of research, i.e., inorganic and organic chemistry, protein chemistry, proteomics, metabolomics, microbial identification, diagnosis

and more. Measurements from MS provides a mass to charge ratio (m/z) with a peak intensity of signal to noise, and provide the means to estimate the mass and/or quantity of particles, with high precision [70, 74].

The general function of mass spectrometry is that, a gas -or solute (in solvent) -or fixed (solid) -sample become ionized, accelerated, separated and then detected. The technique of separation and detection provides information on the specific masses of the particles. Every compound have a specific mass, which become the determining factor in how they are separated. Several technologies have been developed in separating charged particles, and are optimized on the basis of efficiency, cost, analytical resolution, and analyte particle sizes. The MS apparatus generally contains three main modules. The area of analyte ionization is called the *ion source* and serves as the first module. Ions can be produced by various electrical, chemical, photonic, and plasmonic methods, with hard and soft ionization energies. In most biological studies, a soft non-fragmenting ionization method is preferred. One of which is called electrospray ionization (ESI). This method is ideal for liquid samples (most biological samples), and is often directly coupled with liquid chromatography, such as HPLC and UPLC, and is considered the single most popular ionization source [75, 76, 77].

The second module of MS is the *mass analyzer*. Here the particles are separated by their distinct masses and ionization charges, through strong magnetic and electrostatic fields. Another MS system that also utilizes a soft ionization technique, is the matrix assisted laser desorption ionization – time of flight (MALDI-TOF) MS, and operates well with polar compounds, particularly sugars containing nitrogen atoms, such as chitooligomers. Here, MALDI refers to the ion source, while TOF refers to the mass analyzer. The MALDI technique ionizes a solid analyte sample, composed of the analyte and a matrix solution, dehydrated to a crystalline solid. Because this is not a fluid sample, this method is not directly connected to a chromatography system. In the ion source of MALDI, pulsed laser energy is absorbed by the matrix molecules, and typically transfer a cation to the analyte compounds. The ions are then accelerated, by an electric potential within and/or outside the ion source, into the mass analyzer. The TOF mass analyzer is a hollow vacuum tube, and particles are separated simply by the time of flying though the tube. Heavy particles accelerate slower than small particles, and therefore hit the detector last. The detector is the last of the three fundamental MS modules, and operates as an amplifier on the initial energy from the kinetic and ionic force

from the analyte particle. Most common is electron multipliers, which increase signal intensity by a secondary electron emission process [70, 71, 72, 73, 74, 75].

1.7 Protein production

1.7.1 Heterologous protein expression

Protein production by heterologous protein expression can be performed by recombinant DNA technologies, which is used to insert an expression vector, containing the protein coding gene, into a chosen host organism (expression system). The expression systems are often bacterial or fungal organisms, and are cultivated in solution, from which the protein of interest can be harvested. Prior to inserting the gene into the host organism, the gene is often optimized according to nucleotide preferences, and/or guanine-cytosine (GC) -content known for host organism [80, 82].

Growth conditions are optimized in cultivation, e.g., with increased oxygen supply by aeration in aerobic cultivations. Other solvents may be added during cultivation to promote protein production or excretion, such as glycerol addition in later timepoints of cultivation, which is recommended when using e.g. the PichiaPink™ Expression System from Thermo Fisher Scientific [81].

After a period of incubation with the host organism, the protein of interest may be harvested from the culture solution, and further purified, and can be done by various methods depending on the expression mechanism. In fungal expression systems, protein is secreted from the cell into the surrounding solution, while in bacterial systems, the proteins are stored inside the cell, and/or located in the periplasmic region of Gram-negative bacteria. Purification techniques are often performed in sequential manners, in order to obtain the desired protein purity required for the research. Several such methods are described below (1.8.2 Protein purification).

1.7.1.1 Common expression systems

Several types of commercial and non-commercial protein expression systems exist, including bacterial, yeast, mammalian cell, and plant cell host organisms. While bacterial

and fungal host organisms are the most common, bacterial protein expression using the Gram-negative bacterium *E. coli* is the most frequently applied method. This, for various reasons, i.e., *E. coli* is the most studied bacteria, and provides optimal and liable methods with low risks, as well as the growth rate of *E. coli* is very high, compared to that of other possible host strains [83, 84, 85]. Bacterial expression systems with Gram-negative bacteria, typically utilize the double-membrane structure of these organisms, as a means of a primary purification step. Proteins can be secreted through the first cell membrane but may be retained by the second membrane. In this way, the heterologous protein accumulates between these membranes, known as the periplasmic space. The proteins can be released by membrane disruption, also called cell lysis, by osmotic shock procedures, i.e., variations in salt levels. This method aims to disrupt only the outer membrane, thereby retaining most native enzymes within the inner intact cell membrane. If successful, the cells can easily be separated by centrifugation, and the protein of interest should remain in the supernatant, thus simplifying further purification steps [86].

Another alternative for expressing proteins, is by using a fungal organism, such as the PichiaPink™ Expression System [81]. This method was used in expression of *AfuLPMO11B* within the present study. The *Pichia* expression system secretes proteins directly to the extracellular environment and requires no further cell treatment to obtain the heterologous protein. However, many other proteins are also secreted from the fungal cells, and the culture solution is typically of large volumes with low protein concentration compared to the periplasmic technique, mentioned above. Protein purification from culture solution when using fungal expression systems typically require more purifying steps than when using the bacterial system. the fungal system usually includes an up-concentration procedures before further purification are performed by chromatography. Proteins allocated for the periplasmic- or extracellular-space, contain a small N-terminal signal peptide of 18-30 amino acids, which is cleaved off during translocation. The cleavage is performed by signal-peptide peptidases, associated with the inner cell-membrane [87].

Cultivating expression systems is often based on pre-set standard conditions and growth solutions, specific for the host organism, particularly for commercial expression systems. It is however important to evaluate chemical properties of the heterologous protein, e.g. by analyzing the peptide sequence (FASTA), using servers such as ProtParam (ExPASy, Swiss Institute of Bioinformatics [89]), which can provide peptide sequence

information, such as the estimated pI of the protein. It is important that the pH in the growth solution or in enzyme storage buffers are not equal to the protein pI, as this will neutralize charged side-groups in the peptide chain that are important in structural support. Growth and storage buffers should generally have a $\text{pH} \pm 2$ from the pI.

1.7.2 Protein purification

Proteins provide distinct chemical or physical characteristics which can serve as the guideline of the purification method of choice. Purification may consist of a few steps, or multiple extensive steps, depending on the starting material. The first step after cultivation, is typically lysing of the cell membrane of Gram-negative bacteria and separating the proteins from the cells by centrifugation. In the case of protein secretion hosts, cells are directly separated by centrifugation after cultivation. It is essential to track the enzyme and observe improvements in purity between each purification step, to the final enzyme stock. This is commonly done by SDS-PAGE. In some instances, multiple proteins with the same mass can occur in solution and are not always easily detected with SDS-PAGE. This can be avoided, planning in advance, by known interference proteins from the host organism, and selectively choosing an expression system that does not excrete proteins of the heterologous protein size.

Following cell separation, further protein purification is predominantly performed using various forms of liquid chromatography (LC). A vast selection of LC-columns are available, separating proteins by various physiochemical properties, such as net charge, hydrophobicity, and size. Some methods are also based on adding amino acid tags that convey binding affinity towards specific target compounds within the column material. A variation of this method is also developed, where a self-excising peptide module is fused with the protein. The self-excising module has binding affinity towards the column material, and by changing e.g. pH or salt levels, the proteins are released, as the module interacts with itself, and cleaves itself off from the protein. The resulting protein is therefore released without an affinity tag [90]. Some of these LC techniques are briefly explained in the sub-sections below, including SDS-PAGE.

1.7.2.1 Ion-exchange chromatography (IEC)

IEC separates proteins by their intrinsic charge, thus, its electrostatic interaction with the column material. IEC is further subdivided into anion- and cation-exchange

chromatography. Anion exchange columns consist of materials with a positive charge, which can interact with anionic compounds from the mobile phase. Cation exchange columns are, in contrast, made from negatively charge compounds, and form ionic bonds with positively charge molecules from the mobile phase. The ionic interaction with protein occurs in certain pH- or salt-level, or with the ionic strength of the buffer solution.

Proteins can be separated isocratically with IEC if the ionic bond formations are not very strong, allowing for binding and un-binding across the stationary phase. Proteins can also be fixed to the column material at higher ionic bond strength, and thereby be separated by gradient elution, i.e., by a salt gradient. The gradient causes different proteins to elute from the column at different timepoints, depending on their intrinsic charge. The eluate is often fractioned in different tubes, where the different protein types may be sorted. IEC can be carried out at physiological conditions and serves a robust purpose in maintaining the native structure and function of proteins during purification [91, 92].

1.7.2.2 Hydrophobic interaction chromatography (HIC)

HIC operates very similarly to IEC, but rather the inverse in terms of chemical properties, from which hydrophobic residues bind to the stationary phase. Similar to IEC, HIC may also fix proteins in the stationary phase, and gradually eluate proteins with a gradient flow, where the least hydrophobic protein eluates first and most hydrophobic last. High salt levels are usually added to the buffer solution and the running buffer in order to increase the hydrophobic interaction with proteins and the column material. The gradient is thus, a gradual reduction in salt levels. [92, 93].

1.7.2.3 Size exclusion chromatography (SEC)

SEC can be used to separates proteins by size. The SEC column is typically larger than IEC and HIC columns, and is composed of a network of highly crosslinked polymer segments, further connected by flexible polymers (resin). The resin can be composed of e.g. cross-linked agarose and flexible dextran polymers (Superdex, GE Healthcare Life Sciences). The arrangement of this polymer profile provide pores through the resin of various sizes. When the liquid sample pass through the stationary phase, small particles have several

alternative routes passing through this polymer matrix. Large particles have only a few possible routes, and will therefore travel through the column faster than smaller particles. The advantage of SEC is that, particles do not bind to the chromatography resin. Therefore, the buffer composition does not matter in particular, and makes it possible to run SEC directly after other forms of chromatography, such as IEC and HIC, mentioned above. Separated proteins can be collected in fractions, and may operate as the last step in protein purification [94].

1.7.2.4 Sodium dodecyl sulfate – polyacrylamide gel electrophoresis (SDS-PAGE)

Throughout chromatographic steps in protein purification, it is important to track the protein, and make sure that the protein of interest is not lost, and to identify the sampled fractions that contain the protein. This control can be performed using SDS-PAGE. In addition to tracking the protein, SDS-PAGE can also be used quantitatively by relative absorbance (described below), and to visualize the purity of purified protein batches, predominantly though, from other proteins or polypeptide contaminants that are visualized with this technique.

The principle of SDS-PAGE is separating proteins of different sizes in a gel by an applied electric field, and visualize the proteins using staining or fluorescent stain-free techniques. A standard of different peptide lengths are often included in the gel, and is used as a reference to estimate the approximate mass of proteins within a sample. Structure and charge of the analyzed protein(s) is largely eliminated using SDS-PAGE, and the method therefore separates proteins solely by the polypeptide length.

SDS is a strong detergent that break disulfide bridges within a protein, and convert its structure to an open polypeptide chain. SDS bind to the peptide proportional to the peptide length, with a constant ratio of approximately one SDS molecule per two amino acids, as well as covering the peptides intrinsic charge. SDS have a negative charge, and the charge to mass ratio remains equal for all peptide lengths. When an electric field is applied on the gel, the negatively charged peptide migrates towards the positive anode. The migrating peptide fragments are therefore separated by variation in steric hindrance through the polyacrylamide matrix in the gel. Of note, modification on proteins such as glycosylations may alter the apparent mass from on SDS-PAGE analyses from the

theoretical mass for the protein, and does not necessarily correlate to the glycan mass, because of differences in SDS interaction with peptides and carbohydrates [99, 100].

1.7.3 Protein concentration

Final concentration of a protein working stock is highly important in elucidation of enzymatic characteristics, such as determining absolute values in enzyme activity. Protein concentration can be estimated by various methods, where the following three methods are the most common, i.e., Bradford reagent assay, SDS-PAGE relative absorbance, and ultraviolet absorption (UV).

1.7.3.1 Bradford reagent assay

The Bradford reagent assay estimates protein content in a solution by measuring absorption of a coloring complex, where a dye shifts its maximum absorption when bound to protein. The color complex is formed when a dye called 'Coomassie Brilliant Blue' interact with hydrophobic regions of a protein, and further produce ionic bonds with amino- and carboxyl-groups in the protein peptide. The dye shifts its maximum absorption from 465 nanometer (nm) to 595 nm upon binding to the protein. Absorbance of 595 nm (A_{595}) can be measured with spectrophotometry, and in relation to a known protein standard curve, protein concentration can be estimated in the sample. The Bradford method is not a very accurate method, because proteins from the standard curve often differ from sample proteins in both size and chemistry, and lead to either under- or over-estimated concentrations. Concentration estimates based on absorbance of a complex that is formed with protein, make this method more suitable for samples that are not pure, i.e., samples containing other compounds like pigments, lipids and sugars [101].

1.7.3.2 SDS-PAGE based quantification

The SDS-PAGE method described above can be used in quantification. In stain free techniques, such as using the Mini PROTEAN® TGX Stain-Free™ gels, the gel containing the protein is excited by UV light. During excitation, trihalo compounds in the gel interact with aromatic residues such as tryptophan and tyrosine and form key intermediates. These intermediates are then irradiated by a secondary excitation that result in fluorescent emission, which further is measured. These measurements can be performed by stain-free

enabled imagers, and is sensitive down to 20 – 50 nanogram (ng), and can be used in quantification of protein content, based on the relative fluorescent emission intensity. To obtain protein concentration in a sample, a known standard must be applied in the gel alongside the sample [102].

1.7.3.3 UV-absorption

The UV-method is a more accurate method than Bradford and SDS-PAGE in quantifying protein content, but rely on the protein sample to be very pure. The UV-method is based on absorbance at 280 nm (A_{280}) with spectrophotometric analyses, and focuses on aromatic residues in the protein, such as tryptophan, tyrosine, and phenylalanine which have an λ_{max} around 280 nm. The absorbance in the pure protein solution therefore correspond well to the protein content, but may be very inaccurate if there is contaminants in the sample, such as pigments, lipids, etc. In order to estimate protein concentration accurately, the absorbance value should be divided on a molar extinction coefficient (ϵ) derived from analyses on the protein sequence. ϵ can be found according to Beer-Lambert Equation; $A = \epsilon \ell c$, where A = absorbance, ℓ = length of light path through the sample solution in cm, and c = the molar concentration of protein (M). According to the equation, the concentration of the sample must be known to find ϵ . If c and ϵ are unknown, ϵ can be generated for a polypeptide with servers such as ProtParam (ExpASy - ProtParam tool) [89]. The unit of ϵ from ProtParam is in $\text{M}^{-1}\cdot\text{cm}^{-2}$, and the protein concentration can therefore be estimated with the absorption (A) in the following equation; $c = A \cdot \epsilon^{-1} \cdot \ell^{-1}$. To obtain accurate estimates, Absorbance from UV-spectrophotometry should be between 0.1 – 1.0. (depends on the apparatus). Concentration estimates on absorbance values below 0.1, tend to have a reduced accuracy, and with absorbance values above 1.0, tend to be underestimated by due to proteins being in the 'shadow' of others, and therefore have lower absorbance.

1.8 The goal of this study

Due to interesting studies on LPMOs in degrading recalcitrant carbohydrate biomass, alongside accumulating industrial interests, LPMOs have lately become an increasingly popular field of research. LPMOs have shown promise in increasing degradation efficiency on recalcitrant polysaccharides and cut operational costs in biorefineries focused on breaking down and utilize biomass waste materials, as well as gaining attraction in other industries. The LPMO enzyme library continues to grow, readily with new characterized LPMO candidates with putative industrial applications.

So far, the majority of LPMO research have been executed on AA9s and AA10s, and relatively little is known of the remaining AA families; 11, 13, 14, 15, and 16. The general goal of this study was to elucidate functional and structural characteristics of a novel AA11, originating from *Aspergillus fumigatus*, named 'AfuLPMO11B'. This study provides additional insight in enzyme functions of family AA11 and expanded knowledge about LPMOs in general. Characterizing this enzyme also provides a new LPMO candidate for further developments in enzyme technology systems for biomass waste decomposition.

AfuLPMO11B was produced and purified, and was further used in experiments aiming to find the relevant substrate for the AA11, analyze reaction products, find optimal temperatures for activity, and illustrate catalytic rates. Further, demonstrate activity together with a GH, as well as demonstrate activity using H₂O₂ as the catalytic co-substrate. Additional experiments includes protein glycosylation studies, and how glycosylation affect enzymatic activity, substrate specificity and protein stability. The study also includes protein crystallization, and structural visualization of *AfuLPMO11B* from modelled- and experimentally determined protein structures.

2. Methods and materials

2.1 Solutions

2.1.1 Water

All sterile experiments were performed with Milli-Q water (MQ-water) (Ultrapure water system, Milli-Q® Advantage A10), autoclaved at 15 psi and 120 °C for 20 min. All non-sterile experiments were performed, each with fresh MQ-water tapped directly into a new 50 ml falcon tube (50 ml CELLSTAR® Polypropylene Tube).

2.1.2 Buffers

Buffers used in sterile work, such as cultivation, were sterilized through autoclavation or filtration as described below. Buffers used in non-sterile enzyme experiments were prepared in stock of 0.5 – 1 liter (L), and was portionated into a new 50 ml falcon tube (50 ml CELLSTAR® Polypropylene Tube) through syringe filtration with a 0.2 µm polyethersulfone (PES) membrane (Filtropur S 0.2, Sarstedt AG & CO, KG) prior to every individual experiment. Commercial buffers, such as the buffer in the Protein Thermal Shift study or SDS-PAGE described below, was either used directly or diluted and used without any pretreatment. Dilution was performed with MQ-water according to section 2.1.1.

Bis-tris buffer with 50 mM concentration and pH 6.5 was primarily used in enzyme experiments, with a few exceptions described below. In the making of e.g. 1.0 L Bis-tris buffer, 10.46 g crystalline Bis-tris powder was weighed, with a three-digit precision scale, and transferred to a 1.0 L beaker, where 10.46 g correspond to $(50 \text{ mM} / 1000 \text{ mM}) \times 209.24$ (molecular weight of Bis-tris). MQ-water was added up to the 0.8 L mark, and buffer was adjusted with HCl to pH 6.5 while stirring with a magnet spinner, and measuring the pH with a 826 pH mobile (Metrohm) pH-meter continuously. When pH stabilized at 6.50, MQ-water was added to the final volume in a 1.0 L measuring cylinder, and stirred with a magnet spinner.

The mixed buffer solution was then vacuum filtered, into two separate 500 ml, newly rinsed blue-top glass bottles, using a 0.2 µm polyether sulfone membrane (VWR® Filter Upper Cup 250 ml bottle top filter) applied on a vacuum manifold. The bottles were closed with plastic screw caps, and stored at 4 °C.

2.1.3 Eluents

Eluents used in chromatography systems, explained below, were all filtered through a 0.2 µm polyether sulfone membrane (VWR® Filter Upper Cup 250 ml bottle top filter) applied on a vacuum manifold, prior to use. The eluent solutions were filtered into newly rinsed blue top glass bottles, rinsed with MQ-water to minimize dust contamination in the chromatography columns. These solutions were made in similar manners to the buffers in section 2.1.2. above.

2.1.4 Ascorbic acid reductant

Ascorbic acid solutions used in activity assays were produced by mixing ascorbate salt with commercial metal-free “trace select” water (Merck), and proportionated to 10 µl fractions of 250 mM in individual PCR tubes and frozen and stored at -20 °C. When applying ascorbic acid in LPMO activity experiments, the ascorbic acid was thawed on ice in avoidance of light, then quickly added to reaction mixtures to initiate activity by LPMO. Thawed ascorbic acid solutions were never re-frozen, but rather discarded. Therefore, fresh ascorbic acid was used for each individual experiment.

2.1.5 H₂O₂ co-substrate

A 250 µl high molar stock of 5.2 M H₂O₂ was produced by mixing commercial liquid H₂O₂ also with “trace select” water (Merck) in an 1.5 ml Eppendorf tube and encapsulated with aluminium foil (avoid light), then frozed down at -20 °C. Directly prior to any experiments, where H₂O₂ operates as catalytic co-substrate for LPMOs, the 5.2 M stock was thawed on ice in avoidance of light, and a small sample was taken out and diluted to the appropriate concentration for the experiment with MQ-water. The diluted H₂O₂ solution was kept on ice and encapsulated with aluminium foil until it was applied in reaction mixtures. Diluted H₂O₂ solutions was only used once, and the 5.2 M H₂O₂ stock solution was again frozen and reused similarly at later timepoints.

2.1.6 Enzyme stocks

After protein purification described below, diluted enzyme working stocks were produced by taking a small sample of the primary enzyme stock, and dilute it with fresh MQ-water in new 2 ml Screw Cap Micro Tubes (Sarstedt AG & CO, KG). This was done to minimize pollution risk to the primary enzyme stocks, and thereby increasing reproducibility of experiments. Enzyme stocks were always stored in Micro tubes (2ml, PP, Sarstedt) at 4 °C, and kept on ice during experiments, and otherwise kept cold as consistent as possible.

2.1.7 Substrates

Substrates (Table 4) that were only used in qualitative substrate activity screening described in section 2.3.2 below, were commercial premade and in-house prepared substrate solutions diluted in MQ-water and frozen at -20 °C. In progression curves from LPMO activity, chitin substrates were used, and was prepared differently. α - and β -chitin (Table 4) substrate solutions were prepared individually by mixing dry powder of ≤ 0.8 mm grain size β -chitin or ≤ 0.2 mm grain size α -chitin with fresh MQ-water in sterilized 50 ml blue-top glass bottles corresponding to a concentration of approximately 30 g/l.

Additionally, a small magnet stirrer was cleaned with 70 % ethanol, and rinsed with MQ-water, then added to the substrate solution bottles. Because the substrate is insoluble in water, and separates easily in solution from the water phase, the magnet stirrer was added to increase homogeneity of the substrate solution when taking substrate samples and adding it to reaction mixtures. This will better ensure similar substrate concentration between parallel experiments, thus increase the reproducibility. The substrate stock solutions were stored in 4 °C, and substituted every 2 months, or if any abnormal peaks were detected when controlling the substrates with chromatographic studies.

2.2 Protein production

Pichia pastoris (PichiaPink™ Yeast Expression System, Thermo Fisher Scientific) was used to produce protein through heterologous protein expression [81], starting by cultivating an in-house prepared and gene optimized *P. pastoris* strain (Invitrogen, CA, USA) containing the

AfuLPMO11B gene including the native signal peptide (UniProt ID: B0XZD3, Gene name: AFUB_044010). The strain was produced (Petrovic, Varnai and Eijsink, unpublished results) similar to what has been described elsewhere [119]. *P. pastoris* induces extracellular protein expression, such that the protein of interest can be extracted directly from the culture solution [81]. The following cultivation and purification steps (section 2.2.1 – 2.2.4) were performed more than three times, yielding individual *AfuLPMO11B* enzyme stocks (Table 7, Fig 4).

2.2.1 Cultivation of *Pichia pastoris*

Buffered glycerol complex medium (BMGY) was used as growth medium in cultiating the *P. pastoris* strain. Cultivation was initiated by inoculating a blob of *P. pastoris* cells, from a single strain - YPD agar stab, with a sterile toothpick into 50 ml BMGY growth medium in a 250 ml Erlenmeyer flask with ventilation caps. The culture flask were closed with sterile aluminium foil, and incubated over night at 29 °C with vertical rotation of 200 RPM on a sticky surface tray (Multitron Standard, Infors HT). On day 2, the 50 ml *P. pastoris* culture was transferred into 400 ml freshly mixed BMGY-minimal medium, in a 2000 ml Erlenmeyer flask with ventilation caps. The culture mixture was further incubated for 2 more days at 29 °C, 200 RPM. On day 3, 50 ml (10 % Glycerol) was added to the culture solution, then moved back to the incubator for further growth and protein expression over night. On day 4, Incubation was terminated, and proteins harvested. All work involving adding and mixing solutions during cultivation was performed in a sterile fume hood (Safe 2020 Class II, Thermo Fisher Scientific) with sterile equipment. This cultivation procedure was performed in quadruplets at a time to increase final enzyme amount.

BMGY growth medium recipe for V = 1020 ml;

(n.b. in BMGY-minimal medium, BMGY-base was substituted with MQ-water).

- A. 100 ml - KPi
- B. 100 ml - 10 x YNB
- C. 100 ml - 10 % Glycerol
- D. 700 ml - BMGY-base
- E. 20 ml - 50 x Biotin

Stock solutions for BMGY growth medium were prepared accordingly;

- A. KPi: 1 M (Potassium Phosphate Monobasic) pH = 6.0 buffer was prepared by dissolving 136.1 grams (g) of KPi to 80 % of a final volume of 1.0 liter (L) with MilliQ-water (MQ-water). pH was adjusted with Potassium Hydroxide (KOH), before adding MQ-water to final volume (V_f). The solution was placed in a 1.0 L blue cap glass bottle and autoclaved at 15 psi and 121 °C for 20 min, and stored at 4 °C.
- B. 10 x YNB: 13.4 % (Yeast Nitrogen Base, with Ammonium Sulfate, without amino acids) solution was prepared by dissolving 134 g YNB in MQ to a V_f of 1.0 L. The solution was filter sterilized with syringe filtration (Filtropur S 0.20 μ m) in a sterile fume hood (Safe 2020 Class II, Thermo Fisher Scientific) in a sterilized 1.0 L blue cap glass bottle, and stored at 4 °C.
- C. 10 % Glycerol: 10 % (Glycerol) solution was made, mixing 59.0 milli-L (ml) of 85 % Glycerol stock solution with 441.0 ml MQ-water to a homogenous mixture. The Solution was autoclaved at 15 psi and 121 °C for 20 min in a 500 ml blue cap glass bottle, and stored at 4 °C.
- D. BMGY-base: (Buffered Glycerol Complex Medium)-base solution was prepared by dissolving 20 g yeast extract and 40 g peptone in MQ-water to volume V_f = 1.4 L. The solution was autoclaved at 15 psi and 121 °C for 20 min in 2 separate 1.0 L blue cap glass bottles, and stored at 4 °C.
- E. 50 x Biotin: 0.002 % Biotin solution was prepared by dissolving 2.0 mg Biotin in 100 ml MQ-water. The solution was filter sterilized with syringe filtration (Filtropur S 0.20 μ m) into a 100 ml sterilized blue cap glass bottle, performed in a sterile fume hood (Safe 2020 Class II, Thermo Fisher Scientific) and stored at 4 °C.

2.2.2 Purification of protein

Since the PichiaPink™ expression system, express proteins extracellularly, there was no lysis of the cells, as the protein of interest was already in the growth medium. Hence the *Pichia* cells were separated from the solution after cultivation, whereas the supernatant was further

processed to the final enzyme stock. Purification of the protein occurred chronologically as described in the methods below.

2.2.2.1 Cell separation

The *Pichia* cells were separated from the culture solution by centrifugation with 10,000 RCF for 20 min at 4 °C using an Avanti J-26S Series (Beckman Coulter) centrifuge. The supernatant was quickly transferred to a beaker, to avoid cell re-suspension. The supernatant was vacuum-filtered with a VWR® Filter Upper Cup 250 ml bottle top filter with 0.45 µm polyether sulfone (PES) membrane, into blue-top glass bottles.

2.2.2.2 Confirming LPMO expression

Expression of *AfuLPMO11B* was confirmed (Appendix B, Fig B1) in the filtered supernatant (filtrate) with stain-free SDS-PAGE (Mini PROTEAN® TGX Stain-Free™ Gels – BioRad). Samples for SDS-PAGE was prepared by upconcentrating 5 ml of filtrate + 10 ml MQ-water to 1.5 ml, using Amicon® Ultra-15 centrifugal filter, regenerated cellulose membrane, 10,000 MWCO (Millipore), in centrifugation at 3600 RCF using an Hareus Multifuge (Thermo Fisher Scientific). Addition of 10 ml MQ-water and upconcentration to 1.5 ml was repeated twice. The final concentrate was prepared and analyzed with SDS-PAGE as described in section 2.4.1 below.

2.2.2.3 Vivaflow filtration

The filtrate solution (~ 4.0 liters) from cell separation in section 2.2.2.1 above was dialyzed against 50 mM Bis-tris (pH = 6.5) and concentrated to 100 ml with a VivaFlow 200 – tangential crossflow concentrator column (MWCO 10 kDa, Sartorius Stedim Biotech, Germany) with peristaltic pump flow (Masterflex Economy Drive Peristaltic Pump 115 V, Sartorius Stedim Biotech, Germany).

To adjust the solution to the Bis-tris buffer, the 4.0 L solution was first concentrated with the vivaflow system to 150 ml, then 450 ml Bis-tris buffer was added in two portions during concentration towards the final 100 ml. During concentration, the solution was always kept on ice, as well as the buffers that were added. The Bis-tris buffer pH was adjusted with HCl and/or NaOH.

2.2.2.4 Hydrophobic interaction chromatography (HIC)

Prior to HIC, the 100 ml concentrated protein solution in 50 mM Bis-tris buffer (pH 6.5) was adjusted to 2 M ammonium sulfate by slow addition of crystalline powder salt to the solution in a 100 ml blue-top glass bottle, while stirring with a magnet mixer, on ice. Some precipitates were formed after salt addition, and was separated out of the solution by centrifugation at 20,000 RCF for 10 min at 4 °C using an Avanti J-26S Series (Beckman Coulter) centrifuge. The precipitate was not protein, confirmed by SDS-PAGE (not shown).

HIC was performed on the 100 ml, 2 M ammonium sulfate adjusted protein sample with a HiTrap™ phenyl FF (HS) 5 ml hydrophobic column (GE Healthcare) installed on an ÄKTA Prime™ Plus chromatography system, with live monitoring using a Primeview 5.0 (UNICORN) Software. The column was calibrated to buffer A (50 mM Bis-tris buffer (pH 6.5) with 2 M ammonium sulfate), thereafter the protein sample was loaded on the column with 1.5 ml min⁻¹ flow through buffer A injection tube, fixing the protein to the column material. During protein sample addition, the sample was contained in a blue-top glass bottle sealed with parafilm, and kept on ice. After sample loading, buffer A injection was continued until UV absorbance at 280 nm (A_{280}) with live monitoring (Appendix G, Fig G1) re-stabilized after the first increase by the sample bypass flow. After A_{280} stabilized at base absorption (no absorption), a gradient was set towards buffer B (50 mM Bis-tris buffer, pH 6.5) where 100 % B is reached after 35 ml with 1.5 ml min⁻¹ flow. The protein was eluted from the column when buffer B became prominent. When A_{280} increased because of protein elution, 1.8 ml fractions were collected until A_{280} re-stabilized at base absorption.

Protein was identified in the fractions by SDS-PAGE (Appendix B – Fig B1), then pulled together and adjusted to 20 ml with 50 mM Bis-tris buffer (pH 6.5). The protein sample was further concentrated to 1.5 ml through centrifugation with a Vivaspin 20 Centrifugal Concentrator 10,000 MWCO PES (Sartorius Stedim Biotech, Germany), and 3600 RCF at 4 °C, using an Hareus Multifuge (Thermo Fisher Scientific) centrifuge.

2.2.2.5 Size exclusion chromatography (SEC)

SEC was performed on a HiLoad® 16/600 Superdex® 75 pg column (GE Healthcare) on an ÄKTApurifier chromatography system (GE Healthcare), with live monitoring (UPC 900) by

UV-absorbance at 280 nm, and operated with a Unicorn 5.20 Workstation software. The column was calibrated to 100 % buffer B (50 mM Bis-tris buffer (pH 6.5) + 150 mM sodium chloride). Thereafter, the 1.5 μ l protein sample was injected on the column with a polypropylene syring through an injection valve, and underwent isocratic separation with 0.75 ml min⁻¹ flow. 1 ml fractions were collected when UV-absorption started to increase. Fractions containing the pure protein was identified with SDS-PAGE (Appendix B, Fig B1), and pooled.

2.2.3 Copper saturation

LPMOs must be Cu-saturated to ensure all LPMO contains a copper atom in the histidine brace. Cu-saturation was done by adjusting the protein sample (pooled SEC fractions) to 10 x copper(II) sulfate (CuSO₄) to that of the protein concentration, and incubate it for 4 hours (h) at 4 °C. After incubation, excess copper was removed by repeated centrifugal filtration (Vivaspin 20 Centrifugal Concentrator 3,000 MWCO PES, Sartorius Stedim Biotech, Germany) with 3600 RCF at 4 °C using an Hareus Multifuge (Thermo Fisher Scientific) centrifuge. The sample was concentrated from 20 ml to 2 ml, then pure Bis-tris buffer (pH 6.5) was added up to 20 ml. This was repeated so that original CuSO₄ concentration was diluted 10,000 times. The final concentrated protein solution was filter sterilized through a 0.22- μ m-pore-size Millex-GV filter (Merck Millipore, Burlington, MA, USA) into a Micro Tube 2ml, PP (Sarstedt), and stored at 4 °C.

2.2.4 Protein concentration

UV-A₂₈₀ absorbance (A) was measured of the protein solution with a spectrophotometer (Eppendorf Biophotometer D 30, Eppendorf, Hamburg, Germany) with UV-cuvettes (UVette® Eppendorf disposable cuvettes, 50–2000 μ l, 220 – 1600 nm, Eppendorf, Hamburg, Germany), and protein concentration (c) was estimated with the extinction coefficient (ϵ) of the FASTA format for *Afu*LPMO11B (Table 7) calculated using ProtParam [89] through the formula $c = A \cdot \ell^{-1} \cdot \epsilon^{-1}$, where $\ell = 1$ (cm), corresponding to the UV-cuvette size. Concentration is given in M⁻¹·cm⁻¹.

2.3 Experimental setups

Most LPMO activity reactions were performed with the native glycosylated *Afu*LPMO11B. If not told otherwise, this is the LPMO that was used, and is simply referred to as *Afu*LPMO11B with no glycosylation status prefix. LPMO activity reactions were performed predominantly on α -chitin with ≤ 0.2 mm grain size, and β -chitin with ≤ 0.8 mm grain size, and will simply be referred to as α -chitin and β -chitin, without size prefix, unless otherwise is mentioned.

2.3.1 Deglycosylation

- Testing deglycosylation:

A small sample of *Afu*LPMO11B was first deglycosylated by the commercial Endo-H (Endoglucosidase H, NEB), following the commercial protocol [52]. With this protocol, deglycosylation is performed on a native functional, and a denatured non-functional version of the protein of interest. This is done to see, if the milder incubation conditions, where the protein should remain intact, are equally effective in the removal of the N-linked glycans. Several reactions were set up with lower Endo-H concentration and higher *Afu*LPMO11B concentrations than in the protocol, as well as shorter incubation periods with lower temperatures. This optimization was done, because the enzyme should be functional and preferably as clean as possible, for crystallization and activity assays, and Endo-H have similar mass and isoelectric point (pI) as *Afu*LPMO11B which make them difficult to separate after incubation.

- Comparing Endo-H and *Ef*Endo18A:

When reaction conditions were optimized, N-linked deglycosylation efficiency was compared between EndoH and *Ef*Endo18A [53] (Appendix G, Fig G4), in reactions with 0.45 μ M of either enzyme, reacting on 26 μ M *Afu*LPMO11B, respectively, in 50 mM sodium acetate buffer (pH 6.0) with a 60 μ l total reaction volume. The samples underwent static incubation at 30 °C. Samples were taken at 5, 10, 15, 20, and 30 min, where reactions were stopped by adding them directly to SDS denaturing buffer (3x, LDS buffer (NuPAGE® LDS Sample Buffer, Invitrogen, CA, USA). And boiled at 100 °C for 5 min with a Grant QBD2 sample boiler. SDS-PAGE was analyzed according to section 2.4.1.

- Upscaling deglycosylation using *Ef*Endo18A:

The optimized reaction condition was upscaled to deglycosylate a large portion of the *Afu*LPMO11B stock solution. The reaction was composed of 140 μ M *Afu*LPMO11B and 3.4 μ M *Ef*Endo18A reacting in 50 mM sodium acetate buffer, pH 6.0 in a total reaction volume of 5 ml, contained in a 5.0 mL Eppendorf micro centrifuge tube (Eppendorf, Hamburg, Germany). The reaction solution was mixed by pipetting up and down a few times, and further underwent static incubation at 30 °C for 1 h in a Heratherm™ Refrigerated Incubator (Thermo Fisher Scientific), then followed by static incubation at 4 °C for 24 h in a storage fridge.

- Purifying and concentrating the deglycosylated enzyme:

After the deglycosylation reaction above, the 5 ml sample was diluted in 100 ml Bis-tris, pH 6.5. The 100 + 5 ml sample was adjusted to 2 M ammonium sulfate and underwent HIC as described in section 2.1.2.4, but with sampling of 1 ml fractions during gradient elution. Sample fractions from HIC was analyzed with SDS-PAGE as described in section 2.4.1. Fractions containing substantial amount of supposed *Ef*Endo18A bands by SDS-PAGE analysis, was separated from the fractions with supposed *Afu*LPMO11B bands. The pooled fractions of the deglycosylated *Afu*LPMO11B was Cu-saturated with a ten-fold surplus of CuSO_4 , incubated and desalted in the same manner as described in section 2.2.3.

2.3.2 Substrate screening

Activity for glycosylated- and deglycosylated *Afu*LPMO11B was tested on all substrates listed in table 4, in reaction mixtures of 100 μ l, containing 0.2 – 0.6 % substrate, 1 μ M enzyme, 1 mM ascorbic acid, in Bis-tris buffer (pH 6.5), incubated for 24 h in an Eppendorf Thermomixer (Eppendorf, Hamburg, Germany) at 30 °C and 1,000 rpm. Control reactions were performed in the absence of AscA. Additional substrate control reactions were set up similar as described above, but with ascorbic acid and without enzyme. Reactions were stopped by filtrating the soluble fraction from the insoluble substrate using a 96-well filter plate (Millipore) applied on a vacuum manifold. The sample filtrate was analyzed with Ion chromatography (HPAEC-PAD) described in section 2.4.2 below, with a 50 min gradient elution. The chitin samples from the LPMO screening reactions with and without ascorbic acid was additionally analyzed with HILIC UPLC as described in section 2.4.3, where product oxidation state was determined.

Activity for the glycosylated *Afu*LPMO11B was also tested on soluble chitooligomers, i.e. tetraacetyl-chitotetraose, pentaacetyl-chitopentaose, and hexaacetyl-chitohexaose (Purity: > 95 %, Megazyme). Reactions were performed similar to reactions above, but incubated at 45 °C. The samples were also analyzed with ICS-5000⁺ HPLC, but with a 30 min gradient elution.

2.3.3 Protein melting point

The apparent melting temperature of glycosylated and deglycosylated *Afu*LPMO11B was assessed with the use of the Protein Thermal Shift™ Dye Kit, provided by Thermo Fisher Scientific, Applied Biosystems® by *life technologies*™. The experiment was executed according to the protocol for the Protein Thermal Shift™ Dye Kit [125]. Quadruplet reactions of 20.0 µl were set up for each reaction type, i.e. glycosylated and deglycosylated *Afu*LPMO11B and a no-enzyme control, in a MicroAmp™ Optical 96-Well Reaction Plate (Thermo Fisher Scientific, Applied Biosystems™) on ice. The reaction samples were composed by adding the following reagents in the order they are presented; 5.0 µl Protein Thermal Shift™ Buffer, 5.0 µl MQ-water, 2.0 µl Bis-tris buffer (500 mM, pH 6.5), 5.5 µl enzyme solution (17 µM), and 2.5 µl diluted Protein Thermal Shift™ Dye (8x). In no-enzyme control reactions, enzyme was substituted with MQ-water.

After all the reagents were added, the reaction solutions were mixed by pipetting up and down 10 times. The 96-well plate was then sealed with a MicroAmp® Optical Adhesive Film (Thermo Fisher Scientific), and centrifuged with a 5430 R centrifuge (Eppendorf) at 1000 rpm. The sample plate was kept on ice in avoidance of light until it was injected and analyzed with a Real-Time PCR System, described in section 2.4.6 Thermal shift analysis, below.

2.3.4 H₂O₂ production by LPMO in the absence of substrate

The H₂O₂ production by *Afu*LPMO11B at room temperature and pH 6.5 was measured in time with an assay using horseradish peroxidase (HRP) and Amplex Red, bought from Sigma-Aldrich, St. Louis, USA. The formed H₂O₂ by the LPMO is used by HRP in conversion of Amplex Red to resorufin with an absorption maximum (λ_{max}) of 542 nm. Therefore, resorufin formation was monitored with a Thermo Scientific Multiscan FC Microplate Photometer, measuring absorbance at 540 nm with 7 readings per min for 60 min.

The reactions were set up in a Nunc™ MicroWell™ 96-Well Microplates with a total volume of 200 µl each, and contained 1 µM *Afu*LPMO11B, 50 mM Bis-tris pH 6.5, 5 u/ml HRP, 100 µM Amplex Red, and 50 µM ascorbic acid reductant. The reaction was initiated by quickly adding the reductant to the premixed reactions. Control reactions were performed where ascorbic acid was substituted with MQ-water. H₂O₂ standard reactions were produced of 2.5, 5.0, 10.0, and 20.0 µM, and was incubated at room temperature for 5 min after adding ascorbic acid, prior to analysis, to ensure all the H₂O₂ was covered by HRP and resorufin corresponded to the H₂O₂ concentration of the standards. The standard reactions were identical to the negative control reactions, but where *Afu*LPMO11B was substituted with the H₂O₂. All reactions were performed in triplicates. After the addition of the reductant, the samples were mixed by a vertical rotation session by the multiscan plate reader sampler unit and then proceeded with A₅₄₀ measurements.

An additional control was implemented in the final figure (Figure 10) of H₂O₂ production, and was imported from another experiment, performed by PhD stipendiat Lukas Rieder at the faculty of chemistry, biotechnology and food sciences (KBM) at the Norwegian University of Life Sciences (NMBU), Ås, Norway. The control was composed identically as reactions described above, but contained 5 µM CuSO₄ (copper sulfate), and is usually a control in stoichiometric amounts to the enzyme concentration in order to see the enzymatic contribution to H₂O₂ production from the pure copper atoms interacting with reductants and molecular oxygen (O₂). Because H₂O₂ production by *Afu*LPMO11B was performed with 1 µM enzyme, the H₂O₂ produced in the CuSO₄ control reactions were divided by 5, to give an approximation to what 1 µM CuSO₄ might produce in this conditions. However, this may vary from a true control with 1 µM CuSO₄.

The standards showed a stable absorption (A₅₄₀) throughout the analysis of 60 min, and the average absorbance of these measurements produced a linear standard curve (Appendix A – Fig A1, panel A) used in calculating the progression curve of H₂O₂ formation. A separate standard curve was used in producing the H₂O₂ progression curve from the CuSO₄ control reactions (Appendix A – Fig A1, panel B).

2.3.5 Temperature screen

Optimal temperature for stable catalytic activity by *AfuLPMO11B* was approximated with a variable temperature screening assay, where *AfuLPMO11B* reacted and degraded α - and β -chitin and oxidized product formation was measured in samples taken at different timepoints. Reactions with α - and β -chitin was set up identically. The reactions contained 1 μ M *AfuLPMO11B*, 10 g/l substrate, 50 mM Bis-tris buffer (pH 6.5), 1 mM ascorbic acid, with a final reaction volume of 300 μ l. The reactions were initiated by addition of ascorbic acid, and was incubated at 30, 37, and 45 °C and 1000 rpm for 24 h in Eppendorf Thermomixers (Eppendorf Thermomixer, Eppendorf, Hamburg, Germany). Reactions were performed in triplicates.

To execute the experiment, a master master mixture was made, and contained water, buffer and substrate (one for each substrate). This method ensures more homogenous conditions amongst the different reactions, i.e. more similar substrate concentration. Master mixture (approx. 275 μ l, depending on the enzyme and ascorbic acid concentration and volume to be added) was proportionated into 2.0 ml reaction tubes with flat bottoms. The master mix was contained in a 50 ml falcon tube (CELLSTAR® Polypropylene Tube), and was proportionated to reaction tubes by first vigorous pipetting up and down with wide tip pipettes to ensure homogeneity in the solution. After mastermix was added to the 2.0 ml reaction tubes, the tubes were randomized by shuffling, then placed in the Eppendorf Thermomixers, and incubated for 5 min. After the 5 min primary incubation, *AfuLPMO11B* was added, and then ascorbic acid at time zero, and MQ-water in control reactions.

30 μ l samples were taken at different timepoints during the 24 h incubation. The reactions were stopped in the 30 μ l samples by separating the soluble solution from the insoluble substrate by filtration with a 96-well filter plate with 0.22 μ m membrane (Millipore) operated by a vacuum manifold. The reaction stops by this method because *AfuLPMO11B* is only active on insoluble chitin substrates. The soluble fraction from each sample was further degraded with 1.0 μ M chitobiase (*SmGH20*) (CHB), with static incubation at 37 °C for 24 h in a Heratherm™ Refrigerated Incubator (Thermo Fisher Scientific). This treatment convert a complex product profile of various oxidized and non-oxidized chitooligomers from LPMO activity, to a simple product profile of only two products, i.e. GlcNAc (native monomers) and GlcNAcGlcNAc1A (oxidized dimers, where GlcNAc1A is N-acetylglucosaminic acid, with oxidation at carbon 1). The simplified product solution was quantified, using an RSLC system described in section 2.4.5 below, where oxidized product amount correspond, to some extent,

the LPMO catalytic activity. Progression curves of oxidized product formation were generated according to section 2.5.2, with the standard curve from Appendix A – Fig A1, panel C.

*2.3.6 Comparing activity with *AfuLPMO11B* and *BcLPMO10A**

Activity and substrate specificity was compared between *AfuLPMO11B* and the tetra-modular *BcLPMO10A*. The enzymes reacted on two α -chitin substrates with ≤ 0.2 mm and ≤ 0.8 mm grain size, and one β -chitin substrate with ≤ 0.8 mm grain size, respectively. 300 μ l reactions were set up for each enzyme reaction, and contained 1 μ M *AfuLPMO11B* or *BcLPMO10A* in 20 mM Bis-tris with pH 6.5 for the former- and pH 6.0 for the latter enzyme. All reactions also contained 10 g/l substrate and 1 mM ascorbic acid. *AfuLPMO11B* reactions were incubated at 30 °C, while 37 °C for *BcLPMO10A* in Eppendorf Thermomixer with 1000 rpm for the former- and 800 rpm for the latter enzyme, for a total of 6 h. The reactions were initiated by addition of the ascorbic acid at time zero, and in control reactions, ascorbic acid was substituted with MQ-water. All reactions were performed in triplicates. Samples were collected and processed with CHB as described in section 2.3.5 above. Oxidized products GlcNAcGlcNAc1A were quantified, using an RSLC system described in section 2.4.5, and progression curves of oxidized product formation were generated according to section 2.5.2, with the standard curve from Appendix A – Fig A1, panel D.

*2.3.7 Comparing activity with glycosylated and deglycosylated *AfuLPMO11B**

Activity and substrate specificity was compared between the glycosylated and deglycosylated *AfuLPMO11B* reacting on both α - and β -chitin, respectively. The reaction mixtures contained 1 μ M glycosylated or deglycosylated *AfuLPMO11B*, 10 g/l substrate, 50 mM Bis-tris (pH 6.5), and 1 mM ascorbic acid, and were incubated at 30 °C and 1000 rpm in an Eppendorf Thermomixer for a total of 24 h. The reactions were initiated by addition of the ascorbic acid at time zero, and in control reactions, ascorbic acid was substituted with MQ-water. All reactions were performed in triplicates. Samples were collected and processed with CHB as described in section 2.3.5 above. Oxidized product (GlcNAcGlcNAc1A) was quantified using an RSLC system described in section 2.4.5, and progression curves of oxidized product formation were generated according to section 2.5.2, with the standard curve from Appendix A – Fig A1,

panel E. The reaction samples were also analyzed with MALDI-TOF MS, described in section 2.4.4.

2.3.8 Synergy experiment

The synergy experiment was performed in concert with the comparative experiment above (section 2.3.7), therefore the glycosylated *Afu*LPMO11B reactions there, was used as the LPMO control here. The synergy reaction was performed with chitinase-C (*Sm*ChiC) in reactions together with *Afu*LPMO11B in a 1:1 molar ratio, reacting on α - and β -chitin respectively. The assay was performed with 6 different reaction types including 2 controls, on either substrate type; 1: LPMO alone + ascorbic acid, 2: Chi-C alone, 3: LPMO + ascorbic acid and Chi-C, all added at time zero, 4: Chi-C added at time zero and LPMO + ascorbic acid added after 6 h, 5: LPMO alone without ascorbic acid, 6: ascorbic acid, but with no enzymes.

All reactions contained 10 g/l substrate, 50 mM Bis-tris (pH 6.5), and 1 μ M enzyme, or 2 μ M enzyme if LPMO and chitinase were both present in the reaction. The reactions containing reductant contained 1 mM ascorbic acid. In reactions without some reagents, i.e. LPMO, Chi-C and/or ascorbic acid, these were substituted with the adequate volume of MQ-water. two master mixtures of buffer, substrate, and MQ-water (one per substrate type) was blended and proportionated in the 2.0 ml reaction tubes, as described in section 2.3.5 above. In reactions with only Chi-C, MQ-water was added after 6 hours, as a means of control to the 6 h LPMO + ascorbic acid addition (reaction type 4). The reactions were initiated by the following addition order at time zero; 1: LPMO, 2: ascorbic acid, 3: Chi-C (n.b. with MQ-water substitution in the relevant reactions)

All reaction types were performed in triplicates, and incubated at 30 °C and 1000 rpm in Eppendorf Thermomoxers C. Samples were collected and processed as described in section 2.3.5 above. Oxidized dimers (GlcNAcGlcNAc1A) and native monomers (GlcNAc) were quantified using an RSLC system described in section 2.4.5, with the standard curve from Appendix A – Fig A1, panel E and F, and calculated towards % substrate conversion of theoretical maximum as described in section 2.5.3. The samples were analyzed in two turns, first, directly after CHB treatment, where the oxidized product was analyzed, and secondly, after approximately 20 – 50 x sample dilution with MQ-water, where the native product was analyzed. Dilution was necessary, because the samples contain very high concentrations of

native products. Oxidized products were analyzed first, simply because dilution of 20 – 50 x would make the oxidized product concentration too low for chromatographic detection.

2.3.9 H₂O₂ feeding experiment

Several different types of H₂O₂ feeding experiments were performed with *Afu*LPMO11B reacting on β -chitin, and will be explained individually. Common for all reactions however, is that they contain 50 mM Bis-tris (pH 6.5) and 10 g/l substrate, and a total reaction volume of 300 μ l, incubated at 30 °C and 1000 rpm in an Eppendorf Thermomixer, in 2.0 ml reaction tubes with flat bottoms. All reactions were performed in triplicates, and the reaction volume was kept konstant so that addition of H₂O₂ at the given feeding regime resulted in a reaction volume of 300 μ l before every sampling of 30 μ l. Therefore, several diluted H₂O₂ solutions were made according to the preferred H₂O₂ reaction concentration, H₂O₂ feeding regime, and sampling timepoints.

Diluted ascorbic acid and H₂O₂ solutions were kept on ice in avoidance of light until they were added to the reaction mixtures. Sampling volume was always 30 μ l, and reactions were stopped by filtration and processed with CHB as described in section 2.3.5, analyzed with an RSLC system according to section 2.4.5, and progression curves of oxidized product formation were generated according to section 2.5.2, with the standard curve from Appendix A – Fig A1, panel G – L. In control reactions without LPMO, and/or ascorbic acid, and/or H₂O₂, these were substituted with MQ-water. Section A – D below correspond to the panels in figure 17, and section E correspond to figure 18, panel A. The reaction mixture was composed of a master mixture of buffer, substrate and MQ-water proportionated in the reaction tubes, and the reaction was initiated by addition of LPMO, H₂O₂, and ascorbic acid at time zero in the given addition order in the sections below.

- A. H₂O₂ reactions, screening with different H₂O₂ concentrations, where activity was measured of 1 μ M *Afu*LPMO11B reacting in the presence of 0, 20, 35, and 50 μ M H₂O₂ respectively and 1 mM ascorbic acid. The reactions were initiated by addition in the following order; 1: LPMO, 2: ascorbic acid, and 3: H₂O₂ at time zero. H₂O₂ was added every 15 min for 3 hours, and samples were always taken with a volume of 30 μ l.

In the first hour, 30 μ l samples were taken every 15 min, and H₂O₂ was quickly added after sampling. The next 2 h, samples were taken every 30 min. The reaction

- volume was kept so that addition of H₂O₂ every 15 min resulted in a reaction volume of 300 µl before every sampling of 30 µl. Samples were also taken after 4 and 6.5 h. but with no further H₂O₂ addition. Three negative- and one positive control reactions were included in the experiment; (1-) LPMO + 50 µM H₂O₂ added every 15 min, without ascorbic acid. (2-) ascorbic acid + 50 µM H₂O₂ added every 15 min, without LPMO. (3-) LPMO, without H₂O₂ and ascorbic acid. (4+) LPMO with ascorbic acid, but without H₂O₂.
- B. H₂O₂ reactions, screening with different H₂O₂ concentrations, similar to reactions described above (A), but with 0, 50, 80, 120 and 200 µM H₂O₂. The reaction occurred for 6 h, with addition of H₂O₂ every 15 min, and 30 µl sampling every hour. The reactions were initiated by addition of, 1: LPMO, 2: ascorbic acid, and 3: H₂O₂ at time zero. Two negative- and one positive control reactions were included in the experiment; (1-) LPMO + 50 µM H₂O₂ added every 15 min, without ascorbic acid. (2-) LPMO, without H₂O₂ and ascorbic acid. (3+) LPMO + ascorbic acid, but without H₂O₂.
- C. H₂O₂ reactions, screening with different LPMO concentrations. The reactions were set up of 0.05, 0.1, 0.2, 0.4, and 1.0 µM *Afu*LPMO11B reacting in the presence of 1 mM ascorbic acid, and with additions of 40 µM H₂O₂ every 30 min. The reactions were initiated by addition of; 1: LPMO, 2: ascorbic acid, and 3: H₂O₂ at time zero. 30 µl samples were collected every 30 min directly prior to H₂O₂ addition. It was included two negative- and one positive control reactions in the experiment; (1-) ascorbic acid + H₂O₂ (the latter added every 30 min), but without LPMO. (2-) 1 µM LPMO, but without ascorbic acid and H₂O₂. (3+) 1 µM LPMO + ascorbic acid, but without H₂O₂.
- D. H₂O₂ reactions, screening with different ascorbic acid reductant concentrations. The reactions were set up of 0.2 µM LPMO with 40 µM H₂O₂ additions every 30 min, and the reactions were initiated by addition of 10, 20, 70, 150, or 1000 µM ascorbic acid. 30 µl samples were collected directly prior to H₂O₂ addition, every 30 min within the first hour, then every hour up to 6 h in total. The reactions were initiated by addition of; 1: LPMO, 2: H₂O₂, and 3: ascorbic acid at time zero. There is one negative- and one positive control reaction included in the experiment; (1-) LPMO + 40 µM H₂O₂ added only at time zero, but without ascorbic acid. (2+) LPMO + 150 µM ascorbic acid, without H₂O₂.

Addition order was rearranged in this experiment, as opposed to section A, B and C above, in order to minimize ascorbic acid consumption by the molecular oxygen reaction pathway by the LPMO. It came clear that 50 μM H_2O_2 did not notably inactivate the LPMO (H_2O_2 screen, section A), therefore the addition order may not denature the LPMO. By using 0.2 μM LPMO and 40 μM H_2O_2 additions every 30 min it was, based on the previous experiment (section C), estimated that LPMO activity with H_2O_2 consumption and H_2O_2 addition would be balanced with a slight accumulation of H_2O_2 . The increase of H_2O_2 was done to avoid the LPMO from using the O_2 pathway if H_2O_2 was depleted before the next addition. The accumulated H_2O_2 must also be kept at low concentrations, apparently below 80 μM , to avoid inactivation of the LPMO.

- E. H_2O_2 reactions, screening with different H_2O_2 concentrations and 15 μM ascorbic acid. The reactions contained 1 μM LPMO reacting in the presence of 1 mM ascorbic acid, with H_2O_2 concentrations of 0, 20, 35, and 50 μM added every 15 min in a total incubation of 3 h. The reactions were initiated by addition of; 1: LPMO, 2: ascorbic acid, and 3: H_2O_2 at time zero. 30 μl samples were collected, directly prior to H_2O_2 additions, every 15 min the first hour, then every 30 min for the rest of the time. Two negative- and one positive control reactions were included in the experiment; (1-) LPMO + 50 μM H_2O_2 (the latter added every 15 min), but without ascorbic acid. (2-) ascorbic acid + 50 μM H_2O_2 (the latter added every 15 min), but without enzyme. (3+) LPMO + ascorbic acid, but without H_2O_2 .

2.3.10 Protein-substrate binding

A Binding experiment was performed with glycosylated and deglycosylated *Afu*LPMO11B binding to both α - and β -chitin, with LPMO in reduced and non-reduced state, at different timepoints. Reactions were set up of 600 μl with 2.95 μM glycosylated- or 2.37 μM deglycosylated *Afu*LPMO11B, and 2 g/l of either substrate type, with and without 1 mM ascorbic acid. The reactions occurred in 50 mM Bis-tris buffer (pH 6.5), incubated in Eppendorf thermomixers at 30 $^\circ\text{C}$ and 1000 rpm for a total of 24 h. 50 μl samples were taken at 0.5, 1, 2, 4, 6, and 24 h, and filtered with a 96-well filter plate, similar to previous experiments, with a 96-well filter plate with 0.22 μm membrane (Millipore) operated by a vacuum manifold.

unbound enzyme was quantified with relative absorbance of SDS-PAGE according to section 2.4.1, with the standard curve from Appendix A – Fig 1, panel M and N, and calculated for % bound enzyme according to section 2.5.4. In reactions with ascorbic acid, oxidized product (GlcNAcGlcNAc1A) was also quantified with an RSLC system according to section 2.4.5, with a pretreatment of the samples with CHB described in section 2.3.5. Quantification of oxidized products were performed to see how enzyme binding appear in correlation with the catalytic activity. Progression curves of oxidized product formation were generated according to section 2.5.2, with the standard curve from Appendix A – Fig A1, panel O. Negative control reactions for protein binding were performed with the same enzyme concentration and buffer, but in the absence of substrate and ascorbic acid. The binding reactions without ascorbic acid, but with substrate were used as negative control for LPMO activity. All reactions were performed in triplicates. N.b. to obtain lower standard deviation among the triplicates in the SDS-PAGE analysis for protein quantification, a sample loading of at least 20 µl on the gel was necessary. Therefore, 10-well SDS-PAGE stain free gels were used, as they have a larger well volume.

2.3.11 Crystallization

Crystallization of glycosylated and deglycosylated *AfuLPMO11B* was attempted in two primary steps. In the first step, the enzyme was screened with a commercial kit in several ways, and in the second step, promising crystall forming chemical conditions were reproduced, where the enzyme was screened with more specific variations.

2.3.11.1 Primary crystallization screen

Crystallization screening of glycosylated and deglycosylated *AfuLPMO11B* was performed using the commercial crystal screening kit JCSG-plus™ MD 1-37 (Molecular Dimensions), as this crystallization kit is optimal for initial screens. The kit contains 96 different chemical conditions for crystal formation (Appendix F – Table F1). The screening was performed with hanging-drop crystallization technique using 48-well VDX plates with sealant and a well diameter of 9.0 mm, and covered with 12 mm circle glass cover slides, both from Hampton Research, CA, USA.

Prior to the hanging-drop setup, two high concentration enzyme stock were produced, of 22 g/l and 20 g/l of glycosylated- and deglycosylated *AfuLPMO11B*, respectively. Such

high enzyme concentrations led to relatively small final volumes, and caution was made in deciding the necessary volume for the screening, and avoid overusing the primary enzyme stocks that were also used in the other experiments. The concentrated enzyme solutions was made by taking a portion of the primary enzyme stocks, that were produced as described above, and concentrated to the appropriate volume that corresponded to the desired final protein concentration. Enzyme up-concentration was performed with Amicon® Ultra 0.5 mL centrifugal filters with 3 kDA MWCO membranes (Millipore), centrifuged at 4000 rcf at 4 °C, using an Hareus Multifuge (Thermo Fisher Scientific), until desired volume was achieved. Concentrated solution was collected from the filter membranes by reverse spin centrifugation at 1000 rcf at 4 °C for a couple of minutes, in which the filters were placed upside down into a polypropylene tube. The concentrated protein solutions were transferred to 1.5 ml Eppendorf tubes, and a small sample was diluted and measured at UV – A₂₈₀ as described in section 2.2.4, in triplicates, to determine the protein concentration. The sample was adjusted toward 20 g/l with slight addition of Bis-tris buffer (pH 6.5), given that the concentration was a little to high initially, and resulted in a 22 g/l concentration for the glycosylated enzyme, and 20 g/l for the deglycosylated enzyme. Some of the 22 g/l enzyme solution was used to make a dilution towards 11 g/l.

The hanging drop assay was performed by first adding 150 µl of the crystal condition solutions in respective wells of the 48-well plate, 8 conditions at a time. Then a drop of 1:1 ratio of crystal condition and protein with a total drop volume of 1 µl and 1.5 µl of glycosylated- and deglycosylated *AfuLPMO11B*, respectively, was mixed on the 8 first circle glass covers. Then, the glass covers with a 1 µl drop was placed over the well, with the drop facing down, and pressed onto the siliconized edge of the well to ensure the well was sealed. This, then proceeded until all 96 conditions were used on the 11 g/l and 22 g/l glycosylated enzyme, and the 20 g/l deglycosylated enzyme. Observations were made regularly using a stereoscopic optical microscope, and crystal formations were photographed through the lens with a smartphone camera.

2.3.11.2 Expanded crystallization screen

Three crystal screen condition, that resulted in nice geometric crystals with a clean crystal surface, were reproduced, and an extended crystal screen was set up, using these

condition solutions. The relevant conditions were *Tube#* 1-8, 1-15, and 1-19, (see Appendix F, Table F1). Condition 1-8 contain 0.2 M ammonium formate and 20 % w/v poly(ethylene glycol) (PEG) 3350 Da (average molecular weight). Condition 1-15 contain 0.1 M diethanol glycine (BICINE) and 20 % w/v PEG 6000, while condition 1-19 contain 0.1 M sodium acetate (pH 4.6) and 8 % w/v PEG 4000. All reagents were made individually.

50 ml, 30 % w/v PEG stock solutions were made by weighing 15.0 g of PEG (3350, 6000 or 4000) into individual 100 ml blue top glass bottles, and MQ-water was added up to the 50 ml mark. A small clean magnet spinner was added to each bottle, and the PEG was slowly dissolved at room temperature by magnetic rotation ~ 300 rpm, and bottles closed. The spinner was set at slow rotation to avoid air bubbles trapped in the viscous solution. When the PEG was successfully dissolved, the solutions were filtered into new 50 ml falcon (CELLSTAR® Polypropylene) tubes by syringe filtration, using a Filtropur S 0.2 µm filter.

The remaining reagents were made by were made in stocks of 1.0 M concentrations. 100 ml was produced of each, and was composed by weighing 0.1 * molecular weight (in grams) of the relevant compounds in crystalline form, and transferring the powder into separate measuring cylinders, and adding MQ-water up to the 100 ml mark. The compounds were dissolved, and the solution were homogenized with magnet spinners. In the case of the sodium acetate solution, MQ-water was added up to the 80 ml mark, then pH was adjusted to 4.6 with small additions of 37 % HCl while solution was mixed with magnet spinners, and finally MQ-water was added up to the 100 ml mark, and mixed. The resulting solutions was filtered by syringe filtration as with PEG above, into new 50 ml falcon tubes.

Each individual crystal screen condition was made by combining the relevant reagents as described for the condition composition above, calculated towards the desired concentrations, with a final volume of 20 ml, adjusted with MQ-water. The mixture was homogenized by vortexing, and filtered by syringe filtration, as in the previous step, into 50 ml falcon tubes.

The extended crystal screen with these conditions were only performed on the deglycosylated *afuLPMO11B*, with the same hanging drop assay, but with a 24-well VDXm plates with sealant, and a well diameter of 14.4 mm, and drops placed on 18 mm circle glass cover slides. Several drops (1 – 5) were produced in a total of 6 cover slides per condition, where 300 µl crystallization solution was added in the wells. The hanging drops

were ranging in proportion of 0.5:1 to 2:1 of enzyme and condition, respectively, with a drop volume between 0.5 – 3.0 μ l.

2.3.12 CHB treatment

Products from enzyme reactions that were used to generate progression curves were simplified using chitobiase (*SmGH20*) (CHB) with static incubation at 37 °C for 24 h in a Heratherm™ Refrigerated Incubator (Thermo Fisher Scientific). This treatment convert a complex product profile of various oxidized (GlcNAc)_nGlcNAc1A and non-oxidized (GlcNAc)_n chitooligomers from LPMO activity, to a simple product profile of only two products, i.e. native monomers of *N*-acetylglucosamine (GlcNAc) and oxidized chitobiose (dimers) (GlcNAcGlcNAc1A), -where GlcNAc1A is *N*-acetylglucosaminic acid, with oxidation at carbon 1).

2.4 Analytical methods

2.4.1 SDS-PAGE analysis

Samples for SDS-PAGE were prepared by mixing 4:1 ratio of sample and 3x LDS buffer (NuPAGE® LDS Sample Buffer, Invitrogen, CA, USA) respectively in 1.5 ml Eppendorf tubes, and heated at 100 °C for 5 min in a Grant QBD2 sample boiler. After sample boiling, the sample tubes were quickly centrifuged with a mini centrifuge followed by brief vortexing, then quickly centrifuged again with the mini centrifuge. The centrifugation and vortexing was done to collect condensed vapor in the upper part of the Eppendorf tubes and homogenize the sample mixture.

SDS-PAGE was performed using 10- or 15-wells Any-kD stain free gels (Mini PROTEAN® TGX Stain-Free™ Gels, Bio-Rad) installed in a mini cell buffer dam connected in a buffer tank, as part of the Mini-PROTEAN® Tetra Cell vertical mini gel electrophoresis system. The mini cell buffer dam and the buffer tank were filled with 1x TGS (BioRad) running buffer prior to sample loading. The prepared SDS-PAGE samples were loaded in the designated gel wells, along with 5 μ l BenchMark™ Protein Ladder (Invotrogen, CA, USA). Particle migration occurred with 200 V for 32 min supplied by a Bio-Rad Power Pac 300 system. The resulting gels were analyzed

with a Gel Doc™ EZ Imager through an Image Lab™ Version 6.0.0 Standard Edition software, both from Bio-Rad Laboratories, Inc.

2.4.2 Product analysis with HPAEC-PAD

LPMO reaction products were analyzed using high-performance anion exchange chromatography with pulsed amperometric detection (HPAEC-PAD). The analysis was performed on an Dionex™ ICS-5000 system, equipped with Thermo Scientific™ Dionex™ CarboPac™ PA1 Analytical (2 x 250 mm) & Guard (2 x 50 mm) Columns, and with electrochemical detection (High-performance ICS-5000+ DC Detector). The system was controlled- and chromatograms analyzed and recorded using a Chromeleon, version 7.2.9, software (Thermo Scientific™ Dionex™ Chromeleon™ 7 Chromatography Data Systems). The analysis was performed on filtered samples from LPMO activity on various substrates, and directly transferred to HPLC vials (0.3 ml Plastic Snap Ring Micro-vials, ND11, VWR™), closed with snap-ring caps (11mm, PTFE/silicone, VWR™) and analyzed with the Dionex ICS-5000 system without sample pretreatments or adjustments.

The HPAEC-PAD was run with a 0.25 ml·min⁻¹ flow rate, and with sample injections of 50 µl. The sample products were separated with a gradient of two running buffers; (A) 100 mM NaOH, and (B) 1 M NaAc + 100 mM NaOH. In a 50 min gradient protocol, previously described [33], the running buffers start initially with 100 % A, towards 10 % B at 10 min, then 30 % B at 35 min, 100 % B at 40 min, and 0 % B at 41 min continuing with 0 % B to 50 min, reconditioning the column to the initial condition. The gradient occurs faster at the 30 min gradient protocol, but retain the same gradient profile as the former protocol.

2.4.3 Product analysis with HILIC UPLC

LPMO reaction products were analyzed with hydrophilic interaction liquid chromatography (HILIC), performed with an Infinity 1290; Agilent Technologies (Santa Clara, CA, USA) UPLC system, equipped with an Acquity BEH Amide Column (130 Å, 1.7 µm, 2.1 x 150 mm) combined with a VanGuard Pre-column, both from Waters, Milford. Prior to analysis, samples from LPMO activity were filtered with 0.2 µm 96-well filter plates as previously described. The soluble fractions were adjusted to 74 % acetonitrile in 1.5 ml Eppendorf tubes, with a total volume of 60 µl. In the case of protein precipitation by the addition of acetonitrile, the samples

were centrifuged with a Thermo Scientific benchtop microcentrifuge at 14,800 rpm for 5 min. 50 μ l of the centrifuged samples were transferred to HPLC-vials and closed with snap-ring caps, from which oxidized products (GlcNAc)_nGlcNAc1A were analyzed by the UPLC system. A mixture of C1-oxidized standards of (GlcNAc)_nGlcNAc1A was included as a reference in the HILIC analysis, with a degree of polymerization (DP) ranging from 1 – 6, GlcNAc1A – (GlcNAc)₅GlcNAc1A, containing 50 μ M of each product. The oxidized standard is an in-house modified native (non-oxidized) standard (95 % purity, Megazyme), using *Fusarium graminearum* chito-oligosaccharide oxidase (*FgChitO*) [59], to convert (GlcNAc)_n to oxidized products with C1 oxidized ends, as previously described [54, 123].

The HILIC Agilent system was run at room temperature with a 0.400 ml·min⁻¹ flow rate and 10 μ l sample injections. The sample products were separated with a gradient of two running buffers; (A) 15 mM Tris-HCl, pH 8.0, and (B) 100 % acetonitrile. In a 12 min gradient protocol, previously described [124], the running buffers start with 74 % B (0-5 min), then 74-62 % B (5-7 min), 62 % B (7-8 min), 62-74 % B (8-10 min), and 74 % B (10-12 min). Products from elution were measured with UV-detection at 205 nm absorbance. The system was operated with the same Chromeleon software described in section 2.4.2 above, where chromatograms were analyzed and recorded.

2.4.4 Product analysis with MALDI-TOF MS

Reaction products from LPMO activity was analyzed with matrix assisted laser desorption ionization – time of flight (MALDI-TOF) mass spectrometry (MS), using an Ultraflex MALDI-ToF/ToF instrument (Bruker Daltonics, Bremen, Germany) equipped with a 337 nm nitrogen laser beam. 1.5 μ l of filtered (using 0.2 μ m membranes) reaction samples were mixed with 1.5 μ l 2,5-dihydroxybenzoic acid matrix solution (9 g/l dissolved in 30 % acetonitrile) and applied onto an MTP 384 target plate ground steel BC (Bruker Daltonics), and air dried. The MS system was operated using FlexControl Version 3.4, -and results analyzed with FlexAnalysis Version 3.4 softwares (Bruker, Daltonics).

2.4.5 Quantification of GlcNAc and GlcNAcGlcNAc1A with RSLC

Oxidized dimeric products (GlcNAcGlcNAc1A) and native monomers (GlcNAc) were quantified on CHB-treated LPMO reaction samples with HPLC, using a Dionex Ultimate 3000 RSLC system,

equipped with a 7.8 x 100 mm Rezex RFQ-Fast Acid H+ (8%) column (Phenomenex, Torrance, CA, USA). Reaction products were separated isocratically by RSLC, with 8 μ l sample injections and 1.0 ml \cdot min⁻¹ flow rate of the mobile phase (5 mM H₂SO₄), operating at 85 °C. Products from elution were measured with UV-detection at 194 nm absorbance. chromatograms were analyzed and recorded with the same Chromeleon software described in section 2.4.2 above.

To quantify GlcNAcGlcNAc1A and GlcNAc, standards with variable concentration of these compounds were always included in each RSLC analysis, with maximum concentration of 1.0 mM of the former, and 2.0 mM of the latter. If reaction samples surpassed these limits, they were diluted with MQ-water, approximating 50 % of the maximum limit. The oxidized standard (GlcNAcGlcNAc1A) is in-house produced using *FgChitO*, produced and described elsewhere [59, 54, 123], and the GlcNAc standard is commercial (Megazyme; 95 % purity). Quantification of sample products were based on the height of product peaks in the chromatograms, and converted with the standard curve to product concentration.

2.4.6 Thermal shift analysis

The 96-well plate described above (section 2.3.3) was injected and thermal shift analysis was performed with an Applied Biosystems Step-One Plus™ Real-Time PCR System, with a StepOne™ Software v2.2. The following online orders were executed for the method; Instrument type: StepOnePlus™ Instrument (96 Wells), Experiment type: Melt curve, Reagent type: Other, Ramp speed: Fast, Reaction volume per well: 20 (μ L), Ramp mode: Continuous, starting from 25 °C going towards 99 °C with temperature ramp rate of 2 °C \cdot min⁻¹.

2.5 Calculations

2.5.1 Chemical concentrations

- M: Molecular weight (MW) * (x ml/1000 ml) = 1 M = 10⁶ μ M.
- g/l: (1 M/MW) = 1 g/l
- % w/v: % w = grams, if v = 100 ml total solution
- % solution (x %/stock %) * x ml = ml of stock in final volume (x ml)

2.5.2 Progression curves

Progression curves were first calculated with a simple linear slope equation from the standard curve equation; $y = m \cdot x + b$, and $x = (y - b) \cdot m^{-1}$, where $y = A_{194}$ milli absorbance units (mAU) based on chromatographic product peak height, and $x =$ product concentration. $b = y$ -intercept, and was not included in calculations, as it produced in some cases negative values on small chromatographic peaks, and particularly larger negative values in calculating concentrations on diluted samples.

All LPMO reaction samples were treated with CHB, where 1 μ l CHB was added to 15 μ l reaction sample, and produces a dilution factor of 16/15. Some samples contained too high product concentrations, and was diluted with MQ-water, e.g. with a 4 x dilution factor with 10 μ l sample and 30 μ l MQ-water, giving a dilution factor of 4/1. In the case of additions of reagent during the LPMO reactions, a dilution factor is formed from that timepoint, corresponding to (current reaction volume + addition volume) divided by the reaction volume prior to addition.

To estimate the true product concentration produced by the LPMO in time, all chromatographic raw (mAU) data was divided on the standard curve slope value, resulting in the concentration of the sample. This concentration, and all dilution factors were multiplied. Finally, average values and standard deviation was calculated among the triplicates.

In the case of H₂O₂ addition reactions, a new dilution factor is added for every sampling point, which always correspond to the 30 μ l sampling and 30 μ l H₂O₂ addition. Since initial volumes for H₂O₂ reactions are 300 μ l, dilution factor after first H₂O₂ addition (sampling nr. 2) = 300/270, and (300/270)² for sampling nr. 3, and continues with (300/270)ⁿ⁺¹ for every consecutive sampling.

2.5.3 substrate conversion

Substrate conversion (%) of theoretical maximum was estimated by converting the product concentration in μ M to g/l with the theoretical molecular weight (MW) of [(GlcNAc)₂ – H₂O] (424.40 Da – 18.02 Da = 406.38 Da) for oxidized GlcNAcGlcNAc1A products, and with [GlcNAc – H₂O] (221.21 Da – 18.02 Da =) for native GlcNAc products. Conversion from μ M to g/l was done by rearranging the g/l formula in section 2.5.1 to the following; $g/l = MW \cdot (\mu M$

product/ 10^6). The product g/l value was then divided by the substrate concentration (10 g/l) in the reactions, and multiplied by 100 %.

2.5.4 Protein binding

Protein binding (%) was calculated with relative fluorescent intensity by SDS-PAGE. LPMO samples without substrate were collected simultaneously as samples with substrates, and serves as a 100 % unbound protein control. Each 10-well SDS-PAGE gels contains three samples of each, 100 % unbound control samples, LPMO with α -chitin samples, and LPMO with β -chitin samples. In the last well, a standard of the relevant LPMO with controlled concentration was added. N.b. glycosylated and deglycosylated *Afu*LPMO11B were run on different gels, as they appeared to have different fluorescent properties.

To ensure that relative absorbance correlates to a linear difference in protein concentration, standard curves of both the glycosylated and deglycosylated enzyme was made (Appendix A – Fig 1A, panel M and N). The standard curves contained (0.7, 1.0, 2.0, 2.92 and 3.59 μ M) and (0.7, 1.0, 2.0, 2.68 and 3.46 μ M) *Afu*LPMO11B, glycosylated and deglycosylated, respectively. The controlled concentration enzyme sample added in the SDS-PAGE gels was included to ensure that the analyzed samples were within the linear concentration window, and correspond to the highest concentration of the standards. To first calculate unbound protein (%), an average intensity and standard deviation was calculated with the raw data from fluorescent intensity in each sample triplicate. Then these values were divided by the average intensity in the control (100 % unbound) sample triplicates, and multiplied by 100%, giving % unbound protein, and % standard deviation. The inverse of % unbound protein = % bound protein, and was calculated by 100 % - % unbound protein. % standard deviation remain unaffected.

2.5.5 Average DP estimation on $(\text{GlcNAc})_n\text{GlcNAc1A}$ reaction products

Average DP of oxidized products were estimated by the relationship between oxidized dimers (GlcNAcGlcNAc1A) and native monomers (GlcNAc) on LPMO reaction samples that were treated with chitobiase. The calculation was simply performed by, first, dividing the concentration of GlcNAc on the concentration of GlcNAcGlcNAc1A in each individual sample, which result in the average DP attached to oxidized dimer products. This value was then given

an addition of +2, as the oxidized dimer product constitutes a DP of 2. Average values, and standard deviations were then made for the triplicates of each reaction type. This calculation was done to see differences in released product size (DP) in different H₂O₂ conditions.

Because product DP from LPMO reactions also may vary depending on the degree of substrate degradation, an additional calculation was done to compensate for this effect. Substrate conversion (%) of theoretical maximum was calculated for each datapoint in each sample, as described in section 2.5.3 above, where % conversion correspond to the sum of oxidized dimers and native monomers in each sample, from which average values and standard deviations were made for the triplicates. A figure was then produced with % substrate conversion on the x-axis, and with estimated average DP of oxidized products on the y-axis. With this method, estimated DP values should line up to a common trend, among the different H₂O₂ reaction condition, if % substrate conversion caused the apparent DP variability. If the DP variability however was caused by the differences in H₂O₂ concentration, the apparent DP variation should remain between the different H₂O₂ concentration reactions.

2.6 Bioinformatics

2.6.1 Protein modelling

A protein structure model of *Afu*LPMO11B was generated using SWISS-MODEL Homology Modelling [61]. The protein sequence FASTA format of *Afu*LPMO11B (UniProt ID: B0XZD3, Gene name: AFUB_044010) without the signal peptide (first 18 amino acids) was implemented in SWISS-MODEL, and the protein with the highest sequence ID was chosen as the model structure template, i.e. *Ao*LPMO11 (4mah.1.A) with sequence ID: 49.43 (Appendix D, Table D1). The generated PDB-file for the model structure of *Afu*LPMO11B by SWISS-MODEL was further rendered using PyMOL, Version 2.2 [24], producing figures showing putatively important residues indicated by other bioinformatics analyses and litterature, i.e. catalytic site residues, conserved residues, glycosylation sites, and conserved domains.

2.6.2 Multiple sequence alignment

A multiple sequence alignment was produced (Appendix D, Fig D1), using Clustal Omega [103], on several chitin active LPMOs, i.e. *Bt*LPMO10A, *Sm*LPMO10A, *Sli*LPMO10E, *Jd*LPMO10A,

*Sam*LPMO10B, *Cj*LPMO10A, *Ao*LPMO11, *Afu*LPMO11B, *Td*AA15A, and *Td*AA15B, where the full length FASTA format of all enzymes were implemented. The multiple sequence alignment file from Clustal Omega was further rendered using ESPrpt 3.0 [104] with a confidence limit of 0.7.

2.6.3 Glycosylation site predictions

Glycosylation sites on *Afu*LPMO11B was predicted (Appendix D, Table D2) using NetNGlyc [49] for N-linked glycans, and NetOGlyc [50] for O-linked glycans, using the full length polypeptide sequence for the enzyme (UniProt ID: B0XZD3, Gene name: AFUB_044010)

2.7 *Afu*LPMO11B protein crystal structure

The protein crystal structure of *Afu*LPMO11B was solved by x-ray crystallographic analysis performed by Åsmund Røhr Kjendseth (Scientist at the Norwegian University of Life Sciences, faculty of Chemistry Biotechnology and Food Science). The analysis was performed on the protein crystal (Appendix C, Fig C1 – photo 38) produced in the extended crystal screening explained in section 2.3.11.2, with crystallization solution #1-15 (see Appendix F, Table F1).

2.8 Materials

Table 1. Laboratory equipment, computer softwares and server applications

<i>Equipment</i>	<i>Supplier</i>
SDS-PAGE	
Grant QBD2 sample boiler	Grant
Mini PROTEAN® TGX Stain-Free™ Gels	Bio-Rad
NuPAGE® LDS Sample Buffer	Invitrogen
10x Tris/Glycine/SDS Electrophoresis Buffer (TGS)	Bio-Rad
Mini-PROTEAN® Tetra Cell vertical mini gel eletrophoresis system	Bio-Rad
PowerPac 300, power supply	Bio-Rad
Gel Doc™ EZ Imager	Bio-Rad
Centrifuges	
Mini centrifuge – mySPIN 6	Thermo Fisher
5418 R	Eppendorf
5430 R	Eppendorf
Haerus Multifuge	Thermo Fisher

Avanti J-26S Series centrifuge	Beckman Coulter
Spectrophotometry	
Eppendorf Biophotometer D 30	Eppendorf
UVette® disposable cuvettes, 50–2000 µl, 220 – 1600 nm,	Eppendorf
Tubes and HPLC vials	
1.5 ml Eppendorf Tubes® 3810X	Eppendorf
2.0 ml, graduated, non-siliconized polypropylene (flat bottom)	Merck
Micro tube 2ml, PP	Sarstedt
5.0 ml Eppendorf micro centrifuge tube	Eppendorf
50 ml CELLSTAR® Polypropylene Tube (falcon tube)	Greiner
0.3 ml Plastic Snap Ring Micro-vials, ND11	VWR
snap-ring caps (11mm, PTFE/silicone, for Micro-vials)	VWR
Centrifugal filters	
Amicon® Ultra-15, regenerated cellulose membrane - 10,000 MWCO	Millipore
Amicon® Ultra-15, regenerated cellulose membrane - 3,000 MWCO	Millipore
Vivaspin 20 Centrifugal Concentrator 10,000 MWCO PES	Sartorius
Vivaspin 20 Centrifugal Concentrator 3,000 MWCO PES	Sartorius
Amicon® Ultra 0.5 mL centrifugal filters with 3,000 MWCO	Millipore
Vacuum filters	
Filter Upper Cup 250 ml bottle top filter 0.2 µm PES membrane	VWR
Filter Upper Cup 250 ml bottle top filter 0.2 µm PES membrane	VWR
MultiScreenHTS GV Filter Plate, 0.22 µm, clear, sterile	Merck
Syringe filters	
0.22-µm-pore-size Millex-GV filter	Merck Millipore
Filtropur S 0.2 µm PES membrane	Sarstedt
Thermal Shift Analysis	
Protein Thermal Shift™ Dye Kit	Thermo Fisher
MicroAmp™ Optical 96-Well Reaction Plate	Thermo Fisher
MicroAmp® Optical Adhesive Film	Thermo Fisher
Applied Biosystems Step-One Plus™ Real-Time PCR System	Applied Biosystems
Incubator systems	
Multitron Standard	Infors HT
Eppendorf Thermomixer C	Eppendorf
Heratherm™ Refrigerated Incubator	Thermo Fisher
Vivaflow 200	
Masterflex Economy Drive Peristaltic Pump 115 V	Sartorius
Vivaflow 200 Laboratory Cross Flow Cassette, 10,000 MWCO PES	Sartorius
HIC	
HiTrap™ phenyl FF (HS) 5 ml hydrophobic column	GE Healthcare
ÄKTA Prime™ Plus chromatography system	GE Healthcare
SEC	
ÄKTApurifier	GE Healthcare
HiLoad™ 16/600 Superdex™ 75 µg, column	GE Healthcare
H ₂ O ₂ production	
Nunc™ MicroWell™ 96-Well Microplates	Thermo Fisher

Multiscan FC Microplate Photometer	Thermo Fisher
HPAEC-PAD	
Dionex™ ICS-5000 system	Thermo Fisher
CarboPac™ PA1 Analytical (2 x 250 mm) & Guard (2 x 50 mm) Columns	Thermo Fisher
High-performance ICS-5000+ DC Detector	Thermo Fisher
HILIC	
Infinity 1290; Agilent Technologies UPLC system	Agilent
Acquity BEH Amide Column, 130 Å, 1.7 µm, 2.1 x 150 mm	Waters
VanGuard Pre-column	Waters
RSLC	
Dionex Ultimate 3000 RSLC system	Thermo Fisher
Rezex RFQ-Fast Acid H+ (8%) 7.8 x 100 mm column	Phenomenex
MALDI-TOF MS	
Ultraflex MALDI-ToF/ToF instrument	Bruker Daltonics
337 nm nitrogen laser	Bruker Daltonics
2,5-dihydroxybenzoic acid matrix solution	Bruker Daltonics
MTP 384 target plate ground steel BC (Bruker Daltonics)	Bruker Daltonics
Crystallisation	
JCSG-plus™ MD 1-37 Crystallisation Screening Kit	Molecular Dimensions
48-well VDX plates with sealant, and 9.0 mm well diameter	Hampton Research
24-well VDXm plates with sealant, and 14.4 mm well diameter	Hampton Research
12 mm circle glass cover slides	Hampton Research
18 mm circle glass cover slides	Hampton Research
Online servers	
SWISS-MODEL Homology Modelling – protein structure model	Biozentrum
NetNGlyc – N-linked glycosylation site prediction	DTU Health Tech
NetOGlyc – O-linked glycosylation site prediction	DTU Health Tech
Clustal Omega – multiple sequence alignment	EMBL-EBI
ESPrnt 3.0 – multiple sequence alignment modification	SBGrid
SignalP-5.0 – Signal peptide prediction	DTU Health Tech
UniProt – UniProt ID: B0XZD3, Gene name: AFUB_044010	UniProt
ExPASy ProtParam – chemical properties of protein FASTA sequences	SIB
PyMOL Molecular Graphics System, Version 2.2	Schrödinger
Softwares	
Image Lab™ Version 6.0.0 Standard Edition software	Bio-Rad
StepOne™ Software v2.2	Applied Biosystems
Primeview 5.0 (UNICORN) Software	GE Healthcare
Unicorn 5.20 Workstation Software	GE Healthcare
Chromeleon, version 7.2.9 Software, Chromatography Data Systems	Chromeleon
FlexControl Version 3.4 Software	Bruker Daltonics
FlexAnalysis Version 3.4 Software	Bruker Daltonics
Sterilization fume hood - Safe 2020 Class II	Thermo Fisher
Ultrapure water system, Milli-Q® Advantage A10	Merck
Blue-top glass bottles, VWR Borosilicate 3.3. (25 ml – 2000 ml)	VWR
Automated pipettes (0.20-2.00 µl, 2.00-20.00 µl, 10.0-100 µl, 0.1-1 ml)	Labsystems

Pipette tips	Thermo Fisher
Becton Dickinson hypodermic syringes, polypropylene	Merck
1X Glycoprotein Denaturing Buffer	NEB
1X GlycoBuffer 3	NEB
PichiaPink™ Yeast Expression System	Thermo Fisher
826 pH mobile pH-meter	Metrohm

Table 2. Chemicals

<i>Compound</i>	<i>Distributor</i>
Acetonitrile (ACN)	VWR
Ammonium formate (NH ₂ HCO ₂)	Sigma-Aldrich
Ammonium sulfate ((NH ₄) ₂ SO ₄)	Merck
Amplex® Red	Sigma-Aldrich
Ascorbic acid	Sigma-Aldrich
Bacto Peptone	BD Biosciences
Bacto Yeast Extract	BD Biosciences
BICINE (Dihydroxyethylglycine)	Sigma-Aldrich
Biotin	Sigma-Aldrich
Bis-tris	Merck
Copper(II) sulfate (CuSO ₄)	Sigma-Aldrich
Glycerol 85 %	Merck Millipore
Hydrogen peroxide (H ₂ O ₂)	Sigma-Aldrich
Hydrochloric acid (HCl)	Sigma-Aldrich
Oxygen (O ₂)	Ambient
Polyethylene Glycol (PEG) 3,350 Da	Sigma-Aldrich
Polyethylene Glycol (PEG) 4,000 Da	Sigma-Aldrich
Polyethylene Glycol (PEG) 6,000 Da	Sigma-Aldrich
Potassium hydroxide (KOH)	Sigma-Aldrich
Potassium phosphate monobasic (KPi)	Merck
Sodium acetate (NaAc)	Sigma-Aldrich
Sodium chloride (NaCl)	Sigma-Aldrich
Sodium hydroxide (NaOH)	Merck
Sulfuric acid (H ₂ SO ₄)	Merck
Tris hydrochloride (Tris-HCl)	Sigma-Aldrich
Yeast Nitrogen Base, w Ammonium Sulfate w/o amino acids	Sigma-Aldrich

Table 3. Standards

<i>Type</i>	<i>Producer</i>
BenchMark™ Protein Ladder	Invitrogen
Oxidized chitooligomeric standards (GlcNAc) _n GlcNAc1A (DP1 – DP6)	In-house [54, 123]

Oxidized N,N-diacetyl (GlcNAcGlcNAc1A)	In-house [54, 123]
N-acetyl-D-glucosamine, Purity: > 95 %, (GlcNAc)	Megazyme

Table 4. Carbohydrate substrates

<i>Substrate</i>	<i>Specifications</i>	<i>Supplier</i>
Mannan (Ivory nut)	Purity > 98%. 1,4- β -D-Mannan. Treated with sodium borohydride to lower reducing sugar levels. Traces of arabinose and xylose.	Megazyme
Glucomannan (Konjac)	Purity > 98%. Glucose: Mannose = 40: 60. Acetylated. Viscosity ~ 2 cSt.	Megazyme
Xylan (Birchwood)		Sigma-Aldrich
Xyloglucan (Tamarind)	Purity ~ 95%. High viscosity. Ara: Gal: Xyl: Glc = 3: 18: 34: 45	Megazyme
Starch (Potato)		Merck
Xylan (Beechwood)		Megazyme
Acetyl glucuronoxylan (Aspen)	Approximate mass distribution of 500 Da to 2500 Da. Prepared in-house by Protocol: Biely et al. (2013) [120]	In-house
Heparin (Pig)	100 %	Merck
Chitosan (Shrimp shells)	Grade: practical grade, mol wt: 190-375 kDa, \geq 75% deacetylated	Sigma-Aldrich
Hyaluronic acid	Mol wt 0.6 - 1.1 MDa	Sigma-Aldrich
PASC	Phosphoric acid swollen cellulose. Protocol: Wood et al. [118]	In-house
Avicel	Avicel [®] PH-101, ~50 μ m particle size	Sigma-Aldrich
α -chitin (Shrimp shell)	Alkaline and acid pretreated commercial chitin from shrimp (<i>Pandalus borealis</i>) shell, named Chitinor.	Chitinor AS (Senjahopen, Norway)
β -chitin (Squid pen)	extracted from squid pen (batch 20140101), particle size < 0.8 mm	France chitin, Orange, France
Tetra-N-acetylchitotetraose	\geq 95%	Megazyme
Penta-N-acetylchitopentaose	\geq 95%	Megazyme
Hexa-N-acetylchitohexaose	\geq 95%	Megazyme

Table 5. Enzymes

Enzyme	Organism	Producer
<i>Afu</i> LPMO11B glycosylated	<i>Aspergillus fumigatus</i>	In-house [thesis]
<i>Afu</i> LPMO11B deglycosylated	<i>Aspergillus fumigatus</i>	In-house [thesis]
<i>Bc</i> LPMO10A (tetra-modular)	<i>Bacillus cereus</i>	In-house [45]
<i>Sm</i> GH20 (CHB) chitobiase	<i>Serratia marcescens</i>	In-house [106]
<i>Sm</i> Chi18C (Chi-C) chitinase-C	<i>Serratia marcescens</i>	In-house [121]
<i>Ef</i> Endo18A	<i>Enterococcus faecalis</i>	In-house [53]
Endoglycosidase H	<i>Streptomyces Plicatus</i>	NEB
Horse radish peroxidase (HRP)	<i>Armoracia rusticana</i>	Thermo Fisher

3. Results

In this study, *AfuLPMO11B* was produced, purified and characterized in-depth. This Results section is divided into four subsections, i.e. “3.1 Protein quality & *AfuLPMO11B* characteristics”, “3.2 Reaction kinetics and substrate binding”, “3.3 Crystallization”, and “3.4 Protein structure”. Glycosylated and deglycosylated *AfuLPMO11B* were produced and tested in parallel in various experiments, addressing substrate specificity, catalytic rates, optimal conditions for activity, thermal stability, and the nature of the (oxidized) products formed.

Other experiments were performed with the glycosylated variant of *AfuLPMO11B* only, and included an extended substrate screen with soluble substrates, analysis of H_2O_2 production, and determination of the effect of temperature on the catalytic rate. Furthermore, this glycosylated enzyme was used for comparing activity with another chitin-active LPMO, *BcLPMO10A*, for analyzing synergy with a chitinase, and for additional studies of catalysis focusing on the effect of adding H_2O_2 to the reactions.

Stock solutions of purified glycosylated *AfuLPMO11B* showed significant variation in quality, i.e., difference in progression curves of oxidized product formation under identical conditions, as outlined below. Almost all experiments were done with “Stock 2” (Table 7), which was of the highest quality. “Stock 1” was only used in studies of hydrogen peroxide production and in the comparison with *BcLPMO10A* (Fig 18).

3.1 Protein quality & *AfuLPMO11B* characteristics

3.1.1 Protein specifications and purified enzyme batch quality

Figure 7 shows the amino acid sequence of *AfuLPMO11B* derived from UniProt [105], including the signal peptide, which was predicted using SignalP (Appendix D, Fig D2). Table 7 shows several chemical properties of *AfuLPMO11B* without its signal peptide, i.e., the mature, non-glycosylated protein, derived from the amino acid (FASTA) sequence without the signal peptide, which were calculated using ProtParam [89]. Mature *AfuLPMO11B* is a single domain LPMO consisting of 201 amino acid residues, with a theoretical mass of 21750.15 dalton (Da).

1	10	20	30	40	50	60
MMLSKVVMGLLTASLAAAHMEMSWPYPLRSRFDQPVEEDIDYSMTSPLNSDGSNFPCKGYQTNTPWRA						
70	80	90	100	110	120	130
TAQYTAGQTYNMTITGSATHGGGSCQLSLSYDNGKTFKVIQSMEGGCPLVSKYNFKIPGDVANGQALFAW						
140	150	160	170	180	190	200
TWYNLIGNRELYMNCADVVISGGTGTSSSFESAYPDLFVANVGNCGCSTVEGRETVFANPGDQVIYGGTVT						
210	219					
PSSPAFPICH						

Fig 7. The amino acid sequence of *AfuLPMO11B*. Residues marked in red illustrate the predicted signal peptide, The sequence and information were derived from Uniprot (UniProt ID: B0XZD3, Gene name: AFUB_044010) [105].

The theoretical pI of the protein is 4.76 and the calculated extinction coefficient is 38765 M⁻¹cm⁻¹. Of note, this extinction coefficient (ϵ) was used along with measurements of UV-absorption (A_{280}) to determine the protein concentration in solutions with purified *AfuLPMO11B*, throughout this study.

Table 6. Physiochemical properties of *AfuLPMO11B*. The table shows values for *AfuLPMO11B* without its signal peptide and based on the assumption that all Cys residues form cystines. The displayed values were calculated using ProtParam [89] using the sequence displayed in (Fig 7) excluding the signal peptide.

Property	Value
Number of amino acids	201
Molecular weight	21750.15 g/mol
Theoretical pI	4.76
Extinction coefficient	38765 M ⁻¹ cm ⁻¹

The gene encoding *AfuLPMO11B* had previously been cloned in *Pichia pastoris* for expression and secretion to the culture medium (Petrovic, Varnai and Eijsink, unpublished results). The enzyme was successfully purified from multiple *Pichia* cultures, using HIC and SEC chromatography, as described in detail in the Methods section. Figure G1 (Appendix G) shows a typical example of a chromatographic purification step, whereas Figure B1 (Appendix B)

shows SDS-PAGE analysis, illustrating the gradual increase in protein purity between the chromatography techniques used (methods). Figure 8 shows SDS-PAGE analysis of resulting batches of purified protein, with very low levels of contamination. Table 7 shows key properties of the various resulting enzyme stock solutions (numbered 1, 2 and 3) that were used in the experiments described below.

Table 7. Stock solutions of purified *AfuLPMO11B* used in this study. The stock solutions are numbered 1 – 3 and are the result of three cultivations (Cultivation Batch nr.). The table also shows protein concentrations (Concentration), total volumes of the stock solutions (Volume), glycosylation status (Glycosylation), and in which type of experiments the stock solutions were used.

Cultivation Batch nr.	Concentration ¹⁾		Volume	Glycosylation	Application
	μM	g/l	ml		
1	30.6	0.67	3.0	Yes	(H ₂ O ₂ production & comparative study; Figs. 10 & 14)
2	445.0	9.68	1.3	Yes	Catalytic properties & crystallization
3	274.7	5.97	2.0	No	Catalytic properties & crystallization

¹⁾ Calculated by measuring A₂₈₀ and using the theoretical molar extinction coefficient (Table 6) to convert A₂₈₀ to protein concentration.

Figure 8 shows that the glycosylated and deglycosylated protein differ by 5-7 k Da and that the apparent mass of the deglycosylated protein is close to the theoretical mass of 21.7 kDa. As mentioned in the Introduction, the mass difference cannot directly be correlated to the mass of the glycans, as SDS-binding to sugar probably varies from SDS-binding to proteins. portion of *AfuLPMO11B* was denatured by treatment with a commercial protein denaturing buffer (section 3,3,1 - methods) and both the denatured and functionally folded form of the protein were deglycosylated, with the same outcome (Figure 9). It is thus likely that the folded protein was fully deglycosylated, at least when it comes to N-linked glycans. Figure 9 also provides a further illustration of the relative concentrations of *EfEndo18A* and *AfuLPMO11B* in the deglycosylation reactions. The figure shows SDS-PAGE of samples directly after deglycosylation, still containing *EfEndo18A*. Separation of the two proteins was difficult, in that they have similar pI and size, but was achieved using the chromatographic protocol described in section 2.2.2.4, leading to rather clean samples of deglycosylated *AfuLPMO11B*, as depicted in Fig. 8.

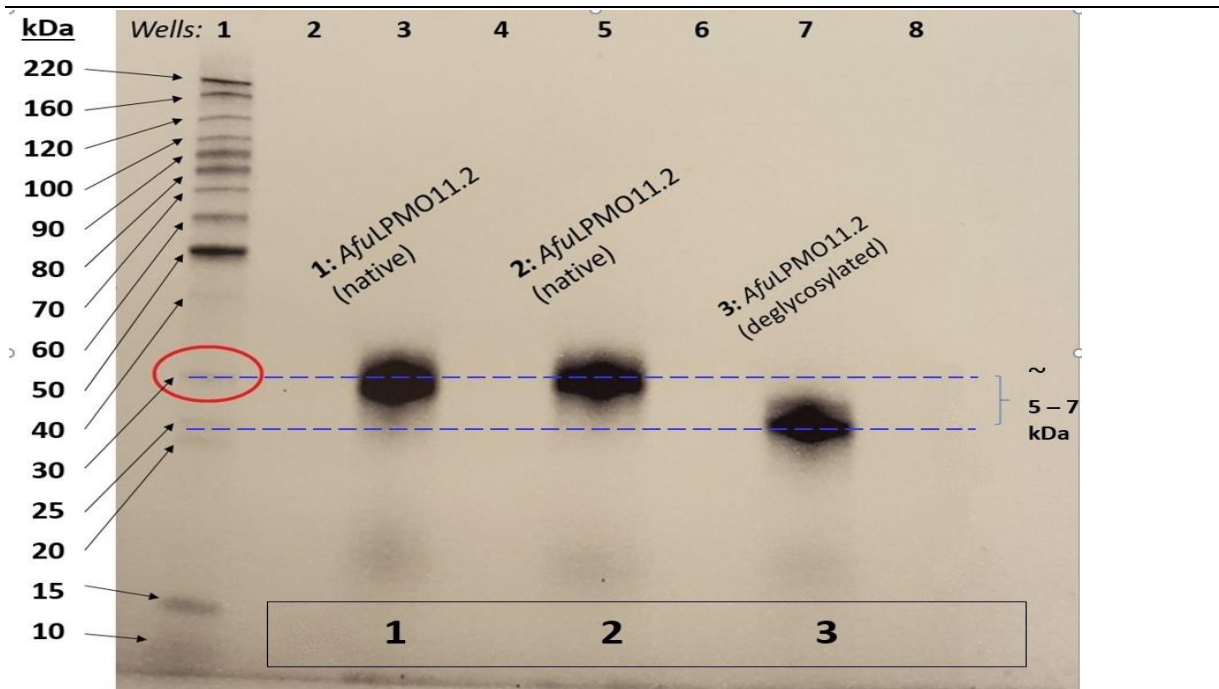


Fig 8. SDS-PAGE of the final working stock solutions with purified *AfuLPMO11B*. The numbers in front of the protein name (*AfuLPMO11.2* = *AfuLPMO11B*) indicate the number of the cultivation from which the protein was purified and the numbers below the bands are the numbers of the resulting stock solutions. See Table 7 for further details and explanation. Lanes 3 & 5 show native proteins possessing glycosylations, whereas lane 7 shows the deglycosylated protein. Lane 1 shows the BenchMark™ Protein Ladder and band sizes are indicated, with the 30 kDa band marked by a red circle. The apparent mass difference between glycosylated and deglycosylated protein is illustrated by the dotted blue lines. The sample size was the same for all three *AfuLPMO11B* containing lanes: 10 μ l of a 10 μ M solution.

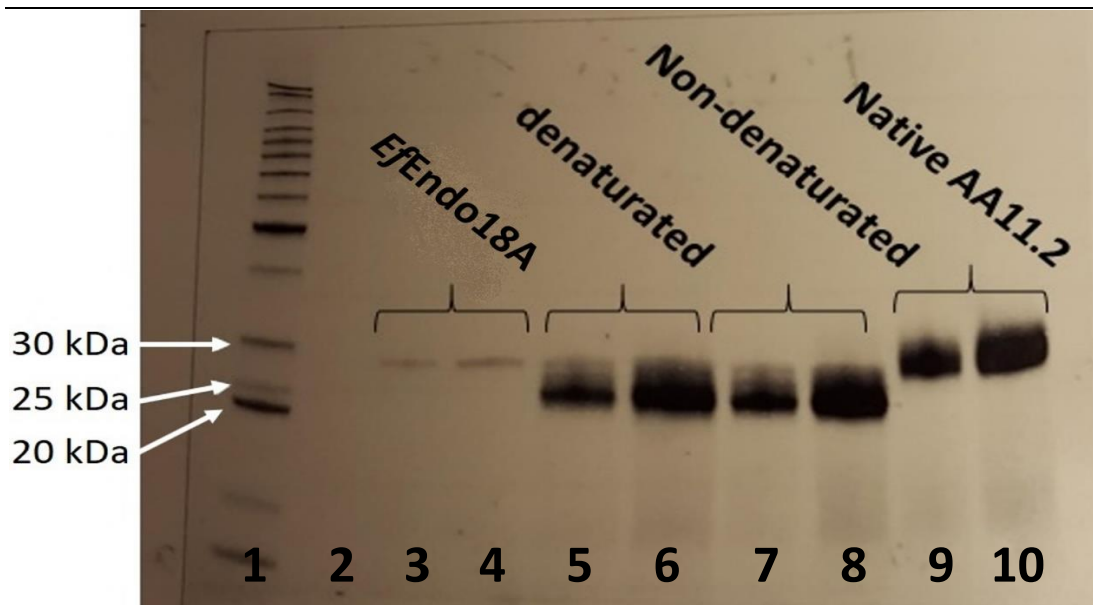


Fig 9. SDS-PAGE analysis of the de-N-glycosylation of *AfuLPMO11B*. Lane 1, molecular mass marker; lanes 3 & 4, *EfiEndo18A* alone; lanes 5 & 6, heat-denaured *AfuLPMO11B* treated with *EfiEndo18A*; lanes 7 & 8, native *AfuLPMO11B* treated with with *EfiEndo18A*; lanes 9 & 10, native *AfuLPMO11B* possessing glycosylations. The masses of relevant bands are indicated on the left side of the figure. Sample sizes used for SDS-PAGE correspond to the concentrations used during the deglycosylation assay.

3.1.2 Functional characterization of *AfuLPMO11B* - Substrate specificity

Both the glycosylated and deglycosylated protein (stock solutions 2 & 3, Fig 8) were tested for activity in aerobic conditions on a variety of substrates, i.e., different carbohydrate types varying in sugar content, chain length, branching, solubility and crystallinity (Fig 10). In the presence of ascorbic acid, *AfuLPMO11B* was active only on α - and β -chitin, whereas no activity was detected on any of the other tested substrates. Importantly product formation from chitin was only observed in reactions with added ascorbic acid reductant together with the LPMO, and not in reactions containing only LPMO (Fig 10, -Ctrl) or only reductant (Fig 11). These products are therefore very likely due to LPMO action and not to an effect of ascorbic acid interacting with the substrate, or otherwise an effect of enzymatic hydrolysis (in the case of protein contamination with an equal size GH in the final LPMO stock solution). It is worth noting that chitosan is closely related to chitin, lacking *N*-linked acetyl groups on most of the glucosamine units, but that *AfuLPMO11B* did not show activity on this substrate.

The results showed that deglycosylation of *AfuLPMO11B* did not effect substrate specificity. Despite a marked difference in the arrangement of the polymer chains in α - and β -chitin, anti-parallel and parallel, respectively, *AfuLPMO11B* was active on both substrates. It is worth noting that product formation was higher in reactions with β -chitin.

Next to clear product peaks in the reaction with chitin, small peaks did appear for all other substrates in the reactions containing ascorbic acid. It was considered that these peaks were not a result of enzymatic activity, but rather products derived from ascorbic acid. Additional control reactions with the same substrates as in Figure 10, where reactions contained ascorbic acid, but not enzyme, showed the same peak formation (Fig 11), confirming that these peaks do not result from enzymatic activity. A large peak was however observed in reaction with Mannan and reductant (Fig 11), which was not observed in reaction with LPMO and reductant (Fig 10), (see Discussion).

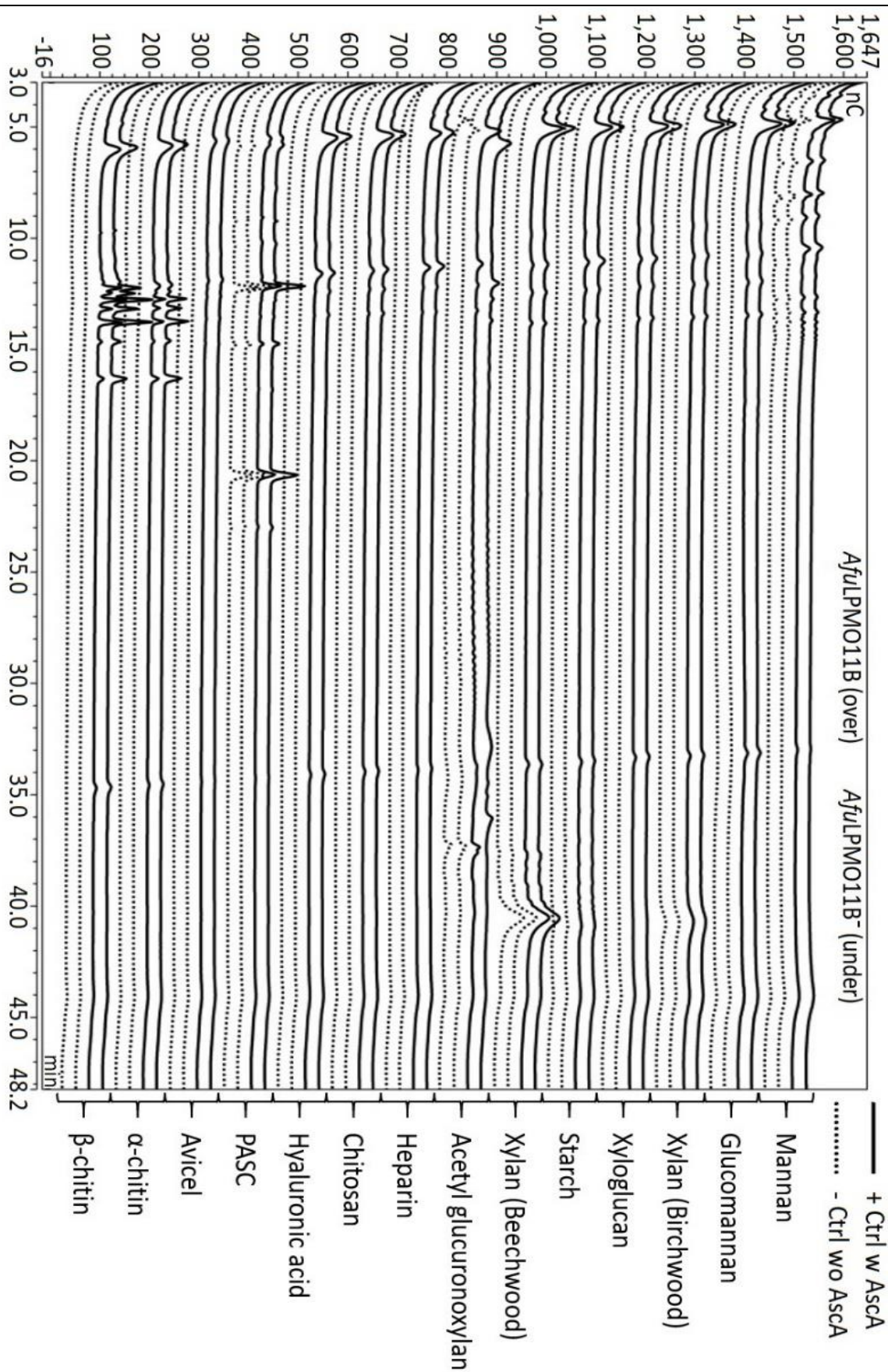


Fig 10. HPAEC-PAD – Chromatographic analysis of products generated in substrate screening reactions with *AfuLPMO11B*. The figure shows *ICS5000* chromatographic analysis with

electrochemical product detection of reaction supernatants obtained after overnight incubation of the indicated substrates (0.2 – 0.6 %, w/v) with 1 μ M *Afu*LPMO11B in 50 mM Bis-Tris buffer (pH 6.5) in an Eppendorf Thermomixer set to 1000 rpm at 30 °C. For each substrate, four chromatograms are shown, for reactions with 1 mM ascorbic acid (solid lines) or without ascorbic acid (dotted lines; in this case ascorbic acid was substituted with MQ-water). For each pair of lines, the upper line is from a reaction with the glycosylated enzyme and the lower line is from a reaction with the deglycosylated enzyme. The Y-axis shows nanoCoulomb (nC) and the X-axis shows time after sample injection in minutes.

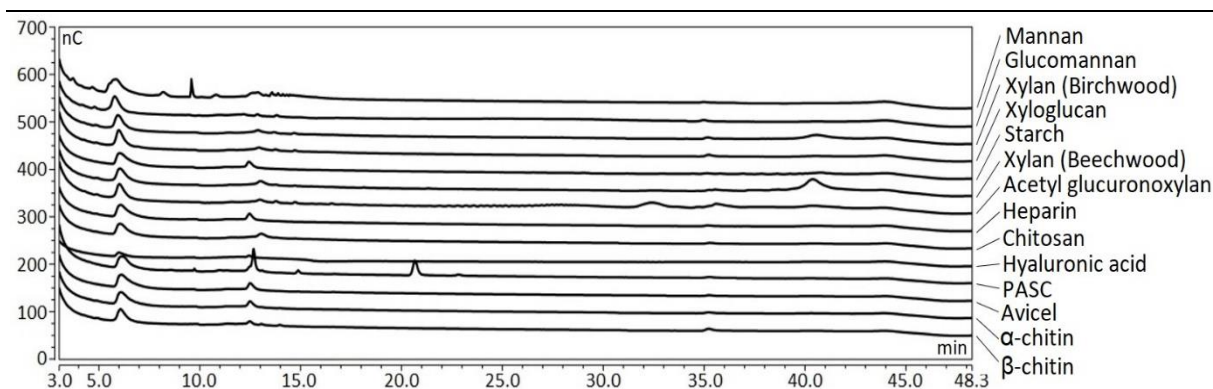


Fig 11. HPAEC-PAD – Chromatographic analysis of products generated in substrate screening reactions without added enzyme. The analytical methods and the reaction set ups used for the experiments depicted in this figure were identical to those in Figure 10, except that no enzyme was added to the reaction mixtures.

The native, glycosylated version of *Afu*LPMO11B was also tested for activity on soluble chitin oligomers [(GlcNAc)ⁿ], with a degree of polymerization (DP) of DP4 to DP6. No apparent activity was observed (Fig 12). As a control reaction, activity was tested without ascorbic acid reductant. Some peaks were however observed on reaction with LPMO and reductant (Fig 12), but closely resemble the peak formation in the previous two figures (Fig 11 and 11), and likely relates to products from ascorbic acid interactions.

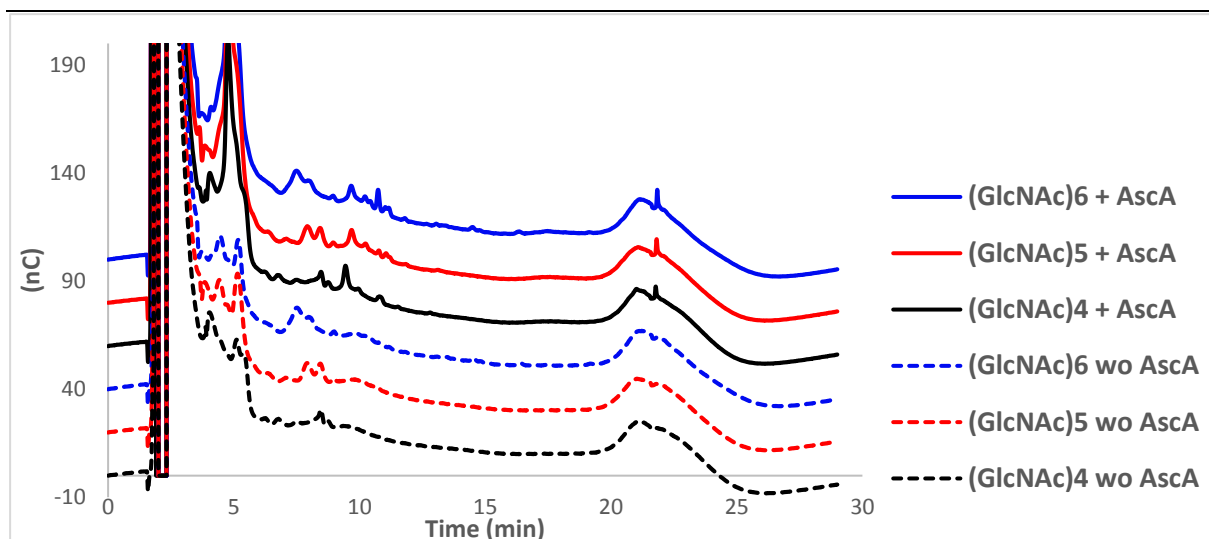


Fig 12. HPAEC-PAD – Chromatographic analysis of products generated in reactions with *AfuLPMO11B* and soluble substrates. The figure shows *ICS5000* chromatographic analysis with electrochemical product detection of reaction supernatants obtained after overnight incubation of $1\mu\text{M}$ *AfuLPMO11B* with 0.2 % (w/v) soluble chitin oligomers in 50 mM Bis-tris buffer (pH 6.5) with 1 mM ascorbic acid, at $37\text{ }^{\circ}\text{C}$, in an Eppendorf Thermomixer set to 1000 rpm. Ascorbic acid was substituted with MQ-water in negative controls (dotted lines). The degree of polymerization (DP) of the substrates varied from 4 - 6 non-oxidized (GlcNAc) units. Potential LPMO activity is expected to occur in reactions containing reductant, with peak formation of oxidized products around 11-14 min. The substrate peaks appear to coelute with the reductant around 3-5 min with low detection.

3.1.3 Functional characterization of *AfuLPMO11B* - Characterization of reaction products

After observing that *AfuLPMO11B* was active on α - and β -chitin (Fig 10), the samples corresponding to those chromatograms were analyzed using another chromatographic method (HILIC; see section 2,4,3) for better resolution (Fig 13). It was found from the analysis that *AfuLPMO11B* is a C1-oxidizing LPMO, as shown by comparison with a standard of C1-oxidized chito-oligosaccharides (In-house prepared [123]). It was interesting to see that both glycosylation variants of *AfuLPMO11B* produced similar amounts of oxidized products from α -chitin, while on β -chitin, the glycosylated enzyme produced nearly twice as much oxidized products. These potential quantitative differences are addressed in more detail, below.

Figure 14 shows a MALDI-TOF MS analysis performed on product mixtures generated from α - and β - chitin with glycosylated and deglycosylated *AfuLPMO11B*. The major peaks in the mass spectrum correspond to sodium adducts of aldonic acids and lactones, confirming that *AfuLPMO11B* indeed is a C1-oxidizing LPMO. C1 and C4 oxidation yield products with identical masses, and it would therefore be difficult to derive oxidation states by MS. C4 oxidation yield

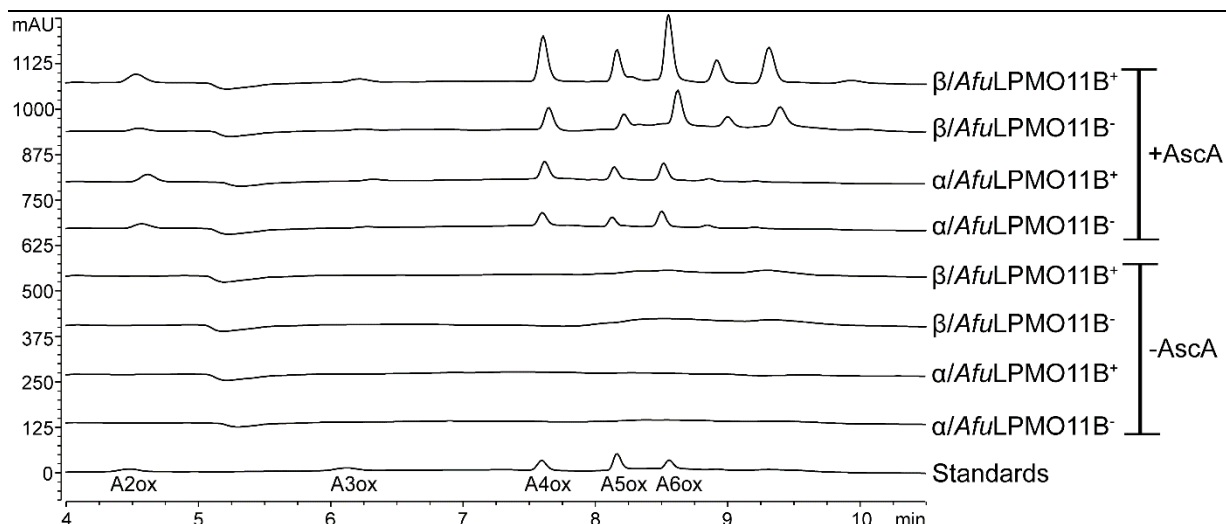


Fig 13. Chromatographic analysis of reaction products resulting from *AfuLPMO11B* activity on chitin substrates. The figure shows HILIC chromatograms of supernatants from overnight reactions carried out at 30 °C with glycosylated (+) and deglycosylated (-) *AfuLPMO11B* on α - and β -chitin respectively. The reaction mixtures contained 1 μ M enzyme and 0.6 % (w/v) substrate, in 50 mM Bis-tris buffer (pH 6.5), and were incubated at 1000 rpm in an Eppendorf Thermomixer. Reactions marked (+AscA) contained 1 mM ascorbic acid, while in reactions marked (-AscA) ascorbic acid was substituted with MQ-water. The bottom chromatogram shows oxidized standards standard mixture in-house generated [123] C1-oxidized chitooligosaccharides (GlcNAc)_nGlcNAc1A with a degree of polymerization (DP) DP1 – DP6 with 50 μ M of each). DP1 is not included in the chromatogram. The y-axis show UV absorption at 194 nm, in milli absorbance units (mAU); the x-axis shows time (min).

4-ketoaldoses that are in equilibrium with gemdiols, where both of these normally form single-sodium adducts. C1 oxidation however, yield lactone products, which further undergo hydrolysis, forming aldonic acids, where the latter dominates in equilibrium at neutral pH. The aldonic acid often result in sodium adduct salts, that include two sodium atoms, which yields characteristic m/z signals. If this sodium salts of sodium adducts are not observed in the MS spectra, it is likely that the oxidation occurred on C4 [95]. The masses (Fig 14) correspond to oxidized chitooligosaccharides with different DP, ranging from DP3 – DP7 ((GlcNAc)₍₂₋₆₎GlcNAc1A), (labeled A3ox – A7ox in the mass spectra), (see Table 8 for a mass list). As an example, the enlarged mass spectrum for the DP6 cluster (Fig. 14B) shows: m/z 1257, lactone, sodium adduct; m/z 1273 (minor signal), lactone, potassium adduct; m/z 1275, aldonic acid, sodium adduct; m/z 1291 (minor signal), aldonic acid, potassium adduct; m/z 1297, sodium salt of the sodium adduct of the aldonic acid; m/z 1313 (minor signal), salt of the aldonic acid with one sodium and one potassium. The other DP_n clusters look similar. Figure 14B also shows almost complete absence of native products (m/z 1259 for the sodium adduction of

DP6), although a slight deviation for the typical isotopic leaflet shape of the 1257 signal at 1259 (see Discussion section) shows that there is some native product. Furthermore, it is

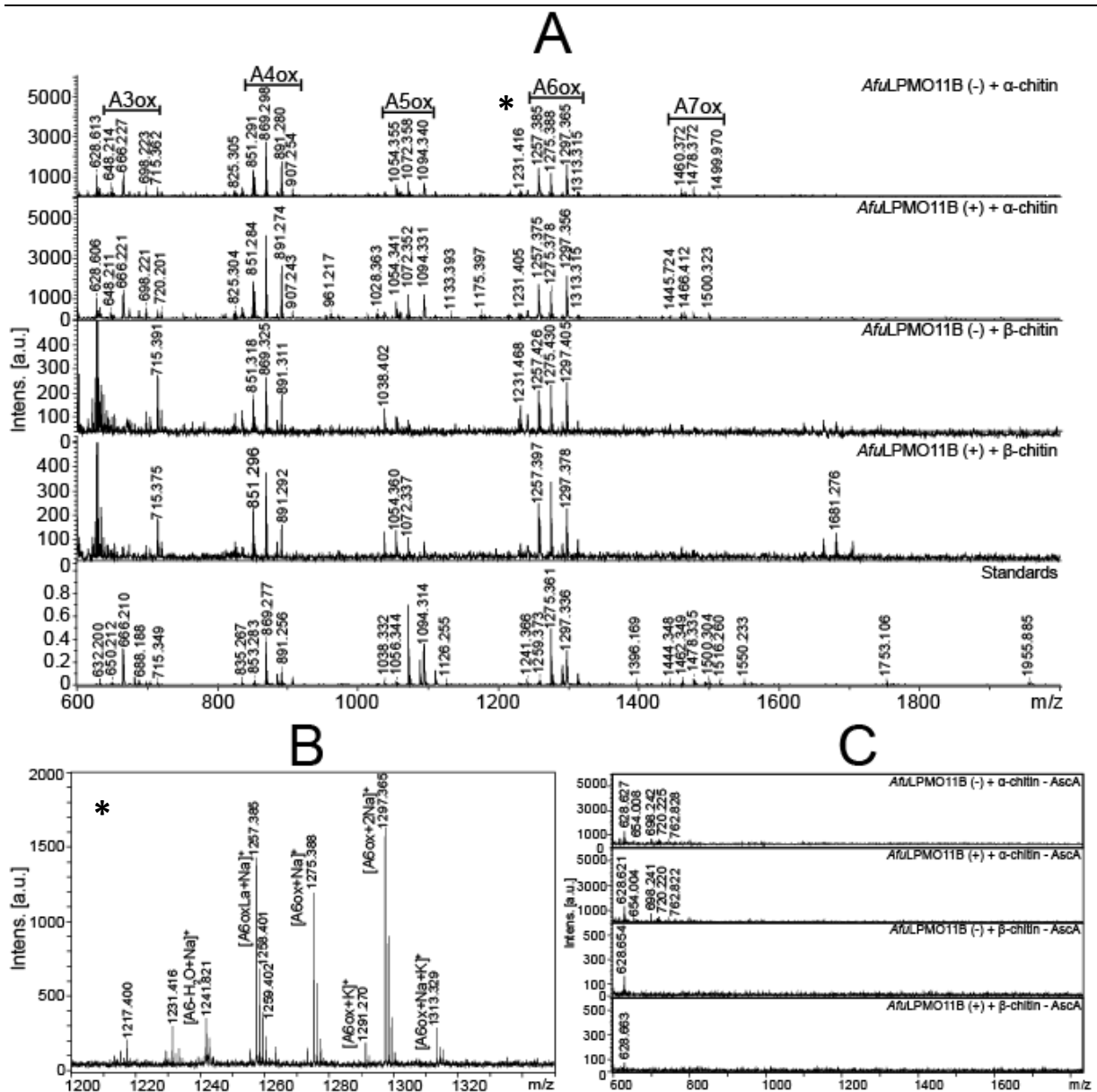


Fig 14. MALDI-TOF MS mass spectra of product mixtures generated by *AfuLPMO11B* from chitin. The analyzed product mixtures result from overnight reactions of 1 μ M glycosylated [(“+”)] or deglycosylated [(“−”)] *AfuLPMO11B* with 10 g/l substrate (α - or β -chitin), in the presence of 1 mM ascorbic acid, in 50 mM Bis-tris buffer (pH 6.5), at 30 °C and 1000 rpm, in an Eppendorf Thermomixer. Panel A show products from both substrates produced by both enzyme variants, respectively. Major masses correspond to sodium adducts of the aldonic acid- and the lactone-form as well as the sodium salt of the aldonic acid (see mass list in Table 8). The bottom mass spectrum in panel A shows oxidized standards with $\Delta DP_{n,ox} = 1 - 7$ (in-house prepared) [123]. Panel B provides a closer look at the DP6 (A6ox) product cluster from panel A (marked with an asterisk). Panel B elucidate masses that may represent non-oxidized native-, deacetylated oxidized-, oxidized – H + Na⁺+K⁺ adducts (see discussion). Panel C shows MALDI-TOF MS analysis of control reactions, that did not contain ascorbic acid.

Table 8. Calculated masses of a selection of possible LPMO products and their various adducts. The Table lists calculated masses (mass per charge, m/z) for various chitin-derived compounds (Product, Adduct type and Product name) commonly observed in product mixtures generated by LPMO action. The left column (DP) indicates the degree of polymerization. Adducts are identified as $[M + nX]^+$ or $[M - H + nX]^+$, where M = Product, H = Hydrogen, n = number of X = cations ($[Na]^+$ and/or $[K]^+$). The list includes some partially deacetylated species (GlcN = glucosamine).

DP	Mass per charge (m/z)	Product	Adduct	Product name
3	666.376	GlcNac ₂ GlcNac1A	$[M + Na]^+$	Aldonic acid
4	827.518	GlcNac ₂ GlcNGlcNac1A	$[M + Na]^+$	Aldonic acid
	851.416	GlcNac ₃ GlcNac1A	$[M + Na]^+$	Lactone
	869.419	GlcNac ₃ GlcNac1A	$[M + Na]^+$	Aldonic acid
	885.500	GlcNac ₃ GlcNac1A	$[M + K]^+$	Aldonic acid
	891.522	GlcNac ₃ GlcNac1A	$[M - H + 2Na]^+$	Aldonic acid
	907.372	GlcNac ₃ GlcNac1A	$[M - H + K + Na]^+$	Aldonic acid
5	1054.513	GlcNac ₄ GlcNac1A	$[M + Na]^+$	Lactone
	1072.523	GlcNac ₄ GlcNac1A	$[M + Na]^+$	Aldonic acid
	1088.631	GlcNac ₄ GlcNac1A	$[M + K]^+$	Aldonic acid
	1094.661	GlcNac ₄ GlcNac1A	$[M - H + 2Na]^+$	Aldonic acid
	1110.480	GlcNac ₄ GlcNac1A	$[M - H + K + Na]^+$	Aldonic acid
6	1191.633	GlcNac ₃ GlcN ₂ GlcNac1A	$[M + Na]^+$	Aldonic acid
	1207.767	GlcNac ₃ GlcN ₂ GlcNac1A	$[M + K]^+$	Aldonic acid
	1233.683	GlcNac ₄ GlcNGlcNac1A	$[M + Na]^+$	Aldonic acid
	1249.811	GlcNac ₄ GlcNGlcNac1A	$[M + K]^+$	Aldonic acid
	1257.693	GlcNac ₅ GlcNac1A	$[M + Na]^+$	Lactone
	1275.707	GlcNac ₅ GlcNac1A	$[M + Na]^+$	Aldonic acid
	1291.847	GlcNac ₅ GlcNac1A	$[M + K]^+$	Aldonic acid
	1297.865	GlcNac ₅ GlcNac1A	$[M - H + 2Na]^+$	Aldonic acid
	1313.718	GlcNac ₅ GlcNac1A	$[M - H + K + Na]^+$	Aldonic acid
	1329.852	GlcNac ₅ GlcNac1A	$[M - H + 2K]^+$	Aldonic acid
7	1460.931	GlcNac ₆ GlcNac1A	$[M + Na]^+$	Lactone
	1478.988	GlcNac ₆ GlcNac1A	$[M + Na]^+$	Aldonic acid
	1494.991	GlcNac ₆ GlcNac1A	$[M + K]^+$	Aldonic acid
	1516.970	GlcNac ₆ GlcNac1A	$[M - H + K + Na]^+$	Aldonic acid
8	1556.145	GlcNac ₄ GlcN ₃ GlcNac1A	$[M + Na]^+$	Aldonic acid
	1572.256	GlcNac ₅ GlcN ₃ GlcNac1A	$[M + K]^+$	Aldonic acid
	1598.168	GlcNac ₅ GlcN ₂ GlcNac1A	$[M + Na]^+$	Aldonic acid
	1614.367	GlcNac ₅ GlcN ₂ GlcNac1A	$[M + K]^+$	Aldonic acid
	1664.283	GlcNac ₇ GlcNac1A	$[M + Na]^+$	Lactone
	1682.320	GlcNac ₇ GlcNac1A	$[M + Na]^+$	Aldonic acid
	1698.339	GlcNac ₇ GlcNac1A	$[M + K]^+$	Aldonic acid
	1704.617	GlcNac ₇ GlcNac1A	$[M - H + 2Na]^+$	Aldonic acid
	1720.337	GlcNac ₇ GlcNac1A	$[M - H + K + Na]^+$	Aldonic acid
9	1885.705	GlcNac ₈ GlcNac1A	$[M + Na]^+$	Aldonic acid
	1901.980	GlcNac ₈ GlcNac1A	$[M + K]^+$	Aldonic acid
10	1920.756	GlcNac ₅ GlcN ₄ GlcNac1A	$[M + Na]^+$	Aldonic acid

possible that the signal at m/z 1241 represents a native product that has lost a water, as indicated in the Figure.

Figure 14A further shows that the glycosylated and the non-glycosylated forms of *AfuLPMO11B* yielded similar product profiles, whereas Fig. 14C shows that product formation did not occur in reactions without added ascorbic acid. Some LPMOs, such as *ScLPMO10B*, generate partially deacetylated oxidized species from chitin, likely because they preferably bind on partially deacetylated regions of the substrate ([129]. Such deacetylated species were not observed immediately, but the possibility of its presence in the mass spectra are further discussed in the Discussion.

3.1.4 Enzymatic H_2O_2 -Production

AfuLPMO11B produced H_2O_2 in the presence of ascorbic acid, with an apparent rate of $0.15 \mu M \text{ min}^{-1}$ (Fig 15). Similar rates have been demonstrated in similar reaction conditions for the

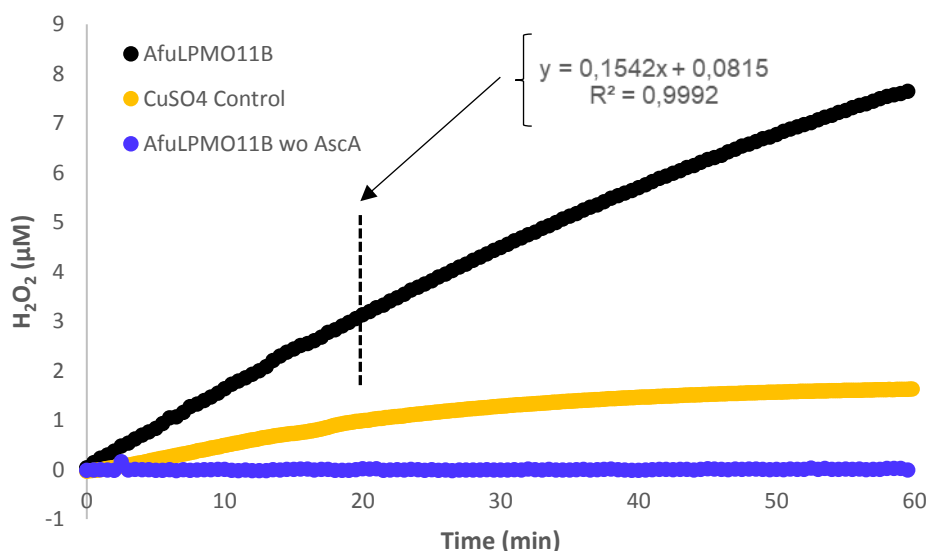


Fig 15. Enzymatic H_2O_2 production. The figure shows the apparent H_2O_2 production by $1 \mu M$ *AfuLPMO11B* in reactions without substrate, in the presence of $50 \mu M$ ascorbic acid in 50 mM Bis-tris (pH 6.5) in standard aerobic conditions at room temperature (black). LPMO was substituted with $1 \mu M$ $CuSO_4$ in control reactions (yellow). Ascorbic acid was substituted with MQ-water in another control reaction (blue). The experiment was performed in triplicates. The SD is not visible in the black and yellow curves as they reside behind the datapoints (closed circles). The SD of the control was excluded because of large variation between the triplets that disturbed the overall figure.

cellulose- and xyloglucan-active LPMO from *Gleophyllum trabeum* (*GtLPMO19B*), with an apparent production of $\sim 0.1 \mu M \text{ min}^{-1}$ [30]. It is important to consider that the *AfuLPMO11B*

stock used in the H₂O₂-production assay was of the lower quality enzyme batch (batch nr 1, Table 7), and the rates of produced H₂O₂ may therefore not be the same as for the higher quality enzyme batches (batch 2 or 3).

3.1.5 Melting Point Analysis

Glycosylation appeared to play a significant role in the thermal stability of *Afu*LPMO11B, in that the glycosylated protein was less stable than the deglycosylated protein (Fig 16). The glycosylated protein denatured with an apparent melting temperature of 54 °C, while the

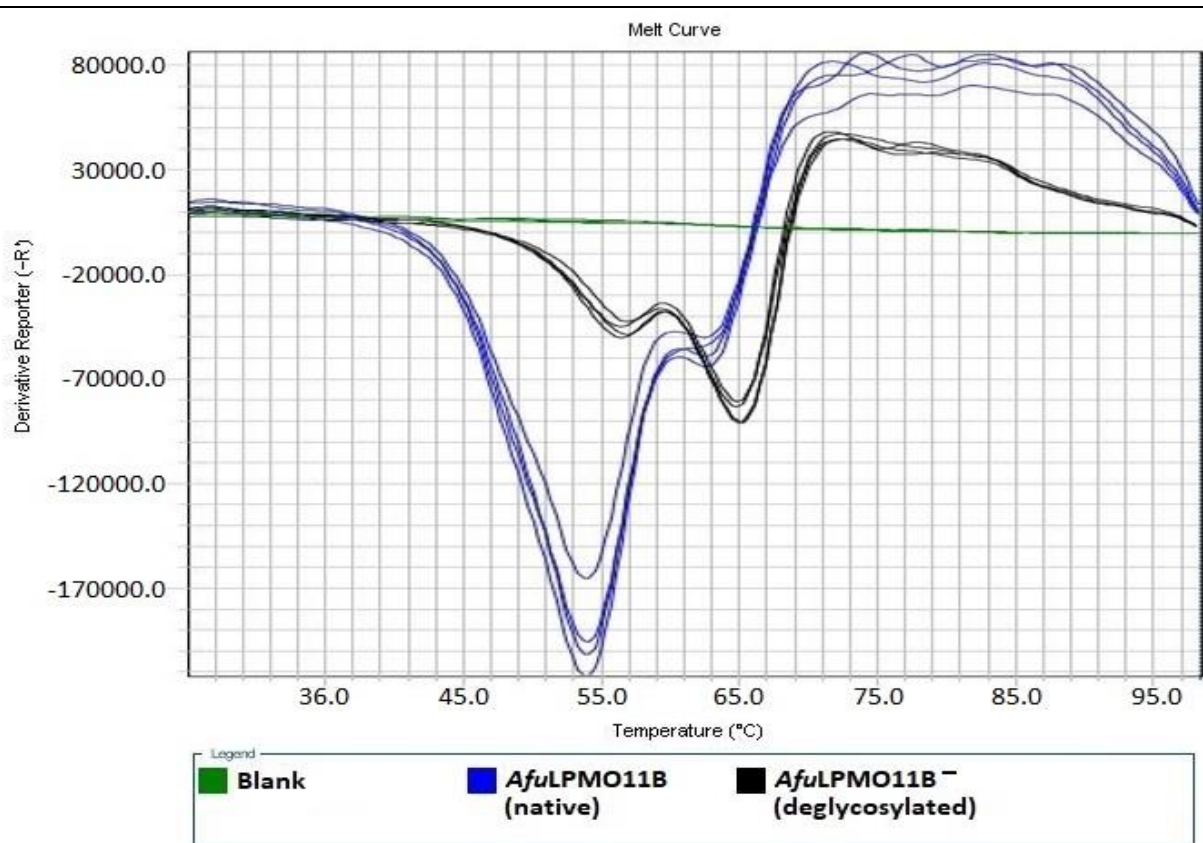


Fig 16. Melting of native and deglycosylated forms of *Afu*LPMO11B. The figure shows apparent melting temperatures for glycosylated/native (blue) and deglycosylated (black) *Afu*LPMO11B. melting curves were determined using the Protein Thermal Shift™ assay (Thermo Fischer Scientific), with real time PCR scanning fluorometry. The temperature was raised from 25 – 99 °C over ~ 56 minutes. The Y-axis indicates intensity of denaturation, whereas the X-axis shows temperature. The experiment was performed in quadruplicates. In blank samples (green), the enzyme solution was substituted with MilliQ-water.

deglycosylated protein showed an apparent melting temperature of 65 °C. There is also a difference in the denaturation or unfolding process between the two, as seen by the variation in the curve. The glycosylated protein denatures when approximating the critical temperature in a seemingly single step denaturation. The deglycosylated protein however, denatures in what appears to be a two step fashion.

3.2 Reaction kinetics & substrate binding

3.2.1 Temperature based activity screen on *AfuLPMO11B*

AfuLPMO11B showed linear product formation at 30 °C on α -chitin, and approximate linearity of product formation on β -chitin, during 24 hours of activity. At 30 °C, the apparent catalytic rate was 0.19 min⁻¹ and 0.34 min⁻¹, on α - and β -chitin, respectively (Fig 17). On α -chitin, activity

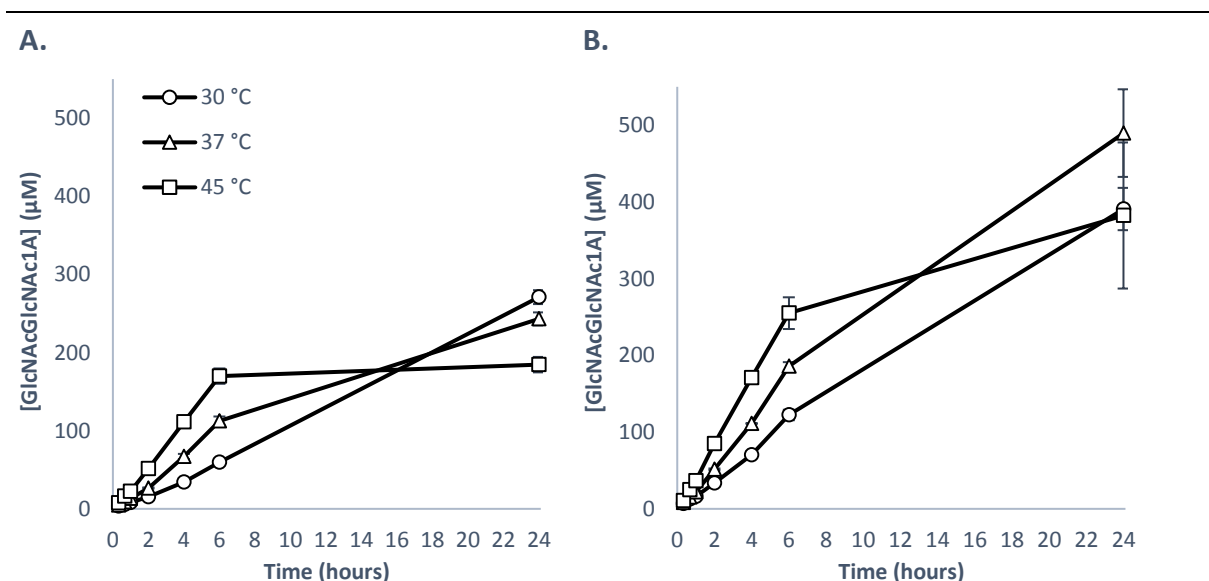


Fig 17. Effect of temperature on the activity of *AfuLPMO11B* (native) on α - and β -chitin. The figure shows progress curves of oxidized reaction products from LPMO activity. The products were converted to oxidized dimers (GlcNAcGlcNAc1A) by CHB treatment (see section 2.3.12). The products formed from reactions with *AfuLPMO11B* with α - (A) or β - (B) chitin. The reactions contained 1 μ M LPMO (glycosylated), 10 g/l substrate, 1 mM ascorbic acid, and 50 mM Bis-tris buffer (pH 6.5), and were incubated at 30, 37 or 45 °C, as indicated in the Figure, at 1000 rpm, in Eppendorf Thermomixers. In control reactions, ascorbic acid was substituted with MQ-water, and the resulting reaction mixtures gave no peaks in the chromatographic analysis (not shown). Error bars indicate standard deviation, n = 3 independent reactions.

stopped completely after 6 hours at 45 °C, but activity was somewhat more stable on β -chitin at the same temperature (Fig. 17). At 37 °C the enzyme showed lineare product formation for 6 hours on both substrates, but showed signs of inactivation within the intervall of 6 – 24 hours. Variation in the initial catalytic rate correlated to variation in temperature for both substrates, with an apparent increase in catalytic speed of $0.020\text{ }^{\circ}\text{C}^{-1}\cdot\text{min}^{-1}$ and $0.024\text{ }^{\circ}\text{C}^{-1}\cdot\text{min}^{-1}$, for α - and β -chitin, respectively. Because 30 °C showed linear product formation for 24 hours, this temperature was used in further activity experiments, in order to avoid complications by enzyme inactivation.

3.2.2 Comparison of *AfuLPMO11B* with another chitin-active LPMO, *BcLPMO10A*

To gain more insight into the activity of *AfuLPMO11B*, comparative studies were conducted using the chitin-active tetra-modular *BcLPMO10A* from *Bacillus cereus*. This enzyme was

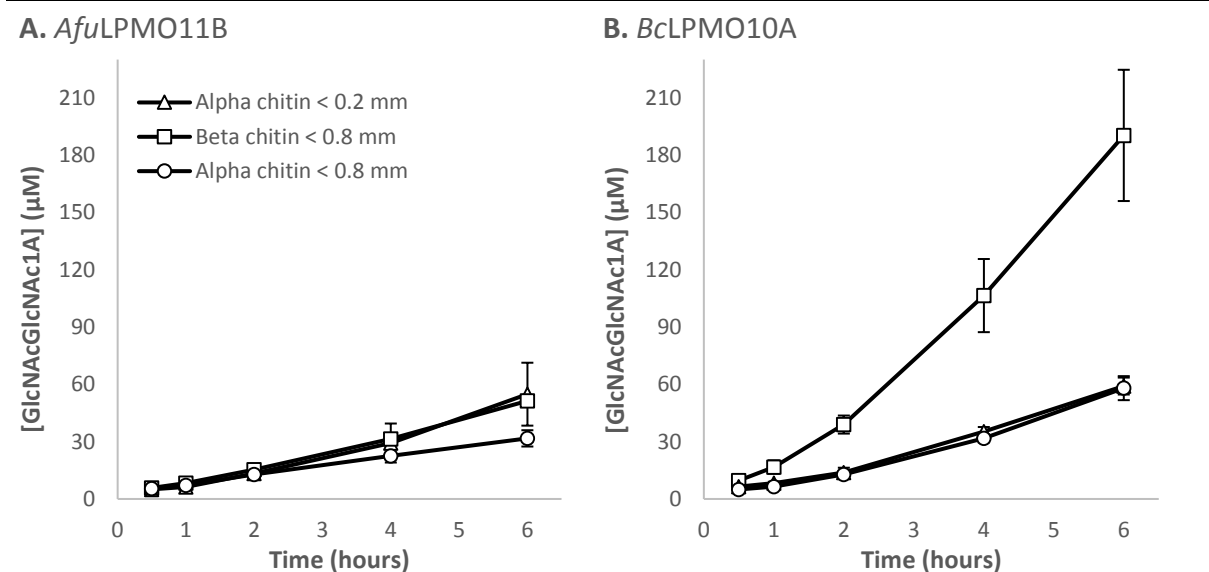


Fig 18. Comparative study of chitin-activity of an AA11 and an AA10 LPMO. The figure shows progress curves for the formation of oxidized products (GlcNAcGlcNAc1A), from reactions with *AfuLPMO11B* (A) and *BcLPMO10A* (B) reacting at 30 °C and 37 °C, respectively, and three different chitin substrates (< 0.2 mm and < 0.8 mm α -chitin, and < 0.8 mm β -chitin). The original reaction products were converted to oxidized dimers with CHB treatment before analysis (see section 2.3.12) The legend in panel A applies to both panel A and B. In the reactions, 0.5 μM LPMO reacted on 10 g/l substrate in the presence of 1 mM ascorbic acid, in 20 mM Bis-tris (pH 6.5) (A) and pH 6.0 (B), at 1000 rpm (A), or 800 rpm (B). In control reactions ascorbic acid was substituted with MQ-water, and no products were detected (not included in the figure). Error bars indicate standard deviations; n = 3 independent reactions.

chosen in the comparison study because it was previously tested in reactions with the same chitinase (*SmChi18C*) as in the synergy experiment in this study (Fig 20), and therefore operates as a good comparative reference in multiple experiments. Fig. 18 shows that *BcLPMO11B* was clearly more active β -chitin compared to *AfuLPMO11B*, and that the two enzymes were equally active on the two tested α -chitin substrates, with differing particle sizes. Thus, while *AfuLPMO11B* showed similar activities on all three substrates (Fig. 18A), *BcLPMO10A* had a clear preference for β -chitin.

3.2.3 The effect of N-glycosylations on catalytic rate

Fig. 19 shows that deglycosylation of *AfuLPMO11B* did not significantly alter the catalytic efficiency on β -chitin. On α -chitin however, the activity was drastically reduced to $\sim 50\%$, in terms of initial catalytic rate (Fig 19). Another interesting finding is that *AfuLPMO11B* in

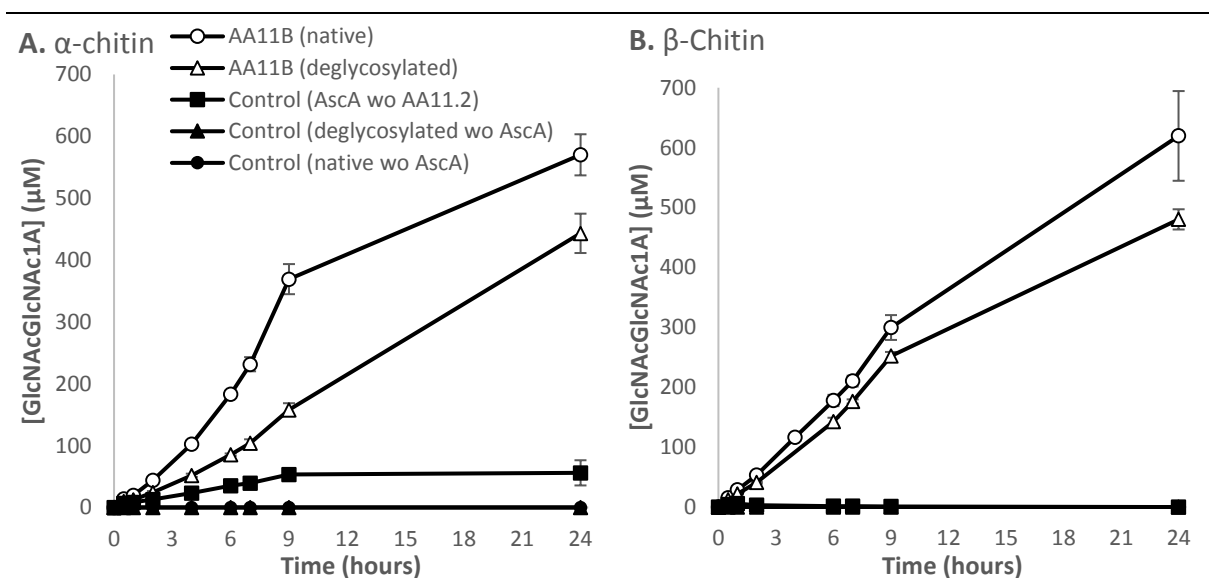


Fig 19. The effect of N-linked glycans on activity of *AfuLPMO11B*. The figure shows progress curves for the formation of oxidized products from LPMO reactions that were converted to oxidized dimers (GlcNAcGlcNAc1A) with CHB treatment (see section 2.3.12), produced by *AfuLPMO11B* with- (circles) and without (triangles) glycosylations, in reactions containing $1\ \mu\text{M}$ enzyme, $10\ \text{g/l}$ substrate and $1\ \text{mM}$ ascorbic acid in $50\ \text{mM}$ Bis-tris buffer (pH 6.5), at $30\ ^\circ\text{C}$ and $1000\ \text{rpm}$, incubated in an Eppendorf Thermomixer. Panel A shows solubilized products formed from α -chitin, while panel B shows product formation from β -chitin. In control reactions, ascorbic acid was substituted with MQ-water (black triangles, black circles), or the LPMO was substituted with MQ-water (black squares). The legend in panel A applies to both panels. Error bars indicate standard deviations; $n = 3$ independent experiments.

deglycosylated form is more active on β -chitin than on α -chitin, a common observation among other chitin-active LPMOs, such as *Sm*LPMO10A (CBP21) and *Bc*LPMO10A [45]. However, when glycosylated, *Afu*LPMO11B becomes more active on α -chitin than on β -chitin (Fig 19). In a control reaction, which included ascorbic acid, but without enzymes, substantial amounts of oxidized products were formed in the reaction with α -chitin only. It is currently unclear why this occurred, but oxidation of the substrate could perhaps be caused by transition metals within the substrate interacting with the reductant and generating powerful reactive oxygen species.

3.2.4 Synergy between the LPMO and a chitinase

When combining *Afu*LPMO11B (glycosylated) and chitinase-C (*Sm*Chi18C (ChiC)), an endochitinase from *Serratia marcescens*, synergy was clearly demonstrated in reactions with both α - and β -chitin (Fig 20). Combination of the enzymes yielded linear product formation for 24 hours in reactions with α -chitin, while the enzymes individually appeared to be inactivated or inhibited after 9 hours, particularly ChiC. After 24 hours, less than 5 % of α -chitin was converted to GlcNAc by the LPMO or ChiC alone, whereas more than 30 % conversion was reached upon combining the two enzymes, indicating a large synergistic effect. Figure 20A shows that addition of the LPMO after 6 hours led to an immediate boost in GcNAc release. Figure 20 D shows that reaction with both enzymes had a beneficial effect of the generation of LPMO products, with an apparent increase of 100%, i.e., 1.3 % to 2.6 % of oxidized dimers of the theoretical maximum.

Synergetic effects were also observed in the degradation of β -chitin (Fig 20B & D), but, in this case conversion was faster and ChiC alone was much more effective, compared to α -chitin. In reactions combining *Afu*LPMO11B and ChiC 85 % substrate conversion was reached after 9 hours, followed by an apparent stop in product formation. It is important to consider that the maximum conversion values may be inaccurate, due to the difficulty to evenly distribute these crystalline non-homogenous substrate suspensions in reactions.

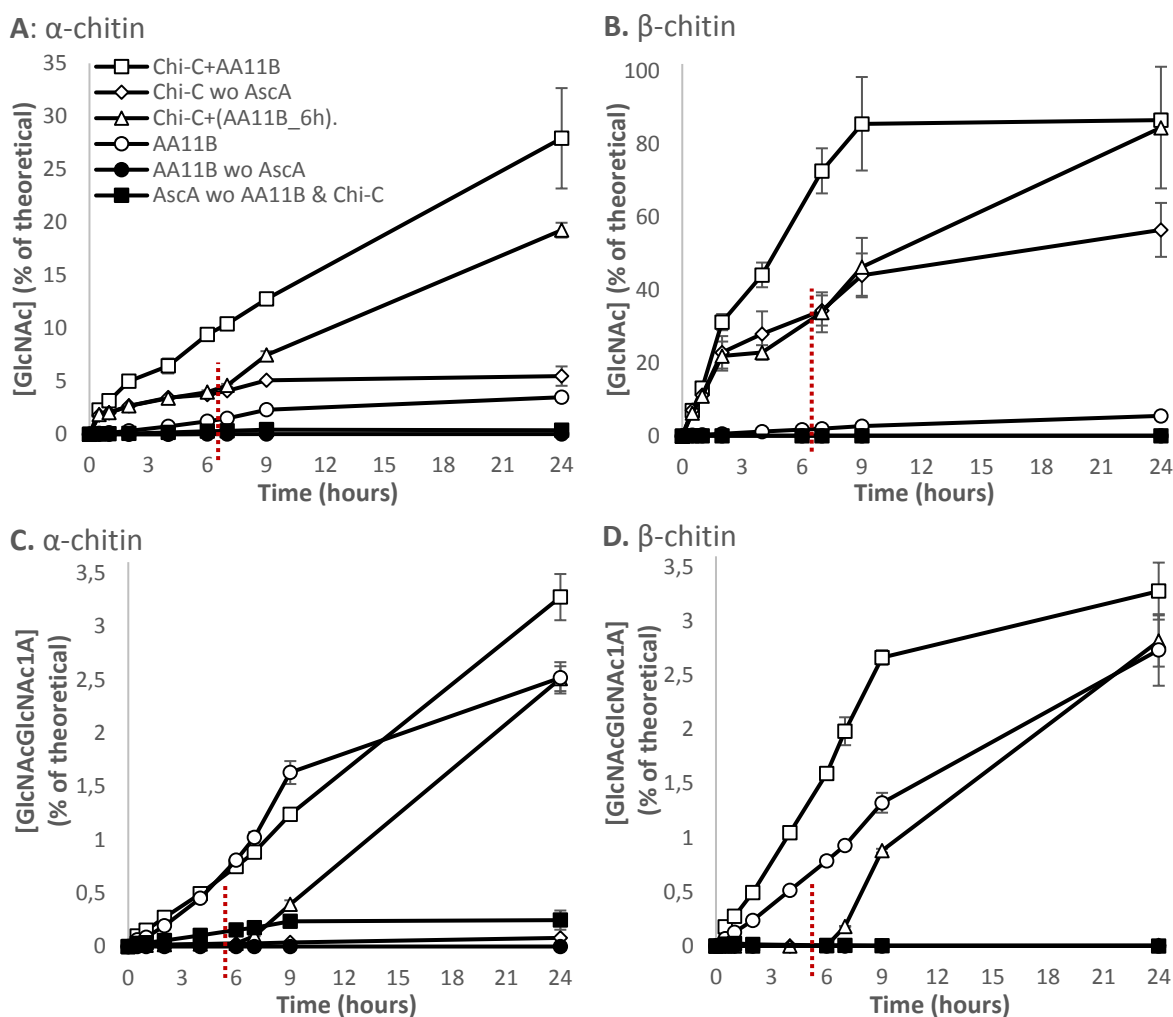


Fig 20. Synergy with *AfuLPMO11B* and Chitinase-C. The figure shows progress for product formation in reactions with glycosylated *AfuLPMO11B* and *SmChi18C* (ChiC), alone or in combination, as indicated in the graph. Original reaction products were treated with CHB (see section 2.3.12). The open triangles apply to a reaction, where the LPMO was added after 6 hours (6 h point, indicated by red dotted lines). Product formation is displayed as % conversion, relative to the theoretical value of complete substrate conversion to monomers (GlcNAc) in panel A and B, and oxidized dimers (GlcNAcGlcNAc1A) in panel C and D. The figure shows progress curves for α -chitin (panel A and C), and β -chitin (panel B and D). The legend in A applies to all panels (A, B, C, and D). Reactions contained 1 μ M LPMO and/or 1 μ M ChiC, reacting with 10 g/l substrate, in the presence of 1 mM ascorbic acid, in 50 mM Bis-tris buffer (pH 6.5), at 30 °C and 1000 rpm, incubated in an Eppendorf Thermomixer. The reactions with only ChiC (diamonds) did not contain ascorbic acid, and in reactions with LPMO addition after 6 hours (triangles), ascorbic acid was added together with LPMO. In control reactions with LPMO only (black circles), ascorbic acid was substituted with MQ-water, and in control reactions with no enzymes (black squares), enzymes were substituted with MQ-water, but ascorbic acid was present with the substrate. Error bars indicate standard deviations; n = 3 independent reactions.

3.2.5 Activity of *AfuLPMO11B* with feeding of H_2O_2 feeding

Fig 21 shows the activity of *AfuLPMO11B* on β -chitin in reactions with added H_2O_2 . Panel A, with H_2O_2 additions every 15 minutes, shows a direct correlation between the amount of H_2O_2 added and product formation. The apparent inactivation after three hours in panel A was not caused by protein denaturation, but because H_2O_2 was no longer added after this time-point. With reference to the control reaction (diamonds) panel A (no added H_2O_2 , only 1 mM AscA), the enzymes using H_2O_2 still seem to be functional after three hours, as the slow product formation rate after three hours is similar to the rate in the control reaction.

Figure 21 B shows progression curves of oxidized products using higher H_2O_2 concentrations. *AfuLPMO11B* showed approximately linear product formation for up to five hours with as much as 80 μM H_2O_2 added every 15 min, although the amount of oxidized products now was considerably lower than the H_2O_2 input. In reactions with more than 80 μM H_2O_2 , i.e. 120 μM and 200 μM H_2O_2 added every 15 min, the LPMO inactivated within two and one hour(s) respectively.

To further assess the role of H_2O_2 , we tested the effect of enzyme concentration. Fig. 21C shows reactions in which 40 μM H_2O_2 was added every 30 min, with different LPMO concentrations. The critical limit appeared to be at 0.2 μM LPMO, since only at concentrations below 0.2 μM there was a clear effect of the enzyme dosage of product formation. At higher enzyme concentrations, the catalytic rate no longer correlated to the LPMO concentration, indicating that another factor, likely the amount of added H_2O_2 , was limiting the reaction. In the reaction with 0.2 μM LPMO, the amount of oxidized products after four hours (appr. 360 μM) was similar to the amount of added H_2O_2 (appr. 360 μM). The slight excess of oxidized products, which is more prominent in reactions containing 0.4 μM and 1 μM LPMO, can be correlated to product formation driven by molecular oxygen, as seen in the 1 μM LPMO control reaction without H_2O_2 (diamond) in panels A, B and C. Interestingly, in this case, one would assume an effect of the LPMO concentration, since the LPMO likely generates its own H_2O_2 from oxygen, which would be rate-limiting. This is indeed observed.

Fig. 21D shows an experiment done to find the number of cycles *AfuLPMO11B* could catalyze after ("priming") reduction by ascorbic acid. Surprisingly (In light of the assumed LPMO mechanism; Fig. 5), the ability of the LPMO to convert the supplied H_2O_2 into products was highly dependent on the ascorbic acid concentration.

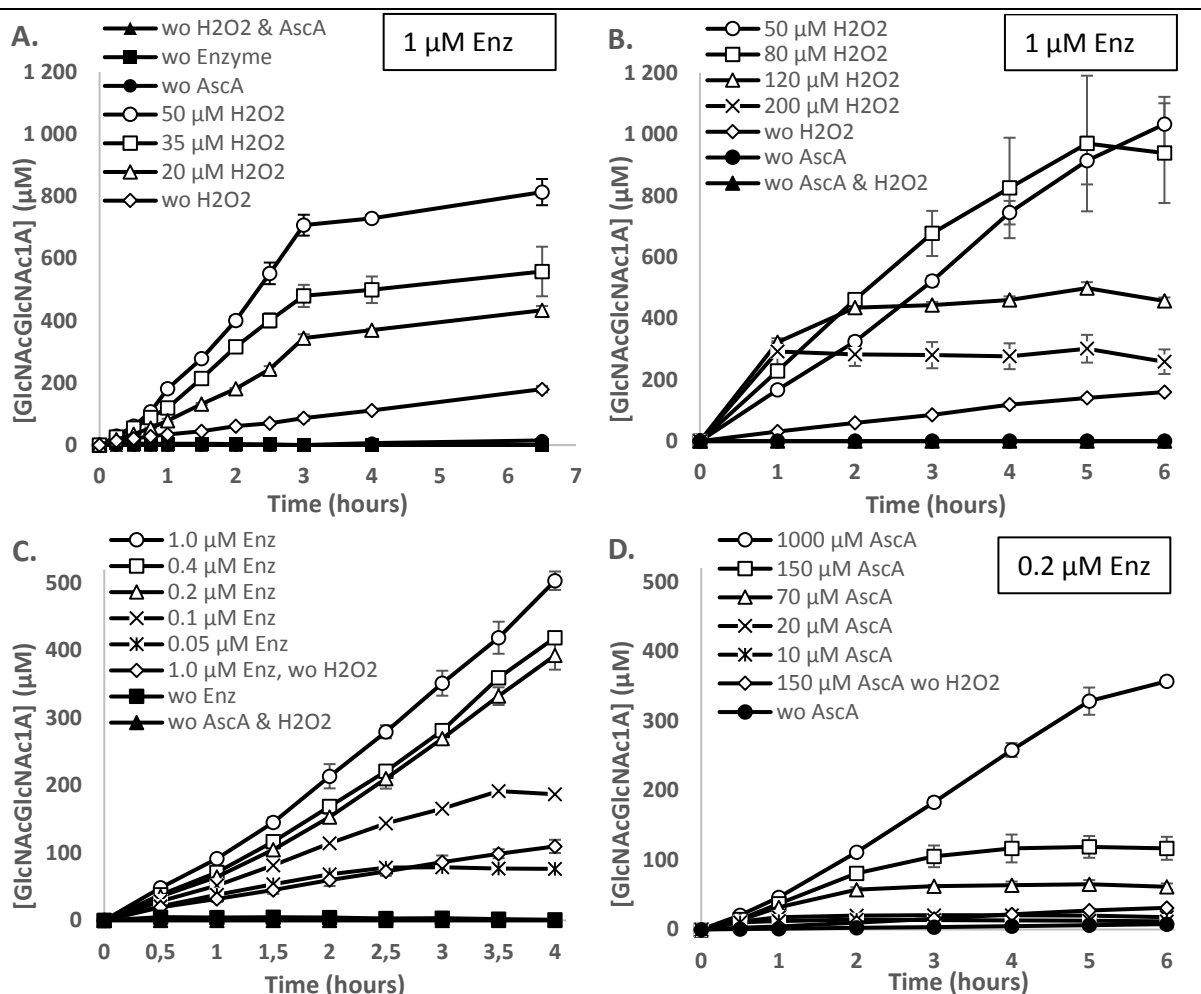


Fig 21. Optimization of H₂O₂ feeding regimes with *AfulPMO11B*. The figure shows oxidized product formation that were (GlcNAcGlcNAc1A) in reactions with *AfulPMO11B* using H₂O₂ as catalytic co-substrate and β-chitin as substrate. The original reaction products were treated with CHB (see section 2.3.12). All reactions were performed with 10 g/l substrate, 50 mM Bis-tris (pH 6.5), at 30 °C, and 1000 rpm, incubated in an Eppendorf Thermomixer. The other reagents differed between the panels; ascorbic acid was only added at time zero. (A) 1 μM LPMO reacting with 1 mM ascorbic acid, and various H₂O₂ concentrations (0, 20, 35, and 50 μM) added every 15 min up to 3 hours. In control reactions, H₂O₂ and ascorbic acid were substituted with MQ-water (black triangles) or the LPMO was substituted with MQ-water (black squares). In the reaction with no ascorbic acid (“wo AscA”), ascorbic acid was substituted with MQ-water and 50 μM H₂O₂ was added every 15 min, for three hours. (B) Similar reaction conditions to that in panel A, but with use of higher concentrations of H₂O₂ (50, 80, 120, and 200 μM) added every 15 minutes up to 6 hours. (C) Reactions contained 1 mM ascorbic acid, were supplied with 40 μM H₂O₂ every 30 min up to 4 hours, and contained varying LPMO concentrations (0.05, 0.1, 0.2, 0.4, 1.0 μM). Control reactions were as in panels A and B. (D) Reactions with 0.2 μM LPMO, supplied with 40 μM H₂O₂ added every 30 min for 6 hours, and with varying concentrations of ascorbic acid (10, 20, 70, 150, and 1000 μM) added at time zero. All panels (A, B, C, D) show control reactions (wo H₂O₂) corresponding to the LPMO reacting under normal aerobic conditions without H₂O₂ (diamonds), where 1 μM LPMO and 1 mM ascorbic acid were used in panels A, B, and C, while 0.2 μM LPMO and 150 μM ascorbic acid were used in panel D. The order of the addition of reagents at reaction initiation (time zero), was 1, LPMO; 2, ascorbic acid; 3, H₂O₂ in panel A, B and C. In panel D, the reaction was initiated as follows: 1, LPMO; 2, H₂O₂; 3, ascorbic acid. Error bars indicate standard deviations; n = 3 independent reactions.

Because of this unexpected finding, another experiment was performed with a low amount of AscA and varying concentrations of H₂O₂. The results, depicted in Fig. 22, shows that under these conditions, product formation was primarily limited by the amount of ascorbic acid, since final product levels resembled the amount of ascorbic acid added and were much lower than the amount of added H₂O₂. This observation confirms that the “priming” mechanism described in the Introduction, implying that a reduced LPMO can catalyze multiple reactions with H₂O₂ without a need for re-reduction, may not hold for *AfuLPMO11B*.

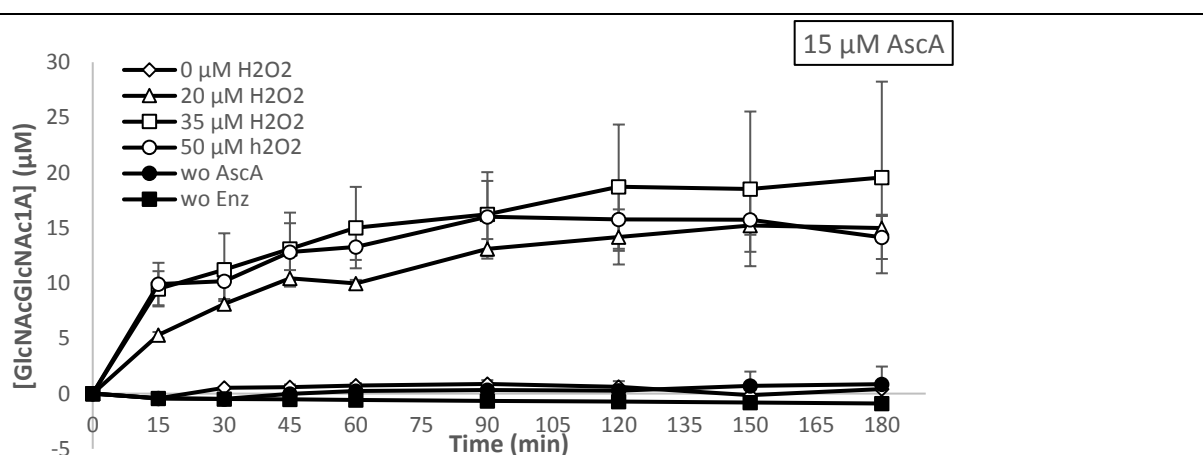


Fig 22. *AfuLPMO11B* reacting with H₂O₂ and 15 µM ascorbic acid. The figure shows oxidized product formation from β-chitin by *AfuLPMO11B* reacting with 0, 20, 35, and 50 µM H₂O₂ respectively, added every 15 min for 3 hours. The reactions contained 1 µM LPMO, 15 µM ascorbic acid and 10 g/l substrate, in 50 mM Bis-tris (pH 6.5) and were incubated at 30 °C, and 1000 rpm, in an Eppendorf Thermomixer. Ascorbic acid was only added at time zero. Reactions were initiated by adding reactants in the following order: 1, LPMO; 2, ascorbic acid; 3, H₂O₂. In control reactions, ascorbic acid was substituted with MQ-water (black circles), or the LPMO was substituted with MQ-water (black squares). Error bars indicate standard deviations; n = 3 independent reactions.

3.2.5.1 Product profile variations in LPMO reactions with H₂O₂

Both oxidized and non-oxidized products were quantified for the progress curves shown in panel Fig. 21A. Since soluble products generated by the LPMO were treated with chitinase before quantification, the oxidized products were only GlcNAcGlcNAc1A, which is *N,N*-diacetylchitobiose with a lactone or aldonic acid group on Carbon 1. The non-oxidized products were regular monomers of *N*-acetylglucosamine (GlcNAc) or DP1. We

analyzed the relative abundance of these two products in time in the various reactions depicted in Fig. 21A, since the ratios between the two provides information about average product length (longer products give more GlcNAc per GlcNAcGlcNAc1A). This approach was performed to see possible variations in the product profile due to different concentrations of H₂O₂. From the results, it was estimated that reactions containing no H₂O₂ released the longest oxidized products, with an average length of DP7.4, and that product length decreased with increasing H₂O₂ concentrations (Fig. 23A).

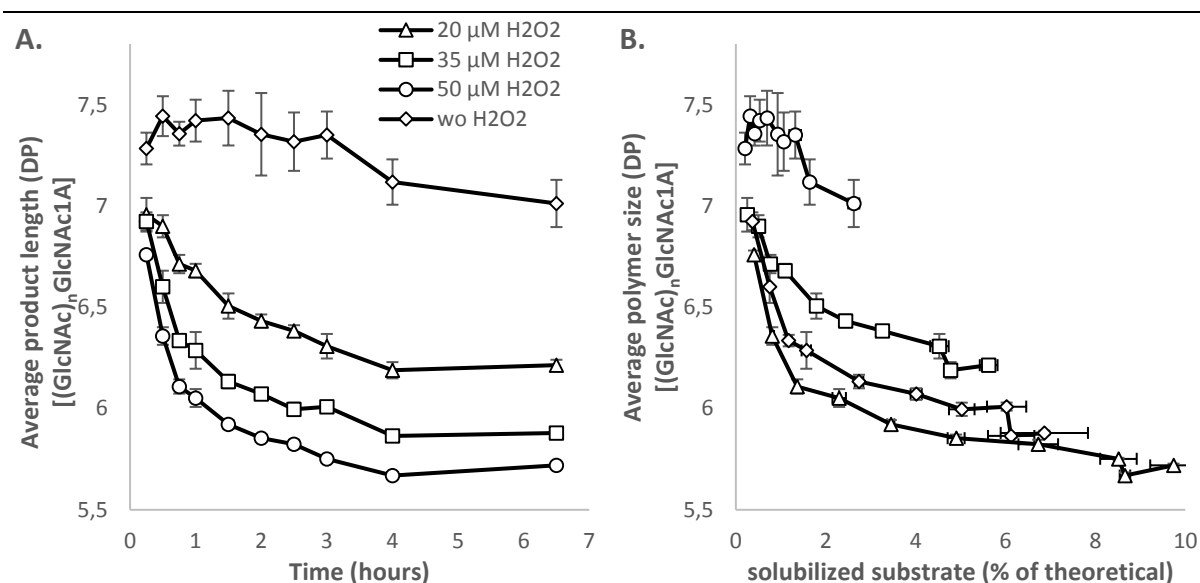
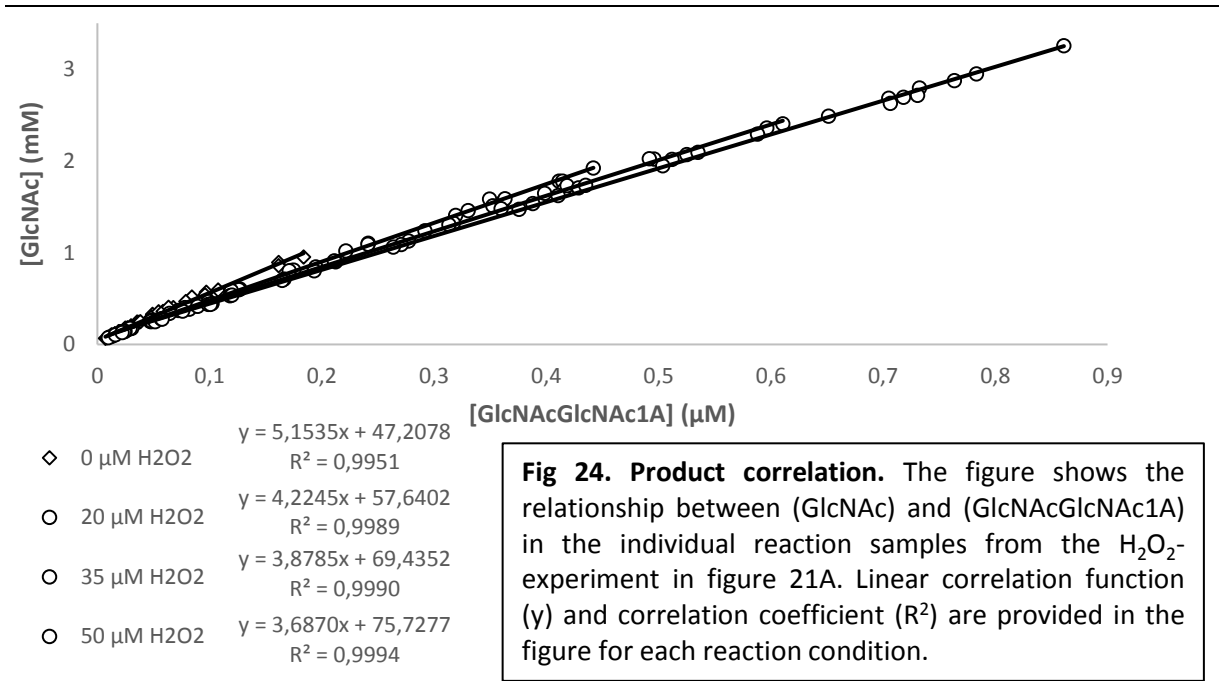


Fig 23. Estimated length of released oxidized products in H₂O₂ feeding reactions. The figures show the estimated degree of polymerization (DP) of solubilized products in H₂O₂ feeding reactions with varying H₂O₂ concentrations, as indicated. The estimate is based on quantification of the oxidized dimer (GlcNAcGlcNAc1A) and native monomer (GlcNAc) from reactions shown Figure 21A (the GlcNAc data are not shown in that Figure). Calculations for the estimates are described in section 2.5.5 (methods). Panel B shows the same average degree of polymerization, but now plotted against the degree of substrate decomposition (solubilized substrate in % of theoretical maximum). The legend shown in panel A applies to both panels. Error bars indicate standard deviations; n=3 independent experiments.

As the length of released products may depend on the degree of substrate degradation, the estimated product lengths were also plotted against the degree of substrate degradation (Fig. 23B). Results depicted in Figure 23B, indicate that the observed difference in length of released products is not a result of the degree of substrate degradation, but rather an effect

caused by different concentrations of H₂O₂. Figure 24 illustrate simple correlations between between measured oxidized dimers (GlcNAcGlcNAc1A) and native monomers (GlcNAc) from



individual reaction samples from the H₂O₂ experiment depicted in Figure 21A (without negative controls). In contrast to Figure 23, the variation in product relativity between oxidized dimers and native monomers appears to be of little significance.

3.2.6 Substrate binding

AfuLPMO11B showed variations in substrate binding, between the reduced and non-reduced state, the glycosylated and deglycosylated state, and the type of substrate, α- or β-chitin substrates (Fig 25). Enzyme activity was also measured in these reactions (Fig. 25A; for reactions with AscA only).

It appears that, in the reduced (active) state, glycosylated *AfuLPMO11B* binds better initially than the deglycosylated form to β-chitin, but the deglycosylated enzyme perhaps binds slightly better to α-chitin. In the non-reduced form, there is a clear difference in binding between α- and β-chitin for glycosylated *AfuLPMO11B*, while for the deglycosylated enzyme

binding appear to be similar on both substrates. The progress curves of panel A (Fig 25) show that LPMO activity stops after 2 hours on β -chitin with the native LPMO and this is accompanied by a reduction in binding (panel B). Likewise, panel C shows that binding decreases as the catalytic activity on β -chitin becomes lower. With α -chitin however, although activity stopped at early timepoints for both LPMO variants, binding appeared relatively unaffected.

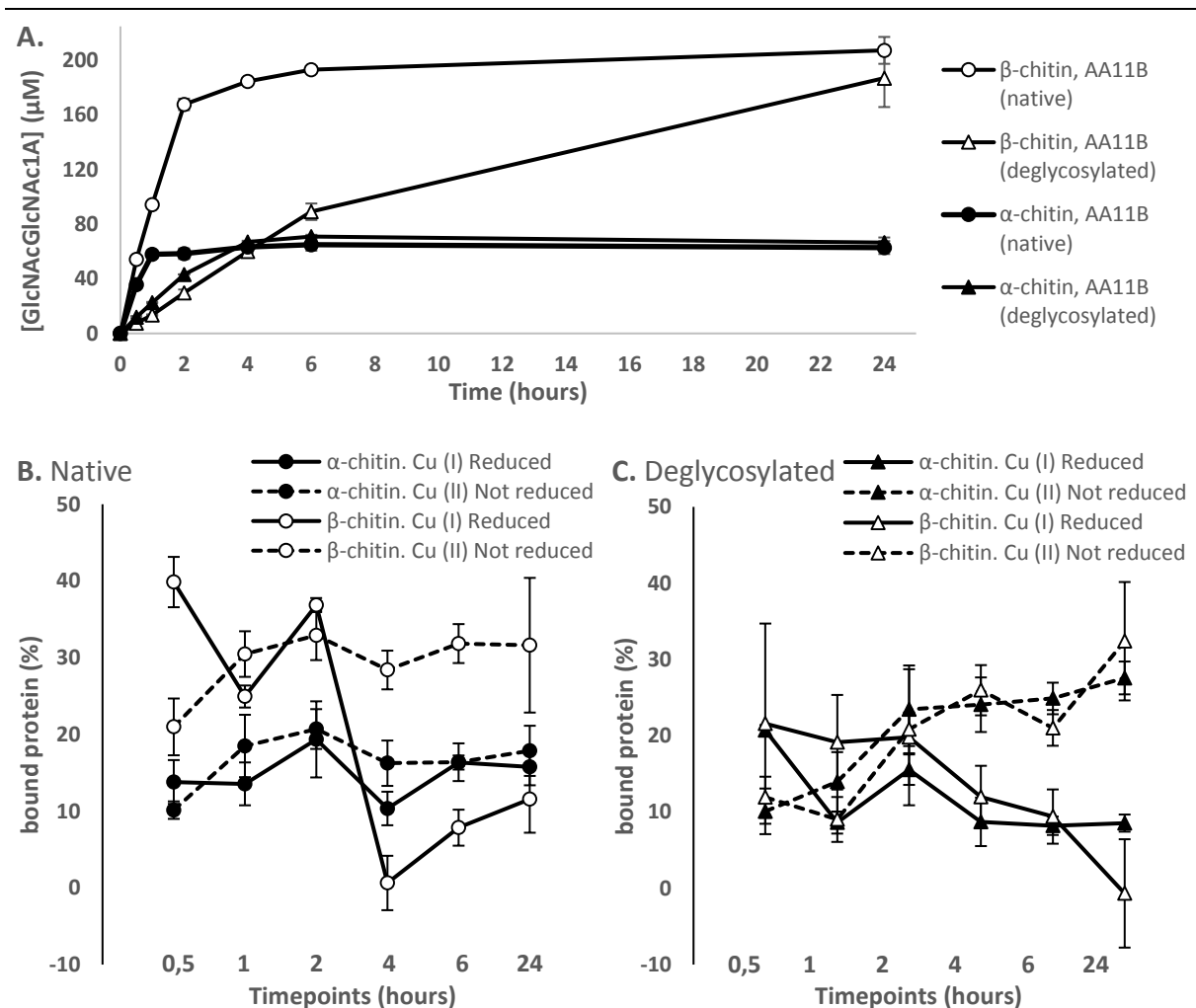


Fig 25. Binding analysis coupled with catalytic activity assay. The figure shows binding (B and C) and oxidized product formation (A) by *Afu*LPMO11B, derived from the same reaction samples. Panel A shows the formation of oxidized chitin dimers (GlcNAcGlcNAc1A) formed from α - and β -chitin in reactions with the glycosylated and deglycosylated enzyme. Original reaction products were treated with CHB (see section 2.3.12). Panels B and C indicate % bound protein as determined by SDS-PAGE analysis of reaction supernatants. Panel B shows binding data of the native (glycosylated) *Afu*LPMO on both substrate types in reduced (full line; presence of AscA) and non-reduced (dotted line; absence of AscA) form. Panel C shows the same experiment for the deglycosylated enzyme. The reactions contained 2.95 μ M glycosylated or 2.37 μ M deglycosylated LPMO, 2 g/l α - or β -chitin, in the presence (“Reduced”) or absence (“Not reduced”) of 1 mM ascorbic acid, in 50 mM Bis-tris (pH 6.5), at 30 °C and

1000 rpm, and were incubated in an Eppendorf Thermomixer. Error bars indicate standard deviations; n = 3 independent experiments. Note that the X-axis in panels B and C are not linear.

Fig. 26 illustrates how binding was quantified using SDS-PAGE. The percentage bound protein depicted in Fig. 25 was calculated by the relative fluorescent intensity in reaction supernatants from reactions containing substrates, and the control reactions which do not contain substrates. The average value of the control reactions was used as 100 % unbound protein standards. The measured value in reactions containing substrates was therefore divided by the average control value, and multiplied by 100 %. This results in % unbound protein, that were simply inverted to % bound protein.

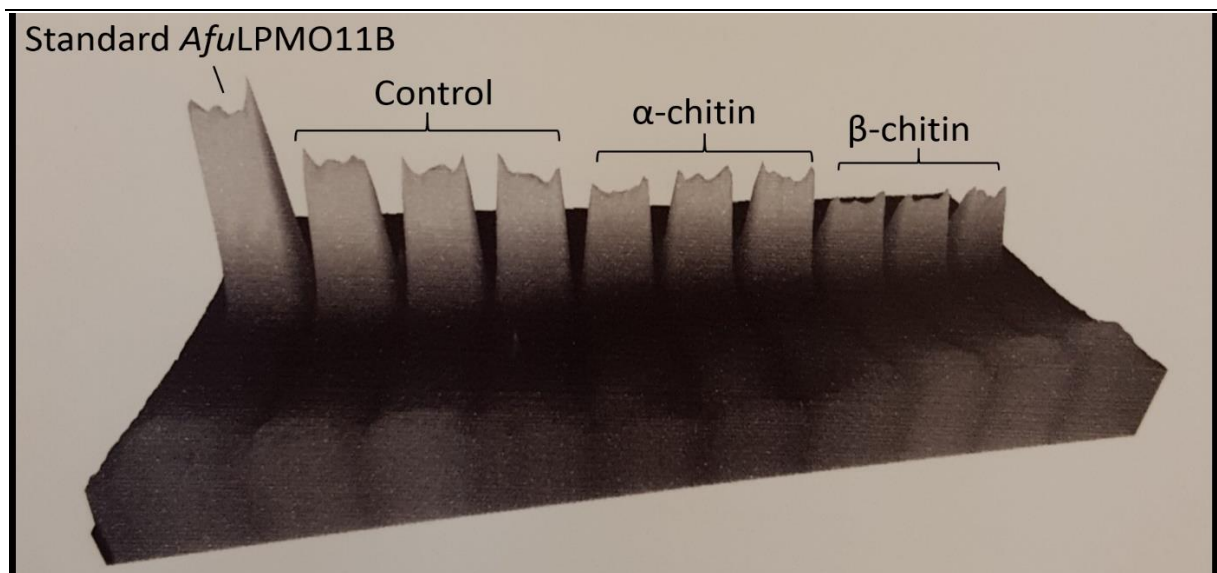


Fig 26. Example of SDS-PAGE binding data. The figure shows an example of the relative difference in protein band UV absorbance on an SDS-PAGE gel (10-well Mini PROTEAN® TGX Stain-Free™ Gel image) from a sample with 2.95 μM glycosylated *AfuLPMO11B* reacting with 2 g/l α - and β -chitin in the presence of 1 mM AsCA in 50 mM BIS-Tris (pH 6.5) at 30 °C and 1000 rpm, after incubation for 0.5 h in an Eppendorf Thermomixer. The lanes: (1) = 3.59 μM *AfuLPMO11B* standard (glycosylated, -upper limit of standards curve, Appendix A, Fig A1). (2, 3, 4) = control reaction with no substrate or ascorbic acid, (5, 6, 7) = reaction with α -chitin, (8, 9, 10) = reaction with β -chitin. This gel shows unbound protein after 0.5 hour from reactions that are also depicted in Figure 25B [Native – Cu(I) Reduced].

3.3 Crystallization of *AfuLPMO11B*

Stock solutions of purified *AfuLPMO11B* with high protein concentrations (~ 20 g/l) were produced and both glycosylated and deglycosylated versions of *AfuLPMO11B* were used for crystallization trials. The glycosylated protein did not yield crystals until several months after the hanging drop screening was initiated, and at the time of crystal formation, several wells were dried out. The deglycosylated protein showed crystal formation early on after the assembly of the hanging drop screening. Pictures of several crystals are shown in Fig C1 (Appendix C).

3.3.1 Crystal screening kit

Table 9 shows the results of a primary screening with glycosylated and deglycosylated *AfuLPMO11B*, performed with crystal screening kit JCSG-plus™ MD 1-37, using the hanging drop crystallization assay. Crystallization conditions are referred to as 1-n or 2-n where n is any number from 1-48, as these are the labels applied by the screening kit supplier. One

Table 9. Crystallization screening. The Table shows various crystallization conditions from the crystal screening kit *JCSG-plus™ MD 1-37 (box 1 & 2)*, which were tested in a hanging drop crystallization assay, where, eventually, crystals were formed in most samples, both with *glycosylated (+)* and *deglycosylated (-)* *AfuLPMO11B*. Details of the conditions are specified in Table D1 (Appendix D) The crystallization setup is described as follows: crystallization sample number (*N*), crystallization condition (*Tube#*), Enzyme stock concentration (*Enz. g/l*), hanging drop size (*Drop μl*), protein glycosylation status (*Glc. +/-*), approximate crystal formation period (*Time: ~ months*), and description of observed crystals (*Crystal description: Nr. – crystal system – Size*), where *Nr.* is the number of crystals, *Crystal system* describes the apparent crystal system mainly within the 7 main crystal-system categories [110], and *Size* indicates a relative size. Highlighting in grey indicates conditions that yielded putative protein crystals, and that were reproduced in an expanded crystallization assay.

<i>N</i>	<i>Tube#</i>	<i>Enz. g/l</i>	<i>Drop μl</i>	<i>Glc. +/-</i>	<i>Time: ~ months</i>	<i>Crystal description: Nr. – Crystal-system – Size</i>
1	1-2	11	1	+	4	3 – Orthorhombic – Big
2	1-3	11	1	+	4	1 – Non specific – Medium
3	1-5	11	1	+	6	4 – Tetragonal – Tiny
4	1-12	11	1	+	2	2 – Tetragonal – Medium
5	1-15	11	1	+	6	1 – Cubic – Small
6	1-19	11	1	+	4	4 – Triclinic – Medium
7	1-27	11	1	+	4	1 – Non specific – Medium
8	2-1	11	1	+	2	4 – Cubic – Small
9	2-13	11	1	+	4	1 – Non specific – Large
10	2-31	11	1	+	4	1 – Orthorhombic – Small
11	1-2	22	1	+	5	1 – Non specific – Medium

12	1-3	22	1	+	3	2 – Tetragonal – Medium
13	1-9	22	1	+	5	1 – Orthorhombic – Small
14	1-15	22	1	+	5	9 – Cubic – Medium
15	1-26	22	1	+	5	1 – Cubic – small
16	1-27	22	1	+	5	2 – Orthorhombic – Medium
17	1-35	22	1	+	4	>10 – Orthorhombic – Variation
18	1-40	22	1	+	2	3 – Orthorhombic – Small
19	1-2	20	1.5	-	1	1 – Tetragonal – Medium
20	1-8	20	1.5	-	1	1 – Hexagonal – Big
21	1-13	20	1.5	-	2	>100 – Small microcrystalline drops – Tiny
22	1-14	20	1.5	-	2	1 – Non specific – Big
23	1-15	20	1.5	-	2	1 – Cubic – Huge
24	1-19	20	1.5	-	3	1 – Orthorhombic – Big
25	1-21	20	1.5	-	1	>5 – Clustered hexagonal plates – Big
26	1-25	20	1.5	-	1	>5 – Clustered square plates – Big
27	1-28	20	1.5	-	3	1 – Cubic – Large
28	1-35	20	1.5	-	2	4 – Snow flakes – Huge
29	1-40	20	1.5	-	0.5	7 – Irregular sharp squares – Big
30	2-8	20	1.5	-	2	1 – Boat like – Huge
31	2-22	20	1.5	-	0.5	1 – rose flower like – big
32	2-26	20	1.5	-	0.2	1 – Cubic – huge
33	2-29	20	1.5	-	1	1 – clustered branches 90° – big
34	2-38	20	1.5	-	1	>30 – bubbles, possible crystallization - small
35	2-39	20	1.5	-	0.5	>5 – packed plates – medium
36	2-42	20	1.5	-	2	1 – Cubic – large

formed crystal from the glycosylated enzyme sample (Table 9) with crystallization solutions #1-15 appeared to have a promising structure in terms of protein structure geometry (see Table D1 (Appendix D)). This crystal was sent for X-ray crystallographic analysis carried out by Åsmund Røhr Kjendseth (Norwegian University of Life Sciences – Faculty of Chemistry, Biotechnology and Food Science). Results revealed that the crystal contained salt, and no protein diffraction data was generated.

3.3.2 Reproducing crystallization conditions

Several conditions listed in Table 9 yielded putative protein crystals. Conditions for these crystals were remade in-house, and an expanded crystallization assay was performed using the deglycosylated enzyme using these conditions, as outlined in Table 9. A large crystal was formed in the expanded crystallization trial, as highlighted in Table 10, and depicted in Fig C1, photo 38 (Appendix C). This crystal was analyzed by x-ray crystallography, resulting in a protein structure (see below).

Table 10. Expanded crystallization assay using deglycosylated *AfuLPMO11B*. The table shows in-house produced crystallization conditions (*Tube#*), using ingredients described for the *JCSG-plus™* crystallization kit (Appendix F, Table F1) for condition 1-8, 1-15, and 1-9. The setup is described as follows; A 20 g/l *AfuLPMO11B* (deglycosylated) stock solution was used, where crystallizing droplets were made by mixing approximately 0.7 μ l protein solution with 0.7 μ l crystallizing solution (see method section 2.3.11.2). The Table indicate which type of crystallizing conditions that are used (*Tube#*), concentration of the protein stock solution (*Enz. g/l*), ratio between protein stock solution 'm' and crystallizing solution 'n' (*Ratio m:n*) where R = random, hanging drop size (*Drop μ l*), approximate crystal formation period (*Time: ~ months*), number of drops in total for each described condition (*Nr. of drops*), and a description of observed crystals (*Crystal description*) including number of observed crystals, crystal-system [110], and size.

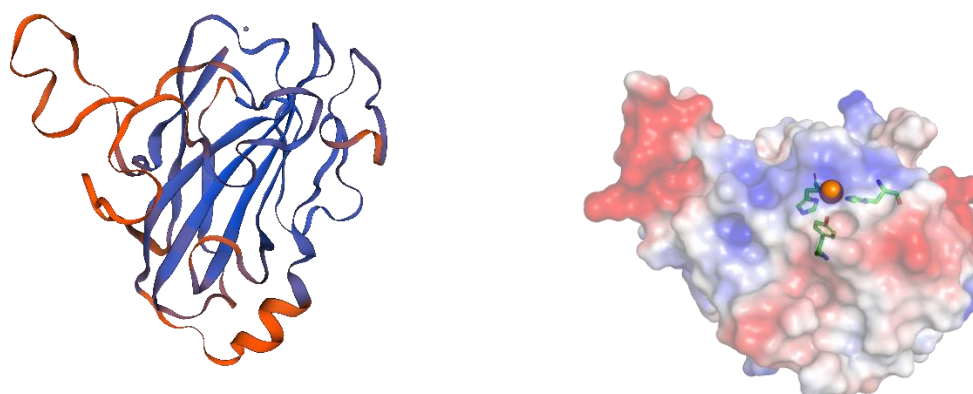
<i>Tube#</i>	<i>Enz. g/l</i>	<i>Ratio m:n</i>	<i>Drop μl</i>	<i>Time ~ months</i>	<i>Nr. of drops</i>	<i>Crystal description N – Crystal-system – size</i>
1-8	20	1:1	2	-	6	Pending...
1-8	20	1:2	1.5	-	6	Pending...
1-8	20	2:1	1.5	-	1	Pending...
1-8	20	R	0.5-3	-	2	Pending...
1-15	20	1:1	2	-	6	Pending...
1-15	20	1:2	1.5	3.5	6	1 – Tetragonal – Big
1-15	20	2:1	1.5	-	1	Pending...
1-15	20	R	0.5-3	-	2	Pending...
1-19	20	1:1	2	-	6	Pending...
1-19	20	2:1	1.5	-	6	Pending...
1-19	20	1:2	1.5	-	1	Pending...
1-19	20	R	0.5-3	-	4	Pending...

3.4 Protein structure

3.4.1 Structural analysis by modelling

A protein model of *AfuLPMO11B* was generated (Fig 27), using SWISS-MODEL Homology Modelling [61], using the one and only published LPMO11 crystal structure as template (*AoLPMO11*, PDB accession code; 4mai/4mah; 49 % sequence identity). The model reached the quality thresholds and was determined as a good model by the SWISS-MODELS' QMEAN criteria. With the use of PyMOL (The PyMOL Molecular Graphics System, Version 2.2 Schrödinger, LLC.) [24]. A close-up figure was generated, focusing on the catalytic site of *AfuLPMO11B*, which was revealed to have the same amino acid residues as *AoLPMO11* in the first and second shell of the copper environment (Fig 28). In addition to the obligatory His-

brace motif (His 1 and His 71 in *Afu*LPMO11B) for LPMOs, *Afu*LPMO11B contains the conserved Glutamate residue (Glu 131), important for chitin binding, as previously mentioned in the introduction (see Fig 4). The enzyme also contains the conserved and buried aromatic tyrosine residue (Tyr 133) facing the catalytic copper ion.



A **B**
Fig 27. modelled structure of *Afu*LPMO11B. The figure display a structure of *Afu*LPMO11B generated using SWISS-MODEL. Panel A displays the model in cartoon representation, where the catalytic site is pointing upwards showing the Cu-atom at top-middle (light blue dot). Colors in A represent QMEAN, where *blue* score positive, and *red* negative on a scale of $-6 - +2$ (the more blue, the more realible the model; note that the catalytic region is blue). Figure (B) displays the protein's charge distribution, which was calculated and illustrated using PyMOL. The model in figure (B) is tilted forward relative to to panel A and shows the Cu-ion as an orange sphere. Figure (B) also show the histidine brace, typical for LPMO's, as well as a relatively conserved Tyr-residue buried near the catalytic site. Colors in figure (B) display charge, where red = negative, blue = positive and white = neutral.

Because of the high similarity in the catalytic site (Fig 28), it was interesting to compare a larger area of the substrate facing side of the two AA11s. This was illustrated with another figure (Fig 29), which highlights identical amino acids between the two enzymes extending from the active copper site. Figure 29 shows that next to the conserved copper environments, *Afu*LPMO11B and *Ao*LPMO11 share additional conserved amino acid residues extending from the catalytic site, and that the variations in sequence identity may be focused on the looping regions. *Afu*LPMO11B, as mentioned earlier on, was glycosylated. It is not experimentally determined where the N-linked glycan occurred on the protein, but this position was however predicted using the NetNGlyc server [49], shown in Figure 30A. To

complement this glycosylation site, a general multiple sequence alignment was generated to potentially illustrate if the glycan site was in close proximity to a conserved residues, or

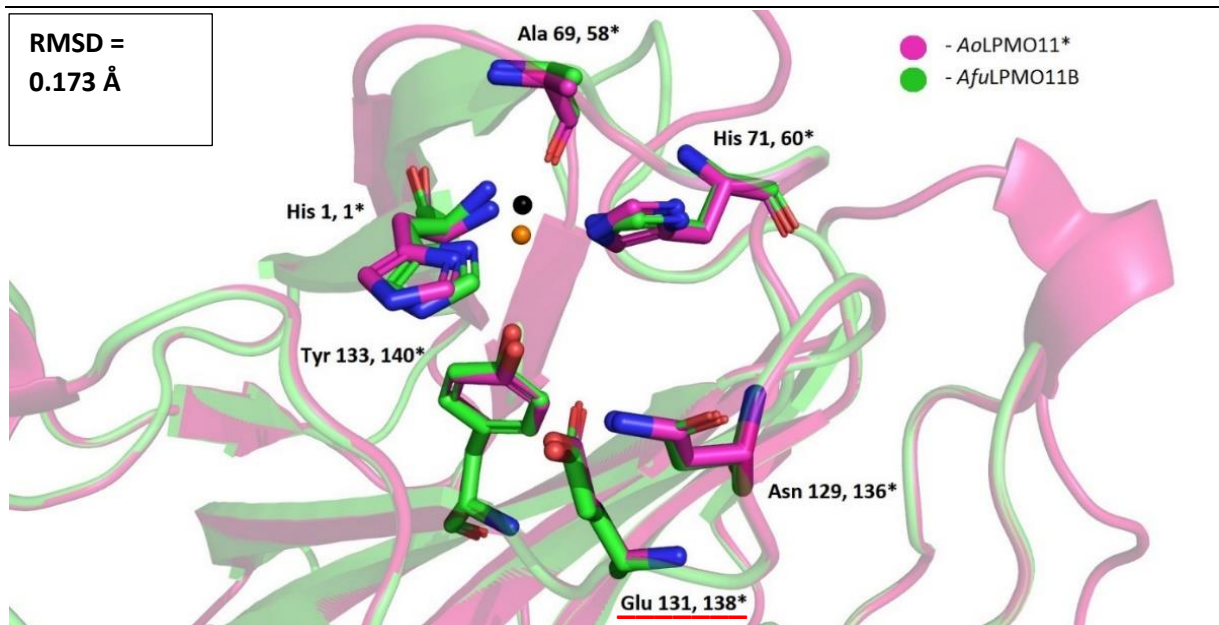


Fig 28. Structural alignment of LPMO11 catalytic sites. The figure shows a superposition of residues surrounding the active site in *AfuLPMO11B* (model; green) and the *AoLPMO11* crystal structure (PDB accession code; 4mah) (magenta). Residues are labeled with three letter codes and the sequence position number (signal peptide excluded). The left number refers to *AfuLPMO11B*, whereas the right number, with an asterisk, refers to *AoLPMO11*. The residue marked by red underlining (*Glu 131, 138**) shows the highly conserved *Glu / Gln* residue, present in all LPMOs, pointing towards the catalytic copper center. His 1 and His 71 illustrate the histidine brace motif in *AfuLPMO11B*. The conserved tyrosine buried beneath the Cu-atom (*Tyr 133, 140**) is also shown. Two copper (Cu) atoms are shown in the figure, where the orange Cu belongs to *AoLPMO11*, and the black Cu is the predicted Cu position in *AfuLPMO11B*. This figure was generated in PyMOL. The structural alignment was performed in PyMOL using the atomic coordinates of the labeled residues (all atoms). RMSD = 0.173 Å.

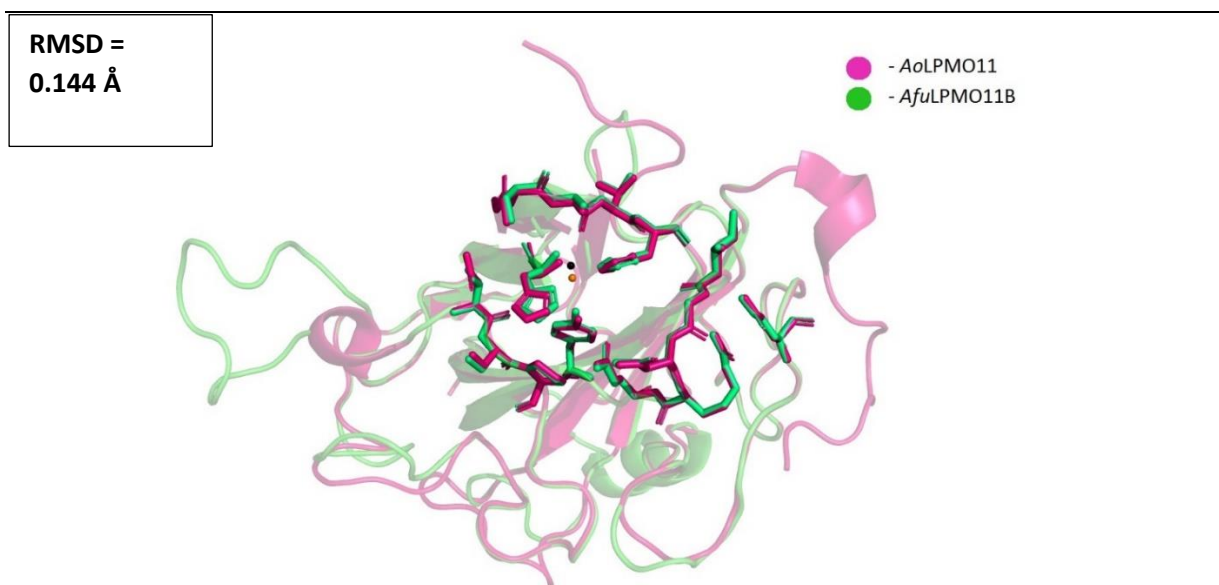


Fig 29. Structural alignment LPMO11s highlighting putative surface-exposed residues putatively interacting with substrate. The figure shows several identical residues (side chains shown as sticks)

between *AoLPMO11* (magenta) and *AfuLPMO11B* (green), surrounding the catalytic site. The structural alignment was performed using all atoms of each protein, where residual superposition complement the sequence alignment (Appendix D, Table D1) . RMSD = 0.144 Å. The figure was generated in PyMOL.

wether this was located in non conserved regions. Combining knowledge of conserved residues and glycosylation sites, may shed light on whether the glycosylation itself is a conserved feature of the LPMO. *AfuLPMO11B* is a fungal LPMO, and it is therefore likely glycosylated in its native host. The multiple sequence alignment was generated included a few selected chitin active LPMOs, i.e. six randomly selected AA10s, two AA15s and the two AA11s discussed above. Sequence alignment was performed with Clustal Omega [103], and rendered with ESPript 3.0 [104], with a visual confidence limit of 0.7. Clustal Omega utilize seeded guide trees and HMM profile-profile techniques to better align protein sequences. The seeded guide three are based on known conserved sequence motifs from a protein database, while the HMM (hidden markov model) give penalty score in peptide alignments based on chemical properties of different amino acids. A hydrophobic and aromatic residue for example would have a low penalty with another amino acid with those characteristics. Possible glycosylation sites (both N-glycans and O-glycans) were predicted with NetNGlyc [50] and NetOGlyc [51]. The results are visualized in Figure 30, whereas the sequence alignment itself is provided in Fig D1 (Appendix D).

Fig. 30A shows that the potential glycosylation sites are located quite far from the catalytic center. The enzyme used for deglycosylation (*EfEndo18A*) cleaves N-linked glycans, but not O-linked glycans. It is therefore likely that the observed deglycosylation effects relate to changes in the blue area of the figure in panel A (Fig 30). In panel B in the same figure, the orange colored areas correspond to an alignment score above the 0.7 confidence limit, but where *AfuLPMO11B* deviates from the other aligned LPMOs, while yellow indicate an alignment score above the confidence limit, but where *AfuLPMO11B* have a similar functioning amino acid. When comparing panels, A and B, one can see the N-glycan site resides in a conserved area. Note that Fig. 30B shows that there is only a few conserved residues above the confidence limit between the selected LPMOs, and that *AfuLPMO11B* and *AoLPMO11* often deviate simultaneously from the commonly conserved residues among the remaining LPMOs. This deviation profile in Fig D1 (Appendix D). It appears that only a few amino acids are conserved among the selected chitin active LPMOs according to the sequence alignment, yet

they all have the same core structure, i.e. the chitin-binding type-4 domain (illustrated in black for the *AfuLPMO11B* model in Fig 30). This, again, demonstrate the flexibility in functions of polypeptides across different amino acid sequences.

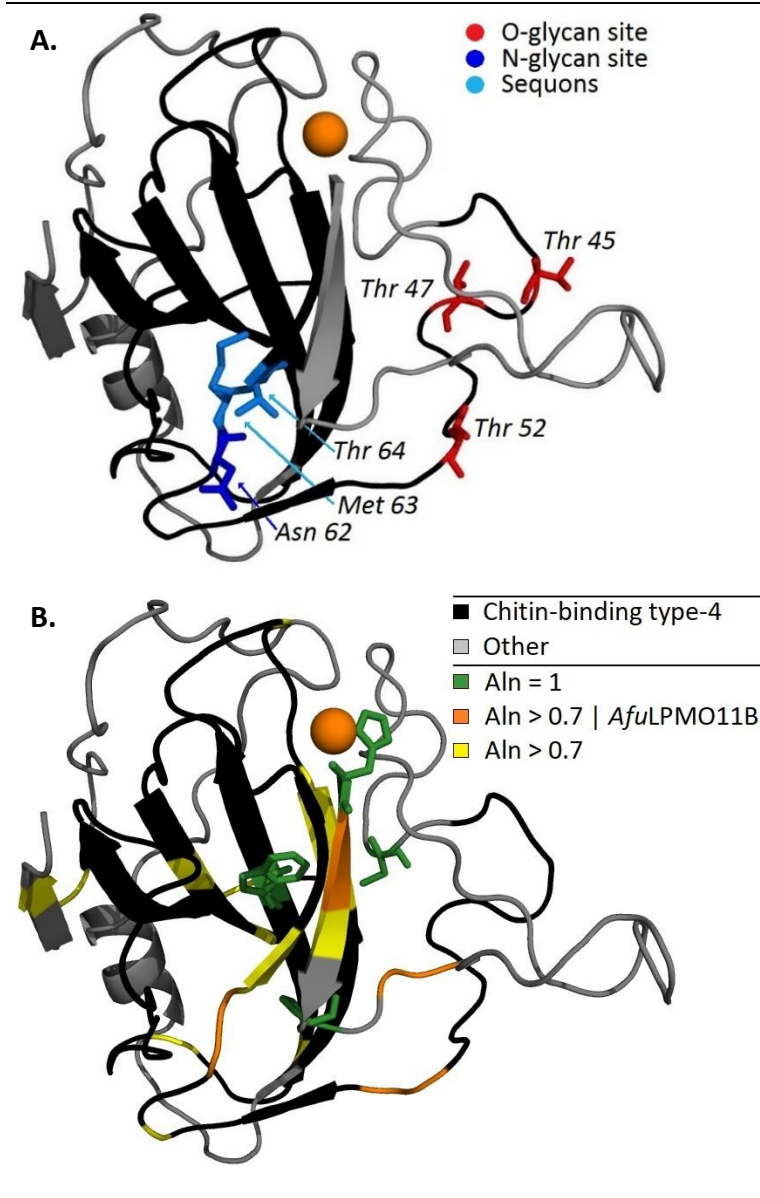


Fig 30. Predicted glycosylation sites and conserved residues in *AfuLPMO11B*. The peptide chain in (A) and (B) is colored in *black* or *grey*, where *black* indicates the Chitin-binding type-4 domain, recognized by *Uniprot* (UniProt ID: BOXZD3), while *grey* regions fall outside this domain. Panel (A) shows predicted glycosylation sites in *AfuLPMO11B* with a probability of > 0.5, either for N- (blue) or O- (red) glycosylation, predicted by *NetNGlyc* and *NetOGlyc* respectively [51, 50]. The single N-linked site also shows supporting *sequons* (light blue). Panel (B) shows conserved residues from the multiple sequence alignment (Appendix D, Figure D1), *green* indicates an alignment (Aln) score of 1 (strict), while *yellow* indicate Aln score > 0.7 (high). *Orange* indicate the same as yellow, but where *AfuLPMO11B* is an outlier. The protein is oriented with the catalytic site upwards, exposing the copper atom (orange sphere).

3.4.2 Protein structure by X-ray crystallographic analysis

Just before concluding the writing of this thesis, the crystal structure of *AfuLPMO11B* was solved (Fig 31), by X-ray crystallography using a crystal depicted in Appendix C (Fig C1 – photo 38) that emerged in the extended *AfuLPMO11B* crystal screen (Table 10, highlighted in grey).

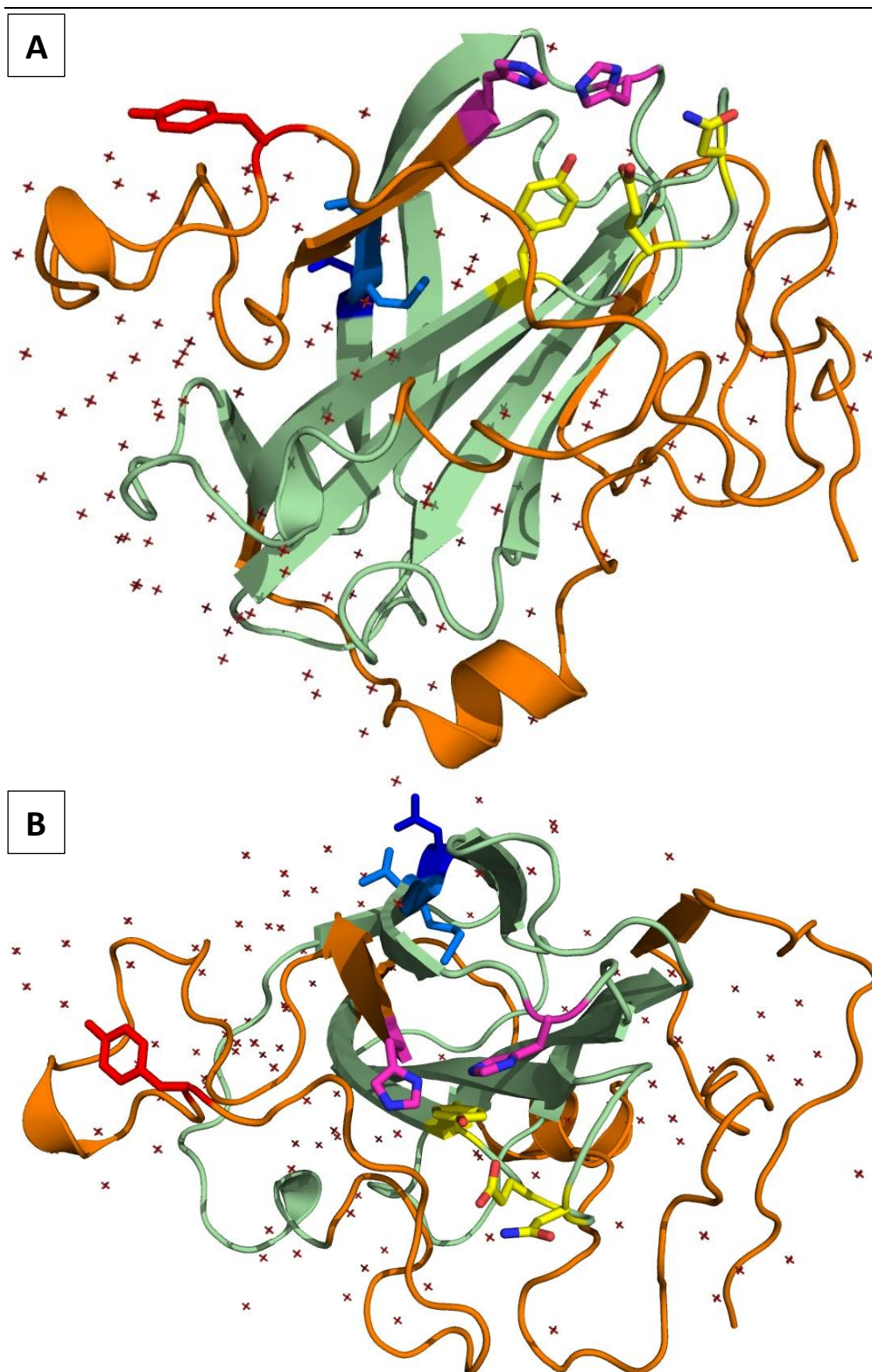


Fig 31. X-ray crystal structure of AfuLPMO11B. Panels A and B show the crystal structure of AfuLPMO11B without copper in the active site, from different angles. Both panels show the chitin-binding type-4 domain (res 42-139; green main chain), the histidine-brace (stick representation; purple carbons), important residues in the second shell of the copper site (sticks, yellow carbons), the predicted N-linked glycan site (dark blue sticks) with the supporting sequons (light blue sticks), and a surface exposed tyrosine residue, potentially important in substrate binding (red sticks). Red crosses indicate water molecules.

The X-ray analysis of the protein crystal and structure elucidation of *AfuLPMO11B* were kindly performed by Åsmund Røhr Kjendseth (Scientist at the Norwegian University of Life Sciences, Faculty of Chemistry Biotechnology and Food Science). The result was a complete protein structure, containing the full mature polypeptide of *AfuLPMO11B*, but lacking a metal ion in the catalytic center. Because of time constraints, an in-depth structural analysis is yet to be performed. It is clear though, that the crystal structure is very similar to the structural model discussed above. A structural alignment was performed on the modelled structure and the crystal structure of *AfuLPMO11B*, and resulted in an RMSD of 1.252 Å, a relatively low deviation. However, when comparing crystal structures of *AfuLPMO11B* with *AoLPMO11*, an RMSD as low as 0.750 Å. This low deviation thus suggest that *AoLPMO11* and *AfuLPMO11B* are highly related in terms of structure, despite that sequence of the full-length peptides only results in a sequence identity of 40 %. These estimates were generated with PyMOL (not included here).

4. Discussion

4.1 Protein purification and quality control

AfuLPMO11B was purified to relatively high purity. No other protein bands were visible in the SDS-PAGE gel (Fig. 4), except for some potential impurities appearing in the 15 kDa region. The vague band seen here likely does not represent protein, since it is not well defined. Due to the binding of SDS, proteins are expected to have a fixed mass to charge ratio, resulting in well-defined bands on the gel. The potential impurity was considered non-significant in terms of protein function and measurements of protein concentration.

The stability of the *AfuLPMO11B* in the stock solutions used for protein characterization was not assessed and it cannot be excluded that the purified enzyme gradually lost some activity during storage, although there were no clear indications of loss of enzyme activity over time (no precipitation, no unexpectedly low activities), absolute quantitative values reported should be interpreted with care. Of note, the stock solutions of glycosylated and non-

glycosylated enzyme were prepared almost at the same time and handled identically throughout the study. Nevertheless, it cannot be excluded that glycosylation affects storage stability of the enzyme.

4.2 *Afu*LPMO11B - functional characteristics

4.2.1 Substratespecificity

From an initial extensive substrate screening (Fig 10), it became clear that the only substrate showing obvious product formation was chitin. The enzyme generated more products from β - than from α -chitin, which is expected based on existing data for chitin-active LPMOs (45, 11) and considering that the degree of crystalline rigidity is stronger in α -chitin due to the antiparallel polymer packing [11]. The activity observed on these substrates may not directly prove however, that *Afu*LPMO11B is truly active faster on α - and/or β -chitin polymer arrangements, considering that these substrates may have amorphous regions on the substrate surface, that may have been favored by the LPMO. Chitin substrates also contain a fraction of deacetylated sugars, which is sometimes favored by LPMOs [129]. The degree of deacetylated chitin may vary between substrate stocks, and therefore reflects another issue in comparing efficiency of chitin degradation in relation to chitin polymorphs. Similar activity to *Afu*LPMO11B have also been found on other AA11s, such as *Ao*AA11 [22] and *Ff*AA11 [131], which have both shown activity on α -chitin substrates. Looking closer at the control reactions (Fig 11), a large peak of unknown nature also appeared from mannan interacting with the reductant. This is not observed in Figure 10 however. It is unclear why this peak formed in reaction with ascorbic acid, but not in reaction with ascorbic acid and LPMO. It is a possibility however, that the LPMO in those reactions interacted with ascorbic acid and further produced H_2O_2 , which may have interacted with the surrounding reductant, and/or somehow have prevented this unknown product formation.

Additionally, substrates are known to contain (varying) amounts of transition metals (e.g., see [4] for chitin) and these metals can again interact with the reductant and/or H_2O_2 . Thus, a lot of redox chemistry may have been going on and it can, for example, not be excluded that the LPMO became fully inactivated (see also discussion of progress curves, below) before slow

product formation became detectable. Reactions with lower ascorbic acid concentration could thus have been tried out. Alternatively, since low concentrations of H₂O₂ can drive LPMO reactions and can potentially lead to higher activity [27, 28, 29, 78], one could also have carried out the substrate screening in reactions driven by H₂O₂.

AfuLPMO11B was confirmed to be active on crystalline chitin, and it was therefore natural to see if it could catalyze soluble chitin (Fig 12). The enzyme (glycosylated) was tested on chitin tetramers, pentamers and hexamers (A4, A5 and A6). At first glance, it may appear that products are formed, because peaks appear in the reactions with added LPMO that are not seen in the negative control reactions lacking ascorbic acid. Nevertheless, the enzyme is likely not active on soluble chitin, firstly, because these peaks resemble peaks in Fig 10 that were likely a product caused from ascorbic acid, and secondly, oxidized chitin products are expected to appear at retention times between 11 – 17 minutes as visible in Fig 10, and such peaks were not observed.

A more detailed analysis of reaction products using both chromatography and mass spectrometry clearly showed that *AfuLPMO11B* generates typical C1 oxidized products from chitin. It is worth noting that, while the standard sample contained 50 μM of every (GlcNAc)_nGlcNAc1A compound, the peaks for the various compounds differed drastically in intensity, which is due to variation in absorption properties. While this complicates quantitative interpretation of the chromatograms, it seems nevertheless clear that *AfuLPMO11B* produces substantially higher amounts of even-numbered products, compared to odd-numbered products. Similar observations have been made in earlier studies on the chitin-active LPMOs, including *SmLPMO10A* also known as CBP21 [16]. This phenomenon has been ascribed to the findings that CBP21 have shown a strong preference for cleaving every second glycosidic bond, and that the LPMO need to approach the substrate from one side, i.e., the LPMO must be oriented according to the direction carbohydrate polymer [16]. This therefore suggests that two sugars (at least) is needed to properly orient the enzyme toward the preferred position in order to execute activity. If this were to be true, The LPMO would always face one direction in respect to the substrate, and therefore result in even numbered products from activity. Sugars in, e.g. chitin or cellulose have an alternating orientation of 180° in respect to each other, between each sugar in the polymer. Keeping this in mind, it seems likely that LPMOs have a binding preference for either of these orientations on its substrate

facing side. However, to restrict the LPMO to one direction on the polymer, the reducing end of the polymer sugar is likely a necessary aspect for the LPMO binding and/or catalysis.

The MS analysis of products showed groups of signals typical for C1-oxidized products, that were spaced by m/z 203, corresponding well with the monoisotopic mass of dehydrated *N*-acetylglucosamine, that equals 221.2255 Da (GlcNAc) – 18.0105 Da (H₂O) = 203.215 Da. Generally, the MS signals showed characteristic isotope leaflets with typical exponential reduction patterns, as expected based on the natural occurrence of ~ 1.1 % of the ¹³C isotope in nature. The major peak with m/z = 1257.365 showed an abnormal isotopic curve, where the 2*¹³C- lactone isotope has too high intensity. This is caused by the overlap with native GlcNAc₆ (m/z = 1259). The complete mass spectrum of products (Fig 14) shows several peaks which could not be identified using the mass list for “expected compounds” in Table 9. Table 12 shows some alternatives for identification of at least some of these peaks. It must be noted that all these additional peaks were minor, relative to the peaks representing standard C1-oxidized products.

Table 12. Potential compounds corresponding to unidentified m/z -values. The table contains all unidentified m/z -values from the MALDI-TOF MS above, with some suggested compounds. The suggested compounds are calculated based on de-acetylation (-43 m/z [Ac]), de-hydroxylation (-17 m/z [OH]), de-hydration ((-18 m/z), and/or hydrogenation/protonation (+1 [H]/[H]⁺) of known compounds in the mass table above. A = *N*-acetylglucosamine (221 Da), L = *N*-acetylglucosaminolactone (219 Da), X = *N*-acetylglucosaminic acid (237 Da), and D = Glucosamine (179 Da). Note that the position of D in the compound chain is not restricted, i.e., it can be at “random” positions. For calculation, [K]⁺ = 39 Da and [Na]⁺ = 23 Da.

m/z	Suggested modification on known compounds	Compound chain	
628.6	DP3; native + [H] ⁺	A-A-A	
648.2	DP3; native + [Na] ⁺	A-A-A	
698.2	-	-	
715.4	-	-	
720.2	DP3; aldonic acid - [H] + 2[K] ⁺	A-A-X	
825.3	DP4; lactone - [Ac] + [H] + [K] ⁺	A-A-D-L	
961.2	?	-	
1028.4	DP5; lactone - [Ac] + [H] + [K] ⁺	A-A-A-D-L	
1038.4	DP5; lactone - [OH] + [H] + [Na] ⁺	A-A-A-A-L	-[OH]
	DP5; native - [H ₂ O] + [Na] ⁺	A-A-A-A-A	-[OH ₂]
1133.4	?	-	
1175.4	?	-	
1217.4	DP6; native - [Ac] + [H] + [Na]	A-A-A-A-A-D	

1231.4	DP6;	lactone - [Ac] + [H] + [K] ⁺	A-A-A-A-D-L	
	DP6;	lactone - [Ac] + [OH] - [H] + [Na] ⁺	A-A-A-A-D-L	+ [OH]
1241.8	DP6;	lactone - [OH] + [H] + [Na] ⁺	A-A-A-A-A-L	- [OH]
	DP6;	native - [H ₂ O] + [Na] ⁺	A-A-A-A-A-A	- [OH ₂]
1445.7		?	-	
1466.4		?	-	
1500.0	DP7;	aldonic acid - [H] + 2[Na] ⁺	A-A-A-A-A-X	

The products displayed in Table 12 include dehydrated native products (Δ -m/z -18) Loss of a hydroxyl group (Δ -m/z -17) Loss of one or more acetyl groups (Δ -m/z -42, -84 and so on) is conceivable since there will be a certain degree of deacetylation in the substrate [132]. The m/z 628.6 signal present in both β -chitin and α -chitin samples, could reflect a proton adduct of a native trimer, but is likely not an LPMO product because analogous peaks do not occur in the other products clusters, for example in the DP4 cluster.

4.2.2 H₂O₂ produced by *Afu*LPMO11B

*Afu*LPMO11B appear to have a H₂O₂ production with a catalytic rate of 0.15 min⁻¹. Similar rates have been observed by other LPMOs, e.g. *Gt*LPMO9B, described by Hegnar et al [33], where the enzyme was shown to produce ~ 0.1 μ M min⁻¹ in reaction with 30 μ M AscA in pH 6.5. The control reaction with 1 μ M CuSO₄ show near to identical H₂O₂ production with a rate of ~ 0.05 min⁻¹. The same production of peroxide was observed in the control reaction here, and therefore indicate to some degree, that the H₂O₂ production rates between *Gt*LPMO9B and *Afu*LPMO11B are comparable. In the paper by Hegnar et al. (2018), they also found that AscA in stoichiometric amounts of 30 μ M were able to remove 54 % of H₂O₂, and that this may mask the true H₂O₂ production in Amplex Red assays. This factor was not accounted for in the assay performed here.

An interesting correlation would be to see if the oxidized product formation and the H₂O₂ production rate of *Afu*LPMO11B are identical. To approximate this comparison, control reactions from the H₂O₂ feeding reactions (Fig 21) can be used to estimate the catalytic rate, showing 160 μ M oxidized product after 6 hours. The H₂O₂ production assay was performed in 20 °C, while 30 °C in the former. By using relative catalytic rate variation observed in the temperature screen (Fig 17 B), 6-hour progression showed 64 μ M variation between 37 °C and 30 °C, giving 8 μ M·°C⁻¹ (n.b. per 6 hours). The product formation from the control (Fig 21) of 160 μ M after 6 hours at 30 °C, would be estimated to 160 - 80 = 80 μ M at 20 °C. This would

give an LPMO catalytic rate of 0.22 min^{-1} . A relatively close approximation to the observed H_2O_2 production rate of 0.15 min^{-1} . Considering also that the LPMO used in the H_2O_2 production assay was performed with a less potent enzyme batch, it could be theorized that the protein batch with higher catalytic rate would also express higher rates of H_2O_2 production.

4.2.3 Effects of temperature on LPMO activity

From the thermal screening reactions with *Afu*LPMO11B (Fig 17), the enzyme showed catalytic stability for 24+ hours at 30 °C on both α - and β -chitin. Looking at panel A (Fig 17), the data is quite conclusive. In 45 °C, the enzyme has linear activity until 6 hours, and is flat-lined from 6 – 24 hours, indicating an abrupt stop after 6 hours. In 37 °C, the enzyme shows catalytic stability for 6+ hours, but with a probable stop around 12 hours, assuming linear product formation until the maximum product formed (product at 24 hours). Based on several studies, a n LPMO reaction would likely operate with a seemingly linear product formation, and later inactivate in a rather quick fashion. It is not likely, as observed in figure 17, that activity have linear activity, and after a certain period, have low activity toward 24 hours. A more realistic reaction curve is rather a linear product formation up to the maximum product formation observed, and from this point, assume an enzyme inactivation. In 30 °C, catalytic rate was almost linear for 24 hours. Looking at B (Fig 17), product formation appeared stable for longer in 45 °C on β -chitin, possibly up to 8 hours, assuming linearity up to maximum product formed. The reason for this variation may be related to difference in binding efficiency on the substrates, as illustrated in the binding experiment (Fig 25).

In 37 -and 30 °C however (Figure 17B), both reactions seem equally stable in terms of product formation. It is also interesting that in 30 °C, product formation seems more stable on α - than on β -chitin, despite the lower binding affinity (Fig 25). One would assume that the LPMO would inactivate faster in this case, as LPMOs are prone to autooxidation and denaturation in un-bound states in the presence of reductant [19].

*Afu*LPMO11B does not appear to be a very rapid enzyme, in terms of chitinous depolymerization, if compared to the apparent catalytic rates compiled by Bizarro et al. [19], on various LPMOs, e.g. the rates calculated by Bizarro and co-workers on *Sm*LPMO10A in reactions with 10 g/l, β -chitin, using 1 mM Asca in BTm-HCl (50 mM, pH 6.0) at 40 °C in

thermomixer at 1,000 rpm. These reaction conditions are fairly similar to those used in e.g. Fig 17. Reactions by *AfuLPMO11B* in the figure show however a ~ 10-fold lower apparent catalytic rate to CBP21, in reference to the 45 °C progression curve (Fig 17B). As well, *AfuLPMO11B* show (Fig 17) approximately a 7-fold lower activity than *BcLPMO10A* reacting at 37 °C, demonstrated by Mutahir et al. [45]. *BcLPMO10A* was tested in parallel with *AfuLPMO11B* reaction on different substrates (Fig 18). Here the catalytic rate was apparently only ~ 3.8 times higher for *BcLPMO10A* than *AfuLPMO11B* reacting on β -chitin. It is important to note however, that the *AfuLPMO11B* enzyme batch, used in this comparison with *BcLPMO10A*, was of lower quality than *AfuLPMO11B* batch '2' and '3'. It is expected, from the data provided, e.g. positive control reactions in H₂O₂ feeding reactions, that *AfuLPMO11B* and *BcLPMO10A* would have similar catalytic rates.

The melt curve (Fig 16) show apparent melt temperature of both glycosylated and deglycosylated *AfuLPMO11B*. Interestingly, temperature dependent structural integrity appears to increase when the glycosylation(s) on the protein is removed. This goes against other findings in protein deglycosylation studies, where glycosylations have shown to increase thermal stability [51]. The native (glycosylated) *AfuLPMO11B* protein melts at ~ 54 °C, while at ~ 65 °C when deglycosylated. This may reflect alternative outcomes of glycosylations, and a possible use in designing proteins towards selected temperatures. It is also important to evaluate experimental conditions when continuing experiments on deglycosylated proteins, and whether the current optimal conditions for catalytic activity still applies. It would therefore be of good interest to perform a temperature dependent catalytic screen on both the glycosylated and deglycosylated version of *AfuLPMO11B* in future research.

4.3 Kinetics

4.3.1 Comparing *AfuLPMO11B* and *BcLPMO10A*

A clear preference is observed for β -chitin by *BcLPMO10A* compared to that of *AfuLPMO11B* (Fig 18), yet the mentioned substrate is also preferred for the latter protein to some extent. In this experiment (Fig 18), *AfuLPMO11B* seem to have similar catalytic rate on (α -chitin < 0.2 mm) and β -chitin < 0.8 mm), and lower rate on (α -chitin < 0.8 mm). Comparably, *BcLPMO10A* show a strong preference for β -chitin, and equal product formation rate on both the α -chitin

variants, supporting similar results found by Mutahir et al [45], in both cases using the *BcLPMO10A* full length protein. In comparing these enzymes, it is pivotal to regard the temperature difference between the two reactions, and that *BcLPMO10A* comprise an LPMO domain, two fibronectin type III (FnIII)-like domains, and carbohydrate-binding module (CBM5), and that the enzymatic function strongly depended on the CMB5 [45]. *AfuLPMO11B* reacted with substrate in 30 °C, while 37 °C for *BcLPMO10A*.

BcLPMO10A was determined “a powerful chitin active LPMO” [45], thus implying that *AfuLPMO11B* is a powerful chitin active LPMO. Perhaps even more so, since *BcLPMO10A* is composed of 4 functional domains, where CBM is specifically important in binding, and prevent catalytic inactivation by autooxidation, while *AfuLPMO11B* is composed of a single LPMO domain. It would be valuable to expand the comparative study between other single domain LPMOs that also have low levels of inactivation during reactions.

4.3.2 Synergy with *AfuLPMO11B* and *SmChi18C*

Synergistic action was observed when combining stoichiometric amounts of Chitinase-C (*SmChi18C*) and *AfuLPMO11B* converting both α - and β -chitin substrates to soluble products (Fig 20). On α -chitin (panel A), an increase of about 70 % non-oxidized products was measured after 9 hours when reacting ChiC with the LPMO, compared to the sum of non-oxidized products formed by ChiC and LPMO respectively. When LPMO was added at a later timepoint (6 hours) to the ChiC reaction, product formation increased to match the rate of product formation in the reaction where both enzymes were added at time zero, while the ChiC control reaction, where only water was added, did not show further significant product formation after 6 hours. The highest substrate conversion was observed on β -chitin (B), with ~ 85 % substrate conversion after 9 hours with both ChiC and LPMO, and ~ 45 % by ChiC alone.

A conversion of 86 % of the substrate theoretical amount, could potentially represent 100 % of the true value, and it is possible that this is the reason for the abrupt stop in product formation, as seen in figure 20B. A portion of the curve however appear slower, from 9 – 24 hours, but is likely caused by the lack of measurements between this interval as discussed above. In both substrates in figure 20A and B, the catalytic capability of ChiC alone seemed to diminish after 9 hours, while remain active in the presence of LPMO. In α -chitin reactions (panel A), ChiC alone was only able to convert ~ 5.5 % of the substrate after 24 hours, while ~

28 % with both enzymes, indicating an increase in product formation of ~ 500 %. However, in β -chitin reactions, the catalytic inactivation was likely caused by a lack of substrate, and would potentially display much greater conversion variation when increasing the substrate amount.

The findings in A and B (Fig 20) clearly shows the importance of *AfuLPMO11Bs* contribution for substrate degradation by ChiC, especially in later timepoints when ChiC becomes inactive, as it appears that the LPMO may render the substrate favorable for ChiC activity. Importantly, from the α -chitin reaction (Fig 20A), both the LPMO and ChiC show catalytic inactivation when operating alone, while in synergistic settings, they produce complete linearity in product formation for 24+ hours. This shows an extraordinary complementation of the combination of these two enzymes in both product yield and catalytic stability. Future synergy assays on α -chitin should be prolonged to at least 72 hours, and determine if these two enzymes single handedly can convert 100 % of α -chitin substrates.

In the paper by Mutahir et al. [45], synergistic action with *BcLPMO10A* - full length and a cocktail of chitinases (*SmChi18A*, B and C), had a rapid and 8-hours linear substrate conversion of crystalline α -chitin, reaching ~ 27 % conversion. After 8 hours, conversion rate drastically reduced, but remained almost linear up to 48 hours, reaching a final conversion of ~ 50 %. Unfortunately for comparative reasons, synergetic reactions with *AfuLPMO11B* and ChiC (Fig 20) did reach ~ 28 % conversion not until 24 hours, which also is the last timepoint. Because of the lack of experimental overlap between these experiments, it cannot be assumed whether 28 % substrate conversion perhaps is a common limit in these reactions on α -chitin, or if *AfuLPMO11B* with ChiC would express further linearity in product formation beyond 28 % conversion. But again, the reduction from initial synergetic catalytic rate and later catalytic rates can also be a result of the enzymatic interplay in these reactions. Where e.g. at initial timepoints, the crystalline substrate is depolymerized by both enzymes without a particular need of each other's contribution, but at later times when the substrate crystallinity is scarce, or not favorable for one (LPMO) or the other (GH) enzyme, they may depend on their individual activity to strip away partially connected oligomeric units on the otherwise crystalline substrate.

When looking at the early initial rates (2 hours) on both substrates (panel A and B) in figure 20, it does not appear to be a synergetic function in terms of catalytic rate on β -chitin (B), but rather in terms of final substrate conversion. On α -chitin however, synergy is observed both in initial catalytic rate, and final substrate conversion.

As it was shown that *Afu*LPMO11B help ChiC in its catalytic capability (Fig 20A and B), experiments were also carried out, showing the effects ChiC have on LPMO activity (Fig 20C and D). First, reacting with α -chitin (panel C), ChiC did not appear to aid the LPMO producing oxidized products. The LPMO alone even appeared to perform better, noticeably at the 9-hour time point. The LPMO did however, decrease its production after 9 hours when reacting alone, while remaining completely linear for 24 hours in combination with ChiC. Secondly, reacting with β -chitin (D), the rate of oxidized product formation was increased by a two-fold in presence of ChiC together with *Afu*LPMO11B, keeping linear product formation up to 9 hours. The reduction in product formation after 9 hours was likely, as mentioned above, a lack of substrate.

It appears by the findings that, *Afu*LPMO11B aid Chitinase-C in maximizing substrate conversion on both α - and β -chitin, and that ChiC aid the LPMO reaction to a 2-fold increase in oxidized product formation on β -chitin, but with no visible contribution on α -chitin. The combination of these enzymes also appears to complement each other both in catalytic longevity and maximal substrate conversion.

Despite the apparent effect ChiC may have on the LPMO catalytic efficiency, there is a good chance that the observed variation is simply due to the increased release of oxidized products that were stuck on the substrate by ChiC. As observed from other Figure 18, *Afu*LPMO11B appear to have similar active rates on α - and β -chitin. The difference in substrate conversion observed in the synergy experiment is therefore likely correlated to ChiC's ability to operate on these two chitin polymorphs. Additionally, as much as 50 % oxidized products have been found, that were stuck on the substrate after LPMO action [108, 109]. this may readily be released in solution when combining LPMO with chitinase.

4.3.3 H_2O_2 -feeding reactions

Reactions with *Afu*LPMO11B using H_2O_2 as co-substrate for the catalytic execution yielded a multitude of interesting results (Fig 21). As mentioned in the figure text, AscA reductant was in all cases only added at time zero, and H_2O_2 was added every 15 minutes in (A) and (B), while every 30 min in (C) and (D). First, the enzyme was able to have a linear product formation for 3 hours with stoichiometric amounts of oxidized products to H_2O_2 input (A). The reduction in oxidized product formation after 3 hours is not caused by LPMO inactivation, but because

H₂O₂ was only added for the first 3 hours. After which, the enzyme continued product formation using O₂ as the catalytic co-substrate, with a progression curve like that of the control reaction with no H₂O₂. This indicated that the enzyme was not denatured in the H₂O₂ condition.

Secondly, since the *Afu*LPMO11B seemed unharmed when reacting with 50 μM H₂O₂, higher concentrations of H₂O₂ (50, 80, 120 and 200 μM) was used in the second assay (B). Here, the upper limit of H₂O₂ for stable catalysis, appeared to be between 80 and 120 μM, with activity inactivation of the former concentration after 5 hours. The 50 μM H₂O₂ reaction in both (A) and (B) should in theory have the same product yield, but appear higher in (A). The difference between the assays are that in (B), a higher concentration and lower volume of H₂O₂ was added every 15 min, because the reaction volume was kept constant, and samples from reactions was in both cases 30 μl, and samples in (A) was taken every 15 min in the first hour, while every 30 min for the entire incubation in (B). Speculatively, the higher H₂O₂ concentration inputs may have harmed the LPMO on the H₂O₂ solute contact surface, before H₂O₂ was uniformly distributed in the solvent. The control reaction without H₂O₂ in both (A) and (B) show similar catalytic rate, suggesting no other (apparent) external factors caused the variation. The 1-hour initial rate of 120 μM and 200 μM H₂O₂ (B) showed similar product formation, and was used to estimate reaction conditions for the third H₂O₂ assay (C), screening with variations of LPMO concentration in 40 μM H₂O₂ with additions every 30 min.

Oxidized product formation in the progression curves (C), showed linear and stoichiometric amounts of products to H₂O₂ in reactions containing > 0.2 μM LPMO. Reactions containing 0.2 and 0.4 μM enzyme showed similar progression rates, suggesting that in both cases, all H₂O₂ was consumed between each feeding interval. Reactions containing 1 μM enzyme showed more than stoichiometric amounts of products to H₂O₂, but the excess amount can be correlated to the product production of the control reaction, containing no H₂O₂. The difference in product amount formed by the (1.0 μM Enz) and (0.2 μM Enz) after 4 hours is ~ 110 μM, while the control (1.0 μM Enz, wo H₂O₂) produced ~ 109 μM. This suggests that the H₂O₂ is rapidly consumed in the (1.0 μM Enz) reaction, and uses O₂ as co-substrate most of the time within each H₂O₂ feeding interval. Because of mentioned relativities, and the proportionate variation in production rates and enzyme concentration between 0.05 – 0.2 μM enzyme reactions, the 0.2 μM enzyme reaction seems to show a good balance between utilizing the H₂O₂, and with minimal O₂-pathway reactions. The chemical conditions

concerning that particular sample was used in the next H₂O₂ assay (D), screening product formation progression with varying ascorbic acid concentrations.

As mentioned in the introduction, the proposed catalytic mechanism for LPMOs using H₂O₂ as co-substrate (Fig 5), AscA concentrations are in several cases found to be in sub-stoichiometric amounts to oxidized products. The H₂O₂ based reaction pathways is thus predicted to only require the priming reduction of LPMO, Cu(II) → Cu(I) by an external electron donor, further using H₂O₂ in the catalytic reactions mechanism, also causing Cu(I) oxidation back to Cu(II), but whereby the hydroxylation of C1 or C4 leads to a simultaneous re-reduction of the copper atom, back to the “primed” state, Cu(I) [19]. The LPMO would therefore ideally only require a first-time reduction by an external electron donor, and be able to continue catalytic activity only by using H₂O₂. Kuusk et al. demonstrated this, showing suprastoichiometric amounts of oxidized products relative to reductant, produced by ScLPMO10C in reaction with H₂O₂, leading to the deduction of the priming theory [40]. This was however not observed in H₂O₂ reactions with *Afu*LPMO11B (Fig 21D) and (Fig 22), where, despite the addition of H₂O₂, oxidized products showed consequently stoichiometric amounts to that of Ascorbic acid (AscA) reductant.

In the reactions (Fig 21D) H₂O₂ was added before AscA, to ensure that AscA was not consumed prior to H₂O₂ addition. While in (Fig 22), AscA was added before H₂O₂, in the case that H₂O₂ denatured the protein before initiating the reaction. No significant variations were observed between the addition order however. This complements previous results from Kuusk et al. [40], where it was also not found any significant variation depending on the AscA and H₂O₂ addition order for reaction initiation.

The findings that *Afu*LPMO11B did not produce suprastoichiometric oxidized product amounts, compared to that of AscA reductant are particularly interesting, as they suggest that, although the priming and re-reduction mechanism are observed in reactions with CBP21, it may not apply in all LPMOs. For example, in the paper by Hegnar et al, *Gt*LPMO9B also seems to produce stoichiometric amounts of oxidized product to the added reductant concentration [33]. This will furthermore raise new questions in why some LPMOs could utilize H₂O₂ re-reduction mechanisms, while others may not. The crystal structure of *Afu*LPMO11B will therefore be highly valuable in finding key characteristics in the H₂O₂ catalytic reaction pathway.

A common observation in many LPMO catalytic progression curves on crystalline substrates in aerobic conditions are, a gradual increase in apparent catalytic rate in time (as seen in e.g., Figures 18 or 19). Several speculations on the phenomenon have been suggested. Amongst them are, that, in the initial reaction on crystalline substrate, portions of the oxidized products stay attached on the substrate, and are not solubilized. After some time of LPMO catalysis, the crystalline substrate becomes more amorphous with partially loose oxidized polymers, that may fall easier off the substrate in further catalysis. This effect would then mask the true initial catalytic activity, and show a progressive increase in product formation.

Another theory is that, when crystalline substrates becomes less crystalline because of LPMO action, the binding affinity to the substrate decreases, as LPMOs active on crystalline substrates explicitly, would naturally prefer crystalline polymer arrangements. When the binding decrease however, H₂O₂ production by LPMO is thought to increase, (as mentioned un-bound LPMO show H₂O₂ production) and rapidly be consumed by LPMO in substrate oxidation. This would then perhaps produce the observed progression curves with gradual increase in apparent catalytic rate. Interestingly in this H₂O₂ feeding experiment (Fig 21), the phenomena are still seen. Mostly in (A) and (C), a gradual increase in apparent catalytic rate is observed, and may therefore suggest that this phenomenon is not caused by the increase in H₂O₂ production by unbound LPMO in aerobic reactions, as H₂O₂ would always be present in these reactions, thereby masking the implications of H₂O₂ production by the enzyme.

Considering the findings in this H₂O₂ reaction assay, specifically Figure 21C, *Afu*LPMO11B showed a maximum of ~ 27-fold increase in product formation in presence of H₂O₂ compared to reaction in standard aerobic conditions, and seem to correlate with increased rates found on other LPMOs using H₂O₂ [33, 115]. The 27-fold estimation above was based on comparison of oxidized product formation between the reactions (0.05 μM Enz) and (1.0 μM Enz, wo H₂O₂) in said figure at the 1-hour timepoint.

An additional control estimation was made (Fig 23), evaluating if variation in size of released oxidized products from H₂O₂ reactions, would pose a problem in comparing the actual difference in catalytic speed of LPMO reactions with and without H₂O₂. It appears that the longest products are released in reactions without H₂O₂, and it would imply that progression curves with H₂O₂ could be underestimated, as more oxidized product are stuck on the substrate. The effect appear, so far, to be of little significant, but it should nevertheless be considered.

4.4 The role of N-linked glycosylation on *AfuLPMO11B*

The protein band on SDS-PAGE appeared higher than initially expected for *AfuLPMO11B* (Fig 8). It was thought to be around the theoretical weight of 21 kDa (Table 6). This deviation from theoretical mass, and the known fact that fungal LPMOs often are glycosylated [11] led to the speculation that *AfuLPMO11B* was glycosylated, which later was proven true, by removing N-linked glycosylations with *Ef*Endo18A. The protein was deglycosylated, primarily to optimize crystallization for x-ray diffraction analysis. It was further tested in binding and variation of activity on substrates such as α - and β -chitin and compared in terms of possible activity on other substrates, and in temperature dependent structural stability. These tests were performed to see what role the N-linked glycan(s) may have on the functional characteristics of the protein, -an important factor to assess when e.g. developing applied enzymatic systems, such as degradation- or biosynthesis of polysaccharides or carbohydrate-based materials.

On Figure 30A, it is shown four predicted glycosylation sites, where three of these are O-linked sites with threonine residues. The O-linked sites reside within the *Chitin-binding type-4* module *AfuLPMO11B* - (aa: 60-167, indicated by UniProt) of the enzyme and could therefore have substantial effect on the enzymatic functionality, if or if not, these sites possess glycosylations. It was, on the other hand only predicted one N-linked glycosylation site, on *Asn 62* (Seq; excluding the signal peptide), with *Met* and *Thr* as suggested sequons, following the typical (*Asn-X-Thr*) motif, where *X* is any amino acid except proline [47]. As only one N-linked glycan site was predicted by *machine learning* - (NetNGlyc) [49], and *AfuLPMO11B* was proven glycosylated with N-linked glycans, it seems reasonable to accept the suggested N-linked glycan site as a likely position for the bound glycan.

When analyzing the conserved residues from the alignment data (Appendix D, Fig D1), it appears that, the two AA11s often deviate from the common conservation synchronically. Yet, on position sequence (NMTI) in *AfuLPMO11B*, residue (N) = Asn (Appendix D, Fig D1), all other proteins in the alignment file have a proline (P). This particular “substitution” putatively enabled *AfuLPMO11B* to have an N-linked glycosylation in a conserved region, as the N-linked glycan is predicted to be on this very residue. The Asn residue is also within the *Chitin-binding type-4* module and could suggest that the N-linked glycan functions to optimize substrate

specificity. Even more interesting is it that, the neighboring residue to the proposed N-linked glycan site is a *Tyr* residue (Fig 32), and are almost aligned with the important tyrosine (Y54) important in binding to chitin for *SmLPMO10A* (CBP21), mentioned earlier [23].

<i>SmLPMO10A</i>	[Q53 – (Y54) – E55 – P56 – Q57 – S58 – V59]
<i>AfuLPMO11B</i>	[Q77 – T78 – (Y79) – N80 – M81 – T82 – I83]

Fig 32. Illustrating N-glycan position in a conserved sequence motif. The figure illustrates the important tyrosine residue for substrate binding in *SmLPMO10A* (Y54), and a tyrosine possible with similar function (Y79) in *AfuLPMO11B*, and illustrates the predicted N-glycan site (N80) right beside the tyrosine in the latter protein. The figure aim to highlight the possible implications glycosylations may have on a residue likely to interact with substrate.

a tyrosine Y79 in *AfuLPMO11B* is very close to the position of the important binding residue Y54 in CBP21, and therefore, it seems possible that Y79 is also a surface residue with similar significance in substrate binding. Glycosylations on the predicted N-glycan site N80 may therefore be imperative in binding efficiency and/or substrate specificity.

The nature and origin of the N-linked glycosylation on *AfuLPMO11B* are yet to be elucidated and could also be a function in the biosynthetic pathway by *Pichia*, rather than a directed property in the enzymatic function.

However, on closer inspection of the *AfuLPMO11B* crystal structure (Fig 31), a surface exposed tyrosine was indeed observed, likely with the same functionality as Y54 in *SmLPMO10A*. However, this residue was Y43 (full sequence) in *AfuLPMO11B*, and therefore suggest that the sequence alignment failed in elucidate important residues regarding the AA11. This may further be supported by the fact that only one histidine in the histidine brace was observed in the conserved residue model (Fig 30), where 100 % identical residues are depicted in green stick. As mentioned in the introduction, a key characteristic in LPMO function and structure, is the his-brace. It therefore must mean that this multiple sequence alignment was ineffectual for finding AA11 characteristics.

4.4.1 Binding and catalysis

Comparison of glycosylated and deglycosylated *AfuLPMO11B* did produce clear differences in both binding behavior and catalytic activity on chitin substrates (Fig 25). The former shows an initial (0.5 hours) binding efficiency of ~ 40 % in reduced state on β -chitin, while only ~ 22 % for the latter. In reduced state, the initial binding efficiency is interestingly downregulated on

β -chitin (approx. 40 % \rightarrow 21 %) and upregulated on α -chitin (approx. 13 % \rightarrow 21 %) upon deglycosylation. This may then advocate that glycosylation serves a purpose in substrate specific recognition by *Afu*LPMO11B. A similar trend in initial binding is observed on the same figure (Fig 25) when comparing the non-reduced copper LPMOs, where \sim 21 % bound protein on β -chitin decline to \sim 12 % when deglycosylated. On α -chitin however, in the absence of reductant, the binding appears relatively unaffected initially, but appear to improve over time. *Afu*LPMO11B glycosylated or not, show binding efficiency lower than that of *Sm*LPMO10A and *Bc*LPMO10A-T3–(single LPMO domain) as shown by Mutahir et al. in LPMO-Cu(II) oxidized form, comparing 2 hours incubation data on α - and β -chitin [45].

The negative trend in (bound protein (%)) on the reduced reactions (Figure 25B and C) is somewhat expected, as the crystalline substrate become gradually amorphous by the LPMO catalytic activity. LPMO degradation of substrate affects the crystalline surface in such way that enzymes with a crystalline substrate preference (most LPMOs and CBMs), will bind poorer as degradation continues. The LPMO can therefore only catalyze a certain percentage of the substrate, until the crystallinity on the substrate surface is too amorphous, rendering e.g. the monooxygenase dysfunctional.

Comparing figure 25A and B The binding seems to complement the progression curve on e.g. β -chitin (reduced), where percent bound protein changes from \sim 37 % to \sim 1 % between 2 to 4 hours. Similarly, the product formation stops almost completely after 2 hours. From 4 – 24 hours however, it appears to be a gradual increase of bound protein, despite no catalytic activity. *Afu*LPMO11B has shown to be stable in the given reaction condition up to 24 hours (Figs 17, 19 and 20), and is therefore expected to be in functional condition after 2 hours, where product formation stops (Figure 25A). If \sim 99 % of the protein is free in solution, it is estimated with the initial linearity in figure 15 (H_2O_2 production assay), to be a peroxide production rate of $9.25 \mu\text{M hour}^{-1}$. By 24 hours from the 2-hour mark, \sim 203 μM hydrogen peroxide could have accumulated in the reaction mixture, if the peroxide did not indulge in other reactions, and the LPMO remained functional but unbound. By trusting the obtained binding data Fig 25A and B, it may appear that likely peroxide formation and/or protein denaturation increases binding of *Afu*LPMO11B on amorphous oxidized β -chitin. (although this would have to be measured more precisely).

Denatured protein is likely to have increased hydrophobic interactions due to misfolding, and exposure of hydrophobic residues on the protein exterior surface and may therefore

increase in hydrophobic interaction with the chitinous substrate, as that is one of the theorized binding forms by LPMOs to crystalline polysaccharides [23, 43]. Briefly analyzing the H₂O₂-feeding reactions (Fig 21), it appears that *Afu*LPMO11B can remain functional in 80 μM hydrogen peroxide for 5 hours, which then suggest that the initial increase in binding (~ 1 % to 8 %) from the 2- to 4-hour mark (figure 25B, β-chitin. Cu(I) reduced) is not caused by protein misfolding, but rather the presence of H₂O₂. An interesting theory to investigate, would be to see if hydrogen peroxide not only serves as a co-substrate in the catalytic mechanism, but maybe also as a binder intermediate or allosteric promotor in substrate binding for *Afu*LPMO11B, and LPMOs in general.

The deglycosylated *Afu*LPMO11B show a gradual increase in binding, continuing for 24 hours on both substrates in non-reduced form, while the glycosylated having a rapid increase in binding with approx. maximum bound fraction already after one hour. (Figure 25B & C – Not reduced). The rapid vs gradual increase in bound protein fraction may invoke the idea that the enzyme has several binding surfaces with various binding coefficients in deglycosylated state and uses time to orientate on the substrate to the optimal binding side, while upon glycosylation one side may be optimized in favor of β-chitin (as observed here) while compensating the binding ability to α-chitin. It is also worth noticing that, with glycosylation, the enzyme has an initial binding increase of ~ 20 % upon reduction on β-chitin, but only ~ 10 % increase without the N-linked glycan. A hypothesis can therefore be made, with the assumption that the N-linked glycan on *Asn 62* provide an additional affinity towards substrate upon reduction.

Standard deviations are relatively high on the deglycosylated (0.5 h, β-chitin) data however. Again, looking at the binding data (Figure 25B & C), it is unclear why there is an increase in binding at the 2-hour mark in several samples. The binding reactions contained 2,95 μM and 2,37 μM of glycosylated and deglycosylated *Afu*LPMO11B respectively, with 2 g/l substrate with a total volume of 600 μl, making these reactions somewhat different than all other substrate degrading reactions performed in this study, where 1 μM enzyme and 10 g/l substrate in 300 μl total volume, was used. The variation in proportion between enzyme and substrate in the binding experiment, is likely to have had higher enzymatic peroxide production than the other kinetics assays, and could have had a role in this observed binding behavior.

catalytic activity was compared between the glycosylated and deglycosylated version of *AfuLPMO11B*, on α - and β -chitin (Figure 19). The catalytic rate appears relatively similar between the two versions on β -chitin (panel B), and interestingly a large variation in catalytic efficiency is observed on α -chitin (panel A). A 50 % reduction in activity was demonstrated with deglycosylated *AfuLPMO11B* on α -chitin. These results show that N-linked deglycosylation on *afuLPMO11B* significantly alter catalytic efficiency between specific substrates, and show that glycosylation on proteins may have severe implication in the LPMO functionality.

It is however with the current results, not possible to conclude if *AfuLPMO11B* are equally fast on β -chitin and varied on α -chitin or vice versa, as portion of denatured proteins are not known in these protein batches. Variations in catalytic activity between substrates are nevertheless, not an artifact of denaturation, as that would cause an equivalent reduction on both substrates, keeping the catalytic product profile. The most likely reason is therefore a function induced by the N-linked glycan. There is unfortunately substantial product formation in the control reaction (Figure 19A) containing substrate and ascorbic acid without enzyme, and it is dubious that this can be neglected in the interpretation of the findings.

4.4.2 Potential mishaps

It is unclear why the progression curve shows abnormally high catalytic rates on the glycosylated samples (Fig 21A), especially since the product amount has been divided by the enzyme concentration used in the binding experiment, and thereby displaying the catalytic rate as $\mu\text{M product/enzyme}$. It seems obvious that a systematic error must have occurred. Chromatographic data and calculations have been re-checked, with no errors found. It could therefore be a mistake in the enzyme concentration in the reaction, or an anomaly by the reaction itself when operating with higher *AfuLPMO11B* concentrations ($\sim 3 \mu\text{M}$) and lower substrate amounts ($\sim 2 \text{ g/l}$), or possibly a contamination in the substrate causing product formation.

Diluted enzyme stock solutions used for the experiment was additionally measured with UV-absorbance A_{280} and concentration accurately estimated based on the extinction coefficient for the enzyme. For comparison, glycosylated *AfuLPMO11B* shows a consistent production yield from β -chitin at 30 °C in most reactions by; 30.5, 29.5, 30.0, 33.3 $\mu\text{M hour}^{-1}$

in 1 μM enzyme control reactions from *H₂O₂ feeding reactions* and *catalytic variation by N-linked glycans* reactions (Fig 21A, B, C, and Fig 19) respectively. In the binding experiment however, the apparent rate appears to be $94.5 \mu\text{M hour}^{-1}$, a 3-fold increase from expected values. The relative product formation rate on both α - and β -chitin (Fig 25A) between glycosylated and deglycosylated *AfuLPMO11B* respectively, also contradicts the findings in figure 19, where the former shows that the glycosylated enzyme prefers β -chitin and deglycosylated prefer α -chitin, while the latter shows the opposite. The uncertainty of these results makes it difficult to assume any conclusions on substrate specificity, and the experiments should be repeated under more strict conditions.

Additionally, the assays have been performed with different stock solutions of chitinous substrate, but from the same dry-matter. The only difference would be the time the substrate has been submerged in water. The substrates needed to be changed, since in the case of the substrate used in the synergy and binding experiment, unknown peaks appeared after some time (approx. 4-7 weeks) when controlling the substrate with UPLC. An example is shown in (Appendix G, Fig G3), but is an extreme case of the pollutant, and any results derived from such extreme cases of contamination would be discarded. The peak observed in the conserved data in mentioned reactions was only of minimal value and was considered insignificant at the time. The main peak appears to be a non-reduced N-acetylglucosamine dimer, as it converts to non-reduced monomer when treated with chitobiase (CHB). As mentioned, chitobiase performs hydrolytic cleavage of soluble chitin oligomers in a sequential manner, producing monomers, and oxidized dimers in the case of an oxidized end-product [59]. Amongst the peaks (Appendix G, Fig G3) it was also found a smaller (GlcNAcGlcNAc1A) peak, suggesting some oxidative action.

The contaminant has not been addressed, but in case of a fungal spore contamination, one could witness a synergetic scenario between the investigated LPMO and enzymes from the fungal arsenal, and thereby producing abnormal progression curves. The origin of the contamination is thought to come from a 5 ml pipette used in the mixing of the stock solution. The pipette was cleaned with 1 M NaOH and 70 % ethanol, and the contamination was never found in later UPLC analysis on other substrate stock solutions.

Because progression curves (Figure 25A) and protein binding analysis (Fig 25B and C), was analyzed from the same samples, two quality controls were performed simultaneously when bound protein fraction was quantified (% bound protein (B) and (C)). First, because the

quantification was performed with SDS-PAGE relative absorbance, any other proteins in the reaction with significant implications on the progression curve (A) should be visible on the gel. That was never observed. Secondly, a concentration control-sample was included in all the quantifiable SDS-PAGE gels of 3.59 μM and 3.46 μM *Afu*LPMO11B glycosylated and deglycosylated respectively. This ensures that the measured signal intensity of the protein bands, lies within the linear limit of the standard curve (Appendix A, Fig A1 – panel M and N)). This again, confirms that the concentrations of *Afu*LPMO11B in the assay correspond to said concentrations, and that relative variation in signal intensity have a linear correlation with protein concentration. Data can therefore be compared and % un-bound protein ($[E] + [S]$) can be estimated. The inverse of un-bound protein is used to estimate bound protein ($[ES]$).

It must be considered however, that some protein may bind to the filter membrane of the 96-well Microtiter filters (0.2 μm Hydrophilic, low protein binding Duapore membrane), or potentially stuck on omitted crystalline substrate fraction in sample filtration. In these instances, protein-substrate binding may be overestimated. However, control reaction containing only enzyme and no substrate or reductant is likely to compensate for filter membrane-bound proteins.

Another factor that could have major implications on estimating protein bound fraction using filtration techniques on crystalline substrates is that, the frequency of individual protein particles alternating from $[ES] \leftrightarrow [E] + [S]$ are unknown. Most, if not all chemical analyses measuring the state between compounds in solution, derive their data based on average properties. Therefore, a static measurement of protein and substrate reactions would show the average relationship between $[ES]$ and $[E] + [S]$. However, quantification in filtration techniques require the process of filtrating out the crystalline substrate from the samples, which may take between 0.3 – 3 seconds, and therefore the measurement does not correlate to a static binding scenario. It is therefore possible, that during filtration, proteins may wander across the substrate following the filtration flow, by binding and unbinding, causing a protein excretion at the filter-membrane border. This potential factor could grossly underestimate the true binding equilibrium with protein and substrate in solution, and should be considered in protein binding analyses.

Finally, SDS-PAGE (Mini PROTEAN® TGX Stain-Free™ Gels) was chosen as the best current alternative for quantification, on the basis of the following issues. First, UV-A₂₈₀ would yield the most precise concentration estimates if the sample was completely pure. On the binding

experiments however, small oligomeric compounds dissociate from the substrate in inactive reaction, and large amounts of soluble oxidized oligomers are present in the supernatant in the reactive (with ascorbic acid) samples. These compounds showed large interferences in the UV measurements, and the UV-method was ruled out. It should be noted that, filtration of pure, and only buffer in the 96-well Microtiter filters contributed to unexpectedly high A_{280} absorption values, between 0.000 all the way to 0.400. The latter measurement would correspond to 10 μM *AfuLPMO11B* according to $\epsilon = 38765$. That is a very high concentration in context of these studies. This indicates that interfering filter membrane particles dissociates into the analytical sample during filtration. This filtration method is commonly used for sample preparation for UPLC as well, and may be harmful for the UPLC column material.

Secondly, the Bradford reagent assay is commonly used in filtration-based bound-protein quantification analyses. The method did however not work with *AfuLPMO11B*. Several controls were made with other LPMOs and with bovine serum albumin (BSA), where *AfuLPMO11B* was the only protein with strong deviation from expected absorbance A_{595} showing 100 times less protein concentration than the references. By deglycosylation, absorbance improved by a 10-fold, yet showing 10 times less than the reference proteins. It is unclear why this happened, but the Bradford reagent may have caused the proteins to precipitate, ergo low absorbance by the Coomassie Brilliant Blue dye. The Bradford reagent assay was therefore not selected.

The last considered option was using SDS-PAGE relative fluorescent emission intensity. This method will separate proteins from soluble oligomers, which originally was considered a possible issue in the former two methods. The fluorescent measurement is very sensitive, but sample loading and sample migration in the gel, makes the results prone to high standard deviations within the triplicates.

4.5 Crystallization and protein modelling

4.5.1 Crystallization

Crystallization of *AfuLPMO11B* was attempted on various screening conditions (Appendix D, Table D1) on high enzyme concentration stocks (11, 22 and 20 g/l). Crystals were not easily produced on the glycosylated protein in the early stages, but at later timepoints around 4 – 6

months, several sample conditions had crystal formations. Several conditions were also dried out, and it is likely that most of the observed crystals were composed of salts in the condition solution. The lack of observed crystals, and that it was a fungal expressed enzyme, led to the conclusion that the protein may have glycosylations, as previously described.

Crystallization screening on the deglycosylated protein led to rapid crystal formation in some conditions, already within a week (Appendix C, Fig C1), while most other crystals on the deglycosylated protein formed within 1-2 months. Considering that the screening of the proteins with and without glycosylations were performed with the same screening kit, it seemed reasonable to believe that some of the early formed crystals could indeed be protein crystals. Although, salt crystals cannot be ruled out as it is uncertain how variations in the protein may affect the salts in crystal formation.

Crystals of particular interest were, from photo 14 and 25, also 1, 5, 6, 15, and perhaps 26 and 27 showed in the photographs (Appendix C, Fig C1) with corresponding information (Table 9), and with elaborated crystal screening recipe (Appendix F, Table F1). These crystals showed similarity to described and photographed protein crystals [116, 117].

4.5.2 Protein structure by SWISS-MODEL Homology Modelling

There is at the moment, only produced one AA11 structure, *AoLPMO11* (PDB accession code; 4mah), from the fungi *Aspergillus oryzae*. The protein shows a sequence identity of 49 % to *AfuLPMO11B* (Appendix D – Table D1) when excluding the signal peptide (aa 1 - 18 – Figure 7). Because of the lack of AA11 structures and characterized AA11s, and that different LPMO families have relatively low sequence similarity, it is hard to generate a good sequence alignment and further produce a good protein structure models. The model generated by SWISS-Model was nevertheless evaluated as a good model by the WSISS-Model quality estimates GMQE and QMEAN. *AfuLPMO11B* protein models was also generated by PHYRE² [62] and I-TASSER [63], where all the models showed high structural similarity in the LPMO core (blue region) (Fig 27) and the catalytic site (Fig 28), (Models by PHYRE² and I-TASSER and structural alignment data are not included).

In the model, the catalytic site of *AfuLPMO11B* (Fig 28) shows the two Cu-coordinating histidines, His1 and His71, also known as the histidine brace, which are by the LPMO superfamily the only totally conserved feature. The catalytic site in *AfuLPMO11B* also show

the conserved second shell glutamate Glu131, equivalent to Glu138 in *AoLPMO11*, which have been determined important in activity on chitin for *SmAA10A*, with Glu60 in the same position [23]. Upon expanded structural comparison, extending from the catalytic site (Fig 28), *AfuLPMO11B* appears to have several identical residues to *AoLPMO11* on the likely substrate facing side (Fig 29), and the proteins could potentially therefore, exhibit similar catalytic characteristics. The newly discovered crystal structure of *AfuLPMO11B* showed good structural similarity to the modelled structure, and analyses described in this study are reasonable in accordance to the structure of *AfuLPMO11B*.

4.6 Comparability between experiments

Catalytic rate is very difficult to properly determine with enzymatic reactions on crystalline substrates because of the unknown interaction nature with non-soluble particles and enzymes, which further derails from classical chemistry in solutions. Also, as discussed above, progression curves seemed to vary depending on how long the substrate was stored in solution, and could potentially reflect a gradual increase in substrate hydration, that may be important for the LPMO catalysis. The substrate stock solution was commonly made, and then used throughout various experiments in time. It was not experimentally proven that the, sometimes observed variation in catalytic rate was caused by prolonged substrate hydration, but it should nevertheless be examined to ensure reproducibility in further kinetics experiments.

Variation of LPMO catalytic rate was also demonstrated by different stock solutions, as seen by the difference in (Fig 17 and 18). *AfuLPMO11B* stock 2 (Table 7) showed approximately 2 x catalytic speed than that of stock 1. Stock 2 and 3 however, was made in parallel, and appeared to have similar catalytic activity when confirming activity after purification (not shown). Stock 3 was later deglycosylated with *EfEndo18A* and had to be purified in a second HIC and re-Cu-saturated and up concentrated. The protein may therefore experience increased denaturation, by incubation temperature of *EfEndo18A* deglycosylation procedure, temperature fluctuation i.e. purification, Cu re-saturation and concentration, and salt variations when preparing the solution for HIC where the enzyme solution contains 2 M Ammonium Sulfate. Nevertheless, the catalytic rate appear to be somewhat similar on α -chitin, when comparing the glycosylated and deglycosylated version of the protein (Fig 19). It

is however difficult to conclude if the rate itself was manipulated by variation in glycosylation, denaturation or a combination of both.

Variations in catalytic speed may also be induced by the quality of ascorbic acid, as it may interact with metal ions within MilliQ water in stock solutions, or interact with light, and lose its reductive capacity. The issue of metal ion interaction was probably avoided with the use of 'trace select' water as mentioned in ascorbic acid stocks. Preferably fresh Ascorbic acid in metal free water should always be used in LPMO kinetics experiments.

Although it may seem hard to extract conclusions by comparing independent assays considering the abundant factors causing variations in the results, the focus within the present study should not be on absolute values, but rather on the variations within each assay, as these have been performed under close to identical conditions (parallel reactions) with clear and significant results between the deliberate reaction parameters.

5. Conclusion and future perspectives

AfuLPMO11B is a chitinolytic oxidoreductase, active on α - and β -chitin, with C₁-hydroxylating substrate oxidation, using H₂O₂ and, so far to current knowledge, O₂ as catalytic cosubstrate. The enzyme appears to have fairly low catalytic rate, but with relatively good stability at 30 °C, with low degree of catalytic inactivation, even though the protein only comprise a single LPMO domain. The absolute catalytic rate cannot be estimated however, until denatured protein proportion in the enzyme stocks has been established. The protein was generally easy to produce and purify, and did not show any signs of denaturation or protein aggregation during storage at 4°C in BIS-Tris buffer (pH 6.5) within the project period (approx. 8 months).

The N-linked glycosylation on *AfuLPMO11B* showed no apparent effect in catalytic stability, but this perception may change in prolonged reactions of > 24 hours. The N-glycan did rather show purpose in substrate specificity between α - and β -chitin, both in terms of binding efficiency and catalytic rate, and in decreasing temperature stability, where the apparent melting temperature was ~ 54 °C for the glycosylated- and ~ 65 °C for the deglycosylated protein. It is important to note that, the apparent effects by glycosylation on *AfuLPMO11B* shown here, do not necessarily reflect intended or evolutionary adaptations. The enzyme originates from *Aspergillus fumigatus*, while the expression host is *Pichia pastoris*. Glycosylations are as said, post translational modifications, and there is a good chance these

organisms produce different glycosylation complexes. The results show nevertheless that glycosylation have relatively strong impacts on the functional characteristics of *AfuLPMO11B*.

AfuLPMO11B did show good cooperation with chitinase-C, with seemingly a complete conversion of β -chitin to soluble oligomeric products, and with great stability for at least 24 hours in α -chitin degradation. and with using H_2O_2 as catalytic co-substrate. Importantly, it did not seem to be able to utilize the suggested H_2O_2 -mechanism with re-reduction by H_2O_2 , mentioned [19, 40], since *AfuLPMO11B* appears to be dependent on continuous reduction with an external electron donor such as ascorbic acid between each catalytic cycle.

Due to the apparently stable activity with low levels of inactivation, both in oxygen reactions and when using H_2O_2 , this enzyme appear as a promising candidate for industrial applications. This assumption can also be made based on the significant synergy that was observed using only a single chitinase. Simplifying enzymatic cocktails, also simplifies surrounding reaction parameters, and provide the possibility of optimizing reaction conditions for all enzymes involved in developed enzyme cocktails.

References

1. Scarlat, N., Dallemand, J.F., Monforti-Ferrario, F., & Nita, V. (2015). The role of biomass and bioenergy in a future bioeconomy: policies and facts. *Environ. Dev.*, 15, 3-34. <https://doi.org/10.1016/j.envdev.2015.03.006>
2. Bugge, M.M., Hansen, T., Klitkou, A. (2016). What is the Bioeconomy? A review of the literature. *Sustainability*, 8(7), 691. <https://doi.org/10.3390/su8070691>
3. Horn, S.J., Vaaje-Kolstad, G., Westereng, B., & Eijsink, V.G. (2012). Novel enzymes for the degradation of cellulose. *Biotechnology for biofuels*, 5(45). doi:10.1186/1754-6834-5-45
4. Tharanathan, R.N., & Kittur, F.S. (2003). Chitin — The undisputed biomolecule of great potential. *Critical Reviews in Food Science and Nutrition*, 43(1), 61-87, <https://doi.org/10.1080/10408690390826455>
5. García, M.C. (2018). Drug delivery systems based on nonimmunogenic biopolymers. In Anilkumar Parambath (Ed.), *Engineering of biomaterials for Drug Delivery Systems* (pp. 317-344). <https://doi.org/10.1016/B978-0-08-101750-0.00012-X>
6. Varki, A. (2017). Biological roles of glycans. *Glycobiology*, 27(1), 3-49. <https://doi.org/10.1093/glycob/cww086>
7. Partain, E.M. (2000). Industrially important polysaccharides. In Craver, C.C., & Carraher, C.E. (Eds.), *Applied Polymer Science: 21st Century* (pp. 303-323). <https://doi.org/10.1016/B978-008043417-9/50018-0>
8. Kadokawa, J. (2016). Chemical synthesis of well-defined polysaccharides. *Reference Module in Materials Science and Materials Engineering*, (2016). <https://doi.org/10.1016/B978-0-12-803581-8.03769-3>
9. Solomon, E.P., Berg, L.R., & Martin, D.W. (2004). *Biology* (7th Ed.). Cengage Learning. p. 52.
10. LibreTexts. (2019). 5.1: Starch and cellulose. Retrieved from [https://chem.libretexts.org/Bookshelves/Organic_Chemistry/Map%3A_Organic_Chemistry_\(Smith\)/Chapter_05%3A_Stereochemistry/5.01_Starch_and_Cellulose](https://chem.libretexts.org/Bookshelves/Organic_Chemistry/Map%3A_Organic_Chemistry_(Smith)/Chapter_05%3A_Stereochemistry/5.01_Starch_and_Cellulose)
11. Meier, K.K., Jones, S.M., Kaper, T., Hansson, H., Koetsier, M.J., Karkehabadi, S., ... Kelemen, B. (2017). Oxygen activation by Cu LPMOs in recalcitrant carbohydrate polysaccharide conversion to monomer sugars. *Chemical Reviews*, 118(5), 2593-2635. <https://doi.org/10.1021/acs.chemrev.7b00421>
12. Vaaje-Kolstad, G., Horn, S.J., Van Aalten, D.M.F., Synstad, B., & Eijsink, V.G.H. (2005). The non-catalytic chitin-binding protein CBP21 from *Serratia marcescens* is essential for chitin degradation. *J. Biol. Chem.*, 280(31), 28492-28497. doi: 10.1074/jbc.M504468200
13. CAZY. (2019). *Carbohydrate active enzymes database*. Retrieved from <http://www.cazy.org/>
14. Cragg, S.M., Beckham, G.T., Bruce, N.C., Bugg, T.D.H., Distel, D.L., Dupree, ... Zimmer, M. (2015). Lignocellulose degradation mechanisms across the Tree of Life. *Current Opinion in Chemical Biology*, 29, 108-119. <https://doi.org/10.1016/j.cbpa.2015.10.018>
15. CAZY. (2019). *Carbohydrate-binding module family classification*. Retrieved from <http://www.cazy.org/Carbohydrate-Binding-Modules.html>
16. Vaaje-Kolstad, G., Westereng, B., Horn, S.J., Liu, Z., Zhai, H., Sørli, M., & Eijsink, V.G.H. (2010). An oxidative enzyme boosting the enzymatic conversion of recalcitrant polysaccharides. *Science*, 330, 219-222.
17. Hamid, R., Khan, M.A., Ahmad, M., Ahmad, M.M., Abdin, M.Z., Musarrat, J., & Javed, S. (2013). Chitinases: An update. *Journal of pharmacy & bioallied sciences*, 5(1), 21-29. doi:10.4103/0975-7406.106559
18. Danismazoglu, M., Demir, A., Sezen, K., Muratoglu, H., & Nalcacioglu, R. (2015). Cloning and expression of chitinase A, B, and C (*chiA*, *chiB*, *chiC*) genes from *Serratia marcescens* originating from *Helicoverpa armigera* and determining their activities. *Turkish Journal of Biology*, 39, 78-87. doi: 10.3906/biy-1404-31
19. Bissaro, B., Várnai, A., Røhr, Å., & Eijsink, V.G.H. (2018). Oxidoreductases and reactive oxygen species in conversion of lignocellulosic biomass. *Microbiol. Mol. Biol. Rev.*, 82(4), <https://doi.org/10.1128/MMBR.00029-18>
20. Johansen, K.S. (2016). Lytic polysaccharide monoxygenases: the microbial power tool for lignocellulose degradation. *Trends Plant Sci*, 21, 926-936. <https://doi.org/10.1016/j.tplants.2016.07.012>
21. CAZY. (2019). *Auxiliary activities family classification*. Retrieved from <http://www.cazy.org/Auxiliary-Activities.html>

22. Hemsworth, G.R., Henrissat, B., Davies, G.J., & Walton, P.H. (2013). Discovery and characterization of a new family of lytic polysaccharide monooxygenases. *Nature chemical biology*, *10*(2), 122-126. doi:10.1038/nchembio.1417
23. Vaaje-Kolstad, G., Houston, D.R., Riemen, A.H.K., Eijsink, V.G.H., & Van Aalten, D.M.F. (2005). Crystal structure and binding properties of the *Serratia marcescens* chitin-binding protein CBP21. *J Biol Chem* *280*, 11313-11319. <https://doi.org/10.1074/jbc.M407175200>.
24. Harris, P.V., Welner, D., McFarland, K.C., Re, E., Poulsen, J.N, Brown, K., ... & Leggio, L.L. (2010). Stimulation of lignocellulosic biomass hydrolysis by proteins of glycoside hydrolase family 61: Structure and function of a large, enigmatic family. *Biochemistry* *49*(15), 3305-3316. <https://doi.org/10.1021/bi100009p>
25. Agger, J.W., Isaksen, T., Várnai, A., Vidal-Melgosa, S., Willats, W.G.T., Ludwig, R., ... & Westereng, B. (2014). Discovery of LPMO activity on hemicelluloses shows the importance of oxidative processes in plant cell wall degradation. *Proc. Natl. Acad. Sci. U.S.A.*, *111*(17), 6287-6292. <https://doi.org/10.1073/pnas.1323629111>
26. The PyMOL Molecular Graphics System, Version 2.2 Schrödinger, LLC
27. Hedegård, E.D., & Ryde, U. (2017). Multiscale modelling of lytic polysaccharide monooxygenases. *ACS Omega*, *2*(2), 536-545. <https://doi.org/10.1021/acsomega.6b00521>
28. Hedegård, E.D., & Ryde, U. (2018). Molecular mechanism of lytic polysaccharide monooxygenases. *Chem. Sci.*, *9*(15), 3866-3880. <https://doi.org/10.1039/C8SC00426A>
29. Wang, B., Johnston, E.M., Li, P., Shaik, S., Davies, G.J., Walton, P.H., & Rovira, C. (2018). QM/MM studies into the H₂O₂-dependent activity of lytic polysaccharide monooxygenases: evidence for the formation of a caged hydroxyl radical intermediate. *ACS Catal.* *8*(2), 1346-1351. <https://doi.org/10.1021/acscatal.7b03888>
30. Bissaro, B., Røhr, Å.K., Müller, G., Chylenski, P., Skaugen, M., Forsberg Z, ... & Eijsink, V.G.H. (2017). Oxidative cleavage of polysaccharides by monocopper enzymes depends on H₂O₂. *Nat. Chem. Biol.*, *13*, 1123-1128. doi:10.1038/nchembio.2470
31. Beeson, W.T., Phillips, C.M., Cate, J.H., & Marletta, M.A. (2012). Oxidative cleavage of cellulose by fungal copper-dependent polysaccharide monooxygenases. *J. Am. Chem. Soc.*, *134*(2), 890-892. <https://doi.org/10.1021/ja210657t>
32. Frommhagen, M., Westphal, A.H., van Berkel, W.J., & Kabel, M.A. (2018). Distinct substrate specificities and electron-donating systems of fungal lytic polysaccharide monooxygenases. *Frontiers in Microbiology*, *9*, 1-22. doi:10.3389/fmicb.2018.01080
33. Hegnar, O.A., Petrovic, D.M., Bissaro, B., Alfreksen, G., Várnai, A., & Eijsink, V.G.H. (2019). pH-Dependent relationship between catalytic activity and hydrogen peroxide production shown via characterization of a lytic polysaccharide monooxygenase from *Gloeophyllum trabeum*. *Appl. Environ. Microbiol.*, *85*(5). doi:10.1128/AEM.02612-18
34. Kjaergaard, C.H., Qayyum, M.F., Wong, S.D., Xu, F., Hemsworth, G.R., Walton, D.J., & Solomon, E.I. (2014). Spectroscopic and computational insight into the activation of O₂ by the mononuclear Cu center in polysaccharide monooxygenases. *Proc. Natl. Acad. Sci. U.S.A.*, *111*(24), 8797-8802. doi:10.1073/pnas.1408115111
35. Walton, P.H., & Davies, G.J. (2016). On the catalytic mechanisms of lytic polysaccharide monooxygenases. *Current Opinion in Chemical Biology*, *31*, 195-207. <https://doi.org/10.1016/j.cbpa.2016.04.001>
36. Span, E.A., Suess, D.L.M., Deller, M.C., Britt, R.D., & Marletta, M.A. (2017). The role of the secondary coordination sphere in a fungal polysaccharide monooxygenase. *ACS Chem. Biol.*, *12*(4), 1095-1103. <https://doi.org/10.1021/acscchembio.7b00016>
37. Nakagawa, Y.S., Kudo, M., Loose, J.S.M., Ishikawa, T., Totani, K., Eijsink, V.G.H., & Vaaje-Kolstad, G. (2015). A small lytic polysaccharide monooxygenase from *Streptomyces griseus* targeting α - and β -chitin. *The Febs Journal*, *282*(6), 1065-1079. <https://doi.org/10.1111/febs.13203>
38. Vaaje-Kolstad, G., Bunæs, A.C., Mathiesen, G., & Eijsink, V.G.H. (2009). The chitinolytic system of *Lactococcus lactis* ssp. *lactis* comprises a nonprocessive chitinase and a chitin-binding protein that promotes the degradation of α - and β -chitin. *The Febs Journal*, *276*, 2402-2415. doi:10.1111/j.1742-4658.2009.06972
39. Hangasky, J.A., Iavarone, A.T., & Marletta, M.A. (2018). Reactivity of O₂ versus H₂O₂ with polysaccharide monooxygenases. *Proc. Natl. Acad. Sci. U.S.A.*, *115*(19), 4915-4920. doi:10.1073/pnas.1801153115

40. Kuusk, S., Bissaro, B., Kuusk, P., Forsberg, Z., Eijsink, V., Sørli, M., & Väljamäe, P. (2017). Kinetics of H₂O₂-driven degradation of chitin by a bacterial lytic polysaccharide monooxygenase. *The Journal of biological chemistry*, 293(2), 523–531. doi:10.1074/jbc.M117.817593
41. Loose, J.S.M., Arntzen, M.Ø., Bissaro, B., Ludwig, R., Eijsink, V.G.H., & Vaaje-Kolstad, G. (2018). Multi-point precision binding of substrate protects LPMOs from self-destructive off-pathway processes. *Biochemistry* 57(28), 4114-4124. <https://doi.org/10.1021/acs.biochem.8b00484>
42. Crouch, L.I., Labourel, A., Walton, P.H., Davies, G.J., & Gilbert, H.J. (2016). The contribution of non-catalytic carbohydrate binding modules to the activity of lytic polysaccharide monooxygenases. *J. Biol. Chem.*, 291, 7439-7449. <https://doi.org/10.1074/jbc.M115.702365>
43. Frandsen, K.E.H., Simmons, T.J., Dupree, P., Poulsen, J.N., Hemsworth, G.R., Ciano, L., ... & Walton, P.H. (2016). The molecular basis of polysaccharide cleavage by lytic polysaccharide monooxygenases. *Nat. Chem. Biol.*, 12, 298-303. <https://doi.org/10.1038/nchembio.2029>
44. Arora, R., Bharval, P., Sarswati, S., Sen, T.Z., & Yennamalli, R.M. (2019). Structural dynamics of lytic polysaccharide monooxygenases reveals a highly flexible substrate binding region. *Journal of Molecular Graphics and Modelling*, 88, 1-10. <https://doi.org/10.1016/j.jmkgm.2018.12.012>
45. Mutahir, Z., Mekasha, S., Loose, J. S., Abbas, F., Vaaje-Kolstad, G., Eijsink, V. G., & Forsberg, Z. (2018). Characterization and synergistic action of a tetra-modular lytic polysaccharide monooxygenase from *Bacillus cereus*. *FEBS Letters*, 592(15), 2562-2571. doi:10.1002/1873-3468.13189
46. Varki, A. (1993). Biological roles of oligosaccharides: All of the theories are correct. *Glycobiology*, 3(2), 97-130.
47. Stanley, P., Schachter, H., & Taniguchi, N. (2009). N-Glycans. In A. Varki, R.D. Cummings, J.D. Esko, et al. (Eds.) *Essentials of Glycobiology* (2nd ed., Chapter 8). Cold Spring Harbor, NY: Cold Spring Harbor Laboratory Press. Available from <https://www.ncbi.nlm.nih.gov/books/NBK1917/>
48. Brockhausen, I., Schachter, H., & Stanley, P. (2009). O-GalNAc Glycans. In A. Varki, R.D. Cummings, J.D. Esko, et al. (Eds.) *Essentials of Glycobiology* (2nd ed., Chapter 9). Cold Spring Harbor, NY: Cold Spring Harbor Laboratory Press. Available from <https://www.ncbi.nlm.nih.gov/books/NBK1896/>
49. DTU Bioinformatics. (2017). NetNGlyc 1.0 Server. N-glycan-site prediction server. Retrieved from <http://www.cbs.dtu.dk/services/NetNGlyc/>
50. DTU Bioinformatics. (2017). NetOGlyc 1.0 Server. O-glycan-site prediction server. Retrieved from <http://www.cbs.dtu.dk/services/NetOGlyc/>
51. Spiro, R.G. (2002). Protein glycosylation: nature, distribution, enzymatic formation, and disease implications of glycopeptide bonds. *Glycobiology*, 12(4), 43R-56R.
52. New England BioLabs. (2019). *Endo H*. Retrieved from <https://www.neb.com/products/p0702-endo-h#Product%20Information>
53. Bøhle, L.A., Mathiesen, G., Vaaje-Kolstad, G., & Eijsink, V.G.H. (2011). An endo-β-N-acetylglucosaminidase from *Enterococcus faecalis* V583 responsible for the hydrolysis of high-mannose and hybrid-type N-linked glycans. *FEMS Microbiology Letters*, 325,(2), 123-129. <https://doi.org/10.1111/j.1574-6968.2011.02419.x>
54. Vaaje-Kolstad, G., Westereng, B., Horn, S.J., Liu, Z.L., Zhai, H., Sørli, M., & Eijsink, V.G.H. (2010). An oxidative enzyme boosting the enzymatic conversion of recalcitrant polysaccharides. *Science*, 330, 219-222.
55. Phillips, C.M., Beeson, W.T., Cate, J.H., & Marletta, M.A. (2011). Cellobiose dehydrogenase and a copper-dependent polysaccharide monooxygenase potentiate cellulose degradation by *Neurospora crassa*. *ACS Chem. Biol.*, 6(12), 1399-1406. <https://doi.org/10.1021/cb200351y>
56. Forsberg, Z., Vaaje-Kolstad, G., Westereng, B., Bunæs, A.C., Stenstrøm, Y., Mackenzie, A., ... & Eijsink, V.G.H. (2011). Cleavage of cellulose by a CBM33 protein. *Protein Sci.*, 20(9), 1479-1483. <https://doi.org/10.1002/pro.689>
57. Westereng, B., Ishida, T., Vaaje-Kolstad, G., Wu, M., Eijsink, V.G.H., Igarashi, K., ... & Sandgren, M. (2011). The putative endoglucanase PcGH61D from *Phanerochaete chrysosporium* is a metal-dependent oxidative enzyme that cleaves cellulose. *PLoS One* 6(11). doi: 10.1371/journal.pone.0027807
58. Paspaliari, D.K., Loose, J.S., Larsen, M.H., & Vaaje-Kolstad, G. (2015). *Listeria monocytogenes* has a functional chitinolytic system and an active lytic polysaccharide monooxygenase. *The FEBS Journal*, 282(5), 921-936. doi:10.1111/febs.13191
59. Heuts, D., Winter, R.T., Damsma, G.E., Janssen, D.B., Fraaije, M.W. (2008). The role of double covalent flavin binding in chito-oligosaccharide oxidase from *Fusarium graminearum*. *Biochemical Journal*, 413(1), 175-183. doi: 10.1042/BJ20071591

60. Berman, H.M., Westbrook, J., Feng, Z., Gilliland, G., Bhat, T.N., Weissig, H., ... & Bourne, P.E. (2000). The Protein Data Bank. *Nucleic Acids Research*, 28(1), 235-242. <https://doi.org/10.1093/nar/28.1.235>
61. Waterhouse, A., Bertoni, M., Bienert, S., Studer, G., Tauriello, G., Gumienny, R. ... & Schwede, T. (2018). SWISS-MODEL: homology modelling of protein structures and complexes. *Nucleic Acids Res.*, 46(W1), W296-W303. <https://doi.org/10.1093/nar/gky427>
62. Kelley, L.A., Mezulis, S., Yates, C.M., Wass, M.N., & Sternberg, M.J.E. (2015). The Phyre2 web portal for protein modeling, prediction and analysis. *Nature Protocols* 10, 845-858.
63. Yang, J., Yan, R., Roy, A., Xu, D., Poisson, J., & Zhang, Y. (2015). The I-TASSER Suite: protein structure and function prediction. *Nature Methods*, 12(1), 7-8. doi:10.1038/nmeth.3213
64. Nielsen, S.S. (2010). Introduction to Food Analysis. In S.S. Nielsen (Ed.) *Food analysis* (pp. 3-14). New York: Springer.
65. Choudhary, A. (2018). Differences between HPLC and UPLC. Retrieved from <https://www.pharmaguideline.com/2018/04/differences-between-hplc-and-uplc.html>
66. ThermoFisher Scientific. (n.d.) *Liquid chromatography*. Retrieved from <https://www.thermofisher.com/no/en/home/industrial/chromatography/liquid-chromatography-liquid-chromatography-lc.html>
67. ThermoFisher Scientific. (n.d.) *HPLC and UHPLC detectors*. Retrieved from <https://www.thermofisher.com/no/en/home/industrial/chromatography/liquid-chromatography-liquid-chromatography-lc/hplc-uhplc-components/hplc-uhplc-detectors>.
68. Swartz, M. E. (2005). UPLC™: an introduction and review. *Journal of Liquid Chromatography & Related Technologies*, 28(7-8), 1253-1263. <https://doi.org/10.1081/JLC-200053046>
69. Yan, X. (2014). HPLC for Carbohydrate Analysis. In Zou, Y. (Ed.) *HPLC principle, practices, and procedures* (pp. 22). Nova Science.
70. ThermoFischer Scientific. (n.d.) *Overview of mass spectrometry for protein analysis*. Retrieved from <https://www.thermofisher.com/no/en/home/life-science/protein-biology/protein-biology-learning-center/protein-biology-resource-library/pierce-protein-methods/overview-mass-spectrometry.html>
71. Wikipedia. (n.d.) *Mass spectrometry*. Retrieved from https://en.wikipedia.org/wiki/Mass_spectrometry
72. Maurer, H.H., Kraemer, T., Ledvinka, O., Schmitt, C.J., & Weber, A.A. (1997). Gas chromatography-mass spectrometry (GC-MS) and liquid chromatography-mass spectrometry (LC-MS) in toxicological analysis Studies on the detection of clobenzorex and its metabolites within a systematic toxicological analysis procedure by GC-MS and by immunoassay and studies on the detection of α - and β -amanitin in urine by atmospheric pressure ionization electrospray LC-MS. *Journal of Chromatography B: Biomedical Sciences and Applications*, 689(1), 81-89. [https://doi.org/10.1016/S0378-4347\(96\)00348-9](https://doi.org/10.1016/S0378-4347(96)00348-9)
73. Lemièrè, F. (2001). *Mass analysers for LC-MS*. Retrieved from http://alfresco.ubm-us.net/alfresco_images/pharma/2014/08/22/78056c0f-8084-4f13-a5dd-a4c333cd5b89/article-8133.pdf
74. Perkel, J.M. (2009). *Mass spectrometry ionization sources*. Retrieved from <https://www.labcompare.com/18-Mass-Spectrometry-Ionization-Sources>
75. Singhal, N., Kumar, M., Kanaujia, P.K., & Virdi, J.S. (2015). MALDI-TOF mass spectrometry: an emerging technology for microbial identification and diagnosis. *Frontiers in microbiology*, 6, 791. doi:10.3389/fmicb.2015.00791
76. Ho, C.S., Lam, C.W., Chan, M.H., Cheung, R. C., Law, L.K., Lit, L.C., ... & Tai, H.L. (2003). Electrospray ionisation mass spectrometry: principles and clinical applications. *The Clinical biochemist. Reviews*, 24(1), 3-12.
77. De Nys, S., Putzeys, E., Vervliet, P., Covaci, A., Boonen, I., Elskens, M., ... & Duca, R.C. (2018). A novel high sensitivity UPLC-MS/MS method for the evaluation of bisphenol A leaching from dental materials. *Scientific Reports*, 8(6981). <https://doi.org/10.1038/s41598-018-24815-z>
78. Kuusk, S., Kont, R., Kuusk, P., Heering, A., Sørliè, M., Bissaro, B., ... & Våljamäe, P. (2019). Kinetic insights into the role of the reductant in H₂O₂-driven degradation of chitin by a bacterial lytic polysaccharide monooxygenase. *Journal of Biological Chemistry*, 294(5), 1516-1528. doi: 10.1074/jbc.RA118.006196
79. Higel, F., Seidl, A., Sörgel, F., & Friess, W. (2016). N-glycosylation heterogeneity and the influence on structure, function and pharmacokinetics of monoclonal antibodies and Fc fusion proteins. *European Journal of Pharmaceutics and Biopharmaceutics*, 100, 94-100. <https://doi.org/10.1016/j.ejpb.2016.01.005>

80. Cereghino, J.L., & Cregg, J.M. (2000). Heterologous protein expression in the methylotrophic yeast *Pichia pastoris*. *FEMS Microbiology Reviews*, 24(1), 45-66. <https://doi.org/10.1111/j.1574-6976.2000.tb00532.x>
81. Life Technologies Corporation. (2014). *PichiaPink™ Expression System: For high-level and large-scale expression and secretion of bioactive recombinant proteins in Pichia pastoris*. Retrieved from http://tools.thermofisher.com/content/sfs/manuals/pichiapink_expression_system_man.pdf
82. Waltson, J.D., Caudy, A.A., Myers, R.M., & Witkowski, J.A. (2007). *Recombinant DNA: genes and genomes: a short course* (3rd ed.) San Francisco: Cold Spring Harbor Laboratory Press.
83. Sørensen, H.P., & Mortensen, K.K. (2004). Advanced genetic strategies for recombinant protein expression in *Escherichia coli*. *Journal of Biotechnology*, 115(2), 113-128. doi: 10.1016/j.jbiotec.2004.08.004
84. Cooper, G.M. (2000). *The cell: a molecular approach* (2nd ed.) Sunderland, MA: Sinauer Associates. Retrieved from <https://www.ncbi.nlm.nih.gov/books/NBK9917/>
85. Heterologous expression. (2009). In M.D. Binder, N. Hirokawa, & U. Windhorst (Eds.) *Encyclopedia of Neuroscience*. Berlin Heidelberg: Springer. doi:10.1007/978-3-540-29678-2_2190
86. Mergulhão, F.J.M., Summers, D.K., & Monteiro, G.A. (2005). Recombinant protein secretion in *Escherichia coli*. *Biotechnology Advances* 23(3), 177-202. <https://doi.org/10.1016/j.biotechadv.2004.11.003>
87. Baneyx, F. (1999). Recombinant protein expression in *Escherichia coli*. *Current Opinion in Biotechnology* 10(5), 411-421. [https://doi.org/10.1016/S0958-1669\(99\)00003-8](https://doi.org/10.1016/S0958-1669(99)00003-8)
88. Wu, X.C., Lee, W., Tran, L., & Wong, S. (1991). Engineering a *Bacillus subtilis* expression-secretion system with a strain deficient in six extracellular proteases. *Journal of Bacteriology*, 173(16), 4952-4958. doi: 10.1128/jb.173.16.4952-4958.1991
89. Gasteiger, E., Hoogland, C., Gattiker, A., Duvaud, S., Wilkins, M.R., Appel, R.D., & Bairoch, A. (2005). Protein identification and analysis tools on the ExPASy Server. In J.M. Walker (Ed) *The Proteomics Protocols Handbook* (pp. 571-607). Humana Press.
90. Sadilkova, L., Osicka, R., Sulc, M., Linhartova, I., Novak, P., & Sebo, P. (2008). Single-step affinity purification of recombinant proteins using a self-excising module from *Neisseria meningitidis* FrpC. *Protein Science*, 17(10), 1834-1843. doi:10.1110/ps.035733.108
91. Yang, Y.B., Harrison, K., & Kindsvater, J. (1996). Characterization of a novel stationary phase derivative from a hydrophilic polystyrene-based resin for protein cation exchange high-performance liquid chromatography. *Journal of chromatography A*, 723(1), 1-10. [https://doi.org/10.1016/0021-9673\(95\)00831-4](https://doi.org/10.1016/0021-9673(95)00831-4)
92. Coskun, O. (2016). Separation techniques: chromatography. *North Clin. Istanbul*, 3(2), 156-160. doi: 10.14744/nci.2016.32757
93. Queiroz, J.A., Tomaz, C.T., & Cabral, J.M.S. (2001). Hydrophobic interaction chromatography of proteins. *Journal of Biotechnology*, 87(2), 143-159. [https://doi.org/10.1016/S0168-1656\(01\)00237-1](https://doi.org/10.1016/S0168-1656(01)00237-1)
94. GE Healthcare Life Sciences. (n.d.) *Fundamentals of size exclusion chromatography*. Retrieved from <https://www.gelifesciences.com/en/us/solutions/protein-research/knowledge-center/protein-purification-methods/size-exclusion-chromatography>
95. Eijsink, V., Petrovic, D., Forsberg, Z., Mekasha, S., Røhr, Å. K., Várnai, A., ... Vaaje-Kolstad, G. (2019). On the functional characterization of lytic polysaccharide monoxygenases (LPMOs). *Biotechnology for biofuels*, 12, 58. doi:10.1186/s13068-019-1392-0
96. Frandsen, K.E., & Leggio, L.L. (2016). Lytic polysaccharide monoxygenases: a crystallographer's view on a new class of biomass-degrading enzymes. *IUCrJ*, 3, 448-467. doi:10.1107/S2052252516014147
97. Koshland, D.E., & Haurowitz, F. (n.d.). *Protein: biochemistry*. Retrieved 30 April 2019 from <https://www.britannica.com/science/protein>
98. Lesk, A. (2010). *Introduction to protein science: architecture, function, and genomics*. Oxford university press.
99. Medical & Biological Laboratories Co. (n.d.). *The principle and method of polyacrylamide gel electrophoresis (SDS-PAGE)*. Retrieved from <https://www.mblbio.com/bio/g/support/method/sds-page.html>
100. Khalsa, G. (2010). *SDS-Page*. Retrieved 2 May 2019 from <https://askabiologist.asu.edu/sds-page>
101. Bradford, M.M. (1976). A rapid and sensitive method for the quantitation of microgram quantities of protein utilizing the principle of protein-dye binding. *Analytical Biochemistry*, 72(1-2), 48-254. [https://doi.org/10.1016/0003-2697\(76\)90527-3](https://doi.org/10.1016/0003-2697(76)90527-3)

102. BioRad. (2016). *Stain-free imaging technology*. Retrieved from <http://www.bio-rad.com/en-no/applications-technologies/stain-free-imaging-technology?ID=NZ0G1815>
103. Madeira, F., Park, Y.M., Lee, J., Buso, N., Gur, T., Madhusoodanan, ... & Lopez, R. (2019). The EMBL-EBI search and sequence analysis tools APIs in 2019. *Nucleic Acids Research*. <https://doi.org/10.1093/nar/gkz268>
104. Robert, X. & Gouet, P. (2014). Deciphering key features in protein structures with the new ENDscript server. *Nucleic Acids Research*, 42(W1), W320-W324. doi: 10.1093/nar/gku316
105. The UniProt Consortium. (2019). UniProt: a worldwide hub of protein knowledge. *Nucleic Acids Research*, 47(D1), D506-D515. <https://doi.org/10.1093/nar/gky1049>
106. Vaaje-Kolstad, G., Horn, S.J., Sørli, M., & Eijsink, V.G.H. (2013). The chitinolytic machinery of *Serratia marcescens* – a model system for enzymatic degradation of recalcitrant polysaccharides. *The FEBS Journal*, 280(13), 3028-3049. doi:10.1111/febs.12181
107. Signal peptide prediction server, SignalP-5.0. Data retrieved from (<http://www.cbs.dtu.dk/services/SignalP/>).
108. Loose, J.S., Forsberg, Z., Kracher, D., Scheiblbrandner, S., Ludwig, R., Eijsink, V.G.H., & Vaaje-Kolstad, G. (2016). Activation of bacterial lytic polysaccharide monoxygenases with cellobiose dehydrogenase. *Protein Science*, 25(12), 2175-2186. doi:10.1002/pro.3043.
109. Courtade, G., Forsberg, Z., Heggset, E.B., Eijsink, V.G.H., & Aachmann, F.L. (2018). The carbohydrate-binding module and linker of a modular lytic polysaccharide monoxygenase promote localized cellulose oxidation. *J. Biol. Chem.*, 293, 13006-13015. doi:10.1074/jbc.RA118.004269.
110. Geo Gems Mineral Club. (2018). *7 types of crystals structure and shapes*. Retrieved from <http://www.geogemsmineralclub.com/2018/11/23/7-types-of-crystals-structure-and-shapes/>
111. Kang, A. & Lee, T.S. (2015). Converting sugars to biofuels: ethanol and beyond. *Bioengineering*, 2(4), 184-203. doi:10.3390/bioengineering2040184
112. Khanna, M., Crago, C.L., & Black, M. (2011). Can biofuels be a solution to climate change? The implications of land use change-related emissions for policy. *Interface focus*, 1(2), 233-247. doi:10.1098/rsfs.2010.0016
113. Inokuma, K., Hasunuma, T., & Kondo, A. (2016). Ethanol production from N-acetyl-D-glucosamine by *Scheffersomyces stipitis* strains. *AMB Express*, 6(1), 83. doi:10.1186/s13568-016-0267-z
114. Loose, J.S., Forsberg, Z., Kracher, D., Scheiblbrandner, S., Ludwig, R., Eijsink, V.G.H., & Vaaje-Kolstad, G. (2016). Activation of bacterial lytic polysaccharide monoxygenases with cellobiose dehydrogenase. *Protein science*, 25(12), 2175-2186. doi:10.1002/pro.3043
115. Müller, G., Chylenski, P., Bissaro, B., Eijsink, V.G.H., & Horn, S.J. (2018). The impact of hydrogen peroxide supply on LPMO activity and overall saccharification efficiency of a commercial cellulase cocktail. *Biotechnology for biofuels*, 11. <https://doi.org/10.1186/s13068-018-1199-4>
116. McPherson, A. & Gavira, J.A. (2013). Introduction to protein crystallization. *Structural biology communications*, 70(1), 2-20. <https://doi.org/10.1107/S2053230X13033141>
117. Giegé, R. (2013). A historical perspective on protein crystallization from 1840 to the present day. *The FEBS Journal*, 280(24), 6456-6497. doi:10.1111/febs.12580
118. Wood, T.M. (1988). Preparation of crystalline, amorphous, and dyed cellulose substrates. *Methods in Enzymology*, 160, 19-25. [https://doi.org/10.1016/0076-6879\(88\)60103-0](https://doi.org/10.1016/0076-6879(88)60103-0)
119. Várnai, A., Tang, C., Bengtsson, O., Atterton, A., Mathiesen, G., Eijsink, V.G.H. (2014). Expression of endoglucanases in *Pichia pastoris* under control of the GAP promoter. *Microb. Cell Fact.* 13(57), 1-10. <https://doi.org/10.1186/1475-2859-13-57>
120. Biely, P., Cizsarová, M., Uhliaríková, I., Agger, J.W., Li, X., Eijsink, V.G.H., & Westereng, B. (2013). Mode of action of acetylxyylan esterases on acetyl glucuronoxylan and acetylated oligosaccharides generated by a GH10 endoxylanase. *Biochimica et Biophysica Acta*, 1830(11), 2013, 5075-5086. <https://doi.org/10.1016/j.bbagen.2013.07.018>
121. Mekasha, S., Byman, I.R., Lynch, C., Toupalová, H., Anděra, L., Næs, T, ... & Eijsink, V.G.H. (2017). Development of enzyme cocktails for complete saccharification of chitin using mono-component enzymes from *Serratia marcescens*. *Process Biochemistry*, 56, 132-138. <https://doi.org/10.1016/j.procbio.2017.02.021>
122. McCourt, J.A., Tyagi, R., Guddat, L.W., Biou, V., & Duggleby, R.G. (2004). Facile crystallization of *Escherichia coli* ketol-acid reductoisomerase. *Biological Crystallography*, 60(8), 1432-1434. <https://doi.org/10.1107/S0907444904012247>
123. Loose, J.S.M., Forsberg, Z., Fraaije, M.W., Eijsink, V.G.H., & Vaaje-Kolstad, G. (2014). A rapid quantitative activity assay shows that the *Vibrio cholerae* colonization factor GbpA is an active lytic

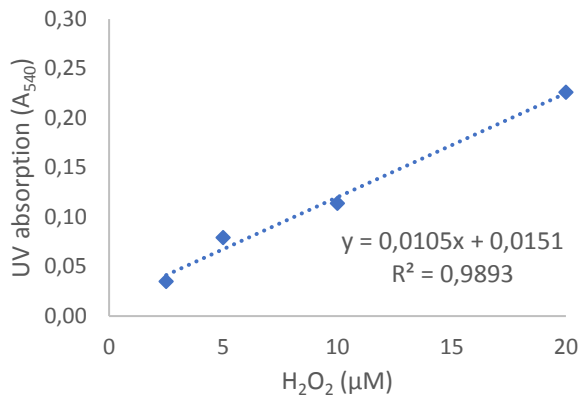
- polysaccharide monooxygenase. *FEBS Letters*, 588(18), 3435-3440.
<https://doi.org/10.1016/j.febslet.2014.07.036>
124. Nakagawa, Y.S., Kudo, M., Loose, J.S., Ishikawa, T., Totani, K., Eijsink, V.G.H., & Vaaje-Kolstad, G. (2015). A small lytic polysaccharide monooxygenase from *Streptomyces griseus* targeting α - and β -chitin. *The FEBS Journal*, 282(6), 1065-1079. doi:10.1111/febs.13203
 125. ThermoFisher Scientific. (n.d.) Protein Thermal Shift™ Dye Kit PDF. Retrieved from <https://www.thermofisher.com/document-connect/document-connect.html?url=https%3A%2F%2Fassets.thermofisher.com%2FTFS-Assets%2FLSG%2Fmanuals%2F4461806B.pdf&title=UHVjdGVpbjBUaGVybWVfIFNoaWZ0JnRyYWRI0yBEeJnRy2l0>
 126. Kaya, M., Mujtaba, M., Ehrlich, H., Salaberria, A.M., Baran, T., Amemiya, C.T, Galli, R., Akyuz, L., Sargin, I., & Labidi, J., (2017) On chemistry of γ -chitin, *Carbohydrate Polymers*, Volume 176, Pages 177-186, <https://doi.org/10.1016/j.carbpol.2017.08.076>.
 127. Synowiecki, J., & Al-Khateeb, N.A., (2003) Production, Properties, and Some New Applications of Chitin and Its Derivatives, *Critical Reviews in Food Science and Nutrition*, 43:2, 145-171, doi: 10.1080/10408690390826473
 128. Tuveng, T.R., Hagen, L.H., Mekasha, S., Frank, J., Arntzen, M.Ø., Vaaje-Kolstad, G., Eijsink, V.G.H., (2017) Genomic, proteomic and biochemical analysis of the chitinolytic machinery of *Serratia marcescens*. *BJL200, Biochimica et Biophysica Acta (BBA) - Proteins and Proteomics*, Volume 1865, Issue 4, Pages 414-421, <https://doi.org/10.1016/j.bbapap.2017.01.007>.
 129. Borisova, A. S., Isaksen, T., Dimarogona, M., Kognole, A. A., Mathiesen, G., Várnai, A., ... Eijsink, V. G. (2015). Structural and Functional Characterization of a Lytic Polysaccharide Monooxygenase with Broad Substrate Specificity. *The Journal of biological chemistry*, 290(38), 22955–22969. doi:10.1074/jbc.M115.660183
 130. Courtade, G., Wimmer, R., Røhr, Å. K., Preims, M., Felice, A. K., Dimarogona, M., ... & Eijsink, V. G. (2016). Interactions of a fungal lytic polysaccharide monooxygenase with β -glucan substrates and cellobiose dehydrogenase. *Proceedings of the National Academy of Sciences*, 113(21), 5922-5927
 131. Wang, D., Li, J., Wong, A., Aachmann, F. L., & Hsieh, Y. (2018). A colorimetric assay to rapidly determine the activities of lytic polysaccharide monooxygenases. *Biotechnology for biofuels*, 11, 215. doi:10.1186/s13068-018-1211-z
 132. Liu, Z., Gay, L. M., Tuveng, T. R., Agger, J. W., Westereng, B., Mathiesen, G., ... Eijsink, V. (2017). Structure and function of a broad-specificity chitin deacetylase from *Aspergillus nidulans* FGSC A4. *Scientific reports*, 7(1), 1746. doi:10.1038/s41598-017-02043-1

Appendices

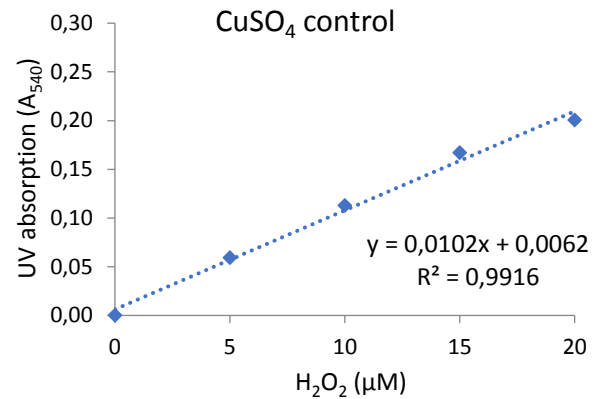
APPENDIX A

Appendix A contains standard curves used to calculate progression curves in the various experiments performed, as described in the methods section.

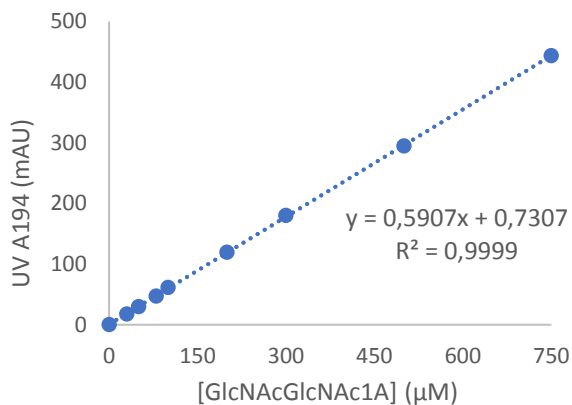
A. H₂O₂ production assay



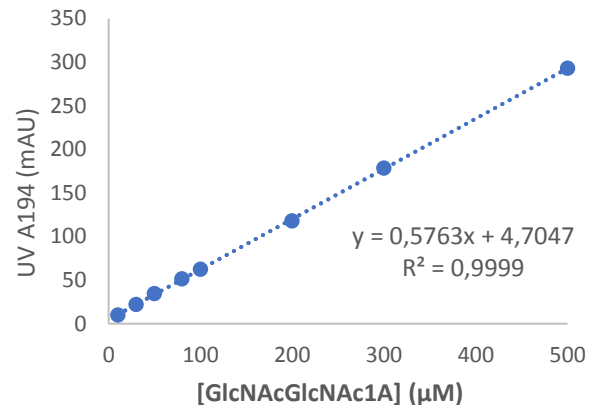
B. H₂O₂ production - imported
CuSO₄ control



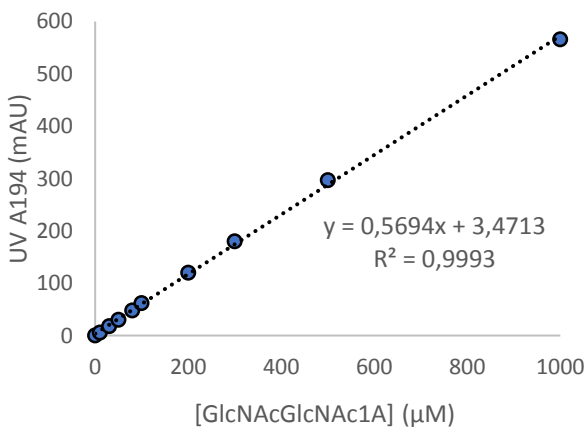
C. Temperature screen



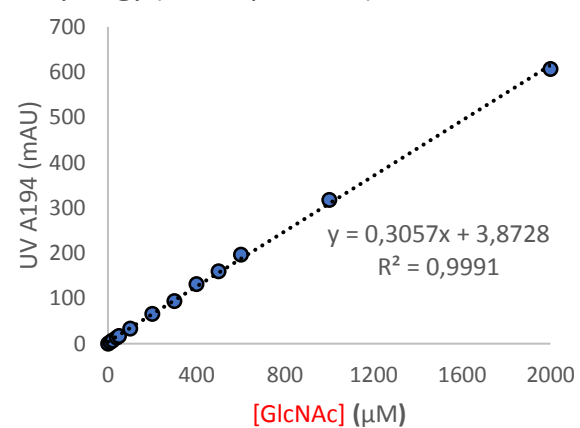
D. *Afu*LPMO11B vs *Bc*LPMO10A



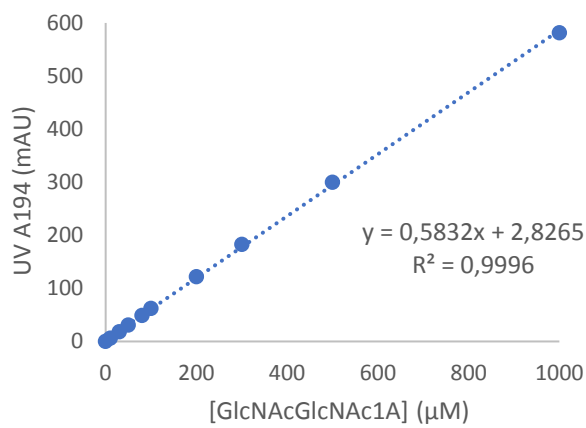
E. Synergy (oxidized products)



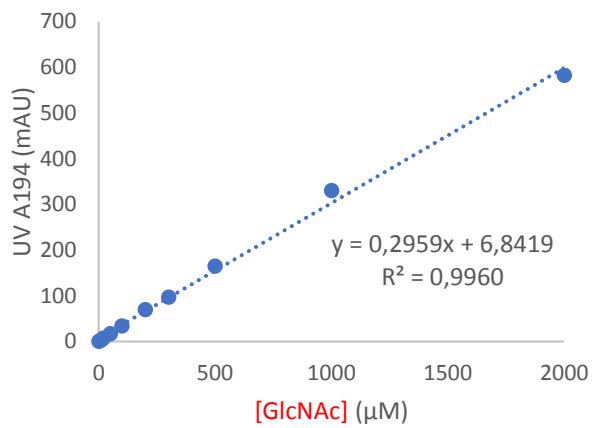
F. Synergy (native products)



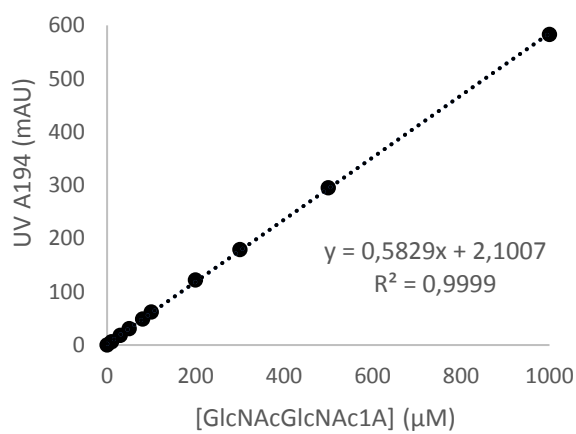
G. H₂O₂ feeding experiment (A)



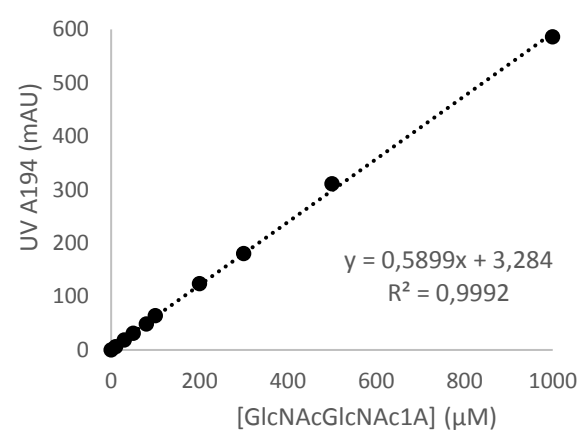
H. H₂O₂ feeding experiment (A)



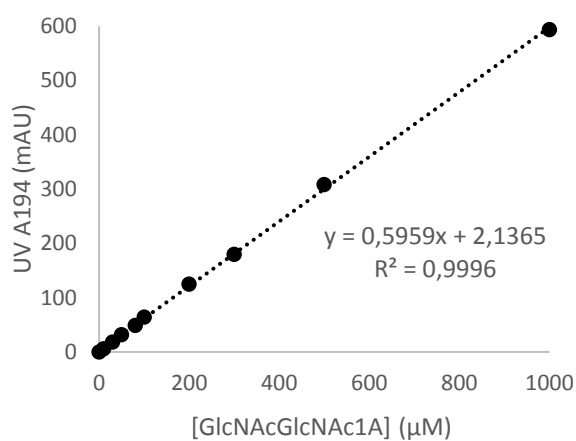
I. H₂O₂ feeding experiment (B)



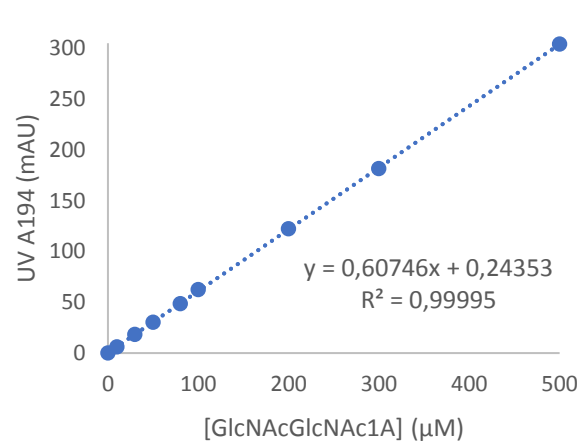
J. H₂O₂ feeding experiment (C)



K. H₂O₂ feeding experiment (D)



L. H₂O₂ feeding experiment (E)



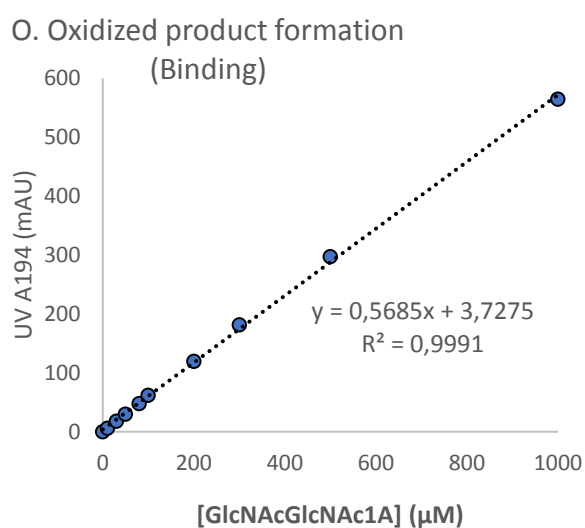
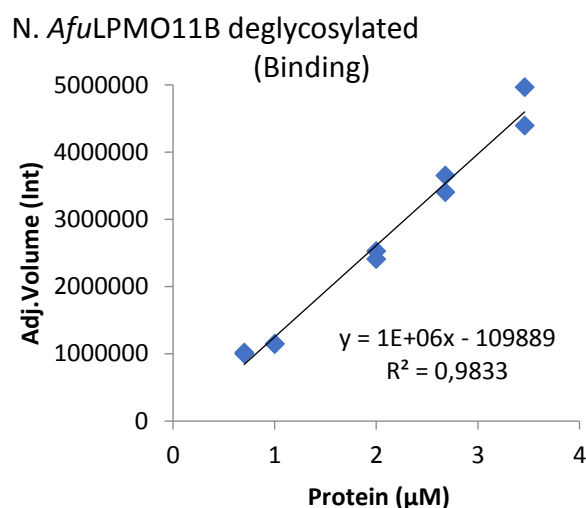
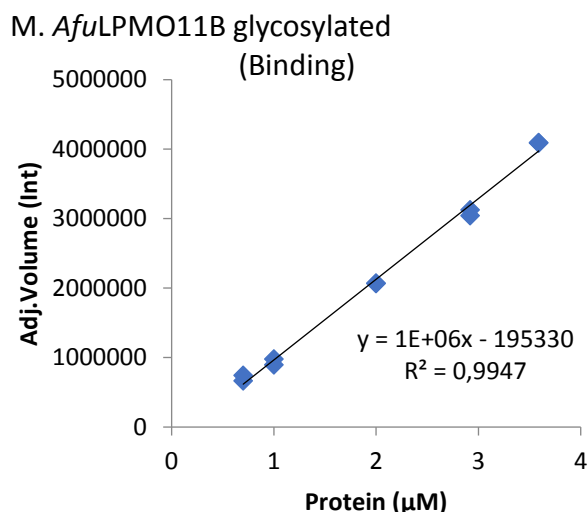


Fig A1. All standard curves used in quantification estimates. All panels show standard curves that were included and analyzed along with the reaction products according to the method described for the relevant experiments (Methods), and used in quantification of H_2O_2 (panel A and B), native GlcNAc (N-acetylglucosamine) monomers (panel F and H), [GlcNAcGlcNAc1A] (N-acetylglucosamine aldonic acids and lactones) oxidized dimers (panel C, D, E, G, I, J, K, L, and O), and protein binding (panel M and N). Each standard curve have a title that correspond to the experiment that they were used for, described in the methods. Measurements were performed in duplicates. Panel A and B were performed in duplicates and triplicates respectively (standard deviation not included), panel C – L and O were performed in singlets, and panel M and N were performed in duplicates with all points included.

APPENDIX B

Appendix B show purification of *Afu*LPMO11B from start to finish.

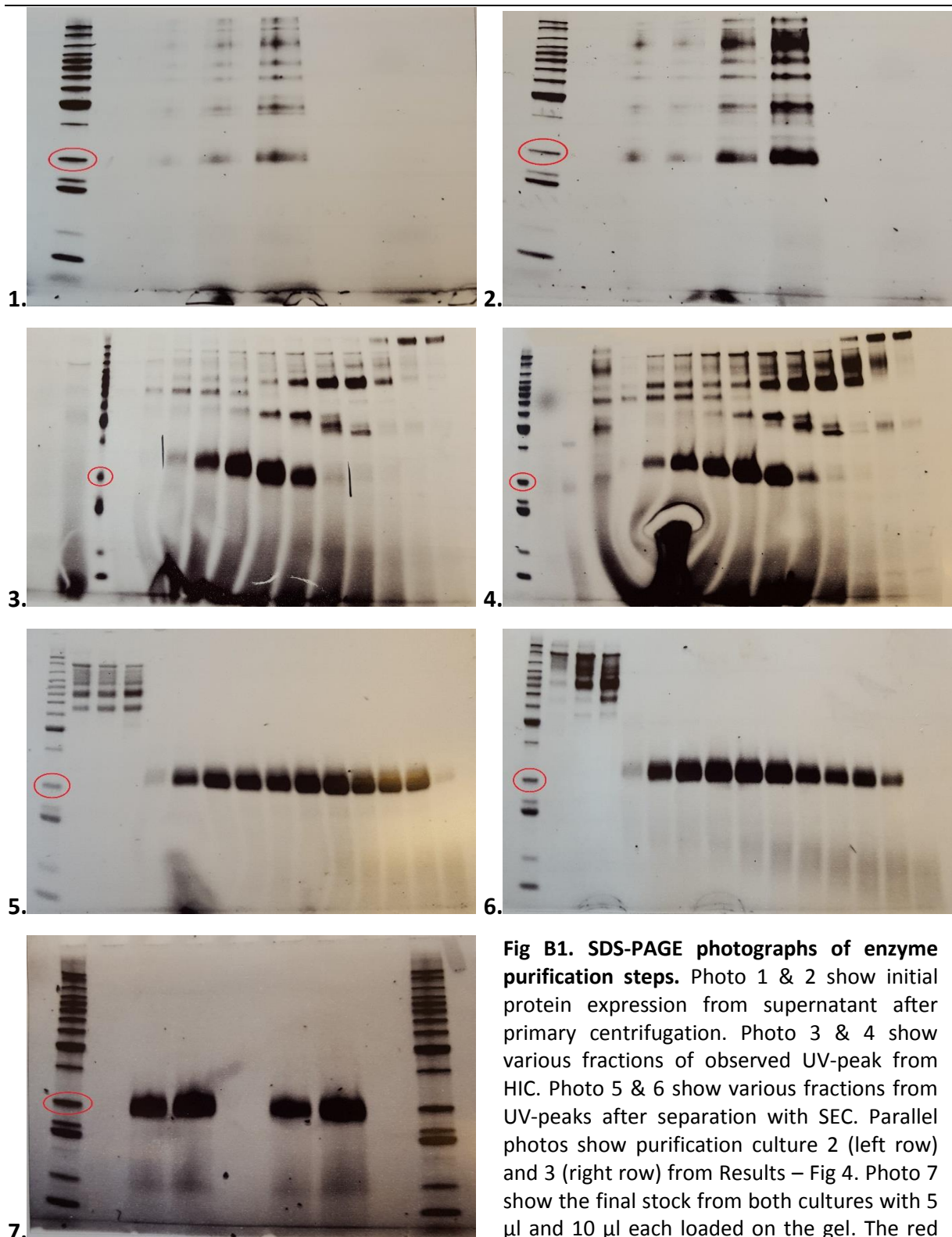
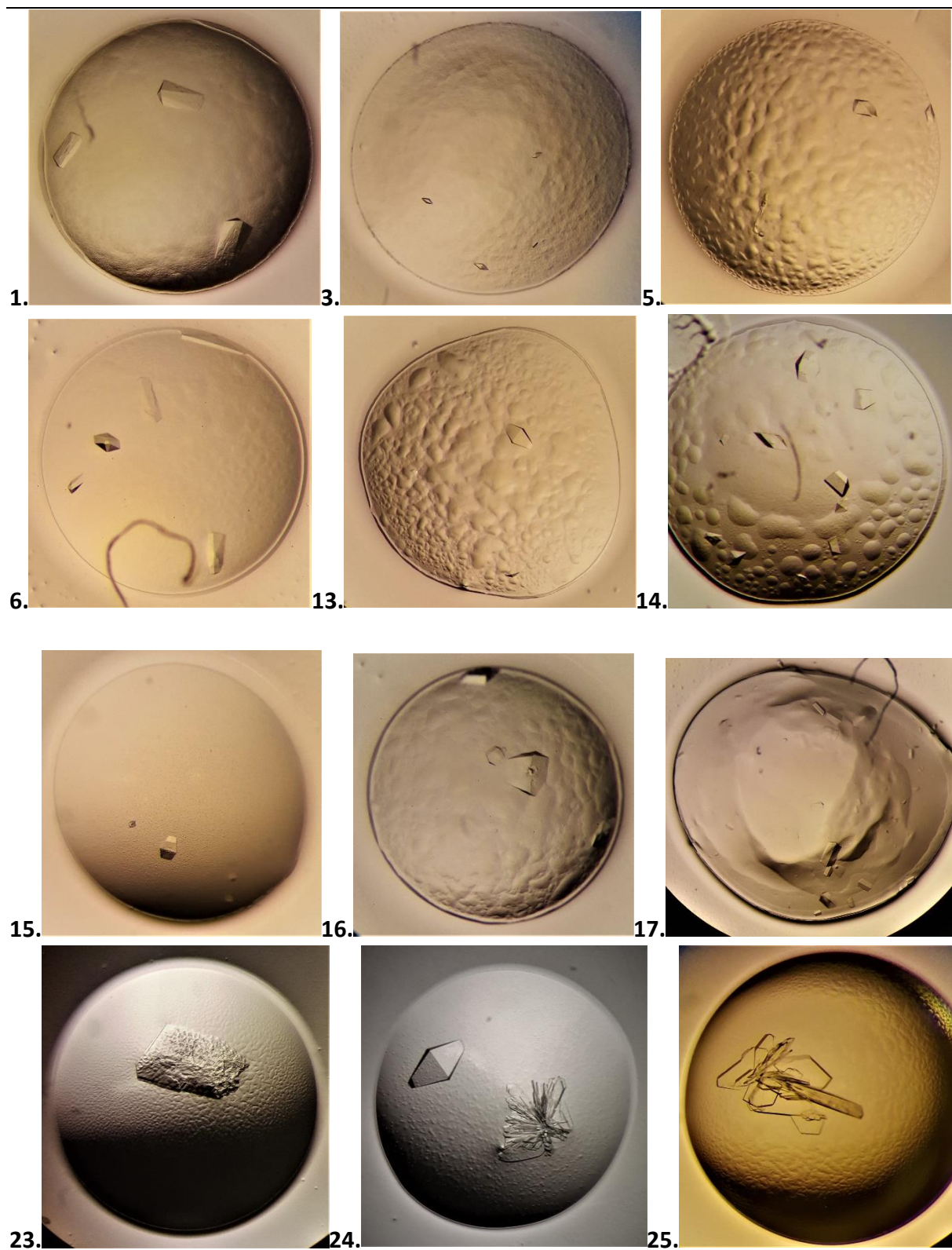


Fig B1. SDS-PAGE photographs of enzyme purification steps. Photo 1 & 2 show initial protein expression from supernatant after primary centrifugation. Photo 3 & 4 show various fractions of observed UV-peak from HIC. Photo 5 & 6 show various fractions from UV-peaks after separation with SEC. Parallel photos show purification culture 2 (left row) and 3 (right row) from Results – Fig 4. Photo 7 show the final stock from both cultures with 5 μ l and 10 μ l each loaded on the gel. The red circle marked on the protein ladder correspond to a mass of 30 kDa.

APPENDIX C

Appendix C contains pictures of several crystal formations from the crystallization screens on glycosylated and deglycosylated *AfuLPMO11B*.



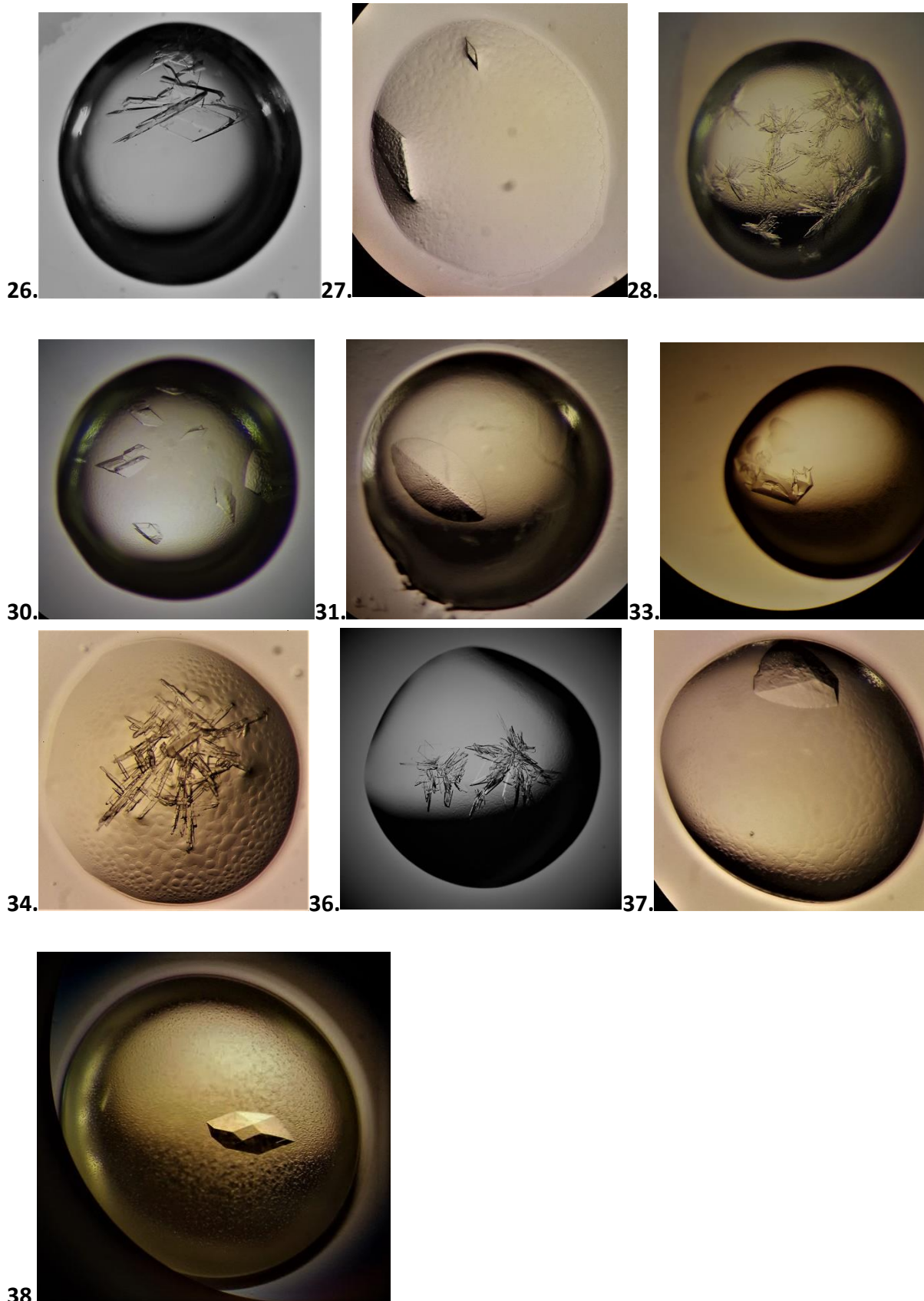


Fig C1. Crystal photo gallery. The gallery shows photographed crystals from the crystallization screens. Photographs are numbered on the left side according to N in table 10 (Results). The last photo (38) shows crystal formation in the in-house produced crystallizing solution #1-15 together with the deglycosylated *AfuLPMO11B*, highlighted in grey in table 10 (Results).

APPENDIX D

Appendix D contain bioinformatic supplementary information, i.e. multiple sequence alignment from several chitin active LPMOs, the full model report by SWISS MODEL in making the *AfuLPMO11B* model structure, glycosylation site predictions on *AfuLPMO11B* by NetNGlyc and NetOGlyc, and signal peptide prediction by SignalP-5.0.

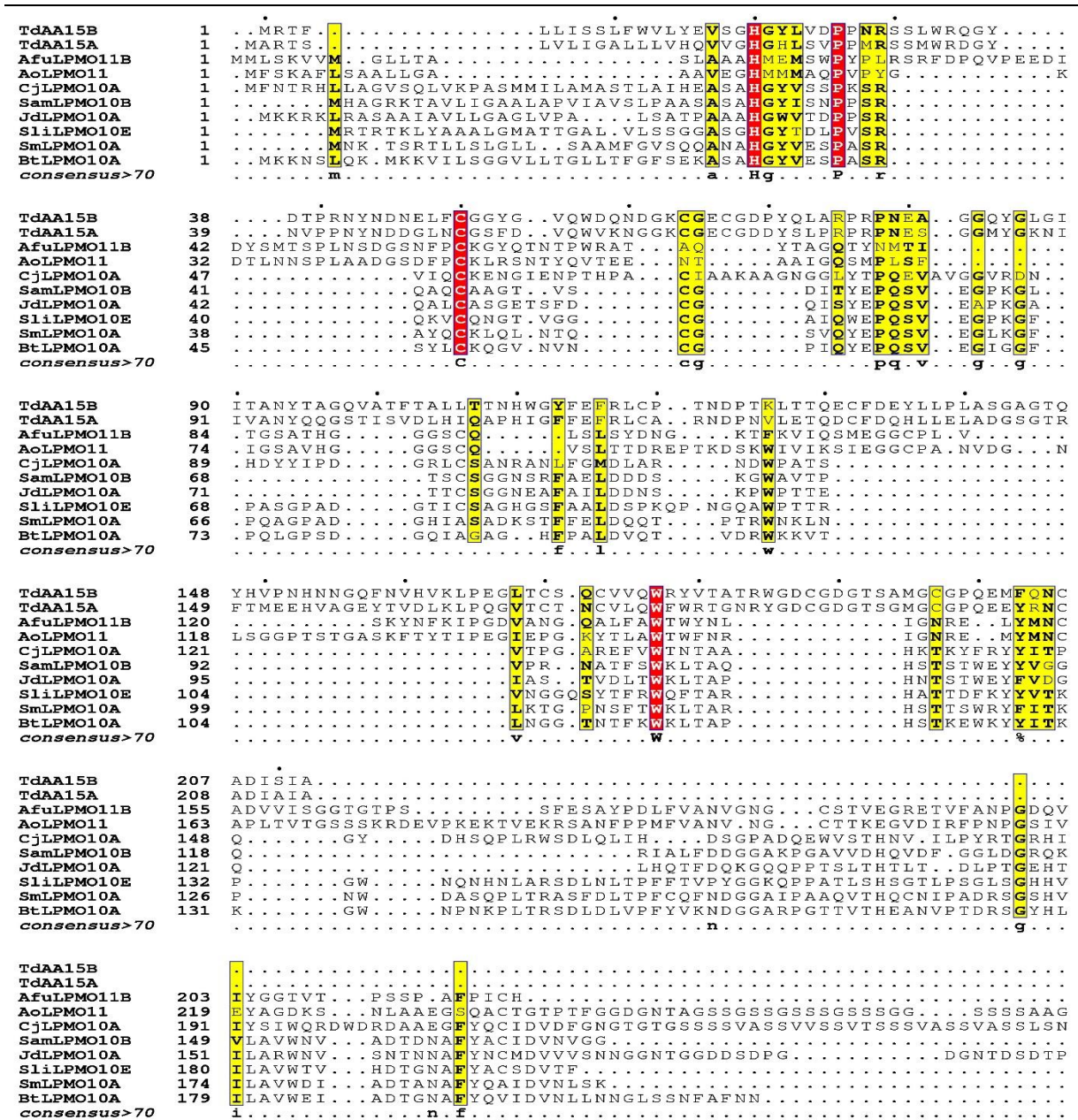


Fig D1. Multiple sequence alignment of chitin-active LPMOs. The figure contains a multiple peptide sequence alignment of chitin active LPMOs, comprising 6 randomly selected AA-family 10, and all AA11s -and AA15s from the CAZy database of characterized LPMOs, and the FASTA sequence for *AfuLPMO11B* (UniProt ID: B0XZD3, Gene name: AFUB_044010). The figure shows only relevant (approx. 1-250) residues alignment, as only a few enzymes had continued sequence, and there was no further significantly conserved residues with > 0.7 confidence. Marked in (red) shows 100 % identical residues in all sequences, while (bold-yellow) shows similar residues above the confidence limit. The alignment was generated with Clustal Omega [103], and modified with ESPrnt 3.0 [104].

Table D1. SWISS-MODEL Homology Modelling Report. The table contains the full protein model report by SWISS-MODEL for the generated structure model of *AfuLPMO11B*.



SWISS-MODEL Homology Modelling Report

Model Building Report

This document lists the results for the homology modelling project "Untitled Project" submitted to SWISS-MODEL workspace on March 18, 2019, 6:15 p.m..The submitted primary amino acid sequence is given in Table T1.

If you use any results in your research, please cite the relevant publications:

- Waterhouse, A., Bertoni, M., Bienert, S., Studer, G., Tauriello, G., Gumienny, R., Heer, F.T., de Beer, T.A.P., Rempfer, C., Bordoli, L., Lepore, R., Schwede, T. SWISS-MODEL: homology modelling of protein structures and complexes. *Nucleic Acids Res.* 46(W1), W296-W303 (2018). [doi>](#)
- Guex, N., Peitsch, M.C., Schwede, T. Automated comparative protein structure modeling with SWISS-MODEL and Swiss-PdbViewer: A historical perspective. *Electrophoresis* 30, S162-S173 (2009). [doi>](#)
- Bienert, S., Waterhouse, A., de Beer, T.A.P., Tauriello, G., Studer, G., Bordoli, L., Schwede, T. The SWISS-MODEL Repository - new features and functionality. *Nucleic Acids Res.* 45, D313-D319 (2017). [doi>](#)
- Benkert, P., Biasini, M., Schwede, T. Toward the estimation of the absolute quality of individual protein structure models. *Bioinformatics* 27, 343-350 (2011). [doi>](#)
- Bertoni, M., Kiefer, F., Biasini, M., Bordoli, L., Schwede, T. Modeling protein quaternary structure of homo- and hetero-oligomers beyond binary interactions by homology. *Scientific Reports* 7 (2017). [doi>](#)

Results

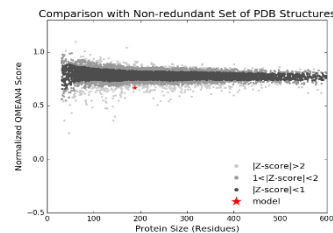
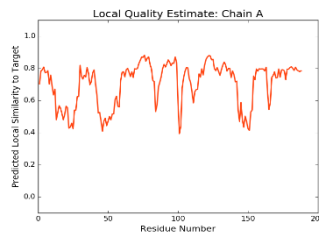
The SWISS-MODEL template library (SMTL version 2019-03-13, PDB release 2019-03-08) was searched with BLAST ([Camacho et al.](#)) and HHblits ([Remmert et al.](#)) for evolutionary related structures matching the target sequence in Table T1. For details on the template search, see Materials and Methods. Overall 80 templates were found (Table T2).

Models

The following model was built (see Materials and Methods "Model Building"):

Model #02	File	Built with	Oligo-State	Ligands	GMQE	QMEAN
	PDB	ProMod3 Version 1.3.0.	monomer	1 x ZN: ZINC ION;	0.67	-2.76

QMEAN	-2.76	
C β	-2.05	
All Atom	-2.79	
Solvation	-2.04	
Torsion	-1.69	



Template	Seq Identity	Oligo-state	Found by	Method	Resolution	Seq Similarity	Range	Coverage	Description
4mah.1.A	49.43	monomer	BLAST	X-ray	1.55Å	0.45	1 - 188	0.87	AA11 Lytic Polysaccharide Monoxygenase

Ligand	Added to Model	Description
ZN	✓	ZINC ION
CL	✗ - Not biologically relevant.	CHLORIDE ION
EDO	✗ - Not biologically relevant.	1,2-ETHANEDIOL

Target HMEMSWPYPLRSRFDPPQVPEEDIDYSMTSPLNSDGSNFPCKGYQTNTPWRTAQYTA--GQTYNMTITGSATHGGGSCQL
 4mah.1.A HMMMAQVPVYGK-----DTLNNSPLAADGSDFPCK-LRSNT-YQVTEENTAIGQSMPLSFIGSAVHGGGSCQV

Target SLSYDNGKT---FKVIQSMEGGCPL-----VSKYNFKIPGDVANGQALFAWTWYNLIGNRELYMNCADV
 4mah.1.A SLTTDREPTKDSKWIVIKSIEGGCPANVDGNLSSGGPTSTGASKFTYTIPEGIEPGKYTLAWTFNFRIGNREMYMNCAPLT

Target ISGGTG-----TPSSFESAYPDLFVANVNGCSTVEGRETVFANPGDQVIYGGTVPSSPAFPICH
 4mah.1.A VTGSSSKRDEVPKKTEVEKRSANFPPMFVANV-NGCTTKEGVDIRFPNPGSIVEYAG-----

Materials and Methods

Template Search

Template search with BLAST and HHblits has been performed against the SWISS-MODEL template library (SMTL, last update: 2019-03-13, last included PDB release: 2019-03-08).

The target sequence was searched with BLAST against the primary amino acid sequence contained in the SMTL. A total of 1 template was found.

An initial HHblits profile has been built using the procedure outlined in (Remmert et al.), followed by 1 iteration of HHblits against NR20. The obtained profile has then be searched against all profiles of the SMTL. A total of 79 templates were found.

Model Building

Models are built based on the target-template alignment using ProMod3. Coordinates which are conserved between the target and the template are copied from the template to the model. Insertions and deletions are remodelled using a fragment library. Side chains are then rebuilt. Finally, the geometry of the resulting model is regularized by using a force field. In case loop modelling with ProMod3 fails, an alternative model is built with PROMOD-II ([Guex et al.](#)).

Model Quality Estimation

The global and per-residue model quality has been assessed using the QMEAN scoring function ([Benkert et al.](#)). For improved performance, weights of the individual QMEAN terms have been trained specifically for SWISS-MODEL.

Ligand Modelling

Ligands present in the template structure are transferred by homology to the model when the following criteria are met: (a) The ligands are annotated as biologically relevant in the template library, (b) the ligand is in contact with the model, (c) the ligand is not clashing with the protein, (d) the residues in contact with the ligand are conserved between the target and the template. If any of these four criteria is not satisfied, a certain ligand will not be included in the model. The model summary includes information on why and which ligand has not been included.

Oligomeric State Conservation

The quaternary structure annotation of the template is used to model the target sequence in its oligomeric form. The method ([Bertoni et al.](#)) is based on a supervised machine learning algorithm, Support Vector Machines (SVM), which combines interface conservation, structural clustering, and other template features to provide a quaternary structure quality estimate (QSQE). The QSQE score is a number between 0 and 1, reflecting the expected accuracy of the interchain contacts for a model built based a given alignment and template. Higher numbers indicate higher reliability. This complements the GMQE score which estimates the accuracy of the tertiary structure of the resulting model.

References

- **BLAST**
Camacho, C., Coulouris, G., Avagyan, V., Ma, N., Papadopoulos, J., Bealer, K., Madden, T.L. BLAST+: architecture and applications. BMC Bioinformatics 10, 421-430 (2009). 
- **HHblits**
Remmert, M., Biegert, A., Hauser, A., Söding, J. HHblits: lightning-fast iterative protein sequence searching by HMM-HMM alignment. Nat Methods 9, 173-175 (2012). 

Table T1:

Primary amino acid sequence for which templates were searched and models were built.

```
HMEMSWPYPLRSRFDQVPEEDIDYSMTSPLNSDGSNFPCKGYQTNTPW RATAQYTAGQTYNMTITGSATHGGSCQLSLSYD  
NGKTFKVIQSMEGGCPL  
VSKYNFKIPGDVANGQALFAWTWYNLIGNRELYMNCADVVISGGTGT PSSFESAYPDLFVANVGNGCSTVEGRETVFANPGDQ  
VIYGGTVPSSPAFPIC  
H
```

Table T2:

Templat e	Seq Identit y	Oligo- state	QSQ E	Found by	Metho d	Resolutio n	Seq Similarit y	Coverag e	Description
4mah.1. A	41.49	monom er		HHblit s	X-ray	1.55Å	0.41	0.94	AA11 Lytic Polysaccharide Monooxygenase

Template	Seq Identity	Oligo-state	QSQE	Found by	Method	Resolution	Seq Similarity	Coverage	Description
4mah.1.A	49.43	monomer		BLAST	X-ray	1.55Å	0.45	0.87	AA11 Lytic Polysaccharide Monoxygenase
5tkf.1.A	22.08	monomer		HHblits	X-ray	2.10Å	0.31	0.77	Lytic polysaccharide monoxygenase
4eir.1.A	21.94	monomer		HHblits	X-ray	1.10Å	0.31	0.77	polysaccharide monoxygenase-2
5x6a.1.A	17.61	monomer		HHblits	X-ray	1.70Å	0.28	0.79	Endoglucanase, putative
6h1z.1.A	17.61	monomer		HHblits	X-ray	1.57Å	0.28	0.79	Endoglucanase, putative
4eis.1.A	17.11	monomer		HHblits	X-ray	1.37Å	0.30	0.76	polysaccharide monoxygenase-3
4eis.2.A	17.11	monomer		HHblits	X-ray	1.37Å	0.30	0.76	polysaccharide monoxygenase-3
4x29.1.A	17.05	homodimer		HHblits	X-ray	2.41Å	0.29	0.44	Fusolin
4ow5.1.A	17.05	homodimer		HHblits	X-ray	1.90Å	0.29	0.44	Fusolin
5b4x.2.A	12.50	monomer		HHblits	X-ray	3.20Å	0.27	0.36	Reelin
3a7q.1.A	12.50	monomer		HHblits	X-ray	2.60Å	0.27	0.36	Reelin
2e26.1.A	12.50	monomer		HHblits	X-ray	2.00Å	0.27	0.36	Reelin
1w8o.1.A	20.31	monomer		HHblits	X-ray	1.70Å	0.29	0.32	BACTERIAL SIALIDASE
2bzd.1.A	20.97	monomer		HHblits	X-ray	2.00Å	0.30	0.31	BACTERIAL SIALIDASE
2bzd.2.A	20.97	monomer		HHblits	X-ray	2.00Å	0.30	0.31	BACTERIAL SIALIDASE
2bzd.3.A	20.97	monomer		HHblits	X-ray	2.00Å	0.30	0.31	BACTERIAL SIALIDASE
2c9p.1.A	11.11	monomer		HHblits	X-ray	2.25Å	0.27	0.31	COPPER RESISTANCE PROTEIN C
1ot4.1.A	11.11	monomer		HHblits	NMR	NA	0.27	0.31	Copper resistance protein C
1m42.1.A	11.11	monomer		HHblits	NMR	NA	0.27	0.31	Copper resistance protein C

Template	Seq Identity	Oligo-state	QSQE	Found by	Method	Resolution	Seq Similarity	Coverage	Description
2c9q.1.A	11.11	homodimer		HHblits	X-ray	1.60Å	0.27	0.31	COPPER RESISTANCE PROTEIN C
1nm4.1.A	11.11	monomer		HHblits	NMR	NA	0.27	0.31	Copper resistance protein C
2c9r.1.A	11.11	monomer		HHblits	X-ray	2.00Å	0.27	0.31	COPPER RESISTANCE PROTEIN C
2bzd.1.A	21.82	monomer		HHblits	X-ray	2.00Å	0.29	0.27	BACTERIAL SIALIDASE
2bzd.3.A	21.82	monomer		HHblits	X-ray	2.00Å	0.29	0.27	BACTERIAL SIALIDASE
2bzd.2.A	21.82	monomer		HHblits	X-ray	2.00Å	0.29	0.27	BACTERIAL SIALIDASE
1w8o.1.A	22.64	monomer		HHblits	X-ray	1.70Å	0.30	0.26	BACTERIAL SIALIDASE
4j9t.1.A	22.00	monomer		HHblits	X-ray	1.40Å	0.29	0.25	designed unnatural amino acid dependent metalloprotein
4j9t.1.A	18.18	monomer		HHblits	X-ray	1.40Å	0.30	0.22	designed unnatural amino acid dependent metalloprotein
5b4x.2.A	21.43	monomer		HHblits	X-ray	3.20Å	0.31	0.21	Reelin
2e26.1.A	21.43	monomer		HHblits	X-ray	2.00Å	0.31	0.21	Reelin
3a7q.1.A	21.43	monomer		HHblits	X-ray	2.60Å	0.31	0.21	Reelin
5t7j.1.A	23.68	monomer		HHblits	X-ray	1.65Å	0.36	0.19	AoAA13
2a9d.1.A	37.50	homodimer	0.00	HHblits	X-ray	1.70Å	0.39	0.16	Sulfite Oxidase
3hbp.1.A	37.50	monomer		HHblits	X-ray	2.40Å	0.39	0.16	Sulfite Oxidase mutant C185S
3hc2.1.A	37.50	monomer		HHblits	X-ray	2.50Å	0.39	0.16	sulfite oxidase
3hbg.1.A	37.50	monomer		HHblits	X-ray	1.90Å	0.39	0.16	Sulfite Oxidase mutant C185S
1sox.1.A	37.50	homodimer		HHblits	X-ray	1.90Å	0.39	0.16	SULFITE OXIDASE

Template	Seq Identity	Oligo-state	QSQE	Found by	Method	Resolution	Seq Similarity	Coverage	Description
2bih.1.A	31.25	homodimer		HHblits	X-ray	2.60Å	0.36	0.16	NITRATE REDUCTASE [NADPH]
2a9b.1.A	37.50	monomer		HHblits	X-ray	2.50Å	0.39	0.16	Sulfite Oxidase
3r19.1.A	37.50	monomer		HHblits	X-ray	2.10Å	0.39	0.16	Sulfite oxidase
5wa0.1.A	25.00	monomer		HHblits	X-ray	2.10Å	0.33	0.16	Putative sulfite oxidase
5k3x.1.A	25.00	monomer		HHblits	X-ray	1.60Å	0.33	0.16	Putative sulfite oxidase
2a9a.1.A	37.50	homodimer	0.00	HHblits	X-ray	2.00Å	0.39	0.16	Sulfite Oxidase
1ogp.1.A	32.26	homodimer	0.00	HHblits	X-ray	2.60Å	0.36	0.15	SULFITE OXIDASE
2ca4.1.A	32.26	monomer		HHblits	X-ray	2.10Å	0.35	0.15	SULFITE\CYTOCHROME C OXIDOREDUCTASE SUBUNIT A
2ca3.1.A	32.26	monomer		HHblits	X-ray	2.00Å	0.35	0.15	SULFITE\CYTOCHROME C OXIDOREDUCTASE SUBUNIT A

The table above shows the top 47 filtered templates. A further 32 templates were found which were considered to be less suitable for modelling than the filtered list.

5aoz.1.A, 5iuc.1.A, 2vtc.1.A, 2ddu.1.A, 4b5q.1.A, 2ber.1.A, 5m2o.1.A, 5o2w.1.A, 4iu2.1.A, 3zud.1.A, 5nlt.1.A, 4qi8.1.A, 3r18.1.A, 5msz.1.A, 4oy7.1.A, 4wkz.1.B, 3eja.1.A, 3a72.1.A, 4yn2.1.A, 5m2s.1.A, 5nns.1.A, 2zf9.1.A, 6ha5.1.A, 5ufv.1.A, 4uyq.1.A, 5n5p.1.A, 5n05.1.A, 5foh.1.A, 4bbw.1.A, 4d7u.1.A, 5no7.1.A, 1eus.1.A

[Swiss Institute of Bioinformatics Contact Us](#)

Table D2. Glycosylation predictions by NetOGlyc & NetNGlyc on FASTA sequence of *AfuLPMO11B*.

The table contains raw data output of predicted glycosylation sites of either O-linked or N-linked glycans with probability score executed by NetOGlyC and NetNGlyc [x, x]. Residues are labeled by sequence number of *AfuLPMO11B* full sequence incl. signal peptide (Table x). Sequence data marked in *red* show predicted sites that was not included in the model produced by SWISS-MODEL.

NetOGlyc 4.0 Server - prediction results

Technical University of Denmark

```

##gff-version 2
##source-version NetOGlyc 4.0.0.13
##date 19-4-12
##Type Protein
#seqname      source  feature  start   end     score   strand  frame  comment
SEQUENCE     netOGlyc-4.0.0.13 CARBOHYD  4       4       0.156505 .      .
SEQUENCE     netOGlyc-4.0.0.13 CARBOHYD  12      12      0.030483 .      .
SEQUENCE     netOGlyc-4.0.0.13 CARBOHYD  14      14      0.0537054 .    .
SEQUENCE     netOGlyc-4.0.0.13 CARBOHYD  23      23      0.0397507 .    .
SEQUENCE     netOGlyc-4.0.0.13 CARBOHYD  30      30      0.104997 .      .
SEQUENCE     netOGlyc-4.0.0.13 CARBOHYD  44      44      0.299444 .      .
SEQUENCE     netOGlyc-4.0.0.13 CARBOHYD  46      46      0.22042 .      .
SEQUENCE     netOGlyc-4.0.0.13 CARBOHYD  47      47      0.132116 .      .
SEQUENCE     netOGlyc-4.0.0.13 CARBOHYD  51      51      0.413602 .      .
SEQUENCE     netOGlyc-4.0.0.13 CARBOHYD  54      54      0.185015 .      .
SEQUENCE     netOGlyc-4.0.0.13 CARBOHYD  63      63      0.50528 .      .      #POSITIVE
SEQUENCE     netOGlyc-4.0.0.13 CARBOHYD  65      65      0.552847 .      .      #POSITIVE
SEQUENCE     netOGlyc-4.0.0.13 CARBOHYD  70      70      0.542678 .      .      #POSITIVE
SEQUENCE     netOGlyc-4.0.0.13 CARBOHYD  74      74      0.434858 .      .
SEQUENCE     netOGlyc-4.0.0.13 CARBOHYD  78      78      0.331824 .      .
SEQUENCE     netOGlyc-4.0.0.13 CARBOHYD  82      82      0.0267761 .      .
SEQUENCE     netOGlyc-4.0.0.13 CARBOHYD  84      84      0.0581215 .      .
SEQUENCE     netOGlyc-4.0.0.13 CARBOHYD  86      86      0.0155773 .      .
SEQUENCE     netOGlyc-4.0.0.13 CARBOHYD  88      88      0.0245874 .      .
SEQUENCE     netOGlyc-4.0.0.13 CARBOHYD  93      93      0.0113561 .      .
SEQUENCE     netOGlyc-4.0.0.13 CARBOHYD  97      97      0.0175839 .      .
SEQUENCE     netOGlyc-4.0.0.13 CARBOHYD  99      99      0.0161223 .      .
SEQUENCE     netOGlyc-4.0.0.13 CARBOHYD  105     105     0.0216104 .      .
SEQUENCE     netOGlyc-4.0.0.13 CARBOHYD  111     111     0.0444566 .      .
SEQUENCE     netOGlyc-4.0.0.13 CARBOHYD  120     120     0.0795099 .      .
SEQUENCE     netOGlyc-4.0.0.13 CARBOHYD  140     140     0.00865163 .    .
SEQUENCE     netOGlyc-4.0.0.13 CARBOHYD  160     160     0.268224 .      .
SEQUENCE     netOGlyc-4.0.0.13 CARBOHYD  163     163     0.140833 .      .
SEQUENCE     netOGlyc-4.0.0.13 CARBOHYD  165     165     0.197325 .      .
SEQUENCE     netOGlyc-4.0.0.13 CARBOHYD  167     167     0.379076 .      .
SEQUENCE     netOGlyc-4.0.0.13 CARBOHYD  168     168     0.285882 .      .
SEQUENCE     netOGlyc-4.0.0.13 CARBOHYD  171     171     0.375648 .      .
SEQUENCE     netOGlyc-4.0.0.13 CARBOHYD  186     186     0.354286 .      .
SEQUENCE     netOGlyc-4.0.0.13 CARBOHYD  187     187     0.0919251 .      .
SEQUENCE     netOGlyc-4.0.0.13 CARBOHYD  193     193     0.148439 .      .
SEQUENCE     netOGlyc-4.0.0.13 CARBOHYD  207     207     0.61683 .      .      #POSITIVE
SEQUENCE     netOGlyc-4.0.0.13 CARBOHYD  209     209     0.530689 .      .      #POSITIVE
SEQUENCE     netOGlyc-4.0.0.13 CARBOHYD  211     211     0.782089 .      .      #POSITIVE
SEQUENCE     netOGlyc-4.0.0.13 CARBOHYD  212     212     0.626415 .      .      #POSITIVE

```

NetNGlyc 1.0 Server - prediction results

Technical University of Denmark

APPENDIX E

Appendix E contains absorption data from the SDS-PAGE analyses used in calculating % bound protein in the binding experiment.

Table E1. SDS-PAGE relative absorbance data used for binding estimation. The table contains average values of all triplicate samples from the SDS-PAGE quantification method used in determining % bound protein (Results – Fig 21, panel B and C). Samples with timepoints (T) in red indicates data from reactions that did not contain ascorbic acid, and timepoints (T) in green indicates samples that did contain ascorbic acid, where oxidized products were also quantified (Results – Fig 21, panel A). Afu(+) indicated glycosylated protein, and Afu(-) indicate deglycosylated protein. 100 % indicate reactions containing no substrate or reductant, and were used as relative value to reactions with LPMO and substrates, α -chitin (dark yellow) and β -chitin (yellow). *Adj. Volume average* = average UV absorbance of triplicates from the protein bands in the SDS-PAGE gels. *SD Adj.V* = standard deviation n=3 from *Adj. Volume* (raw data from triplicates). % of free, bound, and SD was calculated by the relative differences in *Adj.V average* between the control (Afu 100%) and (Afu + substrate).

T	Samples	Adj. Volume average	SD Adj.V	% Free	SD %	Bound %
0,5	Afu(+) 100%	3780277	61428	100,000	1,625	0,000
	Afu(+) alpha	3397184	43054	89,866	1,139	10,134
	Afu(+) beta	2987207	139890	79,021	3,701	20,979
	Afu(-) 100%	3060360	56115	100,000	1,834	0,000
	Afu(-) alpha	2751539	91463	89,909	2,989	10,091
	Afu(-) beta	2694923	82261	88,059	2,688	11,941
1	Afu(+) 100%	4017961	76552	100,000	1,905	0,000
	Afu(+) alpha	3274899	163358	81,506	4,066	18,494
	Afu(+) beta	2793590	119354	69,528	2,971	30,472
	Afu(-) 100%	3148424	149326	100,000	4,743	0,000
	Afu(-) alpha	2709061	122628	86,045	3,895	13,955
	Afu(-) beta	2864235	92671	90,974	2,943	9,026
2	Afu(+) 100%	3800160	30737	100,000	0,809	0,000
	Afu(+) alpha	3013523	98551	79,300	2,593	20,700
	Afu(+) beta	2549213	122789	67,082	3,231	32,918
	Afu(-) 100%	3174694	120223	100,000	3,787	0,000
	Afu(-) alpha	2429975	182590	76,542	5,751	23,458
	Afu(-) beta	2513021	69782	79,158	2,198	20,842
4	Afu(+) 100%	3478385	93340	100,000	2,683	0,000
	Afu(+) alpha	2913248	102755	83,753	2,954	16,247
	Afu(+) beta	2490656	87766	71,604	2,523	28,396
	Afu(-) 100%	1874015	49230	100,000	2,627	0,000
	Afu(-) alpha	1423016	67005	75,934	3,575	24,066
	Afu(-) beta	1387449	61729	74,036	3,294	25,964
6	Afu(+) 100%	3863160	74044	100,000	1,917	0,000
	Afu(+) alpha	3230500	94928	83,623	2,457	16,377
	Afu(+) beta	2633120	98082	68,160	2,539	31,840
	Afu(-) 100%	3513233	232067	100,000	6,606	0,000
	Afu(-) alpha	2638953	72750	75,115	2,071	24,885

	Afu(-) beta	2774427	82258	78,971	2,341	21,029
24	Afu(+) 100%	3807463	258676	100,000	6,794	0,000
	Afu(+) alpha	3127367	124464	82,138	3,269	17,862
	Afu(+) beta	2603370	334178	68,375	8,777	31,625
	Afu(-) 100%	3673871	26519	100,000	0,722	0,000
	Afu(-) alpha	2660785	79124	72,425	2,154	27,575
	Afu(-) beta	2483840	285050	67,608	7,759	32,392
0,5	Afu(+) 100%	3319510	45298	100,000	1,365	0,000
	Afu(+) alpha	2861395	94739	86,199	2,854	13,801
	Afu(+) beta	1996378	108880	60,141	3,280	39,859
	Afu(-) 100%	2743280	120706	100,000	4,400	0,000
	Afu(-) alpha	2175158	18989	79,290	0,692	20,710
	Afu(-) beta	2151192	359949	78,417	13,121	21,583
1	Afu(+) 100%	4344552	89013	100,000	2,049	0,000
	Afu(+) alpha	3755568	121386	86,443	2,794	13,557
	Afu(+) beta	3261096	62411	75,062	1,437	24,938
	Afu(-) 100%	1364834	26104	100,000	1,913	0,000
	Afu(-) alpha	1247376	19545	91,394	1,432	8,606
	Afu(-) beta	1103496	84583	80,852	6,197	19,148
2	Afu(+) 100%	3462386	44415	100,000	1,283	0,000
	Afu(+) alpha	2792312	171727	80,647	4,960	19,353
	Afu(+) beta	2186208	31619	63,142	0,913	36,858
	Afu(-) 100%	3351483	108554	100,000	3,239	0,000
	Afu(-) alpha	2830263	66830	84,448	1,994	15,552
	Afu(-) beta	2687790	298883	80,197	8,918	19,803
4	Afu(+) 100%	3556140	20620	100,000	0,580	0,000
	Afu(+) alpha	3188173	77747	89,653	2,186	10,347
	Afu(+) beta	3533460	126067	99,362	3,545	0,638
	Afu(-) 100%	2985645	26843	100,000	0,899	0,000
	Afu(-) alpha	2725548	94804	91,288	3,175	8,712
	Afu(-) beta	2627710	121547	88,011	4,071	11,989
6	Afu(+) 100%	3788712	194891	100,000	5,144	0,000
	Afu(+) alpha	3169800	34678	83,664	0,915	16,336
	Afu(+) beta	3491472	88941	92,155	2,348	7,845
	Afu(-) 100%	1946929	80940	100,000	4,157	0,000
	Afu(-) alpha	1787370	23420	91,805	1,203	8,195
	Afu(-) beta	1763833	69221	90,596	3,555	9,404
24	Afu(+) 100%	3839917	164475	100,000	4,283	0,000
	Afu(+) alpha	3234997	91548	84,247	2,384	15,753
	Afu(+) beta	3396332	167545	88,448	4,363	11,552
	Afu(-) 100%	2997672	103008	100,000	3,436	0,000
	Afu(-) alpha	2741438	33610	91,452	1,121	8,548
	Afu(-) beta	3017747	212896	100,670	7,102	-0,670

APPENDIX F

Appendix F contains the chemical condition within the commercial crystallization kit (Molecular Dimensions; JCSG-plus™ MD1-37) used in screening for crystal formation of glycosylated and deglycosylated *AfuLPMO11B*.

Table F1. Crystallization conditions: Table contains the various crystallization conditions used when screening for crystal formations of the glycosylated and deglycosylated version of *AfuLPMO11.2*. The screen kit is from Molecular Dimensions; JCSG-plus™ MD1-37 conditions 1- [1-48] (box 1) & 2- [1-48] (box2).

Tube #	Conc.	Salt	Conc.	Buffer	pH	Conc.	Precipitant
1-1	0.2 M	Lithium sulfate	0.1 M	Sodium acetate	4.5	50 % w/v	PEG 400
1-2	-	None	0.1 M	Sodium citrate	5.5	20 % w/v	PEG 3000
1-3	0.2 M	Ammonium citrate dibasic	-	None	-	20 % w/v	PEG 3350
1-4	0.02 M	Calcium chloride dihydrate	0.1 M	Sodium acetate	4.6	30 % v/v	MPD
1-5	0.2 M	Magnesium formate dihydrate	-	None	-	20 % w/v	PEG 3350
1-6	0.2 M	Lithium sulfate	0.1 M	Phosphate / citrate	4.2	20 % w/v	PEG 1000
1-7	-	None	0.1 M	CHES	9.5	20 % w/v	PEG 8000
1-8	0.2 M	Ammonium formate	-	None	-	20 % w/v	PEG 3350
1-9	0.2 M	Ammonium chloride	-	None	-	20 % w/v	PEG 3350
1-10	0.2 M	Potassium formate	-	None	-	20 % w/v	PEG 3350
1-11	0.2 M	Ammonium phosphate monobasic	0.1 M	Tris	8.5	50 % v/v	MPD
1-12	0.2 M	Potassium nitrate	-	None	-	20 % w/v	PEG 3350
1-13	0.8 M	Ammonium sulfate	0.1 M	Citrate	4.0	-	None
1-14	0.2 M	Sodium thiocyanate	-	None	-	20 % w/v	PEG 3350
1-15	-	None	0.1 M	BICINE	9.0	20 % w/v	PEG 6000
1-16	-	None	0.1 M	HEPES	7.5	10 % w/v 8 % v/v	PEG 8000 Ethylene glycol
1-17	-	None	0.1 M	Sodium cacodylate	6.5	40 % v/v 5 % w/v	MPD PEG 8000

1-18	-	None	0.1 M	Phosphate / citrate	4.2	40 % v/v 5 % w/v	Ethanol PEG 1000
1-19	-	None	0.1 M	Sodium acetate	4.6	8 % w/v	PEG 4000
1-20	0.2 M	Magnesium chloride hexahydrate	0.1 M	Tris	7.0	10 % w/v	PEG 8000
1-21	-	None	0.1 M	Citrate	5.0	20 % w/v	PEG 6000
1-22	0.2 M	Magnesium chloride hexahydrate	0.1 M	Sodium cacodylate	6.5	50 % v/v	PEG 200
1-23	1.6 M	Sodium citrate tribasic dihydrate pH 6.5	-	None	-	-	None
1-24	0.2 M	Potassium citrate tribasic monohydrate	-	None	-	20 % w/v	PEG 3350
1-25	0.2 M	Sodium chloride	0.1 M	Phosphate / citrate	4.2	20 % w/v	PEG 8000
1-26	1.0 M	Lithium chloride	0.1 M	Citrate	4.0	20 % w/v	PEG 6000
1-27	0.2 M	Ammonium nitrate	-	None	-	20 % w/v	PEG 3350
1-28	-	None	0.1 M	HEPES	7.0	10 % w/v	PEG 6000
1-29	0.8 M	Sodium phosphate monobasic monohydrate / Potassium phosphate 0.8 M monobasic	0.1 M	Sodium HEPES	7.5	-	None
1-30	-	None	0.1 M	Phosphate / citrate	4.2	40 % v/v	PEG 300
1-31	0.2 M	Zinc acetate dihydrate	0.1 M	Sodium acetate	4.5	10 % w/v	PEG 3000
1-32	-	None	0.1 M	Tris	8.5	20 % v/v	Ethanol
1-33	-	None	0.1 M	Sodium / potassium phosphate	6.2	25 % v/v 10 % v/v	1,2- Propandiol Glycerol
1-34	-	None	0.1 M	BICINE	9.0	10 % w/v 2 % v/v	PEG 20,000 1,4-Dioxane
1-35	2.0 M	Ammonium sulfate	0.1 M	Sodium acetate	4.6	-	None
1-36	-	None	-	None	-	10 % w/v 10 % w/v	PEG 1000 PEG 8000

1-37	-	None	-	None	-	24 % w/v 20 % v/v	PEG 1500 Glycerol
1-38	0.2 M	Magnesium chloride hexahydrate	0.1 M	Sodium HEPES	7.5	30 % v/v	PEG 400
1-39	0.2 M	Sodium chloride	0.1 M	Sodium / potassium phosphate	6.2	50 % v/v	PEG 200
1-40	0.2 M	Lithium sulfate	0.1 M	Sodium acetate	4.5	30 % w/v	PEG 8000
1-41	-	None	0.1 M	HEPES	7.5	70 % v/v	MPD
1-42	0.2 M	Magnesium chloride hexahydrate	0.1 M	Tris	8.5	20 % w/v	PEG 8000
1-43	0.2 M	Lithium sulfate	0.1 M	Tris	8.5	40 % v/v	PEG 400
1-44	-	None	0.1 M	Tris	8.0	40 % v/v	MPD
1-45	0.17 M	Ammonium sulfate	-	None	-	25.5 % w/v 15 % v/v	PEG 4000 Glycerol
1-46	0.2 M	Calcium acetate hydrate	0.1 M	Sodium cacodylate	6.5	40 % v/v	PEG 300
1-47	0.14 M	Calcium chloride dihydrate	0.07 M	Sodium acetate	4.6	14 % v/v 30 % v/v	2-Propanol Glycerol
1-48	0.04 M	Potassium phosphate monobasic	-	none	-	16 % w/v 20 % v/v	PEG 8000 Glycerol
2-1	1.0 M	Sodium citrate tribasic dihydrate	0.1 M	Sodium cacodylate	6.5	-	None
2-2	2.0 M 0.2 M	Ammonium sulfate / Sodium chloride	0.1 M	Sodium cacodylate	6.5	-	None
2-3	0.2 M	sodium chloride	0.1 M	HEPES	7.5	10 % w/v	2-Propanol
2-4	1.26 M 0.2 M	Ammonium sulfate / Lithium sulfate	0.1 M	Tris	8.5	-	None
2-5	-	None	0.1 M	CAPS	10.5	40 % w/v	MPD
2-6	0.2 M	Zinc acetate dihydrate	0.1 M	Imidazole	8.0	20 % w/v	PEG 3000
2-7	0.2 M	Zinc acetate dihydrate	0.1 M	Sodium cacodylate	6.5	10 % w/v	2-Propanol
2-8	1.0 M	Ammonium phosphate dibasic	0.1 M	Sodium acetate	4.5	-	None
2-9	1.6 M	Magnesium sulfate heptahydrate	0.1 M	MES	6.5	-	None

2-10	-	None	0.1 M	BICINE	9.0	10 % w/v	PEG 6000
2-11	0.16 M	Calcium acetate hydrate	0.08 M	Sodium cacodylate	6.5	14.4 % w/v 20 % w/v	PEG 8000 Glycerol
2-12	-	None	0.1 M	Imidazole	8.0	10 % w/v	PEG 8000
2-13	0.05 M	Caesium chloride	0.1 M	MES	6.5	30 % w/v	Jeffamine® M-600
2-14	3.2 M	Ammonium sulfate	0.1 M	Citrate	5.0	-	None
2-15	-	None	0.1 M	Tris	8.0	20 % w/v	MPD
2-16	-	None	0.1 M	HEPES	7.5	20 % w/v	Jeffamine® M-600
2-17	0.2 M	Magnesium chloride hexahydrate	0.1 M	Tris	8.5	50 % w/v	Ethylene glycol
2-18	-	None	0.1 M	BICINE	9.0	20 % w/v	MPD
2-19	0.8 M	Succinic acid pH 7.0	-	None	-	-	None
2-20	2.1 M	DL-malic acid pH 7.0	-	None	-	-	None
2-21	2.4 M	Sodium malonate dibasic monohydrate pH 7.0	-	None	-	-	None
2-22	1.1 M	Sodium malonate dibasic monohydrate	0.1 M	HEPES	7.0	0.5 % w/v	Jeffamine® ED-2003
2-23	1.0 M	Succinic acid	0.1 M	HEPES	7.0	1 % w/v	PEG 2000 MME
2-24	-	None	0.1 M	HEPES	7.0	30 % w/v	Jeffamine® M-600
2-25	-	None	0.1 M	HEPES	7.0	30 % w/v	Jeffamine® ED-2003
2-26	0.02 M	Magnesium chloride hexahydrate	0.1 M	HEPES	7.0	22 % w/v	Poly(acrylic acid sodium salt) 5100
2-27	0.01 M	Cobalt(II) chloride hexahydrate	0.1 M	Tris	8.5	20 % w/v	Polyvinylpyrrolidone
2-28	0.2 M	TMAO	0.1 M	Tris	8.5	20 % w/v	PEG 2000 MME
2-29	0.005 M	Cobalt(II) chloride hexahydrate /	0.1 M	HEPES	7.5	12 % w/v	PEG 3350
	0.005 M	Cadmium chloride hemi(pentahydrate) /					
	0.005 M						

		Magnesium chloride 0.005 M hexahydrate / Nickel(II) chloride hexahydrate						
2-30	0.2 M	Sodium malonate dibasic monohydrate	-	None	-	20 % w/v	PEG 3350	
2-31	0.1 M	Succinic acid	-	None	-	15 % w/v	PEG 3350	
2-32	0.15 M	DL-Malic acid	-	None	-	20 % w/v	PEG 3350	
2-33	0.1 M	Potassium thiocyanate	-	None	-	30 % w/v	PEG 2000 MME	
2-34	0.15 M	Potassium bromide	-	None	-	30 % w/v	PEG 2000 MME	
2-35	2.0 M	Ammonium sulfate	0.1 M	BIS-Tris	5.5	-	None	
2-36	3.0 M	Sodium chloride	0.1 M	BIS-Tris	5.5	-	None	
2-37	0.3 M	Magnesium formate dihydrate	0.1 M	BIS-Tris	5.5	-	None	
2-38	1.0 M	Ammonium sulfate	0.1 M	BIS-Tris	5.5	1 % w/v	PEG 3350	
2-39	-	None	0.1 M	BIS-Tris	5.5	25 % w/v	PEG 3350	
2-40	0.2 M	Calcium chloride dihydrate	0.1 M	BIS-Tris	5.5	45 % w/v	MPD	
2-41	0.2 M	Ammonium acetate	0.1 M	BIS-Tris	5.5	45 % w/v	MPD	
2-42	0.1 M	Ammonium acetate	0.1 M	BIS-Tris	5.5	17 % w/v	PEG 10,000	
2-43	0.2 M	Ammonium sulfate	0.1 M	BIS-Tris	5.5	25 % w/v	PEG 3350	
2-44	0.2 M	Sodium chloride	0.1 M	BIS-Tris	5.5	25 % w/v	PEG 3350	
2-45	0.2 M	Lithium sulfate	0.1 M	BIS-Tris	5.5	25 % w/v	PEG 3350	
2-46	0.2 M	Ammonium acetate	0.1 M	BIS-Tris	5.5	25 % w/v	PEG 3350	
2-47	0.2 M	Magnesium chloride hexahydrate	0.1 M	BIS-Tris	5.5	25 % w/v	PEG 3350	
2-48	0.2 M	Ammonium acetate	0.1 M	HEPES	7.5	45 % w/v	MPD	

APPENDIX G

Appendix G contain other supplementary information mentioned and/or necessary supporting material for other data provided in the result section.

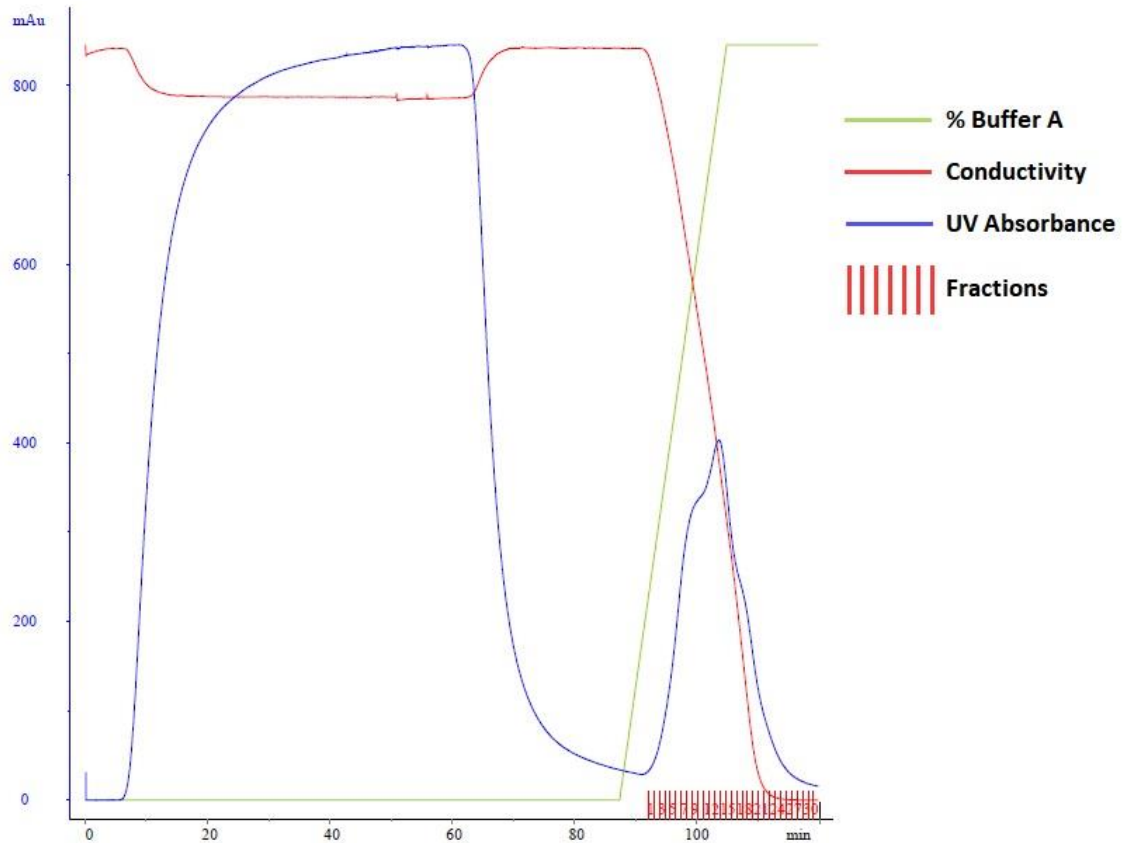


Fig G1. Hydrophobic Interaction Chromatogram (HIC). Figure shows a typical HIC chromatogram, from which fractions were selected based on peak at buffer change retention time. This chromatogram is from *Pichia cultivation 2* [Figure used in kinetic experiments throughout the thesis. Blue line show UV absorbance, indicating chemical content possessing aromatic residues, typically proteins, pigments, or other large organic compounds. Red line show conductivity, indicating salt level variations, decreasing as storage buffer concentration increases. Green line show percentage of storage buffer (50 mM [BIS-Tris], pH=6.5) in the solution, where 100 % is at the top flat-line area. Blue peak at approx. 95 – 115 min. shows chemical content that are released when salt levels decline, most likely the enzyme of interest (AA11.2) + other chemicals with similar interaction with the column material.

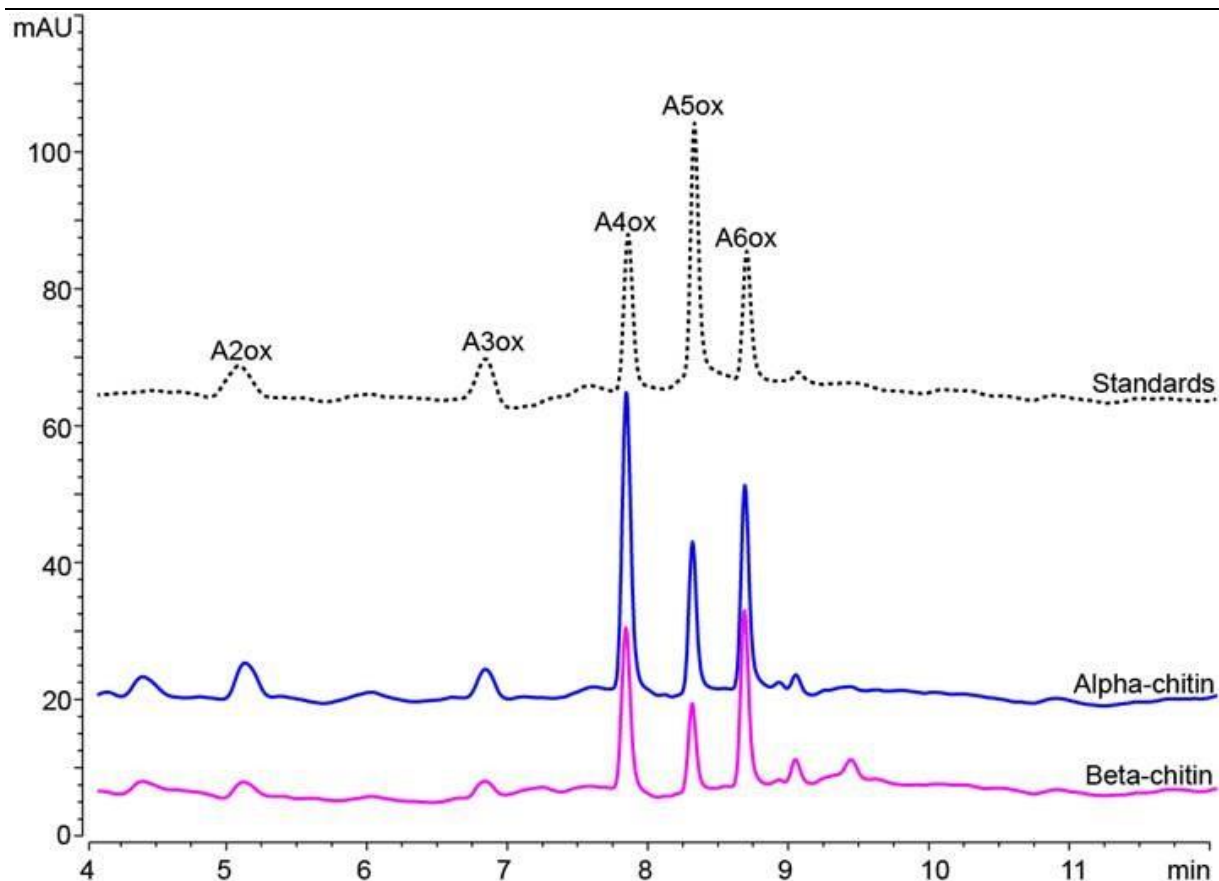


Fig G2. Activity confirmation on *AfuLPMO11B* enzyme stock 1. The figure shows analyzed samples from HILIC – Agilent on overnight reactions on α - and β -chitin *AfuLPMO11B*. The chromatogram shows that the purified enzyme is active. This enzyme stock was used in the enzymatic H_2O_2 production assay (Results – Fig 10) and in the comparison assay with *BcLPMO11B* (Results – Fig 14). The standard is composed of oxidized chitooligomers $(GlcNAc)_nGlcNAc1A$ with a degree of polymerization (DP) of DP1 – DP6, and are described in the method section. DP1 is not shown in the chromatogram.

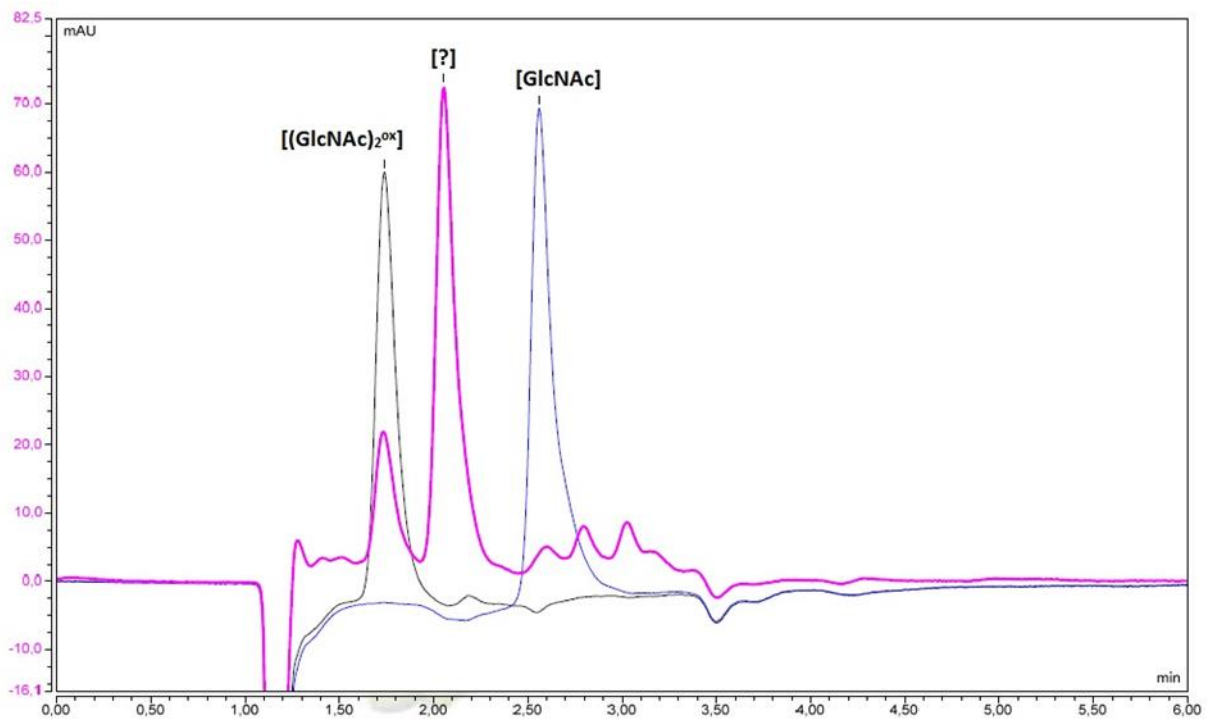


Fig G3. Rezex RSLC UPLC – Analysis of substrate from a contaminated substrate stock solution. The figure illustrates a contamination found in a β -chitin substrate stock solution after some time (magenta). Standards of both oxidized dimer (GlcNAcGlcNAc1A) (60 μ M), and native monomer (GlcNAc) (200 μ M) are included, labeled $[(\text{GlcNAc})_2^{\text{ox}}]$ and $[\text{GlcNAc}]$ respectively.

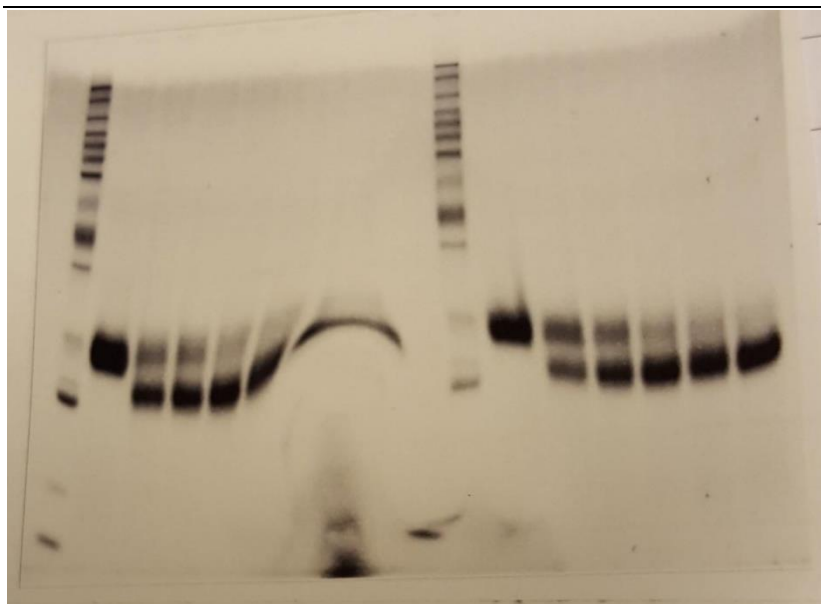


Fig G4. Comparing deglycosylation efficiency between Endo-H and *EfEndo18A*. SDS-PAGE, showing (from left) protein ladder, *AfuLPMO11B* glycosylated control, and successively 5, 10, 15, 20, and 30 min incubation samples from reactions with *EfEndo18A* (left side) and Endo-H (right side).



Norges miljø- og biovitenskapelige universitet
Noregs miljø- og biovitenskapelige universitet
Norwegian University of Life Sciences

Postboks 5003
NO-1432 Ås
Norway